Evaluation and improvement of dehydrogenation conversion and isomerization selectivity in an extractor Catalytic Membrane Reactor

by

Lizelle Doreen van Dyk

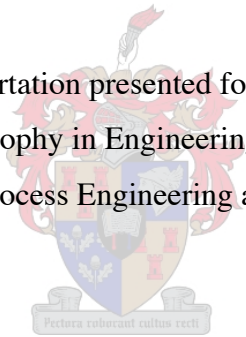

Dissertation presented for the Degree of
Doctor of Philosophy in Engineering (Chemical Engineering)
in the Department of Process Engineering at the University of Stellenbosch.

Promoters:
Prof. Leon Lorenzen
Dr. Sylvain Miachon

April 2005

Declaration

I, the undersigned, hereby declare that the work contained in this dissertation is my own original work and that it has not been submitted previously in its entirety or in part for a degree at any university.

Signature: .....

Date: .....

Summary

Recent advances in inorganic material preparation for membrane fabrication have extended the use of membranes to high temperature and chemically harsh environments. This has allowed inorganic membranes to be integrated into catalytic reactors, resulting in the concept known as Catalytic Membrane Reactors (CMRs). CMRs have overall important benefits of product quality, plant compactness, environmental impact reduction and energy savings. It has found use in a broad range of applications including biochemical, chemical, environmental and petrochemical systems. In these CMRs, the membranes perform a variety of functions, and consequently they are categorized according to the primary role of the membrane: *extractor*, *distributor* or *contactor*.

In this dissertation the different uses of an *extractor* Catalytic Membrane Reactor (eCMR) are evaluated with the help of model reactions. In the eCMR the primary function of the membrane is to selectively extract one of the reaction products from the reaction zone, thereby combining the benefits of separation and reaction in one unit operation. This can lead to a number of advantages, of which the two most important ones include: (a) conversion beyond thermodynamic equilibrium in equilibrium restricted reactions and/or (b) the improvement of product selectivity in consecutive/parallel reaction networks.

The dehydrogenation of isobutane, an equilibrium restricted reaction, was evaluated in a dense Palladium and a MFI-zeolite/alumina composite eCMR. These two eCMRs, consisting of a membrane packed with a Pt/In/Ge-MFI-zeolite catalyst, differed only on the basis of the membrane used. The palladium membrane showed superior extraction and selectivity capability for hydrogen in the reaction mixture compared to the MFI/alumina composite membrane. Regardless of these facts, the performances of the Pd and MFI eCMR, when evaluated at the same reaction conditions, were similar. The isobutane conversion to isobutene, employing high sweep rates (185 ml/min) could be increased up to ca. 37 % at 723 K, compared to 14 % in the conventional packed-bed reactor. The similar performance of the two different eCMRs was evaluated using a Catalytic Membrane Reactor model. Model results showed that in order for the extractor-type CMR to completely draw benefit from the combination of membrane and catalyst in the same unit for conversion enhancement, a very active catalyst should be developed, able to sustain the high extraction ability of the membrane. This was the first time that these

two eCMRs were evaluated at similar reaction conditions in order to study the influence of the nature of the membrane material on the working of the eCMR.

The eCMR was also used to carry out meta-xylene isomerization. This part focused on the extraction of para-xylene from the meta-xylene isomerization reaction zone with a MFI eCMR (MFI-zeolite membrane and Pt-HZSM5 fixed-bed catalyst) in order to improve the reaction selectivity towards para-xylene. Para-xylene is an important industrial chemical used as a precursor for polyester resin, and in order to meet the para-xylene demand, ortho- and meta-xylenes are converted via the xylene isomerization reaction to xylene isomers.

It has been shown that the pore-plugged MFI-zeolite membranes used in this study can selectively extract para-xylene from a mixture of xylenes. Using an extractor type catalytic membrane reactor instead of a conventional fixed-bed reactor for meta-xylene isomerization, can lead to higher para-xylene selectivities. The para-xylene selectivity can even be improved to 100% if the CMR is operated in the permeate-only mode, but this comes at a price of lower para-xylene yields. When operated in combined mode (i.e. mixing both permeate and retentate streams after the reactor), the CMR shows an improvement on both para-xylene productivity (ca. 10 % maximum at conditions studied) and selectivity when compared to the conventional reactor. This is the first time para-xylene selectivity could successfully be improved by employing an extractor Catalytic Membrane Reactor.

This dissertation also led to the design and construction of a new generation membrane reactor testing bench, a first in the Department of Process Engineering, University of Stellenbosch. The bench allows for high temperature evaluation of membranes and Catalytic Membrane Reactors. The design is simple and easily adaptable for use to evaluate various different reactions.

Opsomming

Onlangse ontwikkelinge in die gebied van anorganiese materiaal voorbereiding vir membraan vervaardiging, verbreed die omstandighede waarby membrane gebruik kan word, na hoë temperature toestande en chemiese ongure toestande. Dit het gelei tot die integrasie van membrane in katalitiese reaktore, 'n begrip wat bekend staan as die Katalitiese Membraan Reaktor (KMR). KMRe bied oorhoofs belangrike voordele noemlik produk-kwaliteit, aanleg kompaktiwiteit, omgewingsimpak verlagings en energie besparings. Dit word gebruik vir 'n wye reeks van applikasies in onder andere biochemiese, chemiese, omgewings en petrochemiese sisteme. In hierdie KMRe verrig die membraan 'n verskydenheid van take, en gevolglik word KMRe geklassifiseer volgens die primêre rol van die membraan, naamlik: *ekstraktor, verspreider* of *kontaktor*.

In hierdie proefskrif word die verskillende gebruike van die ekstraktor tipe Katalitiese Membraan Reaktor (eKMR) geëvalueer met behulp van model-reaksies. In die eKMR is die primêre funksie van die membraan om een van die reaksie produkte uit die reaksieomgewing te onttrek. Dit hou 'n aantal voordele in, waarvan die twee hoofvoordele insluit: (a) omsetting verby die termodinamiese reaksie ewewig en/ of (b) die verhoging van produkselektiwiteit in series/ parallel reaksie netwerke.

Die dehidrogenering van isobutaan, 'n ewewig beperkte reaksie, is in 'n digte palladium en saamgestelde MFI/alumina eKMR geëvalueer. Hierdie twee eKMRe, wat betaan uit 'n membraan gepak met 'n Pt/In/Ge-MFI-zeoliet katalis, het slegs op grond van die membraan materiaal wat gebruik is verskil. Die palladium membraan, het in die reaksie mengsel, beter ekstraksie en selektiwiteit tot waterstof getoon in vergelyking met die saamgestelde MFI/alumina membraan. Ongeag hierdie feite, het die palladium en MFI KMRe soortgelyke resultate gelewer toe dit onder dieselfde reaksiekondisies geëvaluëer is. Die isobutaan omsetting in die eKMRe, by 'n teenstroom veegasvloeisnelheid van 185 ml/min kon verhoog word na ongeveer 37 % in vergelyking met die 14 % omsetting wat in die konvensionele gepakte-bed reaktor verkry is. 'n Katalitiese Membraan Reaktor Model is gebruik om hierdie soortgelyke werkverrigtinge van die twee eKMRe te evaluëer. Modellering resultate het getoon dat, indien daar volkome benutting van die kombinasie van 'n membraan en katalis in dieselfde eenheid geput wil word, moet 'n baie aktiewe katalis gebruik word, viz. wat die waterstof ontrekkingstempo kan bevredig. Dit is die

eerste keer dat hierdie twee eKMRe onder dieselfde reaksie kondisies bestudeer is, om die invloed van membraan materiaal op die werking van die eKMR te ondersoek.

Die eKMR is ook gebruik vir meta-xileen isomerisasie. Hierdie gedeelte het gefokus op die ekstraksie van para-xileen uit die meta-xileen isomerisasie reaksie omgewing met ‘n MFI eKMR (MFI-zeoliet membraan en Pt-HZSM5 gepakte-bed reaktor) om die reaksieselektiwiteit tot para-xileen te vebeter. Para-xileen is ‘n belangrike industiële chemikalie en word gebruik as roumateriaal vir die produksie van poliëster harse. Om die para-xileen aanvraag te bevredig word meta- en orto-xileen via die xileen isomerisasie reaksie omgeskakel na a mengsel van xileen.

Daar is getoon dat die porie-gevulde MFI-zeoliet membrane, wat in hierdie studie gebruik is, para-xileen selektief onttrek uit die reaksie omgewing. Die gebruik van die ekstraktor tipe KMR, in plaas van die konvensionele gepakte-bed reaktor, vir meta-xileen isomerisasie, het ‘n verbetering van die para-xileen selektiwiteit tot gevolg gehad. Die para-xileen selektiwiteit kan selfs tot 100 % verbeter word indien die KMR in die permeaat-alleen mode gebruik word. Dit kom egter teen ‘n prys van laer produktiwiteit. Wanneer die eKMR in die gekombineerde mode (menging van die retentaat and permeaat stroom) bedryf word toon die KMR ‘n verbetering ten opsigte van reaksie selektiwiteit en produksie (tot 10 % by die reaksie kondisies wat bestudeer is) in vergelyking met die gepakte bed reaktor. Dit is die eerste keer dat daar suksesvol ‘n verbetering in para-xileen selektiwiteit verkry kon word met die gebruik van ‘n ekstraktor tipe KMR.

Hierdie proefskif het ook gelei tot die ontwerp en konstruksie van ‘n nuwe generasie membraan reaktor toetsbank, ‘n eerste in die Departement van Prosesingenieurswese, Universiteit van Stellenbosch. Die toetsbank kan gebruik word vir die hoë-temperatuur evaluasie van membrane en katalitiese membraan reaktore. Die ontwerp is eenvoudig en maklik aanpasbaar vir die evaluering van verskillende reaksies.

Acknowledgements

This work was completed at the Department of Process Engineering, University of Stellenbosch, South Africa in collaboration with the Institut de Reserches sur la Catalyse (CNRS/IRC), Lyon (France).

I would like to thank the following people and institutions:

- The Institut de Recherche sur la Catalyse (CNRS/IRC), in particular the director Thierry des Courières, for allowing me to spend a total of 15 months at the laboratory in Lyon and enabling me to use the facilities in order to complete parts of this study. I would also like to thank the Centre National de la Recherche Scientifique (CNRS) and CNRS/IRC for the financial contributions they made to my research stays at the CNRS/IRC.
- The French Embassy in South Africa and the National Research Foundation (NRF) of South Africa for financial contributions made to my research stays at the CNRS/IRC through a French Embassy/NRF doctoral fellowship programme.
- The National Research Foundation of South Africa and Department of Process Engineering for financial assistance to this PhD.
- The staff at the Department of Process Engineering for technical, analytical and administrative assistance. A special thanks to the people in the workshop, Jannie, Howard and Anton for their assistance with the construction of the experimental set-up.
- Prof. Przybylowicz from iThemba LABS (South Africa) for his help with PIXE and RBS analysis.
- Süd Chemie for providing me with a xylene isomerization catalyst.
- The GRE group from the CNRS/IRC for welcoming me into their group and providing assistance during my stays. In particular, I would like to extend a special thanks to Dr. Jean-Alain Dalmon for his help as mentor during my stays. Also, to Emmanuel Landrivon for his technical assistance and Dr. Yongsheng Li for some membrane data.
- To Prof. Leon Lorenzen my promotor, a grateful thanks for his role as mentor, and his guidance and wisdom.

- To Dr. Sylvain Miachon for his role as mentor, friend and co-promotor. I want to extend a sincere thank you.
- To my friends for moral support and creating some healthy distractions. Also to all the wonderful people I met in France who made me feel at home.
- To my family, my parents (Pieter and Theresa) and my three brothers (Leon, Pieter and Hermanus), my sincere and loving thanks for all the love and encouragement you have shown me over the years.
- To my Creator, without whom I could not have done any of this.

Table of Contents

List of Tables

List of Figures

1 Introduction

"**membrane** - *gen.* Any thin, often pliable, sheet or layer, esp. one forming a barrier or lining. Also fig." OXFORD DICTIONARY 2002 edition [1]

When faced with an unknown word one will often turn to a dictionary e.g. Oxford English Dictionary for an explanation. Often these dictionaries are not equipped to explain words in their scientific context and after reading this chapter it will become clear to the reader that the definition given above does not capture the true potential of this word. In this chapter the concepts, *membrane separation* and *catalytic membrane reactors (CMRs)*, will be explained and the objectives of this dissertation presented.

The work of this dissertation was done in two laboratories, the Department of Process Engineering, University of Stellenbosch (DPE/US), and the Institut de Recherches sur la Catalyse (CNRS/IRC), Lyon (France). The DPE/US and the CNRS/IRC has been in collaboration since 1998. The collaboration made it possible for me to spend a total of 15 months at the CNRS/IRC working in the Reaction Engineering and Energy Research Group (GRE). The research stays enabled me to gain valuable knowledge on membrane catalysis by working in a well-established world leading research group on membrane reactor technology and also enabled me to make use of the equipment available at the CNRS/IRC. Reference made to *our* group in this dissertation will therefore refer either to the GRE group in France or the Membrane Reactor research group in South Africa.

1.1 Membranes and membrane separation

A membrane is a permeable or semi-permeable phase, e.g. a film, which allows the selective passing of components when certain driving forces are applied. Consequently it can act as a barrier between two adjacent phases (gas or liquid), controlling the exchange of mass between them (Figure 1-1). Typical driving forces are pressure difference, concentration difference, or voltage difference across the membrane [2].

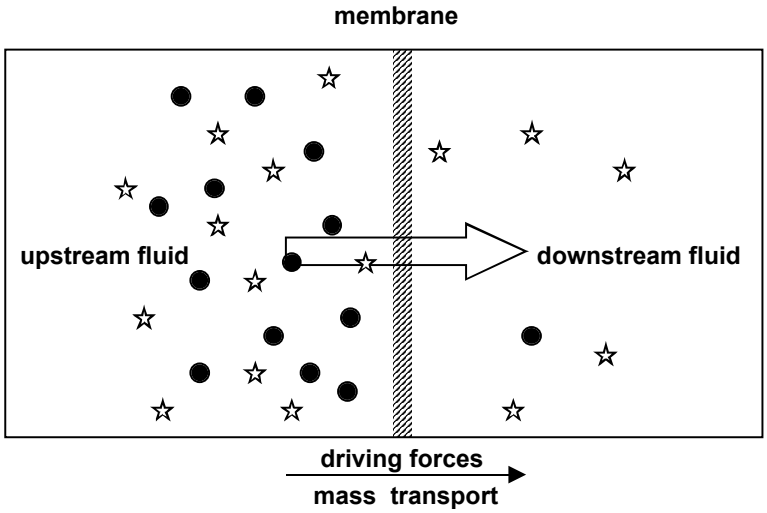

Figure 1-1 Schematic drawing of the basic membrane separation principle.

Conventional industrial separation methods include distillation, absorption, liquid-liquid extraction, gas-liquid extraction, adsorption, etc. Some of these methods are energy intensive and the process equipment is expensive and complex. By utilizing a membrane for separation, one can sometimes save on energy and capital costs, and it even allows for separation of species that have been impossible to separate in the past [3].

Membranes can be dense or porous, and the layer can be made of organic or inorganic material. Inorganic membranes (made from metals, carbon, glass or ceramics) normally possess better mechanical strength, chemical inertness and temperature resistance than organic membranes, making them useful for a much broader range of applications [2]. Many catalytic processes of industrial importance involve the combination of high temperature and chemically harsh environments, for which inorganic membranes, to be used as membrane reactors, are ideally suited [4]. The rest of this discussion will focus on inorganic membranes, but it should be noted that some of the terms and characteristics given below are also applicable to organic membranes.

Dense inorganic membranes are normally made from precious metals (palladium, platinum, silver and its alloys) or solid electrolytes (modified zirconia or perovskites). These membranes are permeable to atomic or ionic forms of hydrogen (Pd, Pt and its alloys) or oxygen (Ag, ZrO_2 or perovskite) [5].

Porous inorganic membranes are made from ceramics (alumina, silica, titania, zirconia, zeolites, etc.), glass, carbon, stainless steel, palladium, etc. The IUPAC classification of average pore diameters (d_p) can be used to classify porous membranes into three groups: macroporous ($d_p > 50$nm), mesoporous (2 nm < d_p < 50 nm) and microporous

(d_p < 2 nm). They allow for the separation of a much broader spectrum of molecules. Typical gas transport mechanisms in porous membranes include:

- d_p > 50 nm - Bulk diffusion, viscous flow and Knudsen diffusion.
- 2 nm < d_p < 50 nm - Knudsen diffusion, surface diffusion and multilayer diffusion/capillary condensation.
- d_p < 2 nm - Surface diffusion (micropores) [6].

Membranes can be uniform in composition or composite (Figure 1-2c), having a symmetrical (Figure 1-2b) or asymmetrical porous structure (Figure 1-2a). A composite membrane is usually made up of a porous support (porous glass, sintered metal, granular carbon or ceramics such as alumina) with a thin, permselective layer deposited on it or inside its pores [4]. The support gives the necessary mechanical stability that the layer doesn't possess without restricting the mass transport, allowing for the use of very thin membranes [3].

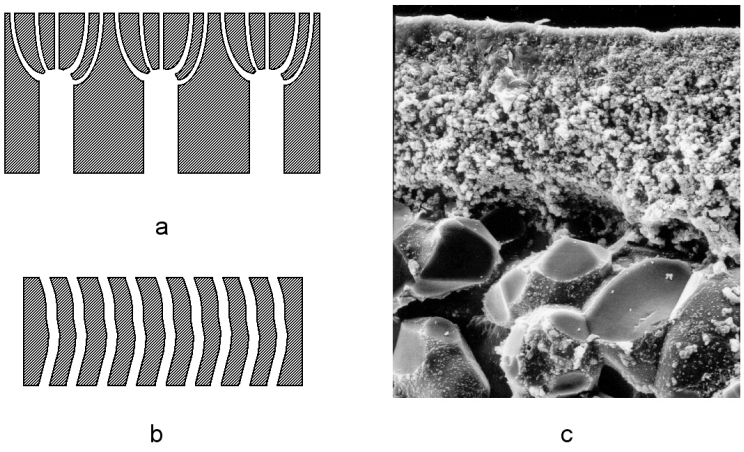

Figure 1-2 Schematic drawings of (a) an asymmetrical (anodized alumina membrane) [6] and (b) symmetrical porous structure. (c) SEM image of a composite membrane (top layer MFI-zeolite) (micrograph H. Mozzanega).

Inorganic membranes are manufactured in different shapes e.g. tubes, flat disks, hollow fibres, or monolithic multi-channel elements for ceramic membranes [2] and foils, spirals or helix for metallic membranes [7].

A membrane's ability to separate components in a mixture can be expressed by selectivity, while the transfer of components through the membrane can be quantified by permeability. These two parameters are usually determined experimentally, although models have been proposed to calculate them based on the characteristics of the membrane

and the components to be separated. Permeability is the flux (molar or volumetric flow per unit area) through a membrane scaled with respect to the membrane thickness and driving force, e.g. partial pressure difference ((mol or m^3).m.s^{-1}.m^{-2}.Pa^{-1}). This parameter is rarely used, because the membrane thickness is often not known. Moreover, this concept of measurement implies an inverse proportionality of the flux with the thickness, which is not always the case, particularly with modern very thin separative layer. Instead, the parameter permeance is used, which is the flux through the membrane scaled with respect to the driving force. The permeance of a component, therefore gives valuable information about the amount of a component that can pass through a unit surface area of the membrane when a certain driving force is applied. The selectivity is a membrane's ability to separate two given species from each other, and one of the ways to estimate it, is to take the permeability ratio of the two components within a mixture [3].

The mass transfer mechanisms through membranes also depend on factors like the interactions between the membrane and the mass species, and the operating conditions (temperature and pressure) [4].

1.2 Catalytic Membrane Reactors (*CMRs*)

A membrane reactor is a device in which a chemical reaction is combined with membrane-based separation in the same unit (IUPAC) [8]. The membrane therefore, does not only play the role of a separator, but also act as part of the reactor. One advantage of such a configuration lies in the fact that it is compact and therefore, sometimes less capital intensive. The possibility of savings in processing costs also exists [3].

Membrane reactors used for catalytic reactions are referred to as catalytic membrane reactors *(CMRs)*. They can offer an additional benefit, obtained from the synergy of both the catalyst and membrane interacting with each other in the same device. In this case, the CMR will demonstrate higher performances than a membrane unit separately coupled with a catalytic reactor.

In the last decade, different classification systems have been proposed, with different degrees of complexity. One may quote Tsotsis' six-configuration sorting [9], based on the combination of the catalyst and the membrane, but in our groups, we tend to use the more simple approach proposed by J.-A. Dalmon [10].

Accordingly, catalytic membrane reactors are classified into three groups depending on the function of the membrane: extractor, distributor and contactor [10, 11].

When the membrane is used as an *extractor* (Figure 1-3), one or more of the reaction products are removed from the reaction zone. There are two advantages to this, (a) in equilibrium restricted reactions greater conversion beyond the equilibrium value can be achieved, or (b) when the desired product is an intermediate, and it is extracted from the reaction zone before it reacts in consecutive reactions, leading to better selectivity [12]. As an example of case (a), one may quote work done here at the Department of Process Engineering, already in collaboration with CNRS/IRC in France, on the dehydrogenation of ethanol and 2-butanol in a Pd-Ag/α-alumina membrane reactor by Keuler *et al.* [13, 14]. During this study highly selective Pd-Ag/α-alumina membrane reactors [15, 16] were used to extract hydrogen from the reaction zone, whereby shifting the equilibrium towards higher yields of 2-butyraldehyde and acetaldehyde. The *extractor type CMR (eCMR)* is discussed in detail in chapters 4 and 5.

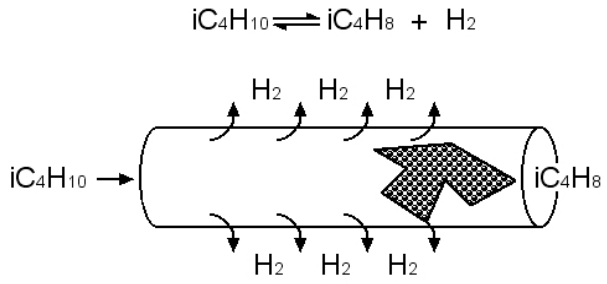

Figure 1-3 Extractor Catalytic Membrane Reactor: Example Isobutane dehydrogenation.

In a *distributor* (Figure 1-4) the membrane is used to feed one or more of the reactants to the reaction zone in a controlled way. This reactor configuration is best suited for reactions accompanied by a network of series-parallel reactions, where controlling the partial pressure of one of the reactants will have a positive kinetic effect on the reaction.

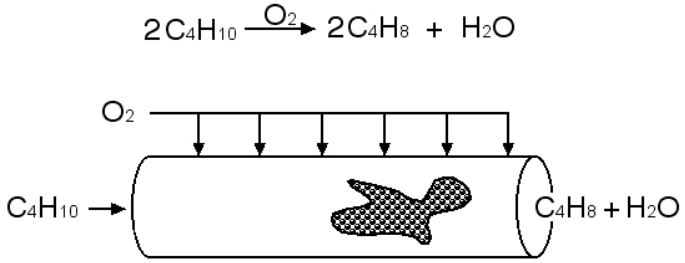

Figure 1-4 Distributor Catalytic Membrane Reactor: Example Butane oxidative dehydrogenation.

Research efforts in this area focus mainly on oxidation reactions, although this technology is also applicable to partial hydrogenation reactions. At the CNRS/IRC it has been applied to the partial oxidation of butane [17], while research by other groups focus on the partial oxidation of alcanes (propane [18-20] and butane [11, 21]), the oxidative dehydrogenation of methanol [22-24] and alcanes (ethane [25-27], propane [28-30], and butane [31, 32]) and oxidative coupling of methane [33].

By feeding the O_2 through the membrane, the O_2 partial pressure in the reaction zone can be kept low, decreasing over-oxidation of the products to CO and CO_2, and leading to better selectivities. The heat formed during the reaction is also distributed more evenly along the reaction zone, which decreases the formation of hot spots, and the possibility of runaway behaviour is minimal. The presence of oxygen at every point in the reaction zone can also prevent coke formation on the catalyst [32]. It has been shown that for the selective oxidation of butane to maleic anhydride, separate feeding of the two reactants can limit flammability problems, with butane-rich feeds impossible to use in a conventional reactor [21]. By using a membrane distributor the range of safe operation of oxidation reactions can also be extended.

Porous membranes are mostly used as oxygen distributors, although dense membranes have also been used, e.g. solid oxide membranes like a PbO catalyst supported on MgO [34] and silver membranes [35, 36]. The added advantage of dense permselective membranes lies in the fact that air can be used as an oxygen source. This can lead to the elimination of feed gas purification plants, thereby saving on capital and operating costs. The main challenges in this field are the difficulties of obtaining high permeation fluxes (achieved with thin dense membranes), while at the same time maintaining the membrane properties during prolonged exposure to operating conditions. Due to the exothermic nature of oxidation reactions mechanical problems such as thermal mismatch of the membrane materials and support can be experienced along with hot zones in the reactor. Development of dense membranes capable of simultaneous oxygen anion and electron conductivity might be a solution to the problem. It has been shown that dense ceramic membranes made of mixed conductors can successfully separate oxygen from air, at flux rates considered commercially feasible. These membranes are finding application for the partial oxidation of CH_4 to syngas [37], and oxidative dehydrogenation of ethane to ethylene [38]. In the study by Rebeilleau-Dassonneville *et al*. (from the same group as where part of this work was carried out) [38], the mixed conductor perovskite

($Ba_{0.5}Sr_{0.5}Co_{0.8}Fe_{0.2}O_{3-\delta}$) membrane [39] used by them, was modified by the deposition of a catalyst (V/MgO or Pd nano clusters) on the membrane surface. Ethylene yields of about 75 % were obtained at temperatures of 1040 K and 1050 K, i.e. yields beyond state-of-the-art steam cracking.

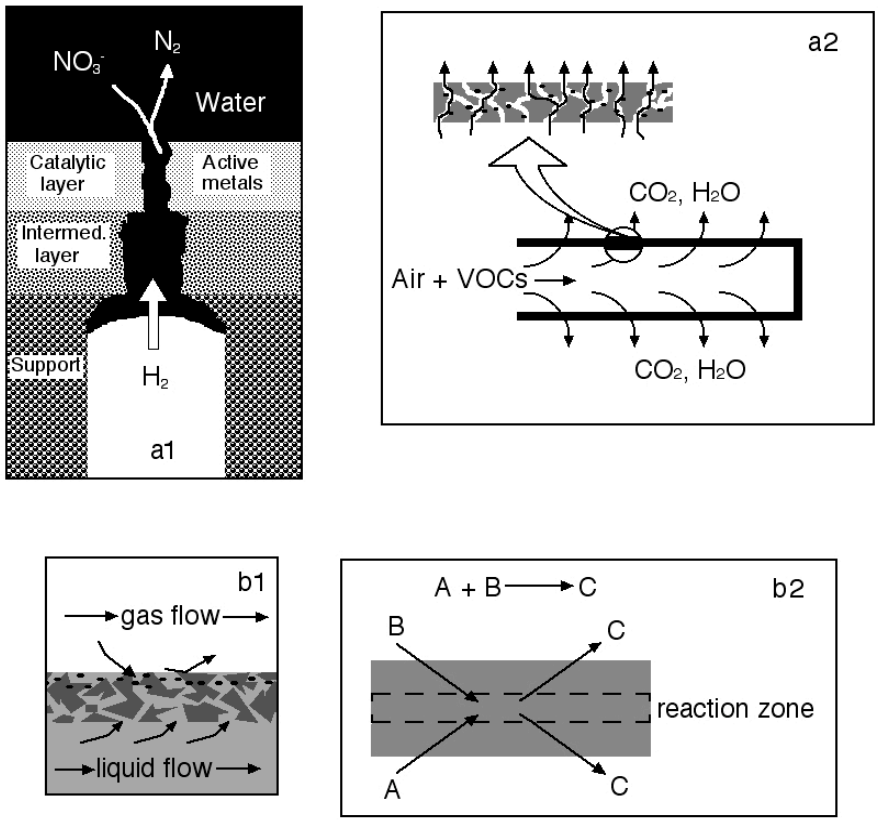

Figure 1-5 Contactor type catalytic membrane reactors: cross-flow contactor examples: (a1) reduction of nitrates in water [40], (a2) combustion of volatile organic compounds (VOCs) [41], and interfacial contactor, examples: (b1) liquid/gas phase reactions, (b2) reactions that require very strict stroichiometric feed mixtures [41].

The *contactor* type catalytic membrane reactor (Figure 1-5) provides for excellent contact between the process stream(s) and the catalyst. The catalyst is either the membrane itself, or situated within the membrane pore matrix. For this application, the membrane does not need to be permselective, just catalytically active [4]. Two types of contactors have been identified: the *cross-flow contactor* (also referred to as the flow-through contactor) and the *interfacial contactor* [42].

The *cross-flow contactor* (Figure 1-5a) allows for precise control of the contact time between the catalyst and reactants, in order to improve the reaction selectivity. The cross- flow contactor is operated in the forced flow mode [4]. This implies that a mixture of the reactants is forced through the membrane, trapped within the membrane pore network, providing intimate contact with the catalyst. A practical example of where this membrane reactor configuration can find application is for the reduction of nitrates in water (Figure 1-5a1). The concentration of nitrates in ground water exceeds tolerance limits due to the excessive usage of nitrate fertilisers. In order to dispose of the nitrates, selective hydrogenation of nitrates in water to nitrogen can be achieved in a cross-flow contactor [40, 43]. Other examples of where this contactor has been applied include, combustion of volatile organic compounds (Figure 1-5a2) [44], *i*-butene oligomerization to *i*-octane [45], methanol to olefins [46] and the selective hydrogenation of 2-hexyne [47]. In the last example, back mixing of the initial reaction products and hydrogen were prevented, due to the fact that the permeating hydrocarbons blocked hydrogen from moving through the pores. So any further hydrogenation of the products were prevented, and this led to a higher selectivity towards 2-cis-hexene.

The *interfacial contactor* (Figure 1-5b) provides for a small reaction zone inside the membrane, with each fluid located on opposite sides of the reactor. The location of the reaction zone depends on the relative bulk concentration, and the interparticle diffusion of the two reactants. The operational conditions are normally chosen in order to ensure that this reaction zone is located within the catalyzed zone in the membrane.

It has been used for reactions that require very strict stroichiometric feed mixtures like the Claus reaction (reaction between hydrogen sulphur and sulphurdioxide) [48], and for kinetically fast, very exothermic reactions like oxidation reactions (e.g. oxidation of carbonmonoxide) [49]. By separating the two feed mixtures and controlling the transport of the reactants through the membrane, it can be manipulated such that at the interphase layer, the reactants are always in their stroiciometric ratios (Figure 1-5b2). This can prevent runaway reactions, and for combustion processes no explosive mixtures will build up.

In triphasic (gas/liquid/solid) reactions (Figure 1-5a1), the reaction rate is sometimes limited by the diffusion of the volatile component through the liquid to the catalyst. This problem is overcome when the *interfacial contactor* is used for such reactions, because the gas doesn't need to diffuse through the liquid. A gas/liquid

interphase is created inside the membrane pores, which is in direct contact with the catalyst. Examples of reactions that have been studied include, nitrobenzene hydrogenation [50], n-hexane oxyfunctionalization by hydrogenperoxide [51], as well as wet air oxidation of formic acid [42, 52-54] [55], which is one of the main applications studied at the CNRS/IRC. The *interfacial contactor* has also been used for oxidation of cyclohexane by tertiary-butyl peroxide [56]. Here the two reacting liquids are immiscible, and the use of a co-solvent normally required. With the use of an interfacial contactor, the co-solvent is not necessary, and problems with preferential sorption of one of the compounds onto the catalyst active sites are eliminated.

Membrane bioreactors

Biotechnology is another area in which catalytic membrane reactors are finding application and there are already many industrial processes using membrane bioreactor (*MBR*) technology [3]. Membrane reactors using biological catalysts (e.g. enzymes, microorganisms and antibodies) can be used in production, processing and treatment operations. Sectors where this technology is finding widespread application include, agro-food, pharmaceutical, biomedical and environmental (biological treatment of contaminated air and water) [57-61]. These applications operate mostly at low temperatures, where inexpensive commercial, organic, or polymeric membranes are used. Industrially important bioreactions, include a broad class of fermentation-type processes, for the production of amino acids, antibiotics, and other fine chemicals [62, 63]. Membrane based reactive separation processes are used here for the continuous elimination of metabolites, necessary to maintain high production rates [3]. Membranes are also used as hosts for the immobilization of bacteria, enzymes, or animal cells in the production of high value-added chemicals [3, 63] [57]. Advantages of this are improved reactor stability and productivity, improved product purity and quality, and reduction of waste [57]. The MBR processes used for the production of fine chemicals and biochemicals produce, in general, high value added products that makes the use of MBR very attractive from an economic point of view.

Research on catalytic membrane reactors therefore explores a very larger array of possibilities.

1.3 Objectives

This dissertation has three primary objectives:

- To design and construct a new generation membrane reactor testing bench for the Department of Process Engineering, University of Stellenbosch.
- To study the internal eCMR mechanism in the case where it has been applied in order to increase reaction conversion (isobutane dehydrogenation), by studying the influence and nature of the membrane material (palladium and MFI-zeolite).
- To explore the use of an eCMR to increase the selectivity of a reaction, using xylene isomerization as an example and using a MFI-zeolite membrane.

1.4 Dissertation layout

In this chapter it was shown that catalytic membrane reactor concepts could find wide application in the chemical synthesis and petrochemical industries. The different types of catalytic membrane reactors were discussed, pointing out the advantages of using a membrane and catalyst in the same unit for doing reactions.

Chapter 2 focuses on the membranes used during this study in *extractor* CMRs. The various mass transport mechanisms and properties of membranes are discussed, with emphasis on palladium supported membranes and MFI/alumina composite membranes. The membranes are characterized through physical techniques as well as through hydrodynamic measurements.

Chapter 3 deals with the design and construction of a catalytic membrane reactor testing-bench for the Department of Process Engineering at the University of Stellenbosch, South Africa. Experimental procedures and protocol for the catalytic membrane reactor tests are given and discussed.

Different uses of the extractor type catalytic membrane reactor are discussed and evaluated in chapters 4 and 5. In chapter 4 the extractor are used to increase the conversion of equilibrium restricted reactions and the model reaction is isobutene dehydrogenation. Chapter 5 deals with the use of the eCMR to enhance the reaction selectivity in the model reaction of xylene isomerization. Chapter 6 gives a synthetic conclusion of this work and in chapter 7 some thoughts are shared on future work.

2 Membranes used in eCMRs

In an *extractor* type Catalytic Membrane Reactor the primary function of the membrane is to selectively extract one reaction product from the reaction zone. The *extractor* membrane must therefore, be highly permeable and selective towards the component to be extracted, and able to maintain these properties over a long period of time.

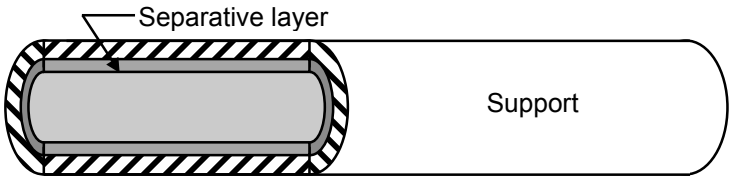

Figure 2-1 Schematic structure of an asymmetric (i.e. multi-layered) selective tubular membrane. The separative top layer (here represented on the tube side) may be based on palladium or MFI zeolite, as is the case in this work.

Two different kinds of supported membranes (Figure 2-1), MFI-zeolite and Palladium, were studied in this dissertation as *extractor* membranes. Each supported membrane is made of a porous support tube and a selective layer, MFI-zeolite or Palladium, deposited on the inside.

In this chapter the characteristics, preparation methods and transport mechanisms through these types of membranes will be explained. Membrane preparation and testing methods are provided, and the membranes used will be characterized with physical methods, gas permeation and gas mixture separation testing for the zeolite-based membranes.

2.1 Literature review

2.1.1 Gas transport mechanisms in membranes

Permselective transport through dense membranes is governed by a solution-diffusion mechanism, while non-permselective transport normally occurs in macro/mesoporous membranes. Microporous membranes can display both permselective and non-permselective transport depending on the chemical nature of the permeating molecule, membrane matter and the pore sizes within the membrane [64].

Permeance is the flux through the membrane divided by the pressure difference across the membrane and is often used to quantify permeation through membranes:

$$P_i^m = \frac{N_i}{\Delta P_i} \qquad (2\text{-}1)$$

with P_i^m the permeance (mol.Pa^{-1}.m^{-2}.s^{-1}) of specie *i*, N_i the molar flux (mol.m^{-2}.s^{-1}) of specie *i*, ΔP_i the trans-membrane partial pressure (Pa) of specie *i*.

Transport through porous membranes

When capillary condensation is absent, the flow of vapours and gases through pores (porous membranes) can be distinguished by four transport mechanisms. The contribution of each mechanism towards transport depends on the properties of the membrane and gases, as well as the operating conditions (temperature and pressure) [65].

Viscous flow is the result of convective flow in the direction of an absolute pressure drop or gradient and therefore, does not take place unless an absolute pressure drop is present. It does not yield any separation, which makes it irrelevant for membrane separation processes. The flux is related to the pore size, $N \propto r_p^2$.

$$P_i^m = \frac{1}{RT}.\frac{g}{\delta}.\frac{r_p^2}{8.\eta_i}.\overline{p_i} \text{ with } \eta_i \propto T \text{ therefore } P_i^m \propto \frac{1}{T^2},\overline{p_i} \qquad (2\text{-}2)$$

Bulk or molecular diffusion is governed by molecular-molecular collisions in the gas phase. It becomes important at relatively large pore diameters or at high system pressure. For a single component system this type of diffusion makes no contribution towards transport.

$$P_i^m = \frac{1}{RT}.\frac{g}{\delta}.D_{ij} \text{ with } D_{ij} \propto T^{\frac{7}{4}},\frac{1}{p_i} \text{ therefore } P_i^m \propto T^{0.75},\frac{1}{p_i} \qquad (2\text{-}3)$$

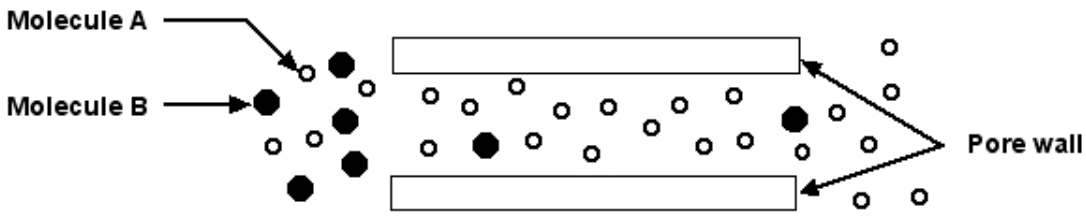

Figure 2-2 Knudsen diffusion through a pore.

Knudsen diffusion (Figure 2-2) is the result of pore wall-molecule collisions. The mechanism prevails when the mean free path of molecules is larger than the pore diameter, e.g. at high temperatures or low pressure.

$$P_i^m = \frac{1}{RT}.\frac{g}{\delta}.D_i^{Kn} \text{ with } D_i^{Kn} \propto T^{0.5} \text{ and therefore } P_i^m \propto \frac{1}{T^{0.5}} \qquad (2\text{-}4)$$

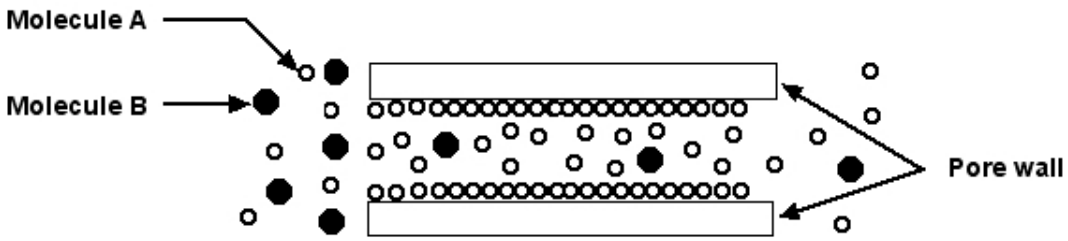

Figure 2-3 Surface diffusion in a pore.

Surface diffusion (Figure 2-3) represents the activated transport of adsorbed species along a pore wall. It can occur in parallel with Knudsen diffusion, which will dominate at high temperatures, as molecules desorbs from the surface. Surface diffusion increases the permeance of the strongly adsorbed compound, while reducing the permeance of other compounds due to the reduction of the effective pore diameter.

$$P_i^m = \rho.q_{sat,i}.g.D_i^s.\frac{\ln(1-\theta_i)}{\Delta p_i} \quad \text{with } D_i^s \propto \exp\left(\frac{-E_{a,i}^s}{RT}\right), \theta_i = f(T, p_i) \quad \text{therefore}$$

$$P_i^m \propto f(T, p_i) \qquad (2\text{-}5)$$

Another transport mechanism that has been hypothesized is *configurational diffusion or diffusion in micropores*. According to the theory, diffusion in micropores, especially in zeolites, is characterized by an active nature. When the gas is not adsorbed onto the micropore surface but retains its gaseous character, activated gaseous diffusion takes place [66].

$$P_i^m = \frac{1}{RT}.\frac{g}{\delta}.\sqrt{\frac{8RT}{\pi M}}.\exp\left(\frac{-E_a^g}{RT}\right) \quad \text{therefore} \quad P_i^m \propto f(T) \qquad (2\text{-}6)$$

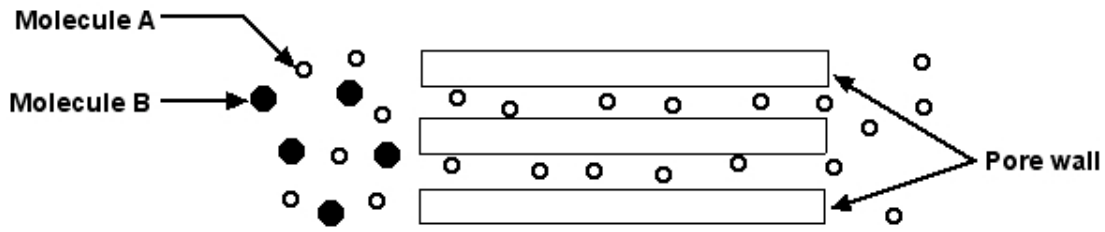

Figure 2-4 Molecular sieving through a pore.

Molecular sieving (Figure 2-4) takes place when compounds are separated purely due to steric reasons on a molecular level. Molecules of kinetic diameter similar to ultra-microporous membranes ($d_k < 0.7$ nm) diffuse through, separating them from larger molecules [6].

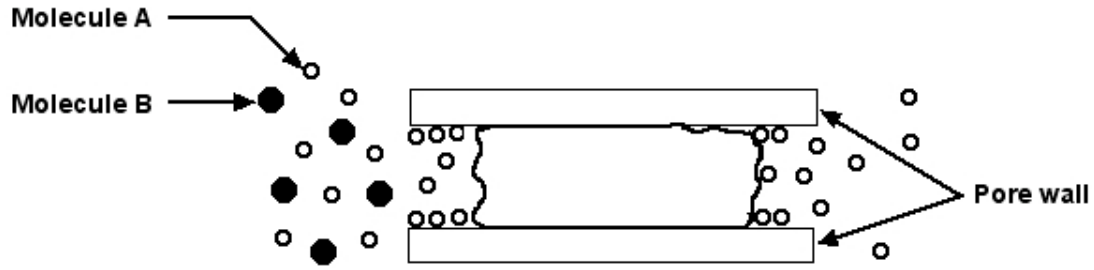

Figure 2-5 Capillary condensation in a pore.

When *capillary condensation* is present, condensable vapour components in a mixture will condense, if the pores are small enough, blocking the gas-phase diffusion of other species. As a result the permeance of the other components will be slow, and in the case of total blockage due to condensation, dependent on their solubility in the condensed component. The condensate evaporates upon exiting at the low-pressure side. The capillary condensation pressure can be determined using the Kelvin equation and is in most cases at 0.5 - 0.8 of the saturated vapour pressure [6].

Dense Inorganic Membranes

Dense inorganic membranes are permeable to atomic and ionic forms of hydrogen (Pd, Pt and its alloys) or oxygen (Ag, ZrO_3 and perovskite). Transport of components proceeds via diffusion under a pressure, concentration, or electrical driving force. The separation of various components of a mixture is related to their diffusivity and solubility in the membrane material.

Hydrogen transport through palladium membranes

Transport of hydrogen through dense palladium membranes occurs via a solution diffusion mechanism. The hydrogen dissociates at the membrane surface on the high pressure side and atomic hydrogen diffuses through the membrane. On the low pressure side the hydrogen recombines. The driving force for hydrogen movement is the hydrogen surface concentration difference across the membrane.

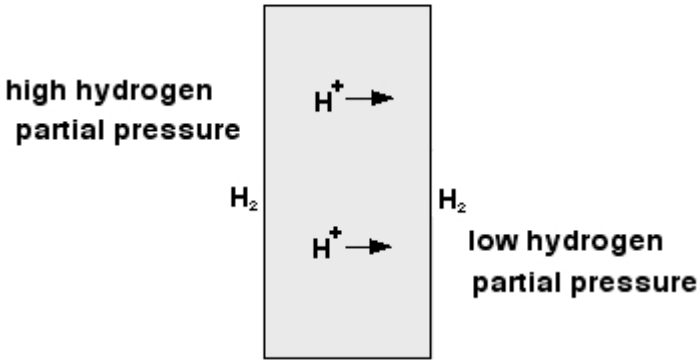

Figure 2-6 Hydrogen permeation through a dense palladium membrane.

The hydrogen flux through Pd membranes is usually expressed by the following equation:

$$N_{H2} = \frac{P_{er}}{l}\left(P_{H2,ret}^{n} - P_{H2,per}^{n}\right) \qquad (2\text{-}7)$$

The value of n is used as an indication of the hydrogen permeation rate-limiting step through composite membranes. If H diffusion through Pd is the rate limiting step, then the hydrogen flux would be directly proportional to the difference of the square root (n = 0.5) of the hydrogen partial pressure on both sides of the membrane (Sievert's law). On the other hand, on thinner membranes, this exponent n is often reported to be closer to 1, as it is assumed that the kinetic importance of the adsorption/desorption steps increases [16].

H_2 transport through Pd is an activated step and if it is assumed that the value of n is independent of temperature, then the relationship between the permeability and temperature can be described by an Arrhenius function [67].

$$P^{er} = P_0^{er} \exp\left(\frac{-E_a}{RT}\right) \qquad (2\text{-}8)$$

It is therefore clear that the permeation behaviour with temperature is a useful way to reveal the rate limiting steps.

Oxygen transport through dense metal and dense mixed-conducting membranes (Figure 2-7)

Oxygen transport through dense silver membranes is similar to hydrogen transport through palladium membranes. The value of n can be taken as 0.5 [68]. Oxygen permeance in a gas mixture through silver is reduced by competitive adsorption of other species.

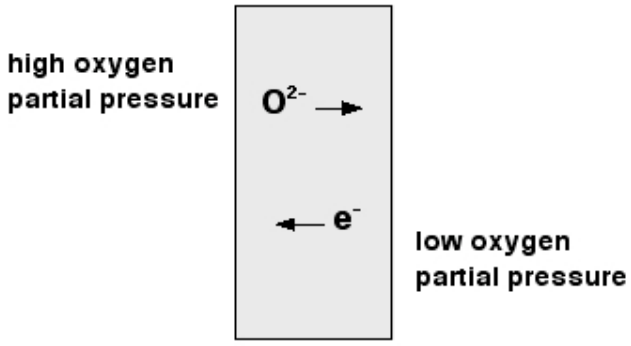

Figure 2-7 Oxygen transport through a mixed conducting OR solid metal membrane.

The driving force for oxygen permeation through dense mixed conducting membranes is an oxygen partial pressure gradient, which causes selective transport of O^{2-} from the high to the low oxygen partial pressure side. The oxygen diffusion process is facilitated by a large concentration of vacant crystallographic sites in the oxygen sublattice of the oxide. Overall charge neutrality in the membrane is maintained by a counterbalancing flux of electrons [69].

2.1.2 Porous support

The flux of components through a membrane is usually a function of its thickness, thinner membranes displaying higher flux values. Very thin membranes do not possess the necessary mechanical strength to be self-supporting. For this reason the membrane layer is deposited on a porous support, which provides the necessary mechanical stability to the membrane without hindering mass transport. The use of a membrane support can also reduce the cost of the membrane considerably [3]. For example: in the case of palladium membranes, self-supporting membranes need to be thicker than 50 – 100 μm in order to have sufficient mechanical strength. At these thicknesses, the hydrogen flux is so low that the economical advantages of using them is overshadowed by the cost of the membrane itself [64].

Membrane supports are usually flat disks, tubes or multi-channel tubes [3]. Tubular and multi-channel membrane supports are stronger than disks and have larger surface areas. Moreover, they offer much higher ratios of membrane per seal surface, thus strongly reducing sealing costs and seal leak influence. They can be manufactured from a variety of materials of which porous glass [70-74] porous ceramics [67, 75, 76] and porous stainless steel [74, 77-79] [80] are mostly used.

The main advantages of using porous stainless steel supports over porous ceramics and glass, are their robustness (resistance to breaking) and weldability. Last mentioned, i.e. weldability, allows for the successful integration of the membranes into a reactor design system, without any leaking problems. In the case of Pd/stainless steel supported membranes, stainless steel and palladium have similar thermal expansion coefficients, but at high temperatures (> 823 K), intermetallic diffusion occurs. This leads to appreciable changes in the hydrogen flux through these membranes [77]. Lee and co-workers [79] found that stainless steel supported membranes have a possibility of failure at high temperatures in the presence of hydrogen, if metal oxide layers are present on the surface of the stainless steel support. The reduction of oxide layers by hydrogen causes pinholes to form. On the other hand, the use of stainless steel porous supports for zeolite membrane has to face a large thermal expansion coefficient difference, that may lead to difficult crack formation problems during calcinations steps or high temperature uses [81].

The pore structure of porous glass membranes is known to collapse at high temperatures, due to meltdown of the internal porous structure [70, 71]. This happens even at temperatures as low as 473 K for untreated Vycor glass. It is therefore, essential to do a high temperature pre-treatment on these membranes before use. However, the porous structure of the membrane support then becomes difficult to control [70]. The small pore size (4 nm) of some Vycor glass supports also contributes largely to the transport resistance of Pd/Vycor glass membranes [74].

Porous ceramics, and in particular α-alumina have been studied extensively, and a broad database of knowledge on the synthesis of membranes on these supports exists in literature. There are however, difficulties in the gastight sealing of ceramic membranes to metallic module parts [64].

Therefor, it is essential that membrane supports have the necessary thermal, chemical and mechanical stability to withstand the harsh conditions associated with membrane reactor applications. In the case of a film-like toplayer (Pd membrane in this

work), support surface smoothness is also important, to ensure that a thin top layer can be applied without the formation of pinholes [82].

Moreover, these porous supports are often of asymmetric structures (i.e. made of a series of layers of reducing pore size), in order to offer a final supporting layer of smaller pore size, but low thickness. This final layer of the support must also be exempt of defects (pinholes) that would end up as pinholes in the final separative material as well.

2.1.3 MFI-zeolite membranes

Zeolite membranes have in recent years received much attention, due to the potential of using their preferential adsorption properties and sieving abilities for separation processes. MFI-type zeolite membranes in particular have been studied in detail due to the following reasons: a broad knowledge base in the synthesis of the MFI structure exist, their micropore size (~ 0.55 nm) is similar to the kinetic diameter of various hydrocarbons, MFI–membrane preparation is relatively easy, modifications in the chemical composition is possible (e.g. cation exchange), and a high thermal and chemical stability due to the high SiO_2/Al_2O_3 ratio [83]. Examples of other zeolite membranes that have been studied, include LTA (NaA) [84-86], FAU (NaX, NaY) [87], MOR [88, 89], CHA (SAPO34) [90], P-type zeolites [91], ETS-4 titanosilicate molecular sieve [92] and β-zeolite [93].

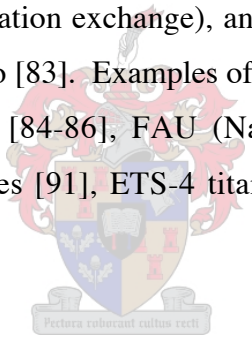

MFI structure

The general chemical formula of a zeolite is $M_{2/n}OAl_2O_3{\cdot}xSiO_2{\cdot}yH_2O$, where M is a non-framework cation with valence n, x is 2 or more, and y is the moles of water in the voids. Zeolites structures consist of silicon (Si^{4+}) and aluminium (Al^{3+}) cations surrounded by four oxygen (O^{2-}) anions. Each oxygen anion connects two cations, which yields a three-dimensional (3D) framework of AlO_4^- and SiO_4 tetrahedra. Although the SiO_4 tetrahedra is charge-balanced, the AlO_4 tetrahedra has a negative charge which is balanced by a positive charge on M, which binds on one of the oxygen anions connected to an aluminium cation [94]

The micoporous structure of zeolites gives it molecular sieving ability in addition to various adsorption properties. The ratio of Si/Al in the zeolite structure, and type and concentration of non-framework cations present in the zeolite crystals controls the surface properties of the zeolite (hydrophobicity, hydrophilicity, acidity, etc.). It has also been shown that the thermal stability of zeolites increase with an increase in the Si/Al ratio [95].

The MFI-zeolite structure group consists of two main types namely: the ZSM-5 and Silicate-1. ZSM-5 (Zeolite Socony Mobil-Five) was discovered in 1972 by Mobil and Silicate-1 was developed by Union Carbide a few years later. The difference between these two zeolites is their Si/Al ratios. ZSM-5 has a Si/Al ratio ranging between 11 and 1000 while Silicate-1 has a ratio higher than 1000. The higher Si content of Silicate-1 gives it more thermal stability and hydrophobic character than ZSM-5 [66].

The chemical formula of an elemental MFI crystal is given by the following formula:

$$\left|Na_n^+\left(H_2O\right)_{16}\right|\left[Al_nSi_{96-n}O_{192}\right]^- \text{ MFI, n} < 27 \qquad (2\text{-}9)$$

The elementary mesh contains 96 tetrahedrons TO_4 (T=Si or Al), as can be seen from the chemical formula. The structure consists of a three-dimensional pore system. The pores are presented in Figure 2-8. There are two kinds of pores: the straight channels, and the cross channels that zig-zag between the straight channels. The straight channels are circular (0.53 × 0.56 nm) in the (010) crystallographic orientation, and the zig-zag (sinusoidal) channels are elliptic (0.51 × 0.55 nm) in the (100) direction. Each "ring" consists of 10 oxygen atoms [96]. The pores provide three types of adsorption sites: those at the intersections, those along the cross channels, and those in the straight channels between the intersections.

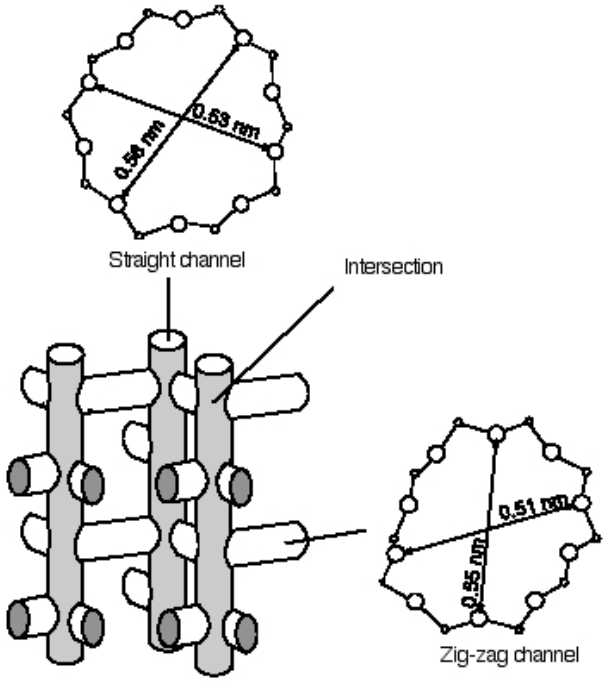

Figure 2-8 MFI-zeolite pore structure [96].

Figure 2-9 is a schematic diagram of the diffusion unit cell in the MFI–zeolite framework.

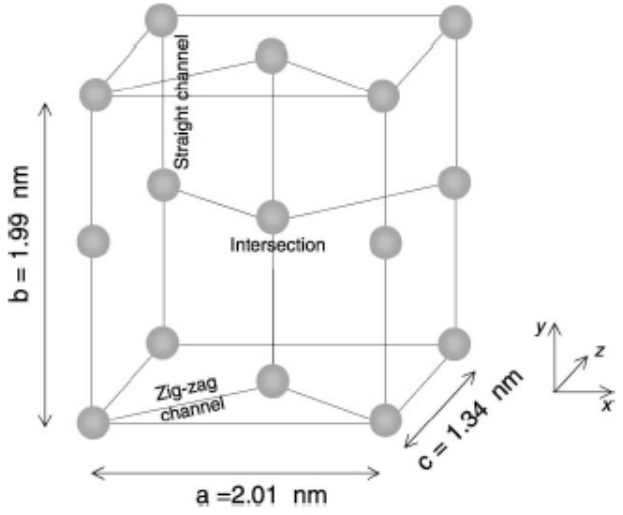

Figure 2-9 Diffusion unit cell for silicate-1 (MFI) [97].

All MFI-zeolites show a polymorphic, monoclinic to orthorhombic, phase transition. The phase transitions are induced by temperature changes and the presence of sorbed molecules within the framework. The transition temperature and mechanism are

closely linked to the composition (content of aluminium and other substituted elements) and defect density of the tetrahedral framework, besides the nature of the molecules adsorbed in the zeolite cavities. For example, at room temperature the as-synthesized ZSM-5 is orthorhombic (Pnma), although H containing ZSM-5 is monoclinic (P21/n). Silicate-1 is monoclinic at temperatures below 225 - 275 K and reversibly transforms to orthorhombic above this temperature range [98, 99]. It has been shown by Yamahara *et al.* [99] through molecular dynamic studies that the thermal expansion coefficient of Silicate-1 becomes negative above 450 K, indicating the existence of a higher temperature orthorombic phase.

Synthesis Methods

Zeolites and in particular MFI zeolite membranes are synthesized using mainly three methods:

- in-situ hydrothermal synthesis,
- synthesis by secondary growth and
- vapour phase transport.

All of these methods require a synthesis solution or gel, which generally consists of silicon, aluminium, sodium and water, although organic structure directing agents (SDAs) may be required to synthesize certain zeolite membranes.

Zeolite membrane synthesis is commonly carried out by in-situ hydrothermal synthesis. The basic procedure requires contacting the support with the synthesis solution or gel, and to allow growth of a zeolite film on the support under hydrothermal conditions. Dalmon and co-workers recently developed a specific synthesis method where the zeolite is formed within the pores of the support, forming zeolite plugs, leading to a composite structure of alumina and MFI zeolite [100-103]. After the hydrothermal synthesis of the zeolite, the supported zeolite membrane and residual synthesis solution/ gel are separated and the membrane is washed, dried and possibly calcined at a high temperature to get rid of the SDA present in the micropores.

Another quite popular method for zeolite membrane synthesis involves a two-step preparation method called secondary (seed) growth. Small (10-500 nm) zeolite crystal seeds are deposited in some way onto the surface of the support. These seeds act as nuclei for further crystal growth under hydrothermal conditions in order to fill the intercrystalline space, and create a continuous layer. This is similar to *in situ* hydrothermal synthesis, although due to the fact that there are no constraints on the hydrothermal conditions in

order to form crystal nuclei on the support, a wider range of hydrothermal conditions can be used. Therefore, crystal growth is the main film mechanism, adding improved flexibility in the zeolite film and membrane preparation. High reproducibility and better control over the membrane microstructure can be achieved using this method [104].

Another synthesis method that is relatively new is called vapour phase deposition. Xu *et al*. [105] discovered that MFI zeolite crystallize from an amorphous dry gel under vapours of triethylamine (Et_3N) and ethylenediamine (EDA) and water. A possible advantage of this method is that it can be used to prepare membranes on supports with relatively complicated shapes, for example honeycombs [106].

Mass transfer models through MFI-zeolites

The transport through microporous (like zeolites) membranes was described by Barrer [107], as a sequence of five activated reversible steps involving interfacial and intracrystalline processes (Figure 2-10). Several models have been proposed to describe the intracrystalline diffusion (step 3) in zeolites, which proceeds via surface diffusion. Some authors have also introduced an *activated gaseous diffusion* at higher temperature. Interfacial effects (steps 1, 2, 4 and 5) are important for very thin membranes and depend on the difference between the activation energy for intercrystalline diffusion and the activation energy for pore entrance.

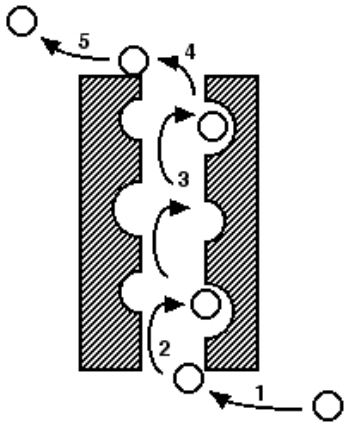

1. Adsorption on external surface.
2. Transport from the external surface into the pores.
3. Intracrystalline transport (transport through pores).
4. Transport out of pores to external surface.
5. Desorption from external surface.

Figure 2-10 Barrer's 5 step transport through zeolites [107].

For weakly adsorbing molecules or at high temperatures, direct entrance into the pores takes place, due to the fact that adsorption onto the external surface becomes negligible. The entrance of bulky molecules into pores is likely to be rate controlling, as a result of higher activation energy required for entry. If the molecule has to change its

conformation upon entering, some extra energy may be required. It is unlikely that desorption from the external surface would be rate limiting. Van de Graaf *et al.* [108] attributes this to the fact that adsorption on the external surface is usually less strong than adsorption within the crystal. It is unclear, however, whether the difference does not lie just on the molecule mobility, obviously higher on the external surface, leading to an apparent lower adsorption enthalpy. Models for mass transfer through MFI-zeolite membranes focus mainly on surface diffusion rate limitations. One model that has been used successfully to describe the mass transfer, is the Maxwell-Stefan formulations. Krishna *et al.* [97, 109-111] applied the Maxwell-Stefan equations, which are generally used to describe the diffusion in bulk fluid phase, to surface diffusion inside micropores. The basis of the Maxwell-Stefan theory is that, the driving force acting on a component for movement, is balanced by the friction experienced by the component.

Previous works in CNRS/IRC demonstrated that in the case of the type of MFI-zeolite membranes used in this work, the M-S surface diffusion model is sufficient enough to adequately describe the temperature dependence of the permeation [112].

Model for single gas transport through zeolite membranes

Ciavarella *et al.* [112] gives a model for the diffusion of a single gas through a zeolite membrane based upon the Maxwell Stefan theory and this model is described below.

The diffusional flux of a component can in general be described in two ways. It is either based on the first law of Fick (Equation (2-10)), or on the approach resulting from the irreversible thermodynamics developed by Maxwell-Stefan (Equation (2-11)) [109].

$$N = -D^F(q)\frac{dq}{dz} \tag{2-10}$$

$$N = -B_C(q)q\frac{d\mu}{dz} \tag{2-11}$$

where N is the molar flux (mol.m^{-2}.s^{-1}), $D_F(q)$ the Fickian diffusion constant (m^2.s^{-1}), q is the concentration of the mobile component in the micropores (mol.m^{-3}), $\frac{dq}{dz}$ is the concentration gradient, $B_C(q)$ is the mobility of the component (mol.Pa^{-1}.m^{-1}.s^{-1}) and $\frac{d\mu}{dz}$ is the chemical potential gradient (J.mol^{-1}.m^{-1}).

Fick's first law assumes that the concentration gradient is the driving force for transport, but the true driving force is actually the chemical potential gradient as proposed by the Maxwell-Stefan approach.

The permeation can be described by Fickian diffusion, by relating $D_F(q)$ to an intrinsic diffusivity (or a Maxwell-Stefan diffusivity), $D_0(q)$, through a Darken type equation:

$$D^F(q) = \Gamma D_0(q) \tag{2-12}$$

where $\Gamma = \frac{d\ln P}{d\ln q}$ is the thermodynamic "correction" factor (or the Darken factor).

The thermodynamic factor relates the chemical potential gradient to the surface occupancy gradient and can be determined from adsorption data.

Adsorption in the micropores can, in most cases be adequately described by the Langmuir isotherm. The Langmuir isotherm is valid if it is assumed that other adsorbed molecules do not influence the adsorption of a molecule, and that all the sites are equivalent. The Langmuir adsorption isotherm for one component is given by

$$\theta = \frac{q}{q_{sat}} = \frac{KP}{1+KP} \tag{2-13}$$

where θ is the fractional surface occupancy (or coverage), q_{sat} is the sorption capacity of the material (in this case the zeolite) (mol.m^{-3}), K the adsorption equilibrium constant or Langmuir parameter (Pa^{-1}) and P pressure (Pa).

By rearranging equation (2-13), an expression is obtained for the pressure in terms of surface concentration:

$$P = \frac{q}{K(q_{sat} - q)} \tag{2-14}$$

Differentiating equation (2-14) with respect to q gives an expression for $\frac{dP}{dq}$:

$$\frac{dP}{dq} = \frac{q}{K(q_{sat} - q)^2} \tag{2-15}$$

The expression of the thermodynamic factor can be rearranged such that:

$$\Gamma = \frac{d\ln P}{d\ln q} = \frac{dP}{dq} \cdot \frac{q}{P} \tag{2-16}$$

By substituting equations (2-14) and (2-15) into equation (2-16) an expression of the thermodynamic factor in terms of occupancy can be obtained:

$$\Gamma = \frac{q_{sat}}{q_{sat} - q} = \frac{1}{1-\theta} = 1 + \frac{\theta}{1-\theta} \tag{2-17}$$

Integration of the equation of single gas transport

An expression for the flux can be obtained by substituting equations (2-12) and (2-15) into equation (2-8), and assuming that the intrinsic diffusion coefficient (D_0) is independent of the concentration in the micropore.

$$\int_0^L N dz = -\int_{q_R}^{q_P} D_0 \frac{q_{sat}}{q_{sat} - q} dq \tag{2-18}$$

where q_R and q_P are the steady state concentrations at the permeate and the retentate side, respectively, and l is the effective thickness of the membrane layer.

After integration of equation (2-18) we obtain:

$$N = \frac{D_0 q_{sat}}{l} \ln\left(\frac{q_{sat} - q_P}{q_{sat} - q_R}\right) \tag{2-19}$$

If the Langmuir adsorption isotherm is used, then the following relationship between the retentate side pressure (P_R) and surface concentration q_R, and the permeate side pressure (P_P) and the surface concentration q_P, can be obtained:

$$\theta_R = \frac{q_R}{q_{sat}} = \frac{KP_R}{1 - KP_R} \tag{2-20}$$

$$\theta_P = \frac{q_P}{q_{sat}} = \frac{KP_P}{1 - KP_P} \tag{2-21}$$

where θ_R and θ_P are the fractional surface occupancy of the retentate and permeate, respectively.

Substitution of equations (2-20) and (2-21) into equation (2-19) gives the following expression for the single gas flux in terms of retentate and permeate pressures:

$$N = \frac{D_0 q_{sat}}{l} \ln\left(\frac{1-\theta_P}{1-\theta_R}\right) = \frac{D_0 q_{sat}}{l} \ln\left(\frac{1-KP_R}{1-KP_P}\right) \tag{2-22}$$

At low occupancy (Henry's regime) in the zeolitic micropores ($KP_R << 1$ and $KP_P << 1$), equation (2-24) simplifies to:

$$N = \frac{D_0 q_{sat}}{l} K\left(P_R - P_P\right) \tag{2-23}$$

At very high coverage in the zeolitic micropores ($KP_R = 1$ and $KP_P = 1$), equation (2-22) simplifies to:

$$N = \frac{D_0 q_{sat}}{l} K\left(\frac{P_R}{P_P}\right) \tag{2-24}$$

Dependence of the flux on temperature

The temperature dependency of D_0 satisfies the Arrhenius-type relationship:

$$D_0 = D_0^{\infty} \exp\left[\frac{-E_D}{RT}\right] \tag{2-25}$$

where E_D is the diffusional activation energy (kJ.mol $^{-1}$) and D_0^{∞} is the intrinsic diffusivity at infinite temperature.

The temperature dependency of the Langmuir parameter (K) can be correlated using the Van't Hoff-type relation, assuming $\Delta U_{ads} \cong \Delta H_{ads}$:

$$K = K_0 \exp\left[\frac{-\Delta U_{ads}}{RT}\right] = \exp\left[\frac{\Delta S_{ads}}{RT} - \frac{\Delta H_{ads}}{RT}\right] \tag{2-26}$$

with K_0 a pre-exponential factor Van't Hoff (1 atm) law, ΔU_{ads} the internal adsorption energy (J.mol^{-1}.K^{-1}), ΔS_{ads} the adsorption entropy (J.mol $^{-1}$.K^{-1}) and ΔH_{ads} is the differential adsorption enthalpy (J.mol^{-1}), for K given in atm^{-1}.

The equation for the single gas flux through a microporous membrane can be obtained (equation (2-27)) by substituting equations (2-25) and (2-26) into equation (2-24) and correcting the intrinsic diffusion constant by a factor, $\frac{\varepsilon}{\tau}$, to account for the geometrical properties of the membrane. ε is the porosity and τ is the tortuosity of the composite membrane.

$$N = \frac{q_{sat}\rho_{MFI}\varepsilon D_0^{\infty}}{\tau l} \ln\left[\frac{1 + P_R \exp\left(\frac{\Delta S_{ads}}{R} - \frac{\Delta H_{ads}}{RT}\right)}{1 + P_P \exp\left(\frac{\Delta S_{ads}}{R} - \frac{\Delta H_{ads}}{RT}\right)}\right] \cdot \exp\left(\frac{-E_D}{RT}\right) \tag{2-27}$$

Multicomponent diffusion in microporous zeolite membranes

The prediction of separation performance of MFI zeolite membranes requires knowledge of multicomponent adsorption and diffusion models in microporous materials. Ideally one would like to be able to predict mixture permeation at various conditions, using single component parameters. Although the description of multicomponent mass transfer in microporous membranes is of great practical importance, studies in the area are limited. Mixture permeation through zeolite membranes has been modelled qualitatively using the generalized Maxwell-Stefan equations with [108] and without [113, 114] adsorbate-

adsorbate interactions. The generalized Maxwell-Stefan equations have proven to be a good choice for the description of multicomponent mass transfer through MFI-zeolite membranes and have been applied to surface diffusion in microporous media by Krishna *et al*. [97, 110, 113]. It permits the generalization of n constituents of the Fick equation and expresses the flux in terms of the chemical potential gradient.

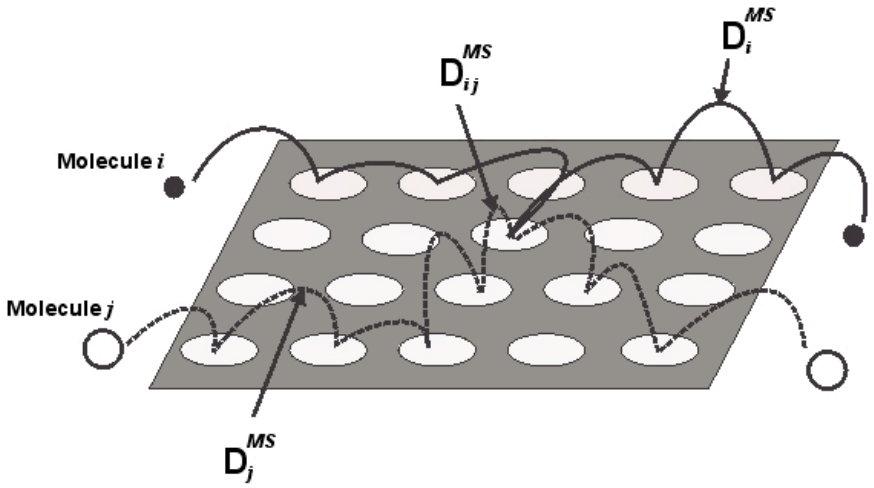

Figure 2-11 Graphical representation of diffusion through a microporous media as in the Maxwell-Stephan formulations [109]. Multicomponent surface diffusion model based on the Maxwell-Stefan equations.

According to the multicomponent surface diffusion model, it is presumed that a molecule is in contact with other molecules as well as the vacant sites. The vacant sites are described as the (1 + n)th pseudo-species in the (surface) system, a similar idea as considered in the Dusty gas model.

The balance of the forces experienced by component *i* during migration on the surface can be written as follows:

$$-\nabla\mu_i = RT\sum_{j=1}^{n}\theta_j\frac{\left(u_i - u_j\right)}{D_{ij}^{MS}} + RT\theta_{n+1}\frac{\left(u_i - u_{n+1}\right)}{D_{i,n+1}^{MS}}, \quad i = 1,2,...,n \qquad (2\text{-}28)$$

with $-\nabla\mu_i$ being the surface chemical potential gradient, the driving force acting on component *i* tends to move along the surface. The first term on the right hand side reflects the friction exerted by adsorbate j on the surface motion of adsorbed component *i*. The second term reflects the friction experienced by the component *i* from vacancies.

The Maxwell Stefan diffusion coefficients are per definition analogous to the Knudsen diffusion coefficients as in the case of the Dusty gas model.

$$D_i^{MS} = \frac{D_{i,n+1}^{MS}}{\theta_{n+1}} \tag{2-29}$$

The cross term diffusivities are determined from the single-component diffusivities by using the empirical relation of Vignes (1966),. They account for the molecule-molecule interactions.

$$D_{ij}^{MS} = D_i^{MS^{\theta_i/(\theta_i+\theta_j)}} D_j^{MS^{\theta_i/(\theta_i+\theta_j)}} \tag{2-30}$$

The cross term diffusivities satisfy the Onsager reciprocity relation.

$$D_{ij}^{MS} = D_{ji}^{MS} \tag{2-31}$$

By rearranging the formula for the molar flux of i, $N_i = \rho_z.q_i.\mathbf{u}_i$, and substituting for c_i using the definition of occupancy, $\theta_i = \frac{q_i}{q_{sat}}$, the linear velocity $\mathbf{u}_i$ is given by

$$\mathbf{u}_i = \frac{N_i}{q_{sat}.\rho_z\theta_i} \tag{2-32}$$

By substituting equations (2-29) to (2-32) into equation (2-28) and taking into account that the vacant sites are immobile ($\mathbf{u}_{n+1} = 0$), one arrives at the general form of the generalized Maxwell-Stefan equations used for surface diffusion.

$$-\frac{\theta_i \nabla \mu_i}{RT} = \sum_{\substack{j=1 \\ j\neq 1}}^{n} \frac{\theta_j N_i - \theta_i N_j}{q_{sat}.\rho_z.D_{ij}^{MS}} + \frac{N_i}{q_{sat}.\rho_z.D_i^{MS}} \qquad i = 1,2,...,n \tag{2-33}$$

Assuming equilibrium between the surface and the bulk fluid gives the following expression for the surface chemical potential of species *i*:

$\mu_i = \mu_i^0 + RT\ln(f_i)$ where μ_i^0 is the standard state chemical potential and f_i is the fugacity of component i in the bulk fluid mixture. For low system pressures, the component fugacities can be replaced by the component partial pressures. The chemical potential can be related to the gradient in the surface coverage by a matrix (Γ) of thermodynamic factors, such that:

$$\frac{\theta_i \nabla \mu_i}{RT} = \sum_{j=1}^{n} \Gamma_{ij} \nabla \theta_i \text{ with } \Gamma_{ij} \equiv \theta_i \frac{\partial \ln p_i}{\partial \theta_i} \qquad i,j = 1,2,...,n \tag{2-34}$$

The surface occupancy, θ_i, is related to the partial pressure by the adsorption isotherm. The choice of the adsorption isotherm determines the mathematical form of the thermodynamic factor, and therefore, influences the complexity of the mathematics. The extended Langmuir equation is often used due to its mathematical simplicity, although

other models, e.g. Ideal Adsorbed Solution Theory (IAST), can also be used. For further derivation of the model the extended Langmuir equation is used.

$$\theta_i = \frac{K_i.p_i}{1+\sum_{j=1}^{n} K_j.p_j},\ K_i.p_i = \frac{\theta_i}{1-\theta_{tot}} \tag{2-35}$$

For the Langmuir isotherm the elements of (Γ) are:

$$\Gamma_{ij} = \delta_{ij} + \frac{\theta_i}{1-\theta_{tot}} \tag{2-36}$$

with δ_{ij} a Kronecker matrix (1 if $i = j$; 0 if $i \neq j$) and θ_{tot} the total fraction of the surface occupied by n species, $\theta_{tot} = \sum_{j=1}^{n} \theta_j$ and $\theta_{tot} = 1 - \theta_{n+1}$.

Equation (2-33) can be written in n-dimensional matrix notation and the geometric factor of the membrane can be incorporated into the equation:

$$-\rho_z.q_{sat}.\frac{\varepsilon}{\tau}.[\Gamma].(\nabla\theta) = [B].(N) \tag{2-37}$$

where the matrix $[B]$ has the elements

$$B_{ii} = \frac{1}{D_i^{MS}} + \sum_{\substack{j=1 \\ j\neq 1}}^{n} \frac{\theta_j}{D_{ij}^{MS}},\quad B_{ij}^{s} = -\frac{\theta_i}{D_{ij}^{MS}},\quad i,j = 1,2,...,n \tag{2-38}$$

For the case of a binary mixture the surface flux of component 1 through the membrane can be given by equation (2-39) using equation (2-37) [66]. In the same manner an expression for the flux of component 2 can be written.

$$N_1^{MS} = -q_{sat}\cdot\rho_z\cdot\frac{\varepsilon}{\tau}\cdot\frac{D_1^{MS}}{(1-\theta_1-\theta_2)}\cdot\frac{\left[(1-\theta_2)+\theta_1\frac{D_2^{MS}}{D_{12}^{MS}}\right]\nabla\theta_1+\left[\theta_1+\theta_1\frac{D_2^{MS}}{D_{12}^{MS}}\right]\nabla\theta_2}{\theta_2\frac{D_1^{MS}}{D_{12}^{MS}}+\theta_1\frac{D_2^{MS}}{D_{12}^{MS}}+1} \tag{2-39}$$

In a special case, called *single-file* diffusion mode, the friction between molecules is much less important than friction with the wall and $D_i^{MS} <<<<<< D_{ij}^{MS}$ and equation (2-33) reduces to:

$$N_1^{s} = -q_{sat}\rho_z\frac{\varepsilon}{\tau}\frac{D_1^{MS}}{(1-\theta_1-\theta_2)}\left[(1-\theta_2)\nabla\theta_1+\theta_1\nabla\theta_2\right] \tag{2-40}$$

Therefore, it can be seen that if the single component diffusivities are known, then a prediction can be made of the multicomponent diffusion through zeolite membranes.

2.1.4 Palladium membranes

Palladium and hydrogen system

In 1866 the Pd/H_2 system became the first metal-hydrogen system to be studied, with the discovery by T. Graham that palladium (Pd) can absorb large quantities of atomic hydrogen (H) [115]. During H dissolution, atomic and electronic structural changes occur in Pd and it can have considerable effects on the physical properties of Pd, for example the Pd-H_x alloy is diamagnetic and superconducting at very low temperatures (1 K for x = 0.75 up to 9 K for x = 1)[116], although Pd itself is strongly paramagnetic [117].

Solid solutions of H in Pd correspond to α-phase regions if the atomic ratio of H:Pd, n_H/n_{Pd}, is less than 0.02 - 0.03, and to β-phase regions if the n_H/n_{Pd} ratio is greater than ca. 0.6. A mixture of both phases are present when the ratio lies between these values at temperatures lower than ~ 573 K and hydrogen pressure below 2.2 MPa (Figure 2-12). In both α- and β-phases, the Pd atoms form an f.c.c. structure, with H atoms occupying octahedral interstitial sites, but the distance between Pd atoms in the β-phase is ca. 3% greater than the α-phase. The α ↔ β-phase transition process is therefore accompanied by distortion of the palladium structure that may lead to crystal defect generation, and eventually crystal disjunction or even rupture in the case of large crystals. This phenomenon is known as hydrogen embrittlement [117-119]. For common hydrogen pressures, it occurs below 573 K, and therefore prevents the use of common palladium membranes at low temperatures for hydrogen separation.

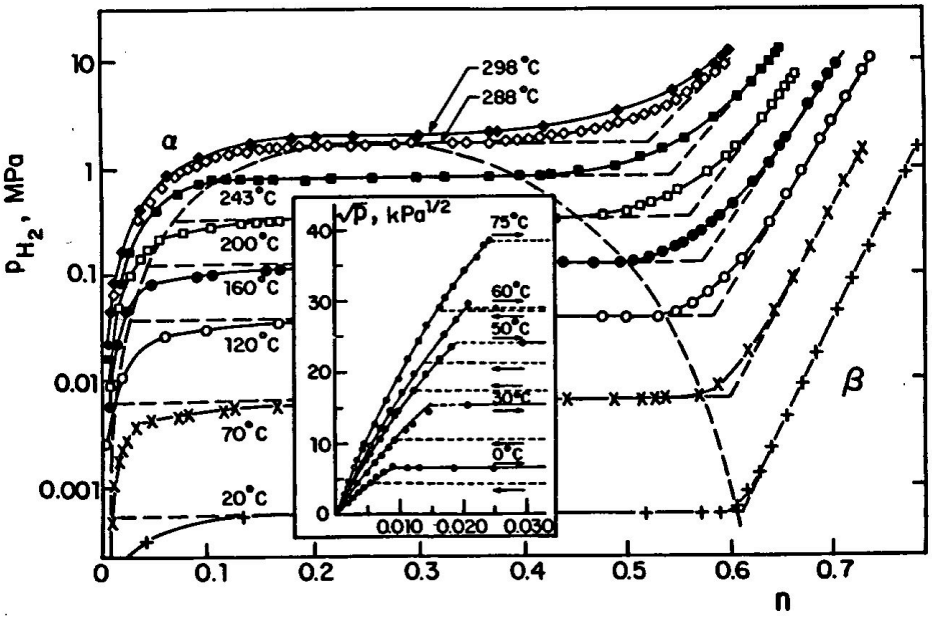

Figure 2-12 Palladium/Hydrogen system [118].

In the case of Pd membranes this leads to cracks in the Pd, destroying the selectivity of the membrane. In order to avoid this from happening, two routes can be followed: the first would be to operate the process under conditions where no phase transition occurs, or the second would be to alloy the palladium in order to suppress $\alpha \leftrightarrow \beta$-phase transition [120]. Figure 2-13 gives the hydrogen permeance values through various palladium-alloy membranes at 623 K and 2.2 MPa hydrogen pressure. Of these alloying metals, silver has been the most widely used for the preparation of palladium-alloy membranes.

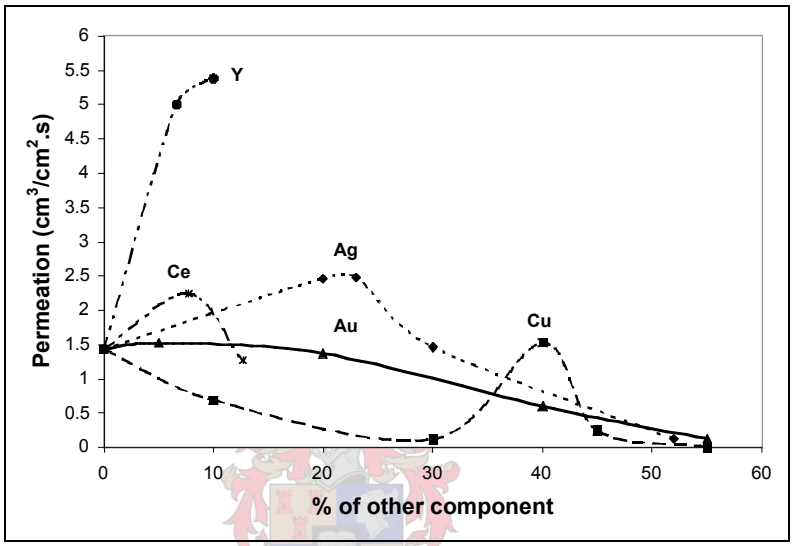

Figure 2-13 Hydrogen permeability through Palladium Alloys 350oC and 2.2 MPa [121].

Another option would be to design palladium membranes with sufficiently small crystals that would not be sensitive to the hydrogen embrittlement phenomenon. The pore-plugging approach was used in CNRS/IRC to achieve this objective, leading to a nanocomposite palladium/alumina membrane [122].

Composite Palladium membrane preparation

Various methods exists to prepare composite palladium membranes, which include, physical vapour deposition (PVD), metal organic chemical vapour deposition (MOCVD), magnetron sputtering, pyrolysis, micro-emulsion techniques, pore-plugging by liquid impregnation, electroplating and electroless plating.

Of these methods electroless plating have been extensively used for composite palladium membrane preparation. Electroless plating is the deposition of a metallic

coating onto a surface by the continuous reduction of an aqueous metal ion to a metal solid via a chemical reaction, without any external electric current [123].

The advantages using this method lie in the fact that the deposit follows all contours of the substrate. It is uniform, dense and the method is simple and inexpensive [123, 124]. Good metal to substrate adhesion is also obtained [14]. Some disadvantages of electroless plating with specific referral to palladium deposition are: impurities might form in the metal layer when certain reducing agents are used (phosphorous along with Pd), which can result in the formation of Pd-P alloys (1 - 2 wt.%P) when hypophosphite is used as reducing agent [124] and boron (3 - 8%) when boronhydride is used [125]. A drawback when using hydrazine as the reducing agent is that the palladium deposition rate decreases rapidly, due to thermal decomposition of hydrazine, even if the palladium concentration is high, leading to losses [124]. Co-deposition of palladium with other metals to form Pd alloys have not been very successful and some difficulties are also experienced when depositing separate metal layer and subsequent alloying [14]. Moreover, the method is highly sensitive to the quality of the support.

Electroless plating chemistry

The electroless plating bath consists of four components namely, an aqueous metal solution, a reducing agent, a complexing agent and a bath stabilizer. The bath is operated at a specific pH, temperature and metal ion concentration.

The reducing agent acts as an electron donor, while the metal ions acts as electron acceptors. The complexing agent acts as a buffer helping to control the pH and maintain control over the *free* metal salt ions available in solution, allowing solution stability. The stabilizer acts as a catalytic inhibitor, retarding the spontaneous decomposition of the electroless bath. The deposition rate is controlled by the pH, temperature, metal ion and reducer concentrations.

For composite palladium membrane fabrication, an electroless plating procedure with hydrazine as reducing agent was used. The electroless plating procedure consists of two steps: activation (deposition of nuclei on the substrate surface) and the electroless plating itself (further growth of nuclei to form a plating layer).

The traditional *activation procedure* for palladium electroless plating is a two-step process of *sensitization* and *activation*. During *sensitization* the substrate is immersed into an acidic $SnCl_2$ solution, and the reducing agent is adsorbed onto the substrate surface. This is followed by *activation*, during which the substrate is immersed in a $PdCl_2$ solution,

leading to the formation of Pd seeds on the substrate surface (nucleation). The substrate is then gently rinsed with deionized water and the whole procedure is usually repeated a couple of times in order to obtain enough Pd seeds for the autocatalytic electroless plating process. The oxidation reduction reaction is given by the following reaction formula:

$$Pd^{2+} + Sn^{2+} \rightleftharpoons Sn^{4+} + Pd^{0} \tag{2-41}$$

This procedure does have a number of disadvantages: (i) The two-step process is time consuming and cumbersome due to the fact that it has to be repeated several times in order to obtain satisfactory activation. (ii) Sn compounds with low melting points can be trapped at the Pd/ceramic interface and at high temperatures, melting and decomposition of the co-deposited impurities will cause the formation of cracks and pinholes within the film. (iii) The uniformity of the Pd-nuclei and adhesion between the metallic film and substrate is questionable due to the fact that it is not known whether the catalization is successful or not [126].

When *hydrazine* is used as the *reducing agent* the plating bath normally consists of an EDTA stabilized Pd-amine complex and hydrazine. An excess amount of ammonium is present in the bath in order to stabilize the bath and to maintain the pH of the solution, and it also serves as a solvent for the EDTA.

$$\begin{aligned} 2Pd(NH_3)_4^{2+} + 4e^- &\longrightarrow 2Pd^0 + 8NH_3 \\ N_2H_4 + 4OH^- &\longrightarrow N_2 + 4H_2O + 4e^- \\ \hline 2Pd(NH_3)_4^{2+} + N_2H_4 + 4OH^- &\longrightarrow 2Pd^0 + 8NH_3 + N_2 + 4H_2O \end{aligned} \tag{2-42}$$

The reaction takes place at the surface of the support, preferentially around the Pd seeds formed during the activation step. The reaction is initiated when hydrazine reacts with hydroxide ions forming nitrogen gas and water with the simultaneous release of electrons. The electrons are transferred across the Pd seeds and used to reduce the Pd^{2+} complex into Pd metal. The palladium is deposited onto the Pd seeds and growth takes place. The deposition rate increases with the amount of Pd sites, and the reaction becomes autocatalytic. Nitrogen and ammonia bubbles are formed during the plating process [124].

The hydrazine solution decomposes rapidly in the presence of Pd metal and temperature. This leads to low plating efficiency of the hydrazine-based plating bath. In the plating bath hydrazine is the limiting reactant. The bath is, however, sensitive for the amount of hydrazine, and an excessive amount of hydrazine can lead to bulk precipitation

of the palladium and poor coating. Cheng and Yeung [124] have suggested feeding the hydrazine to the plating bath in portions, during the reaction, in order to ensure that the maximum available amount of Pd^{2+} in the bath reacts.

Modelling H_2 transport through Palladium membranes

Ward and Dao [127] used a set of mathematical equations to describe a number of sequential steps which takes place during hydrogen permeation (Figure 2-14).

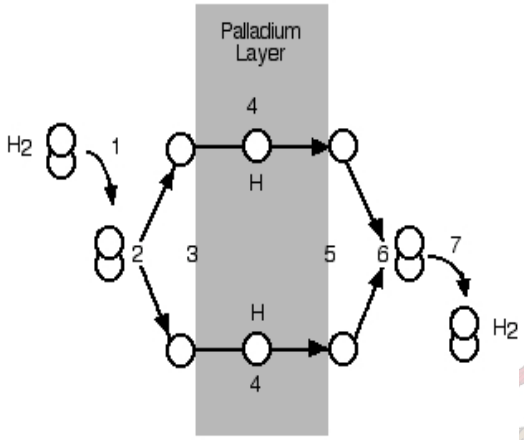

1. Molecular transport from the bulk gas to gas layer adjacent to the surface.
2. Dissociative adsorption onto the surface
3. Transition of H atoms from the surface to the bulk metal
4. Atomic diffusion through the bulk metal
5. Transition from the bulk metal to the surface on the lower pressure side
6. Recombinative desorption from the surface
7. Gas transport away from the surface to the bulk gas

Figure 2-14 Transport of hydrogen through palladium [127].

After investigating the influences of all the transport steps, using rate parameters estimated from surface science and membrane literature the following conclusions were made:

- For pure Pd in the absence of external mass transfer the rate limiting step would be diffusion through the membrane at relatively high temperatures (673 K ≤ T).
- Only at low temperatures will desorption be the rate dominating process.
- At low hydrogen partial pressures or in the presence of surface contamination adsorption is likely to be the rate-limiting factor.
- External mass transfer can become a significant resistance especially on the low-pressure side, when the hydrogen fluxes are high due to the thin nature of the Pd membranes or when a support is present.
- There is very little data available on the effects of microstructural properties on the permeation characteristics of Pd and Pd alloy film, and therefore the fabrication method can also play a role in the permeation characteristics [127].

The mathematical formulation of hydrogen diffusion through the palladium layer has been given in section 2.1.1 (p. 11).

2.2 Experimental: Membrane preparation and testing

2.2.1 The support

The supports (Figure 2-15) used are macroporous, multilayered α-alumina (Pall Exekia T1-70) tubes, 15 cm in length, with an outer diameter of 10 mm, and an inner diameter of 7 mm. The ends are sealed with enamel, incorporated in the support pores over its whole thickness. Each enamel ending is 1 to 1.5 cm in length and they create two non-permeable zones at the membrane endings. The length of the support available for membrane deposition and permeation is consequently 13-12.5 cm. These membranes were purchased from Pall Exekia.

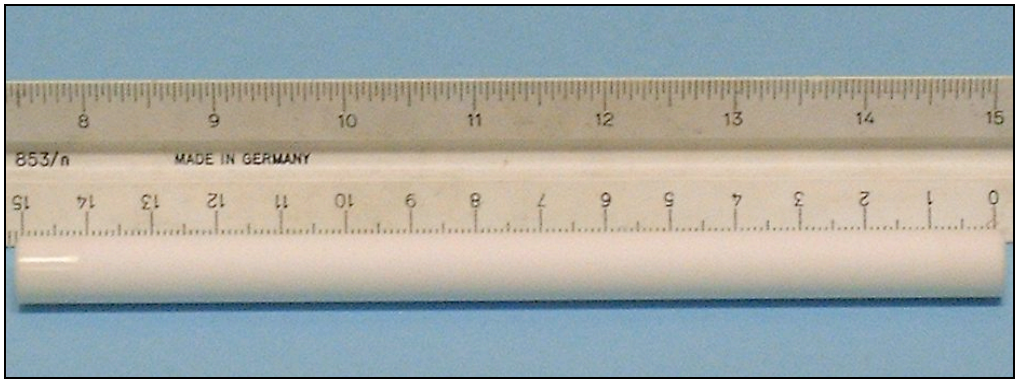

Figure 2-15 Pall Exekia T1-70 membrane support tube (1 cm enamel endings).

The support consists of three α-alumina layers with increasing pore size from the internal to the external layer (Figure 2-16). The characteristics of the three layers are given in Table 2-1.

Table 2-1 Characteristics of the different layers of the Pall-Exekia T1-70 support tube.

	Pore Diameter [μm]	Thickness [μm]
1st Layer	12	1500
2nd Layer	0.8	40
3rd Layer	0.2	20

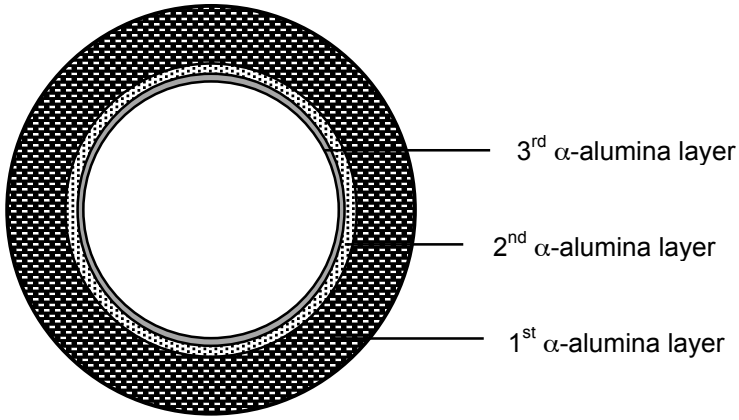

Figure 2-16 Cross–cut of the support tube.

2.2.2 MFI-zeolite membranes

The MFI-zeolite composite membranes used in this study was supplied by the CNRS/IRC. The MFI-zeolite is synthesized within the macroporous structure of the α-alumina support with a pore-plugging technique developed at the CNRS/IRC [101, 102]. The preparation is carried out in four steps:

Preparation of the precursor: A solution of oligomeric silica species are prepared by dissolving commercial silica (Degussa- Aerosil 360) in tetrapropyl ammonium hydroxide (Aldrich-TPAOH) under stirring. A typical precursor solution would consist of 6 g of fumed SiO_2 (Degussa Aerosil 380) and 50 ml of TPAOH (0.9M). This solution is then stirred for 72 hours at ambient temperature. This ageing leads to the formation of silica oligomers with controlled nuclearity during which the size are adapted for the following step in the production process (diffusion within the macroporous support). The precursor is centrifuged for 30 minutes to remove all the unreacted silica and the "clear" oligomeric solution is recovered. The TPAOH play a significant role in the structuring during nucleation and the crystallization of the silicate during the next stage.

Hydrothermal synthesis: The tabular α-alumina support enamelled endings are wrapped in PTFE (polytetrafluoroethylene) tape, and the tube is brought into contact with the oligomeric solution in a stainless steel autoclave. The PTFE tape on the outer surface of the enamel prevents zeolite formation on that area of the tube, to keep it as smooth as possible for further use in contact with seals. The hydrothermal treatment is performed at 443 K for 89 hours. During this time, the hydrothermal treatment temperature is changed with time, as shown in Figure 2-17. During this stage crystallisation of the MFI zeolite

takes place within the pores of the alumina matrix. The exact nature of the diffusion/crystallisation processes, during this temperature profile, is currently under investigation.

Washing and drying: The tube containing the zeolite is obtained after the hydrothermal treatment. In order to remove all the zeolite that has not crystallized onto the support, the membrane is washed three consecutive times. It is then dried at 373 K under nitrogen flow for 12 hours. At this stage the membrane should not display any nitrogen permeance, due to the fact that the support pores are plugged by the zeolite, and the pores of the zeolite are occupied by the molecules of the structuring agent (TPAOH). An N_2 permeance test is performed at ambient temperature to determine whether any defects are present in the membrane at this stage.

Calcination: After washing and drying, the membrane is placed in a quartz cell and calcined at 773 K for 8 hours in air. Calcination leads to the "release" of the porosity of the zeolite.

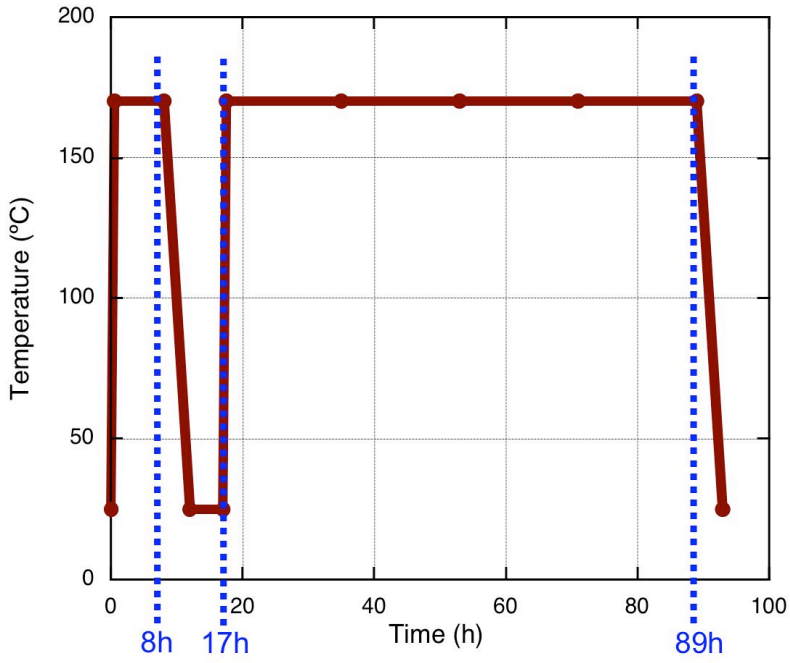

Figure 2-17 Hydrothermal synthesis conditions.

2.2.3 Supported Palladium membranes

Supported palladium membranes were prepared using a batch electroless plating procedure similar to a technique enhanced by Keuler at the DPE/US and CNRS/IRC [14]. The membrane plating procedure was, however, changed in this work: the objective was to plate the same thickness as Keuler in each step. Due to the fact that the membranes used in

this study were shorter (15 cm compared with 25 cm) and from a practical point of view (8 ml plating solution was needed to cover the surface area of the membrane) the plating solution concentration was changed from 2000 ppm to 1625 ppm. No changes were made to the concentration ratios of the technique, meaning that the ratio between Pd:N_2H_2 was kept constant. The preparation is done in three steps, pre-treatment, electroless plating and membrane cleaning:

Pretreatment (Sensitization and Activation): The main objective of support pretreatment prior to electroless plating is to anchor metal nuclei on the plating surface. Metal nuclei's serve as seeding or catalyzing agents, providing catalytic nucleation centres for electroless plating. Prior to pretreatment, the support is washed in distilled water for 30 minutes and allowed to dry overnight at 473 K. The initial mass of the support is then recorded. PTFE tape is wound around the support's outer surface in order to ensure that only the inner surface is activated. The support is stirred in approximately 300 ml of palladium chloride or tin-chloride solution at 2000 rpm (Figure 2-18a) following the pretreatment sequence given in Figure 2-18b. The support is first stirred in $PdCl_2$ for 10 minutes, and then dipped 10 times in distilled water to wash off all the remaining $PdCl_2$ on the tube. The support is then stirred in $SnCl_2$ for 10 minutes, and then dipped 10 times in distilled water. This process is repeated 3 times. The support is once again stirred in $PdCl_2$ for but this time only for 5 minutes, followed directly by stirring in the $SnCl_2$ for 5 minutes, after which the support is dipped 10 times in distilled water. This process is repeated 3 times.

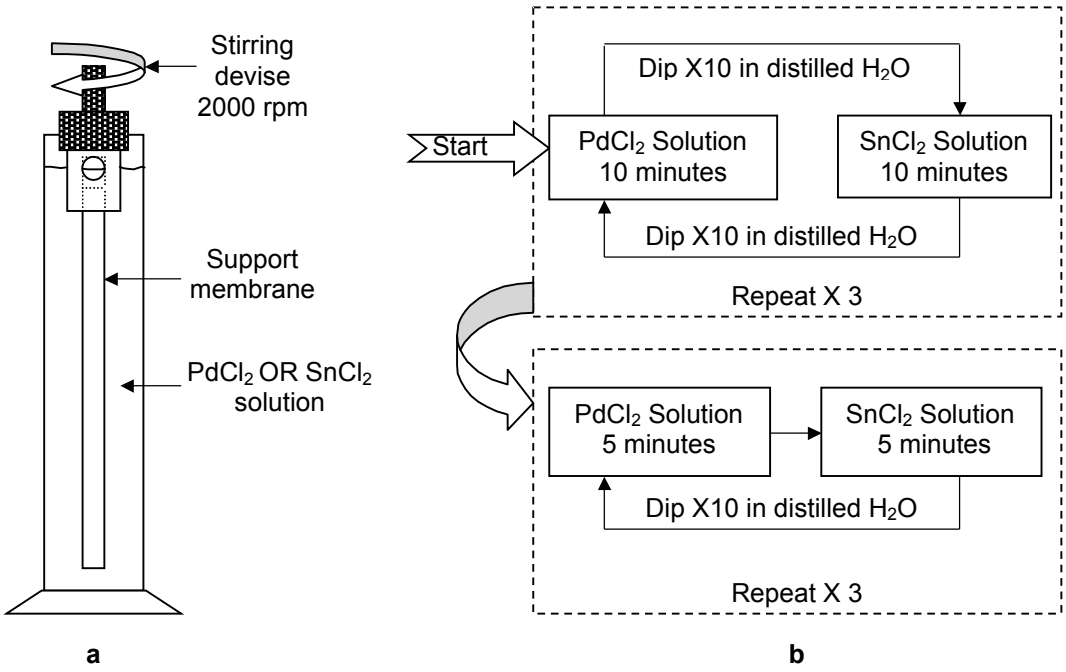

Figure 2-18 Pretreatment (a) equipment and (b) procedure.

The compositions of the activation ($PdCl_2$), and sensitization ($SnCl_2$) solutions are given in Table 2-2 along with the compositions used in previous studies. Acid was added to the solutions of Keuler [14], due to the fact that the $PdCl_2$ (60% Palladium) did not dissolve easily in distilled water. Due to the unstable nature of the $SnCl_2$ solution, fresh solution is prepared before each pretreatment. After pretreatment the PTFE tape was removed, and the membrane stirred in distilled water for an additional 30 minutes.

Table 2-2 Pretreatment solution composition compared to previous studies.

Composition	Yeung *et al.* [128]	Li *et al.* [75]	Keuler [14]	Shu *et al.* [129]	This study
Sensitization					
$SnCl_2.2H_2O$	5 mM	5 g/l	0.45 g/l	1 g/l	0.45 g/l
HCl (37%)	-	1 ml/l	-	1 ml/l	1 ml/l
Temperature [K]	Ambient	323	Ambient	Ambient	Ambient
Activation					
$PdCl_2$	-	-	1.4 g/l (23 wt% $PdCl_2$)		0.322 g/l (60 wt% Pd)
$Pd(NH_3)_4Cl_2$	5 mM	0.5 mM	-		
$Pd(NH_3)_4(NO_3)_2$	-	-	-	0.168 g/l	
HCl_2 (37%)	-	1 ml/l	-	1 ml/l	1 ml/l
Temperature [K]	Ambient	323	Ambient	Ambient	Ambient
Sn: Pd	1.0	44	1.1	7.9	1.1

Electroless Plating: The pretreated membrane is sealed in a teflon reactor with o-rings, creating an external shell side and internal tube side, within the teflon plating reactor. The plating reactor has a single shell side outlet where a vacuum can be drawn. The plating reactor is 13 cm in length, allowing 1 cm (enamelled ending) of the membrane to stick out. At one end a 2-cm silicon tube is placed around the membrane, and the tube is closed off. At the other side, a 15-cm silicon tube is placed round 1 cm length of the membrane. This allows space in order for the plating solution to cover the whole plating area.

The plating reactor is placed in a warm bath (345 K) (Figure 2-19), and 8 ml of plating solution is introduced into the tube side of the membrane. A 1625 ppm palladium solution is used for electroless plating. The composition of the solution is given in Table 2-3. The plating solution is prepared without adding hydrazine, and is then allowed to

stabilize for a minimum of 16 hours before use. The hydrazine is introduced into the plating solution (8 ml) as indicated in Table 2-4 when plating is done.

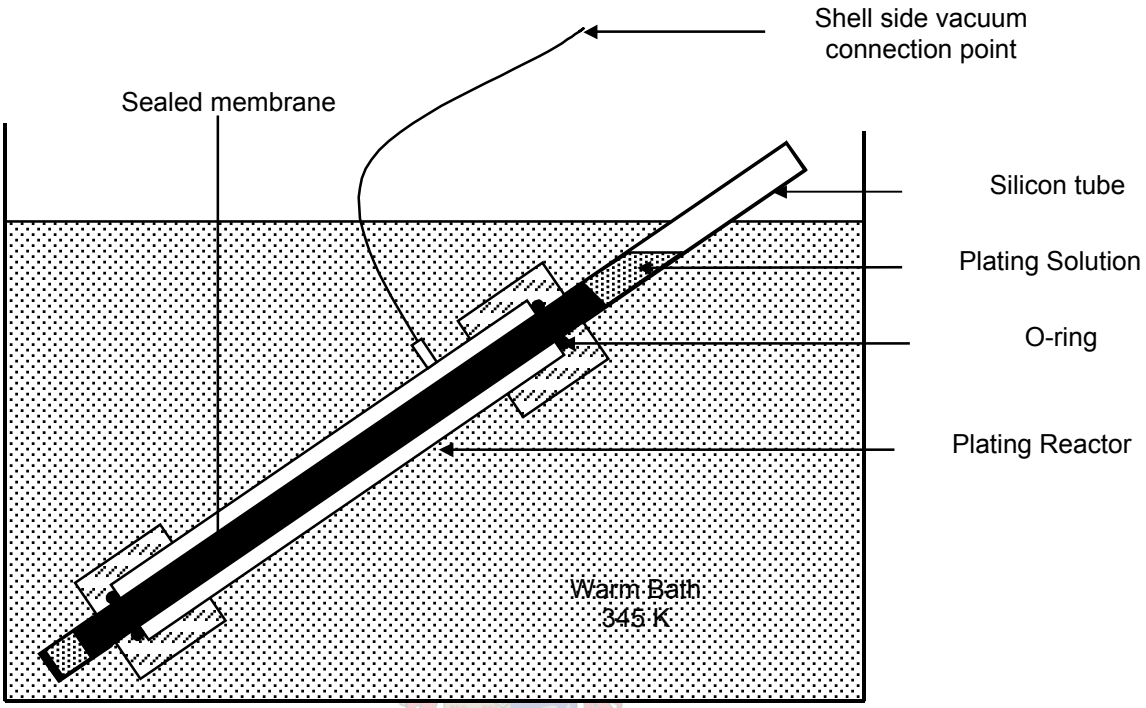

Figure 2-19 Electroless plating bath with submerged electroless plating reactor.

Table 2-3 Composition of the Pd plating solution per litre (1625ppm Pd in solution).

$(NH_3)_4PdCl_2.H_2O$ [g]	4.00
28 wt % Ammonia [ml]	325
EDTA [g]	65
35 wt % Hydrazine	Hydrazine:Pd = 0.35:1 (start reaction) Increased with time
Temperature [K]	345

Table 2-4 Plating procedure for plating one Pd film layer.

Reaction Time (Total) (8 ml plating solution) [min]	1.75 wt% Hydrazine Added (8 ml plating solution) [µl]
0	84.8
20	56.5
40	283
Stop reaction after 60 minutes	

An initial ~ 1 micron palladium base layer is deposited on the inside of the membrane tube, by repeating the procedure three times (8 ml × 3 = 24 ml). The membrane is cleaned (procedure given in next section) and dried overnight before the next layer is plated. The number of layers to be plated will depend on the desired thickness of the palladium film. For example, a membrane with a palladium film of ~ 1.5 µm will be prepared by plating the initial base layer, followed by plating the second layer (8 ml plating solution), cleaning and drying overnight and then plating a third layer (8 ml plating solution) followed by cleaning and drying. After the initial palladium base layer is deposited, a vacuum is applied to the outside of the plating reactor during the following plating sessions. This will result in a denser film, due to the fact that the palladium solution concentrates in the more permeable or defected areas, allowing more plating in weakly plated areas, and the repair of defects in the film, if any.

Post-treatment or cleaning: The post treatment step or membrane cleaning is done to remove EDTA which might be trapped within the membrane pores of the support from the electroless plating step. The same experimental set-up that was used for the pretreatment step is used for the post-treatment. The Pd composite membrane is washed in 300 ml 15 % ammonia solution, stirring speed 2000 rpm for an hour. The solution is then replaced with fresh solution, and the process is repeated, after which the membrane is washed in distilled water for 30 minutes. It is then dried overnight at 373 K. The cleaning process is repeated the next day, and the Pd composite membrane is dried overnight at 513 K.

2.2.4 High temperature pretreatment before use

Before the MFI-zeolite composite and composite Palladium membranes were tested, high temperature pretreatment of the membranes was carried out. This was performed in order to remove surface contaminants and to unblock pores. In the case of palladium composite membranes, this procedure also serves to remove some EDTA that might still be present in the membrane.

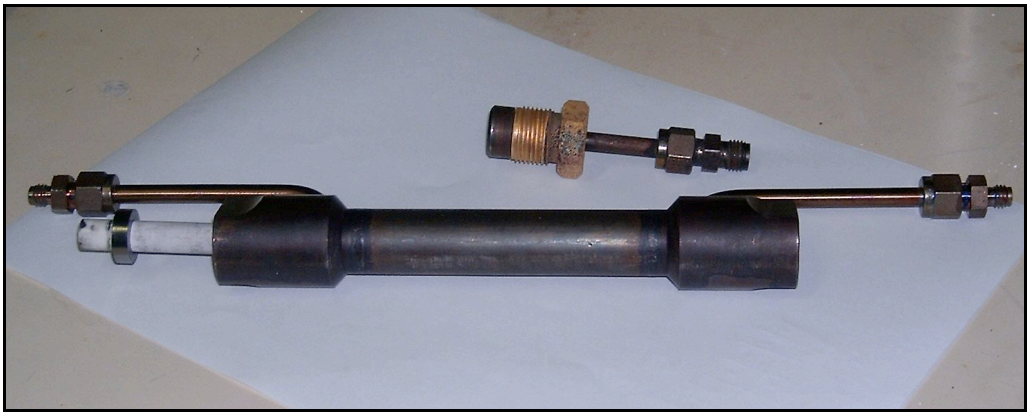

Figure 2-20 Stainless steel membrane reactor module, membrane and graphite ring.

The membrane was fixed in a stainless steel membrane reactor module (Figure 2-20) with graphite rings (Origraph® Cefilac - Garlock), creating internal and external compartments. This membrane reactor module was then placed in a tube furnace, as was the case during single gas permeation testing. A more detailed description of the reactor module and experimental membrane testing bench will be given in chapter 3.

Composite zeolite (MFI) pretreatment

The membrane is heated in under nitrogen flow, 20 ml/min internal flow and 20 ml/min sweep flow to 773 K at a heating rate of 1 K/min. The membrane is then left for 6 hours at 773 K after which testing can commence. The purpose here is to desorb any hydrocarbon or water that easily adsorbs into the zeolite pores. The zeolite prepared is a highly acidic H-ZSM5 (Si/Al = 10), and is therefore very hydrophobic. However, as previous studies suggest [103], water can be removed below 473 K, but some hydrocarbons need no less than 633 K. By using a temperature higher than 633 K, one can be sure of a total desorption process.

Oxidation pretreatment of composite palladium membrane

The oxidation heat treatment of Keuler [14] was used for palladium pre-treatment with a slight change in heating rates from 2.5 K/min, suggested by him, to 1 K/min. This was done in order to prevent any crack formation due to the difference in thermal

expansion coefficients of palladium and α-alumina. The following oxidation pretreatment for palladium membranes was used: heat membrane in nitrogen to 593 K at 1 K/min. Switch from nitrogen to oxygen and force 10 ml/min oxygen through the Pd layer and membrane wall from the feed side to the permeate side for 2 hours. Switch back to nitrogen and heat membrane to 723 K at a heating rate of 1 K/min. Reduce membrane in hydrogen atmosphere for 1.5 hours at 723 K. This pretreatment method was used before the permeation tests were carried out.

Single gas permeation testing

Single gas (N_2 and H_2) permeation tests were performed in the dead-end mode in the palladium membranes. This means that the exit of the membrane was closed as well as one of the sweep side exits, thereby forcing the gas through the membrane at a certain pressure

The molar flux, N_i, is obtained with the following formula:

$$N_i = \frac{Q_i}{A} \tag{2-43}$$

with Q_i being the molar flow rate (mol.s^{-1}) and A, the membrane area (m^2) available for permeation.

The permeance is calculated using equation (2-1):

$$P_i^m = \frac{N_i}{\Delta P_i} \tag{2-1}$$

with P_i^m the permeance (mol.m^{-2}.s^{-1}), N_i the molar flux (mol.m^{-2}.s) and ΔP_i the trans-membrane partial pressure (Pa) of component i. In the case of hydrogen permeation through palladium membranes, equation (2-1) is only valid in certain instances, and therefore the permeance should be calculated using the following equation:

$$P_{H2}^m = \frac{N_i}{\left(P_{H_2,ret}^n - P_{H_2,per}^n\right)} \tag{2-44}$$

Some knowledge of n is therefore required in order to calculate the hydrogen permeance through palladium membranes. The permselectivity, $P_{i/j}^m$, is the ratio of the single gas permeance of component i compared to component j:

$$P_{i/j}^m = \frac{P_i^m}{P_j^m} \tag{2-45}$$

n-Butane/Hydrogen Mixture Separation Testing

n-Butane/hydrogen mixture separation testing as a function of temperature is a standard screening test that is performed on all of the fabricated MFI/alumina composite membranes at the CNRS/IRC.

n-Butane/hydrogen mixture separation tests were performed with a Wicke-Kallenbach method. Due to the fact that n-C_4H_{10} adsorbs strongly in zeolite pores, the separation tests were carried out from high to low temperatures. The experimental conditions used for the MFI-membranes used during the isobutane dehydrogenation and xylene isomerization eCMR testing is as follows:

MFI-membrane used for isobutane dehydrogenation: The pressures of both the feed and the sweep sides, were kept at 1.25 bar and no pressure difference was maintained over the membrane. A mixture of nitrogen, n-butane and hydrogen (composition nC_4H_{10}:H_2:N_2 of 15:12:73) were fed to the internal side of the membrane at a flow rate of 78 ml/min, while a counter-current sweep gas of 78 ml/min of N_2 flowed on the outer side. The composition of the feed and the exit streams (retentate and permeate) were analyzed online with a gas chromatograph, and the flow rates measured. The feed flow rates were controlled with mass flow controllers.

MFI-membrane used for xylene isomerization: The pressures of both the feed and the sweep sides, were kept at 1.2 bar and no pressure difference was maintained over the membrane. A mixture of nitrogen, n-butane and hydrogen (composition n-C_4H_{10}:H_2:N_2 of 14:14:72) were fed to the internal side of the membrane at a flow rate of 77 ml/min, while a counter-current sweep gas of 52 ml/min of N_2 flowed on the outer side. The composition of the feed and the exit streams (retentate and permeate) were analyzed online with a gas chromatograph, and the flow rates measured. The feed flow rates were controlled with mass flow controllers.

The n-butane/hydrogen separation factor (S_f) was determined with the following formula:

$$S_f\left(\frac{nC_4H_{10}}{H_2}\right)=\frac{\left(\left[nC_4H_{10}\right]/\left[H_2\right]\right)_{permeate}}{\left(\left[nC_4H_{10}\right]/\left[H_2\right]\right)_{retentate}} \qquad (2\text{-}46)$$

2.3 Physical characterization of membranes

The manufactured membranes were characterized by physical methods (Scanning Electron Microscopy (SEM), Proton Induced X-ray Emission (PIXE), Raman Back-Scattering (RBS) and Energy Dispersive (EDS).

2.3.1 Zeolite membranes

Results and discussion

Figure 2-21 is a SEM image of the cross-section of a typical zeolite membrane used during this study. The different layers of the support as well as the zeolite crystals are visible. Figure 2-22 is a magnified image of the inner layers of the zeolite membrane.

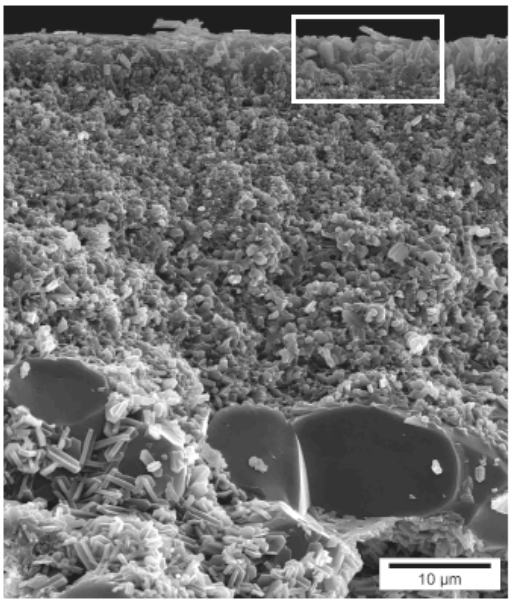

Figure 2-21 Typical SEM cross section image of prepared MFI-zeolite membrane [micrograph H. Mozzanega],

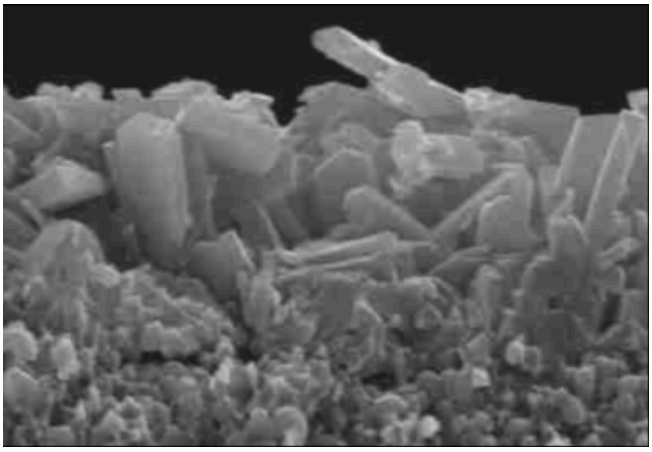

Figure 2-22 Enlarged image of membrane top layer [cross section image] (white block in Figure 2-21) [micrograph H. Mozzanega].

It can be seen that zeolite crystals on the surface are randomly orientated and disjointed. The random orientation is to be expected, considering the preparation method of in situ hydrothermal synthesis. During direct hydrothermal treatment nucleation, crystallization and growth occurs in one synthesis step. Heterogeneous nucleation occurs on the support, and the crystals grow in all directions on the external surface, and within the support pores [130]. Indeed, the crystals are attached to the support in an interlocking way and they extend into the support pore structure. A TEM image (Figure 2-23) was taken in the region of support layer 3 of the cross-section (Figure 2-23).

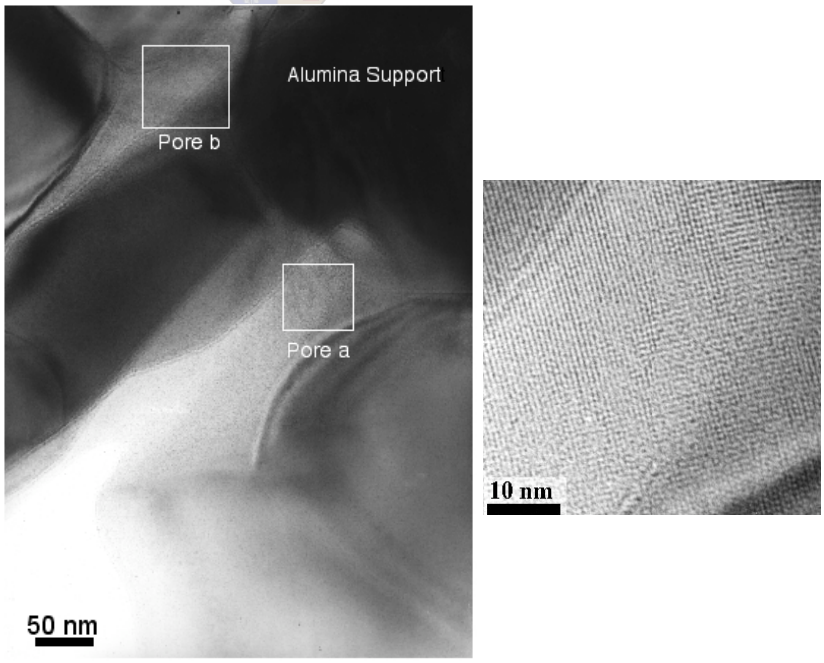

Figure 2-23 TEM of alumina support with pores (a) and (b) (left), and enlarged image of pore (a) (right) [Sample preparation and micrograph M. Aouine].

Figure 2-24 Fast Fourier Transform (FFT) images of pore (a) and (b) [M. Aouine].

The crystals in pore (a) and pore (b) are similar and have the same orientation (FFT), as can be seen from Figure 2-24. The parameters of the crystal in pore (a) was determined to be: a = 2.009 nm, b = 1.974 nm and v = 1.314 nm, orthorombic. The structure has been confirmed to be that of MFI with a Si/Al ratio of 10 given by EDS analysis. It could be expected that the ratio would be less, seeing that a pure Si source was used in the hydrothermal synthesis solution. An explanation for the low Si/Al ratio might be dissolution of aluminium from the α-alumina support membrane. It is a well established fact that when MFI membranes are prepared on α-alumina supports, Al can dissolve and be incorporated into the MFI framework, due to the high alkaline conditions present during synthesis [131]. This very high content of aluminium in an MFI structure is exceptional, and confers to the membrane material a high number of acidic sites.

The TEM image confirms that the pores of the α-alumina support are plugged with MFI-zeolite. The average pore size of the *top* layer of the α-alumina substrate is 200 nm, and in some cases 100 nm, which makes it easy for the solution to disperse and penetrate into the porous substrate. Depth EDS analysis results from a previous study in our group [132] on membranes prepared by the same method are given in Figure 2-25. Si is present throughout the first two layers of the support membrane and indicates that the zeolite crystals extend into the pore structure of the substrate. This diagram gives the overall Si/Al content (Al in substrate and zeolite crystals) and can therefore only be used to estimate to what extent the Si penetrates into the substrate. It is expected that the same phenomena will occur with membranes used in this study, as from previous work [132]. This data confirms that the pore-plugging technique is a successful method, with zeolite crystals localized in the pores of the porous support and extended onto the external surface. The zeolite can be classified as being ZSM-5. This pore plugging composite structure also allows for very good adhesion of the zeolite to the support and leads to higher thermal and

mechanical resistance of the material [101], when compared to conventional film-shaped zeolite membranes.

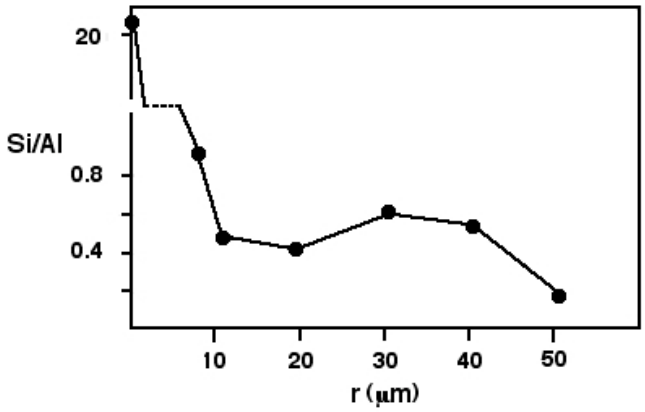

Figure 2-25 Radial distribution profile of Si/Al ratio of the macroporous support [132].

2.3.2 Palladium membranes

Results and discussion

SEM images of the palladium membrane surface were taken during various stages of the electroless plating procedure and thereafter. Figure 2-26a is an image of the membrane surface after the initial ~ 1 μm layer was deposited. Figure 2-26b is an image of the surface after deposition using a vacuum, and Figure 2-26c is the surface after pretreatment and subsequent hydrogen and nitrogen permeation testing had been done on it. From Figure 2-26a it can be seen that the deposited palladium grows into spheres, creating a surface with a relatively high roughness. When applying a vacuum on the layer, the *spheres* get sucked towards the porous support and the grain boundaries decrease, creating a relatively smooth surface. The palladium grains are closely packed, and a uniform, continuous film is formed on the support surface. Individual grain boundaries can still be seen, although they are greatly reduced. After heat treatment and subsequent membrane testing with hydrogen and nitrogen, the grain boundaries almost disappear completely. It is expected that post treatment would lead to a smoother, more integrated surface due to annealing of the palladium in hydrogen at 723 K. This is difficult to see from Figure 2-26c, although the grain boundaries seem to have disappeared. The form of the *spherical* grains changed (Figure 2-27b) and it seems as though the palladium recrystallizes in the grains and the end product appears to be *rose-like* structures. No pinholes can be seen.

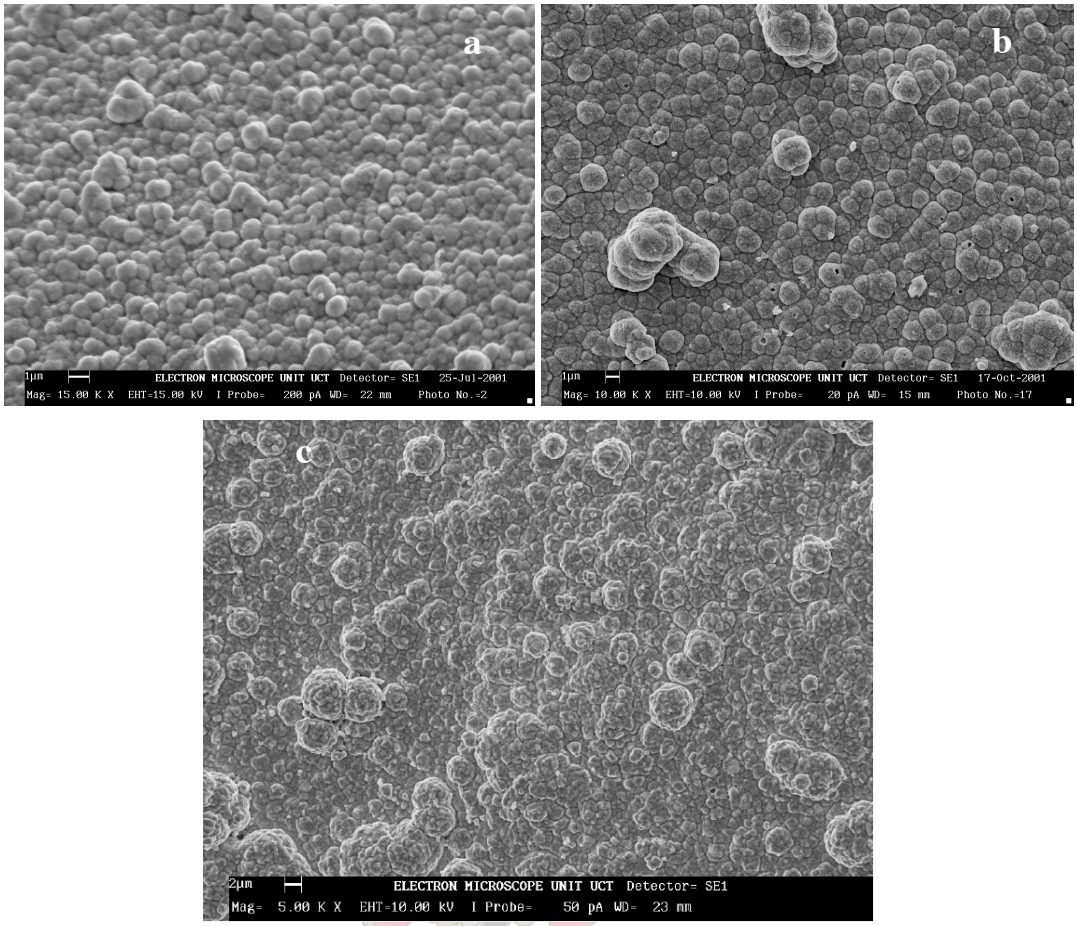

Figure 2-26 SEM Images of the palladium membrane surface during various stages after fabrication: (a) after deposition of initial 1 µm layer, (b) after deposition with vacuum and (c) after heat treatment and hydrogen testing.

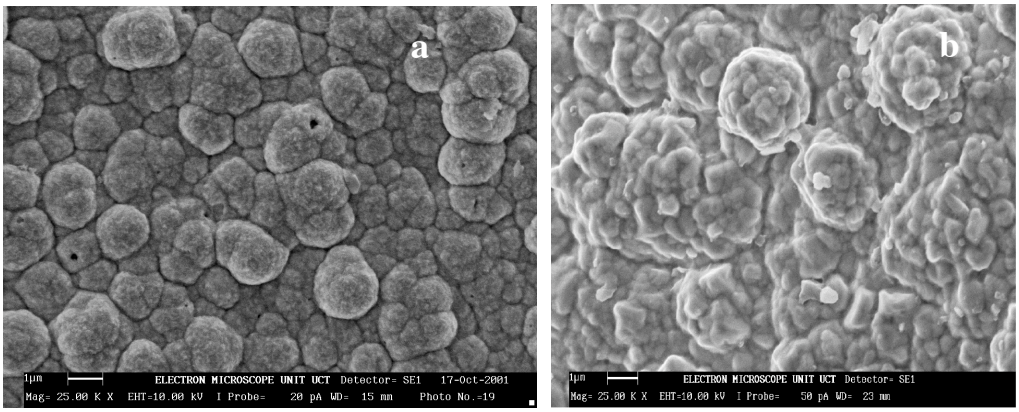

Figure 2-27 Higher resolution SEM images of the palladium membrane surface during various stages after fabrication (a) after deposition with vacuum and (b) after heat treatment and hydrogen testing.

In order to determine the best way to estimate the thickness of the palladium layer, a palladium supported membrane was characterized using various methods (Scanning

Electron Microscopy (SEM), Proton Induced X-ray Emission (PIXE), Raman Back-Scattering (RBS)). The membrane was cut along its length into two parts (e.g. Figure 2-28).

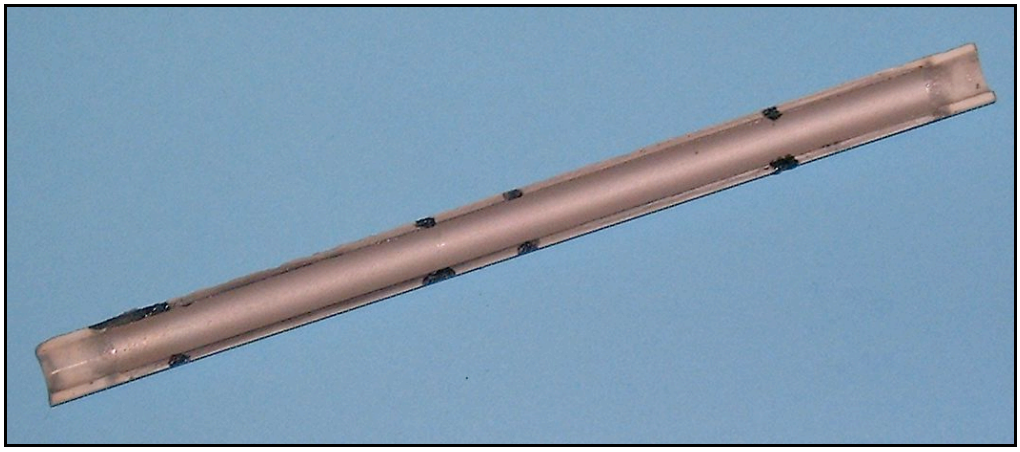

Figure 2-28 Picture of palladium membrane half used for PIXE.

One half was characterized using PIXE and RBS, while the other half was cut into smaller pieces and analysed with SEM.

Figure 2-29 is a typical result of the PIXE scan. It can be seen that palladium and tin are present. Tin was deposited while the electroless pretreatment was done. The red line indicates the curve that was fitted to the data in order to determine the thickness, while the purple curve represents the background.

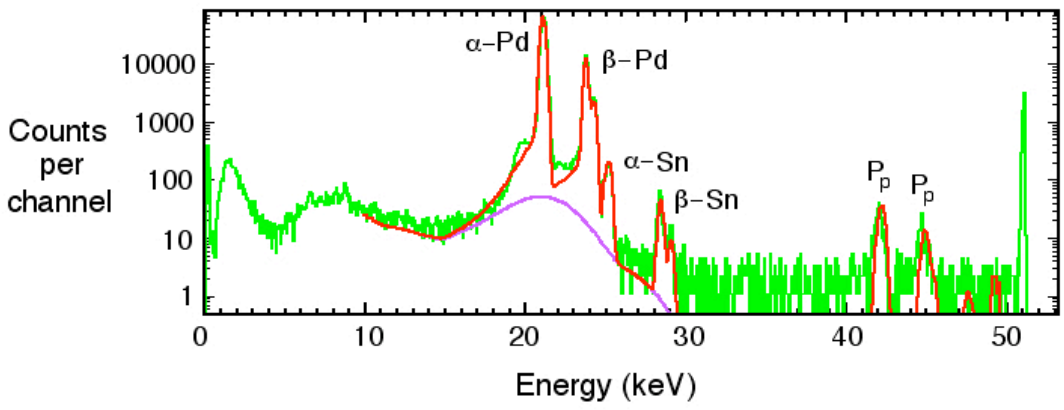

Figure 2-29 Typical PIXE scan.

The backscattering data (Figure 2-30) was also taken from the PIXE scan in order to determine the thickness by RBS analysis.

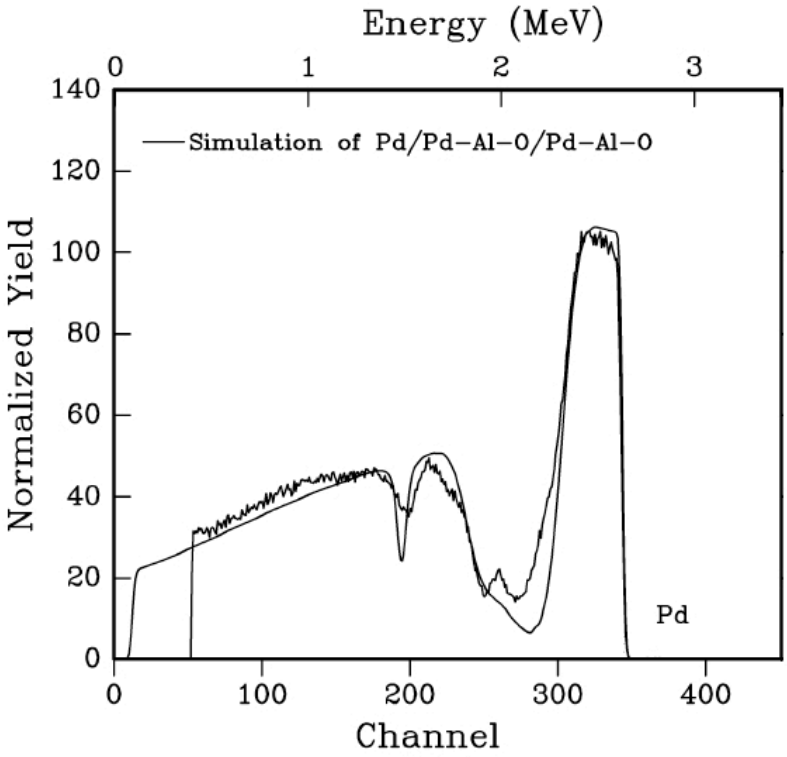

Figure 2-30 Rutterford backscattering diagram and simulation of a palladium supported membrane obtained from PIXE data.

The smooth curve represents the curve fitting for thickness estimation. In this example it was assumed that two layers were present, a solid palladium layer and a mixed palladium/α-alumina layer. It can be seen that this assumption led to a fairly good fit of the curve to the data. Hence, this assumption was used to determine the thickness by RBS analysis. The various thicknesses of the membrane as determined by PIXE and RBS analysis are presented in Figure 2-31. The two methods yield different values for the thickness of the membrane, which may be due to the difference in the analysis technique and the assumptions made to calculate the thickness. Both methods, however, indicate that the thickness along the length of the membrane is relatively even, with some thicker parts at the endings near the enamel.

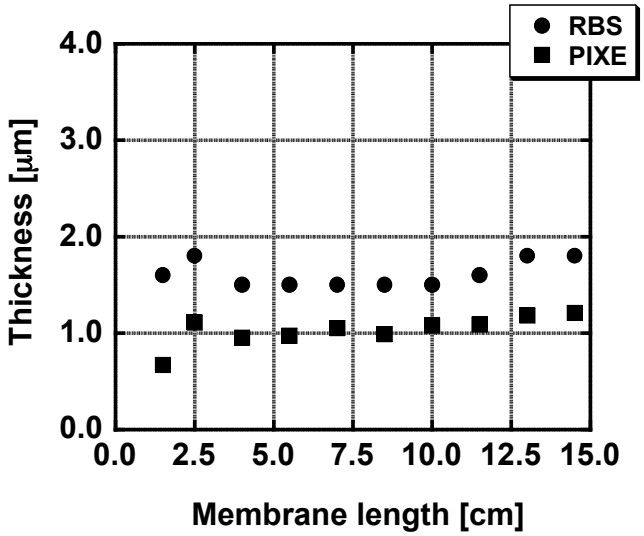

Figure 2-31 Membrane thicknesses as determined from PIXE and RBS (data compliments of Prof. Przybylowicz, iThemba LABS, South Africa).

The other half of the membrane was cut into pieces along the length and cast in resin, and SEM pictures were taken of the pieces at various points around the circumference Figure 2-32.

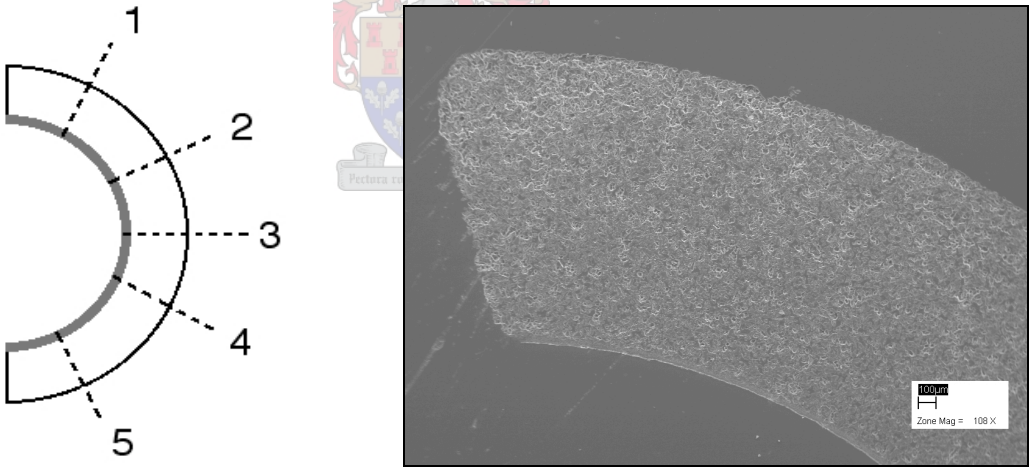

Figure 2-32 Cross-cut section of the membrane (left) diagram of cross-cut with various points of thickness analysis around the circumference of the tube, (right) SEM image of the cross-cut sections.

The thickness of the membrane differs at various points along the circumference as presented in Table 2-5.

Table 2-5 Membrane thickness at various positions along the circumference of the half tube.

Position	Thickness [μm]
1	1.7
2	1.7
3	3.1
4	3.1
5	2.5
Average	2.4

This average thickness is in good agreement with the theoretical calculated thickness of 2.5 μm. The theoretical thickness of the palladium layer was calculated assuming that the plated Pd mass is the sum of the mass increase during plating, plus half of the mass increase obtained after the pretreatment [14]. The volume of the plated Pd was then calculated assuming that the Pd film was solid and dividing the mass by the density of pure Pd (12g/cm^3). The theoretical thickness was consequently calculated using the volume and the area available for plating. It has been shown that some of the palladium penetrated into the support, therefore half of the preplated mass was taken as the amount that penetrated into the support. This is the same method that was used by Keuler [14] to determine his palladium membrane thicknesses.

It can therefore be said that the thickness of the membrane differs around the circumference of the tube, which may account for the difference in the calculated thicknesses through RBS and PIXE analysis from the SEM thickness analysis. The PIXE scans are point analysis and they were taken in the middle of the tube-half. The form of the tube (semi-circle) may have also affected the beam that was reflected off the surface.

2.4 Gas mixture separation and single gas permeation testing of membranes

Mixture (n-butane, hydrogen) separation testing was performed for the MFI-zeolite membranes and single gas (N_2 and H_2) permeation testing was performed on the palladium membranes.

2.4.1 Gas mixture separation testing of MFI/alumina composite membranes

Results and discussion

At the CNRS/IRC the standard procedure for MFI/alumina composite membrane characterization after fabrication, is n-butane/hydrogen mixture separation testing.

The temperature and pressure dependency of single gas permeance for zeolite membranes are fairly complex. In most cases, selectivity for mixture components differ from the ideal selectivity based on single component permeance data. This is because the presence of one component affects the sorption and diffusion properties of the other components in the mixture. For example, the blocking effect of a component with stronger adsorption is observed in many cases (n-Butane/hydrogen mixture separation testing). At low temperatures n-butane blocks the MFI-zeolite pores, due to its higher adsorption capability, making the pores inaccessible for the weaker adsorbing hydrogen [114]. High n-butane/hydrogen separation factor values (at CNRS\IRC a value of 10 is the criteria) at room temperature would therefore be an indication of a *good* quality MFI-zeolite membrane.

Figure 2-33 is a graph of the n-butane/hydrogen separation factor of the MFI-zeolite composite membrane (data complements of CNRS/IRC), used in the isobutane dehydrogenation study, as a function of temperature. It can be seen that the separation factor is higher than 10 (15), which means that the membrane can be classified as high quality (quasi defect free). The decrease in the separation factor with temperature is due to the fact that the adsorption of n-butane becomes less important at higher temperatures, which is a characteristic of the temperature dependant adsorption coefficient of n-butane. The same phenomenon is visible in Figure 2-34.

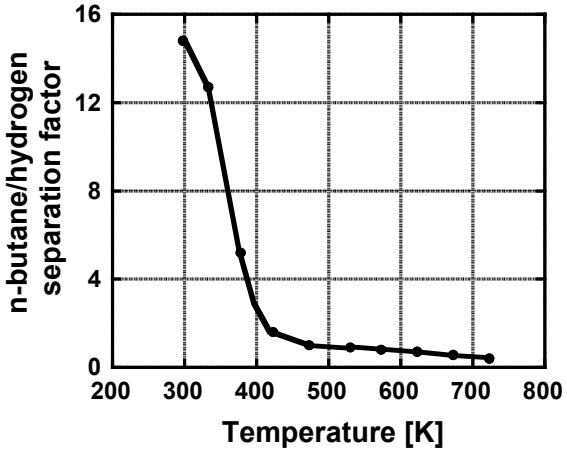

Figure 2-33 n-Butane/Hydrogen separation factor of the MFI-zeolite composite membrane used for isobutane dehydrogenation as a function of temperature.

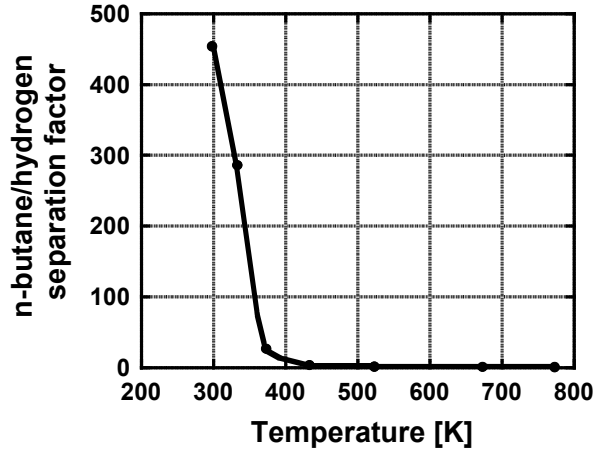

Figure 2-34 n-Butane/Hydrogen separation factor of MFI-zeolite composite membrane used in xylene isomerization study.

Figure 2-34 is a graph of the n-butane/hydrogen separation factor of the MFI-zeolite composite membrane (data complements of Dr. Y. Li, CNRS/IRC) used in the xylene isomerization study, as a function of temperature. It can be seen that the separation factor was very high at room temperature (454), indicating that this membrane was defect free. The first mentioned membrane was prepared on a support with a 0.2μm toplayer, while the support of the MFI-zeolite composite membrane used during the isomerization experiments had a 0.1μm toplayer.

2.4.2 Single gas characterization of palladium membranes

Single gas, nitrogen and hydrogen, permeation testing was carried out on the palladium membranes. For palladium, the high temperature single gas tests lend insight into the quality of the film.

Results and discussion

Nitrogen permeation tests on Palladium membranes

The quality of the Pd film can be determined through nitrogen single gas testing. If the palladium layer is defect free then no nitrogen will go through the layer.

Causes of nitrogen permeance through Pd membranes during single gas permeation testing include:

- leaking through defects in the Pd film,
- leaking at the stainless steel reactor, graphite ring, enamel interfaces, and
- leaking at the porous membrane, non-porous enamel, and Pd film interfaces.

Nitrogen permeance through defects is dependent on the size and number of the defects. A membrane with defects can be described as a porous medium (macro– and mesoporous), with pressure driven separation processes through the porous layer. These transport mechanisms will be viscous flow and Knudsen diffusion. The gas transport will be given by the following equations:

$$N = F_p(P_h - P_l) \tag{2-47}$$

$$F_p = F_{PK} + F_{PV}P_{AVE} \tag{2-48}$$

where F_p is the permeance, F_{PK} is the permeance due to Knudsen diffusion, $F_{PV}P_{AVE}$ is the contribution due to viscous flow, P_{AVE} is the mean pressure, and P_l and P_h the pressure on the low and high pressure sides, respectively. F_{PK} and F_{PV} are given by the following expressions:

$$F_{PK} = \left(\frac{2\varepsilon r_p}{3\tau lRT}\right)\left(\frac{8RT}{\pi M}\right)^{0.5} \tag{2-49}$$

and

$$F_{PV} = \frac{\varepsilon r_p}{8\tau\eta lRT} \tag{2-50}$$

where ε is the medium porosity, η the viscosity of the gas, r_p the mean pore size, τ the tortuosity factor, l the medium thickness, and M the molecular weight of gas. Plots of single gas permeance as a function of average pressure, or temperature, will therefore

give insight into the defects present [133]. If the defects are predominantly mesoporous ($2\ nm < d_p < 50\ nm$) then the contribution of the viscous flow, is negligible when $P_{AVE} < 1$ MPa [6].

Results are presented for each membrane synthesized and the single gas permeance data are used to try and describe the defects present and therefore Pd layer morphology.

Permeance as a function of average pressure can be seen for palladium membranes with thickness 1.9 μm in Figure 2-35. The slopes of the graph at various temperatures are relatively small, which indicate some viscous flow. If one, however, considers the temperature dependency (Figure 2-36) of the permeance, then it seems as though there is no definite temperature dependence. Both viscous and Knudsen diffusion are inversely dependent on temperature which would mean that when the temperature increases then the permeance decreases. The increase in average pressure is small, but significant. Gas transport through leaks display the same permeance behaviour as large pores, showing viscous flow. The permeance here may therefore be due to leaks and not defects.

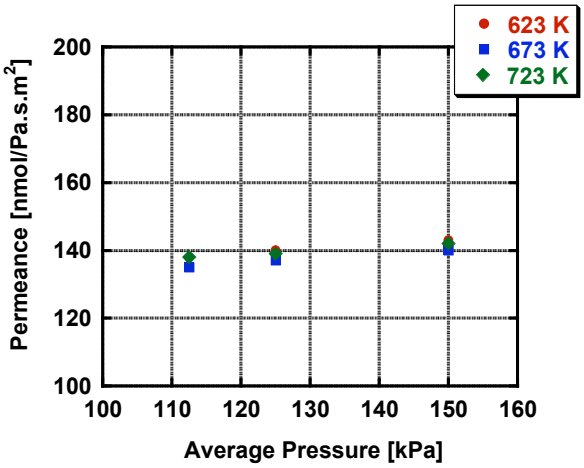

Figure 2-35 Permeance as a function of Average Pressure (membrane 1.9 μm).

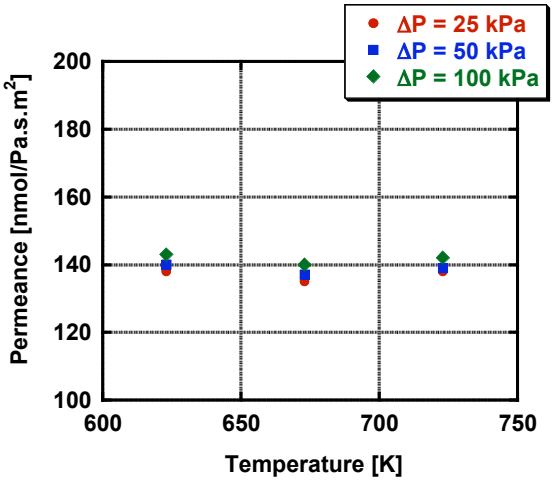

Figure 2-36 Nitrogen permeance as a function of temperature (membrane 1.9 μm).

The same trend can be seen in the nitrogen permeance graphs (Figure 2-37 & Figure 2-38) for the palladium membrane with thickness 4.8 μm. The permeance increases as the average pressure increases (Figure 2-37), however, increases in permeance are more prominent for this membrane. For this membrane, nitrogen permeance is only observed after a certain pressure is applied within the membrane. Dittmeyer *et al.* [64] reported similar results for their palladium membranes, also made by electroless plating, and accounted for the increase in flux with pressure as flow through leaks. It is expected that membranes with a thicker palladium layer would have less defects and therefore the nitrogen flux may to be due to leaking.

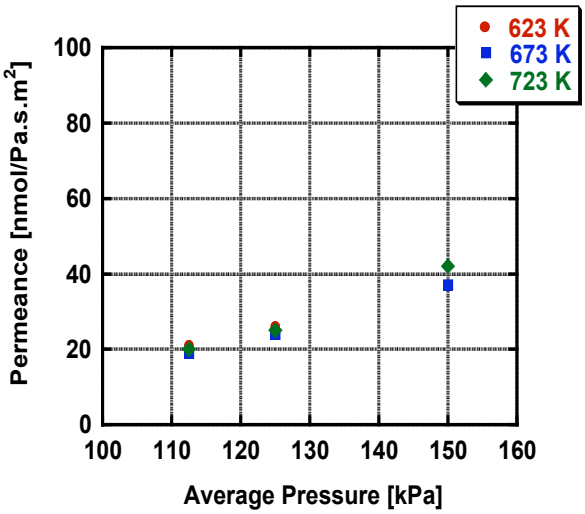

Figure 2-37 Nitrogen permeance with average pressure (membrane 4.8 μm).

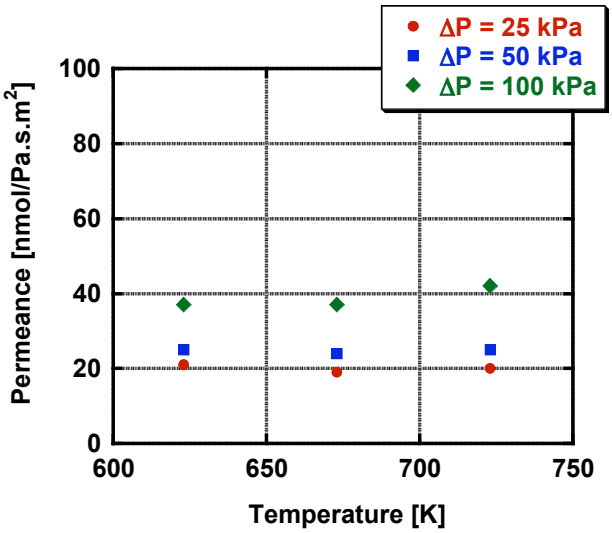

Figure 2-38 Nitrogen permeance as a function of temperature (membrane 4.8 μm).

The membrane with a thickness of 2.9 μm shows a permeance decrease with temperature (Figure 2-39) and increase with average pressure (Figure 2-40). Here there is definite evidence of viscous flow through pores in the membrane, accompanied by Knudsen diffusion. The contribution of Knudsen diffusion is higher than the viscous flow. Viscous flow indicates macro-defects and in the case of palladium membrane films it may be cracks in the membrane layer. Cracks in the membrane could form due to the mismatch in the thermal expansion coefficients (TEC) between the porous ceramic substrate and the Pd film (the TEC difference being in the order of 7 μm/m.K) [76].

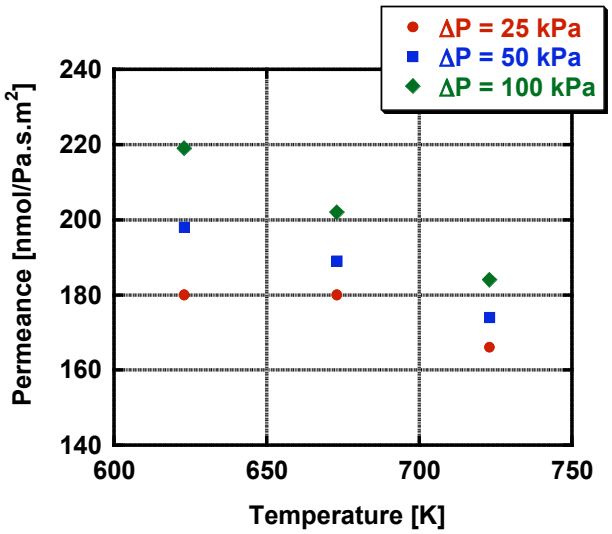

Figure 2-39 Nitrogen permeance as a function of temperature (membrane 2.9 μm).

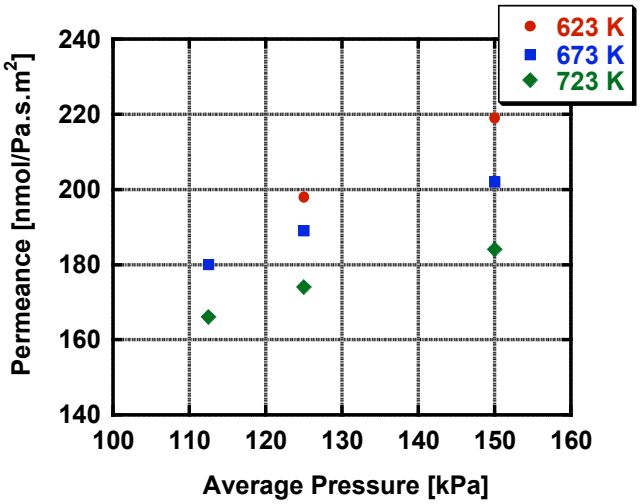

Figure 2-40 Nitrogen permeance as a function of average pressure (membrane 2.9 μm).

Some of the nitrogen diffusion may also be due to leaking. If we compare results obtained for the permeance test during one run (test 1) with another (test 2) (after cooling, membrane storing and subsequent pre-treatment of the membrane), then we get the following graph for nitrogen permeance as a function of average pressure at 723 K (Figure 2-41). If nitrogen permeance during the first permeation test (test 1) was exclusively due to flow through defects then these defects will not disappear when the next test is done, on the contrary some more defects might form. There is a reduction in the nitrogen permeance from test 1 to test 2, which can only be due to better membrane sealing. It has therefore, been shown that some of the nitrogen permeance is due to leaking through membrane seals. It is expected that this would be at the membrane enamel, graphite seal interface.

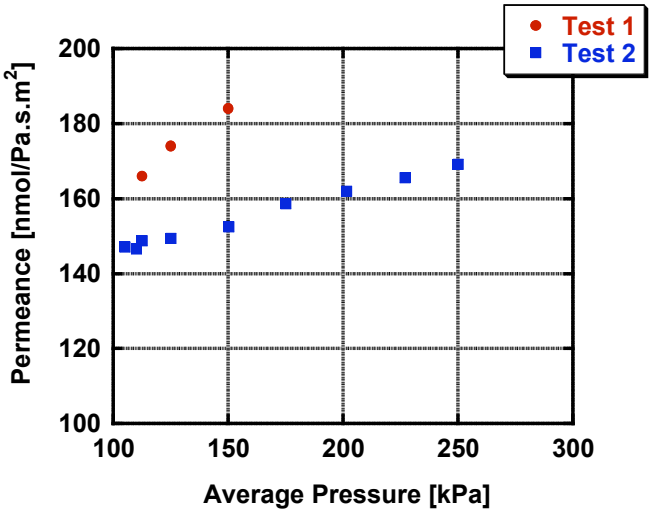

Figure 2-41 Comparison between two different membrane permeation tests performed on membrane 2.9 μm at 723 K.

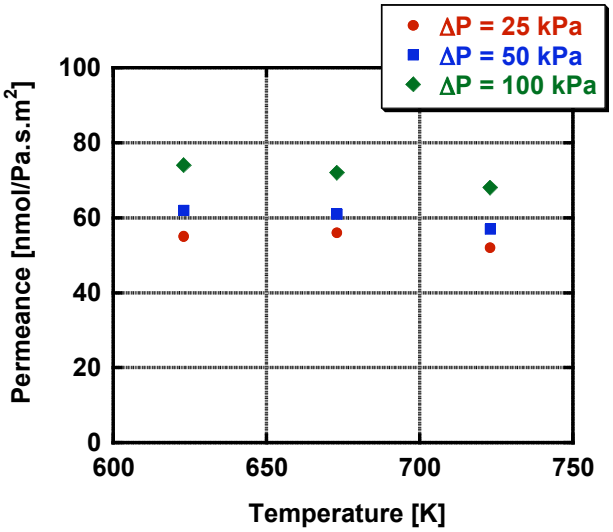

Figure 2-42 Nitrogen permeance as a function of temperature (membrane 4.2 μm)

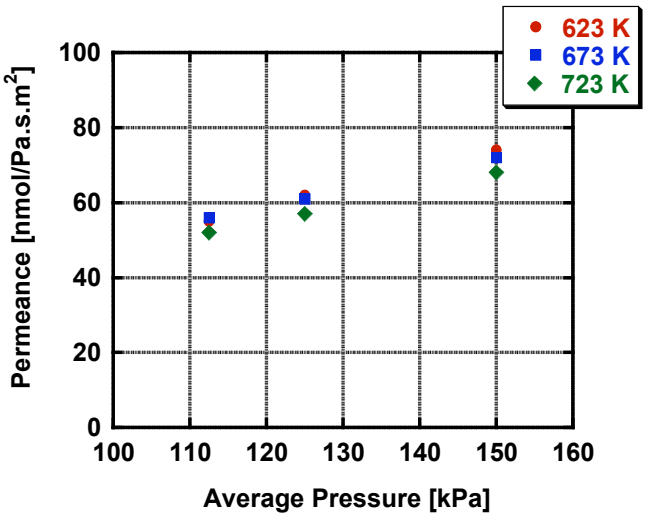

Figure 2-43 Nitrogen permeance as a function of average pressure (membrane 4.2 μm).

The membrane with a thickness of 4.2 μm also displays a decrease in nitrogen permeance with an increase in temperature (Figure 2-42), and an increase in nitrogen permeance (Figure 2-43), with increasing average pressure. The contribution of Knudsen diffusion is less pronounced than for membranes with thicknesses of 2.9 and 1.9 μm at temperatures 623 and 673 K, indicating less mesoporous defects. At 723 K there is no indication of Knudsen diffusion ($F_{PK} < 0$). It is believed that the contribution of the viscous flow is due to leaks as is in the case of the membrane with a thickness of 4.8 μm.

To conclude, it can therefore be said that membranes with predominantly mesoporous defects were produced. Leaking at the enamel, graphite ring interface does however also contribute to the permeance. The magnitude of the leaks are not known and differ from membrane to membrane. The reason for leaking is that it is very difficult to see if a membrane is sealed properly within the stainless steel membrane module. At room temperature the membranes appear to be sealed properly, but at high temperatures and after heat treatment the nitrogen permeance is significantly higher. If the graphite seals are tightened too much then the membranes crack at the membrane enamel, graphite seal interface after high temperature heat treatment. This happened in three cases with membranes not shown here, and the cracking may be due to graphite ring expansion during the oxygen pre-treatment step.

Hydrogen permeance through membranes

As mentioned before, dense Pd membranes are permeable to hydrogen alone. If the membrane contains defects or if leaking occurs, then these effects would contribute to the

total flux of hydrogen through the membrane as measured during experiments. The hydrogen flow path through the composite membrane can be seen in Figure 2-44. If it is assumed that the support membrane's resistance to mass transfer is negligible (macroporous support toplayer 200 nm), then the rate of hydrogen transport through the composite membrane will be dependant on the rate through the defects/leaking as well as through the *dense* metal film.

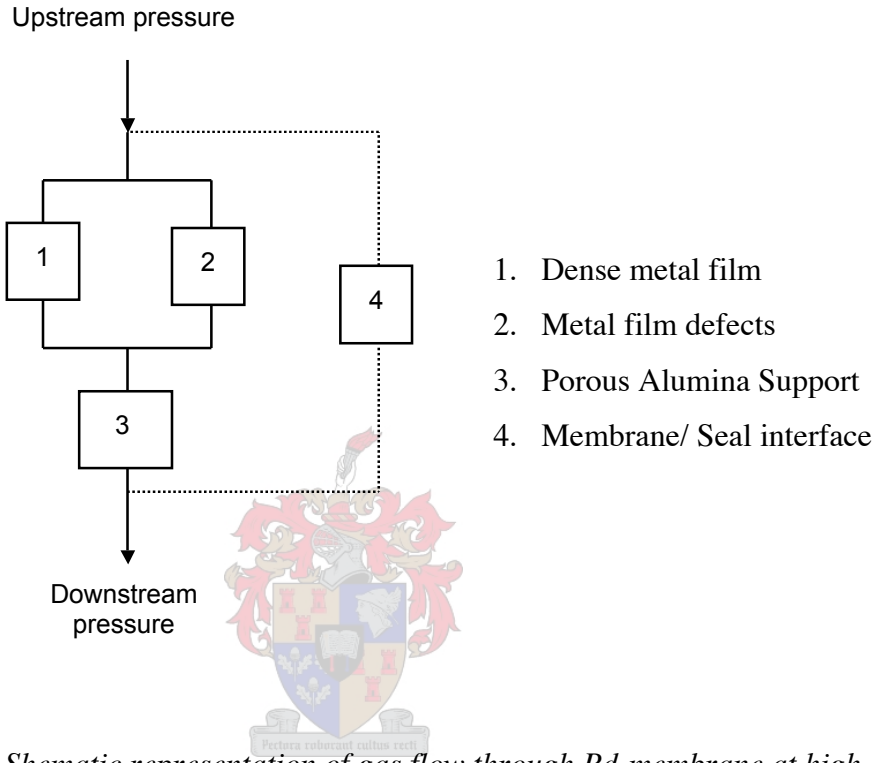

Figure 2-44 Shematic representation of gas flow through Pd-membrane at high temperature.

In order to correct for the contribution of hydrogen flow due to defects, the following equations have been used [134]:

$$F_{PH_2(2+4)} = 3.74 F_{PK(N_2)} + \frac{\mu_{N_2}}{\mu_{H_2}} F'_{PV(N_2)} \qquad (2\text{-}51)$$

$$N_{H_2(2+4)} = F_{PH_2(2+3)}(P_h - P_l) \qquad (2\text{-}52)$$

with $F_{PK(N_2)}$ the intercept, and $F'_{PV(N_2)}$ the slope of the nitrogen permeance vs. average pressure curves determined during nitrogen single gas permeation tests for each membrane (e.g. Figure 2-45).

The effect of defects/leaks on the hydrogen flux values through the palladium membranes are presented in Table 2-6. The contribution of defects/leaks (12 and 11 % compared to 3 and 4 %) towards the hydrogen flux is higher for thinner membranes (1.9

and 2.9 μm) compared to the thicker palladium membranes (4.2 and 4.8 μm). This indicates that the difference in flux values between the various membranes could not solely be attributed to leaks, but that defects were present.

Table 2-6 Hydrogen flux and corrected hydrogen flux at 723 K, ΔP = 250 mBar.

Membrane Thickness [μm]	Hydrogen flux [mmol/m^2/s]	*corrected* Hydrogen flux [mmol/m^2/s]	Hydrogen through defects [%]
1.9	102	90	12
2.9	120	107	11
4.2	78	76	3
4.8	58	55	4

The corrected hydrogen flux values ($N_{H_2(total)} - N_{H_2(2+4)}$) are plotted against the driving force for the permeation pressure. Values of n have been analyzed graphically by finding the R^2 values that best described the data, and in this case it was 1. This is not uncommon, and it has been shown by Dittmeyer *et al.* [64] that in literature, membranes thinner than 4 – 5 μm show hydrogen pressure exponents close to 1. During previous studies the flux data was mostly analyzed graphically and checked to determine if they complied with a pressure exponent of 0.5 or 1. Therefore 4 – 5 μm cannot be taken as the limiting thickness. It has been seen during the analysis of this data, that for the differential pressures used (5000-25000 Pa), the value of *n* did not have a significant effect on R^2. A value of 1 for n indicates that the hydrogen flux does not exclusively depend on atomic diffusion of hydrogen through the palladium, but is influenced to some extent by other processes, e.g. hydrogen adsorption on the palladium surface.

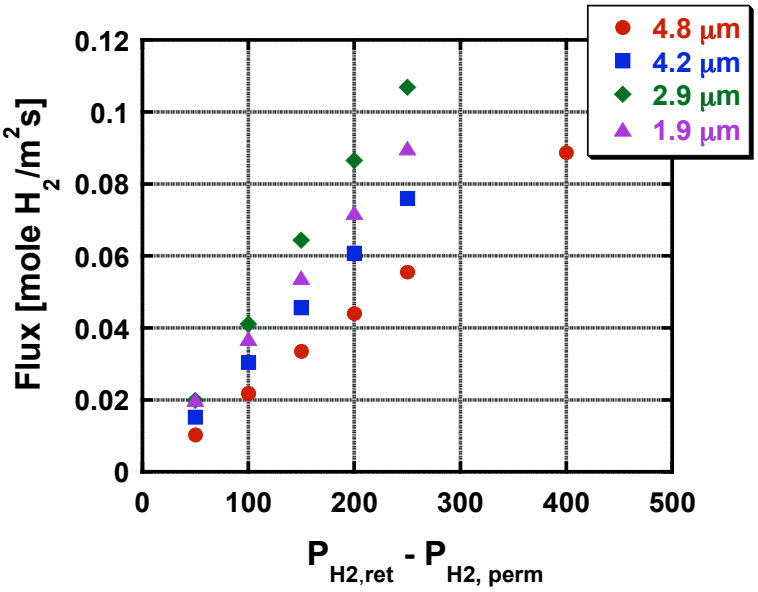

Figure 2-45 Corrected hydrogen flux as a function of driving force at 723 K.

Table 2-7 gives the activation energies as determined by the Arrhenius plots (equation 2-38) of the *corrected* hydrogen permeance values (pressure normalized flux). The temperature ranges used here were 623 to 723 K.

Table 2-7 Activation energies as determined by Arrhenius plots of $ln(\frac{P_{H2}^{er}}{l})$ *vs. 1/T*

Membrane Thickness µm	Activation Energy (E_a) kJ/mol	P_0^{er} 10^{10} mol.m/m^2.s
1.9	11.6	0.47
2.9	17.2	2.1
4.2	20.9	4.2
4.8	26.6	9.1

The activation energies (E_a) range from 12-27 kJ/mol and it increases with membrane thickness. A value for E_a of 22 kJ (433 to 913 K) for thick solid Pd membranes, where diffusion through Pd was definitely the controlling factor, was reported by Holleck [135]. There is a general trend in literature, that the hydrogen permeability factor (P_0^{er}) decreases with decrease in palladium thicknesses below 100 µm [136], as is the case here. In other words the permeability, which is supposed to be independent of membrane thickness, is actually not independent of thickness at thicknesses lower than 100 µm. It has been attributed to many factors, including the increased influence of surface effect,

concentration dependence of the permeability, transport resistance of the substrate material, palladium surface contamination, flow of hydrogen through grain boundaries, thermal history, lattice dilatation and/or lattice defects. It should be noted that electroless plated membrane layers are characterized by a different morphological structure than pure palladium, which might lead to the variation in the E_a from dense palladium. If we assume that grain boundaries still exist within the microstructure of each film produced here, then with thickness increases, more grain boundaries will be present. This leads to an increase in activation energy, due to a combination of surface diffusion effects and bulk metal transition.

The apparent activation energy of membrane 1.9 μm is in good agreement with values obtained in literature (10 – 12 kJ/mol) [67, 137, 138]. Keuler [14] also reported an increase in the apparent activation energies for membranes produced with a similar electroless plating technique.

Palladium membrane ideal selectivities

The ideal selectivity, or permselectivity of palladium membranes represents the ability of the membrane to separate two components from each other in a mixture if no interaction between the components takes place. For palladium, this would not be far from the mixture behaviour due to the fact that the interaction between two components can only manifest itself through movement through the defects. If we look at the various permselectivities from the different thickness membranes then we can see that with an increase in thickness, the permselectivities increase, except for the membrane with a thickness of 2.9 μm. This indicates that with an increase in the membrane thickness the amount of defects in the palladium layers decrease.

The magnitude of the permselectivities indicates the relative importance of defects. It should be noted that in the previous section it was established that some of the nitrogen present in the permeate stream was due to leaks. Because it is difficult to quantify these leaks, it cannot be said with accuracy that these values seen here are representative of the true permselectivities in the membranes. It would, however, represent a worst-case scenario. The permselectivity increases with temperature due to the fact that the hydrogen permeance increases with temperature through the palladium [16] and the nitrogen permeance decreases with temperature through viscous or Knudsen-sized defects, which have the net effect of an increase in permselectivity.

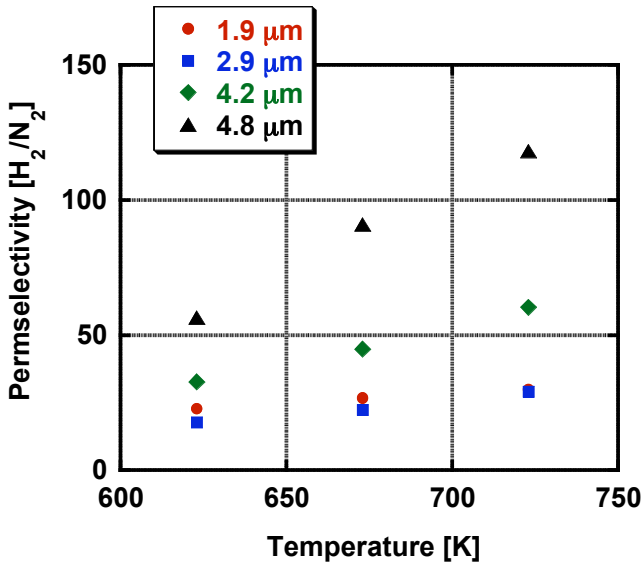

Figure 2-46 Permselectivity as a function of temperature for different membrane thicknesses.

Table 2-8 list some of the hydrogen permeance and permselectivities obtained in literature for various membranes prepared by electroless plating. The hydrogen permeance values agree well with values obtained in the literature for the various thicknesses, except for work done by Keuler [14] and Wu *et al.* [138]. The selectivity values for membranes prepared during this study are, however, lower than others seen here and can be attributed to the *higher* nitrogen permeance values obtained during this study. If the hydrogen permeance values obtained by Keuler are compared with the ones obtained during this study, then it is clear that there is a relatively high difference between these values. The plating procedure used here was similar to Keuler's method, except that the Pd concentration in the plating solution was changed, whilst keeping the concentration ratios of all the chemicals constant. A number of factors could have contributed to the differences in performances of the membranes that were essentially prepared by the same plating method:

- The influence of leaks on the permeance is higher for shorter membranes.
- The supports might have differed in morphology, seeing that no characterization of the supports were performed before plating, for both studies.
- Keuler spent a large amount of time preparing Pd membranes, gradually eliminating supports/membranes that gave low separation factors during experiments.

- Keuler also re-used the same support a large number of times and it may have had an influence on the final Pd membrane obtained.

The objective of this study was not to investigate the electroless plating technique, or to produce membranes with extra high separation factors. It was only necessary to produce palladium membranes that displayed superior hydrogen fluxes compared to the MFI-zeolite/alumina composite membrane, for application in the eCMR for isobutane dehydrogenation. The palladium electroless plating technique is very sensitive to experimental conditions, e.g. surface state of the alumina support, defects in the supports (high bubble flows), and purity of the precursor solutions, to name only a few. This investigation into the electroless plating technique would therefore be a study on its own, and is currently an MSc. project at the Department of Process Engineering, University of Stellenbosch.

Table 2-8 Comparison of the permeance of different palladium-based composite membranes prepared by electroless plating, thickness range 0.3 – 5 μm.

Thickness [μm]	Δ Pressure H_2 [kPa]	Temperature [K]	Permeance [μmol/Pa/s/m^2]	Selectivity (H_2/N_2)	Reference
0.3-0.4	10-45	773	6.3	1140	[126]
1.43	2-8	723	11.7	971	[14]
1.9	25	723	4.1	30	This study
2.1	2.55	723	4.1	-	[139]
2.4	3-11	723	8.4	1465	[14]
2.9	25	723	4.8	29	This study
3.86	4-13	723	6.4	666	[14]
4.2	25	723	3.1	60	This study
4.43	6-16	723	4.7	4297	[14]
4.8	25	723	2.3	118	This study
4.82	25	673	1.7	91	This study
5	100	673	1.42	100-200	[64]

2.5 Summary

The MFI-zeolite/alumina composite membranes used in this study were pore-plugged with zeolite crystals that extend onto the surface layer of the membrane support. The zeolite is confirmed to be ZSM-5 with a varying Si/Al content with penetration into the porous support. Palladium membranes of various thicknesses have been fabricated by an adapted electroless plating technique based on a method developed by Keuler [14]. SEM images indicated that continuous Pd film was formed on the support surface with no visible defects. Nitrogen single gas permeation testing indicated that membranes with predominantly mesoporous defects were produced. Leaking at the enamel, graphite ring interface did, however, also contribute to the permeance. The magnitudes of the leaks are unknown, and differ from membrane to membrane. The permselectivities (H_2/N_2) of the membranes increase with membrane thickness, indicating a decrease in defects with membrane thickness. The hydrogen permeance values are lower than values obtained by Keuler, who used a similar electroless plating technique to produce supported palladium membranes. The objective of this study was not to investigate the plating procedure, but problems associated with the procedure were identified and are consequently being addressed in an MSc. project at the Department of Process Engineering. However, palladium membranes were successfully prepared and are ready to be used in eCMRs.

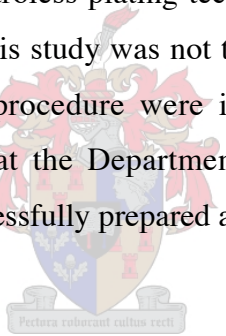

3 Development of a new generation CMR testing bench and experimental procedures

Extractor Catalytic Membrane Reactor experiments were done with the membranes being inert and packed with a catalyst in the lumen of the membrane. In this chapter the various experimental procedures are described for isobutane dehydrogenation and xylene isomerization in eCMRs. Most of the experimental work was performed at the Institut Recherches sur la Catalyse (CNRS\IRC), Lyon (France). The design and construction of a Membrane Reactor Testing Bench for the Department of Process Engineering (DPE), University of Stellenbosch, by me, will also be described.

3.1 Literature review: State of development of industrial eCMRs

Although research in the field of inorganic Catalytic Membrane Reactors are growing, there are very few reports of industrial installations [140]. If we consider this lack of industrial implementation purely from a technical point of view, then the following problems can be identified:

1) The need exists for defect-free, high selective and high permeable membranes. Considerable progress has been made on producing better membranes on lab-scale, but difficulties exist in reproducing lab-scale results on larger scale suitable for commercialization.
2) Metallic and ceramic membranes have to be housed in a reactor assembly with feed/ product lines and other reactor boundaries. Studies on Catalytic Membrane Reactors focus on using tabular membranes with a tube and shell membrane configuration. This is mainly due to the industrial need for membranes in tabular form. An industrial catalytic membrane reactor unit can for instance consist of a cascade of membranes in parallel, fitted into a shell, with different distributors for the feed and permeate. Challenges in this area would be the creation of a pressure driving force for gas phase permeation, heat provision/ uptake from the reactor and temperature control and membrane sealing [141, 142].

3.1.1 Creation of a pressure driving force for gas phase permeation

A pressure driving force for gas phase permeation in membrane reactors can be created using three different design approaches and they are:

1) Application of a pressure difference between the retentate and permeate compartments (evacuation of the permeate if required) – all types of CMRs.
2) The use of an inert sweep gas in the retentate compartment (e.g. nitrogen, helium, etc.) – eCMRs
3) The use of a reactive sweep gas to consume the permeated product – combination of eCMR and distributor CMR.

For eCMRs, the way in which the driving force is created will depend on the application of the product. For industrial application an inert sweep gas to remove an *extracted* product is the worst choice due to the fact that the sweep gas has to be provided and compressed, while rendering a diluted product. If the reaction kinetics allows it, a better alternative is to feed the reacting compounds at an elevated pressure, creating a pressure difference large enough to flush out the extracted product. This, however, requires that the feed gas be compressed while the product is obtained at a lower pressure. An excellent choice if a pure product is required. The third option, i. e. reacting the extracted product with a reactive sweep gas, is promising because it avoids the disadvantages of the other two. An example would be the coupling of hydrogenation and dehydrogenation reactions, if hydrogen is the extracted product [64]. For bench scale experimental experiments an inert sweep gas is the preferred choice due to the complexity of the other two.

3.1.2 Heat provision/ uptake from the reactor and temperature control

So far most bench scale research focuses on providing heat to the membrane by use of an electrical furnace. Research on managing heat effects in membrane reactors focus on:

1) Distribution of the reactor feed in order to control the temperature rise in exothermic reactions.
2) The control of temperature and partial pressure by distributing the fluxes of energy and material along the reactor to manipulate the formation of intermediate products in complex reaction networks.
3) The use of exothermic and endothermic reactions on the permeate and retentate sides of the membrane to satisfy each others' heat needs (thermal coupling).

In the last case the feed of one reaction will be the permeate of the other reaction. This will then lead to the energy needs of one reaction (endothermic reaction) being met, while efficiently using the permeate of the parallel reaction, and therefore eliminating

problems that might arise from obtaining a diluted product. Although in theory this option sounds promising, practical difficulties such as matching the temperature and heat release/ uptake limits the application of this concept [140].

No real progress has been made from a process engineering side to design a membrane reactor heating devise for industrial use.

3.1.3 High temperature sealing of membrane reactors

High temperature sealing of membrane reactors into a membrane housing devise has been a problem up to now. Currently sealing is done with graphite seals, which has shown to be moderately effective for sealing. However, no cheap comparable alternative is available and there has been no recent research aimed at addressing this issue [141]. A way of bypassing the sealing issue is to use stainless steel membrane supports, which can be welded into the membrane reactor housing.

3.2 Reactor/ membrane configuration

The reactor module (Figure 3-1) consists of the membrane placed within a stainless steel reactor, divided into an internal and external compartment (shell and tube configuration), by sealing the membrane into the reactor with graphite rings (Origraph® Cefilac - Garlock).

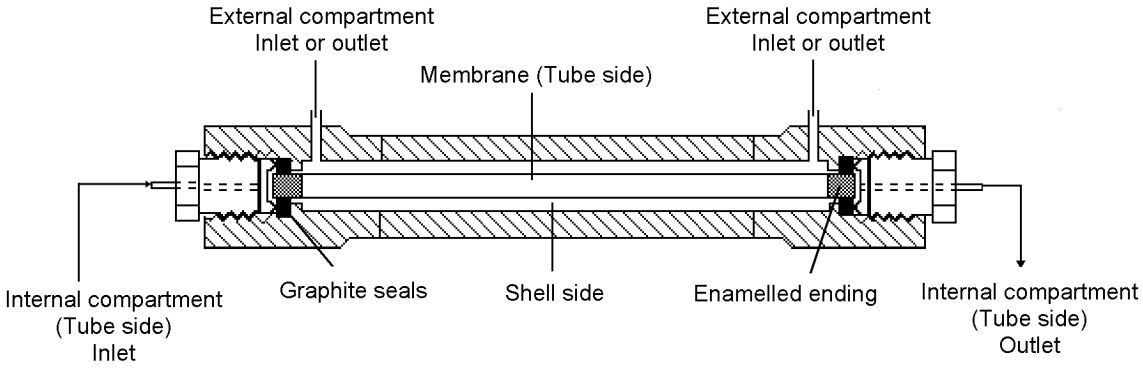

Figure 3-1 Membrane/ stainless steel membrane module configuration.

The graphite rings provide sealing at high temperatures. The rings have the dimensions, inner diameter (ID) of 10.4 mm, outer diameter (OD) of 17.9 mm and a width of 5 mm, and a density of 1.6 g/cm^3.

The reactor module is heated in a cylindrical furnace, length of 30-35 cm (CNRS\IRC, France) or 50 cm (DPE, South Africa), with temperature control. The

thermocouple for furnace temperature control is situated in the middle, on the surface of the stainless steel reactor module. The open endings of the cylindrical furnace are closed off by packing glass wool for isolation, preventing heat loss to the environment. The temperature profile within the membrane is measured with a type K thermocouple (d = 0.5 mm, length 50 cm), placed inside a 1/6" tube, which is located inside of the membrane along the length. The thermocouple can move inside the tube, enabling the user to measure the internal temperature profile of the membrane along its length.

For eCMR experiments the reactions were carried out in the reactor module, with the membrane packed with a catalyst in the lumen of the membrane.

3.3 H_2 and N_2 Single gas testing

Single gas permeation testing was done in the dead-end mode. This means that the exit of the retentate was closed off, forcing the gas through the membrane at a certain internal pressure to the permeate side. The permeate exit next to the retentate inlet was closed off, and the other exit left open to allow the gas to escape at atmospheric pressure. The flow rate of the exiting gas was measured with a Drycal 500 flow meter (CNRS\IRC, France), or a bubble flow meter (DPE, South Africa). Figure 3-2 is a simplified flow diagram to illustrate single gas permeation testing.

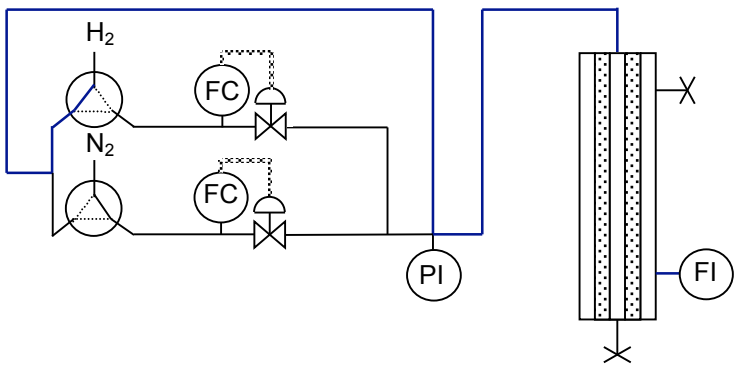

Figure 3-2 Simplified flow diagram of the single gas permeation set-up.

3.4 Isobutane dehydrogenation in an eCMR

Isobutane dehydrogenation testing was done in microporous MFI/alumina composite and dense supported palladium membranes. Hydrogen was extracted from the reaction zone. A description of the experimental procedures used for the evaluation of MFI/alumina and Pd/alumina membranes for isobutane dehydrogenation are discussed below.

3.4.1 Experimental set-up

Figure 3-3 is a schematic diagram of the experimental bench used at the CNRS\IRC, France. Red and blue lines indicate the flow of the feed (blue), and sweep gases (red) during catalytic membrane reaction experiments, or for mixture separation testing, with analysis of the exit gasses (internal and external), and sweep in the counter-current mode.

Various operating modes are possible on this set-up, which include:

- Feed, either internal or external (valve 6).
- Flow through the compartments, either co- or counter current (valve 3).
- Pressure control across the membrane between + 0.5 bar to – 0.5 bar (PC).
- Reactor module feed bypassing (valve 5), allowing the analysis of the feed or pretreatment of the membrane.

The feed and sweep gas flow rates are controlled with Brooks mass flow controllers (FC). The internal pressure is measured by a pressure gauge (Keller PAA23) that is situated after the feed mixing point (PI). It has a range of 0 – 5 Bar (abs). The differential (trans-membrane) pressure between the internal and external compartments of the reactor are measured with a differential pressure indicator (Keller DP22), and regulated with a pneumatic valve (Kammer 800377) situated at the exit of the external compartment. A PID controller (West – 2075) is used to control the pneumatic valve, allowing the user to fix the differential pressure across the membrane, except when the injection valve is open. The regulation of the differential pressure can also be performed manually, by using valves 11 and 12. The Kammer valve can be bypassed (valve 10) if no control or manual control of the differential pressure is required.

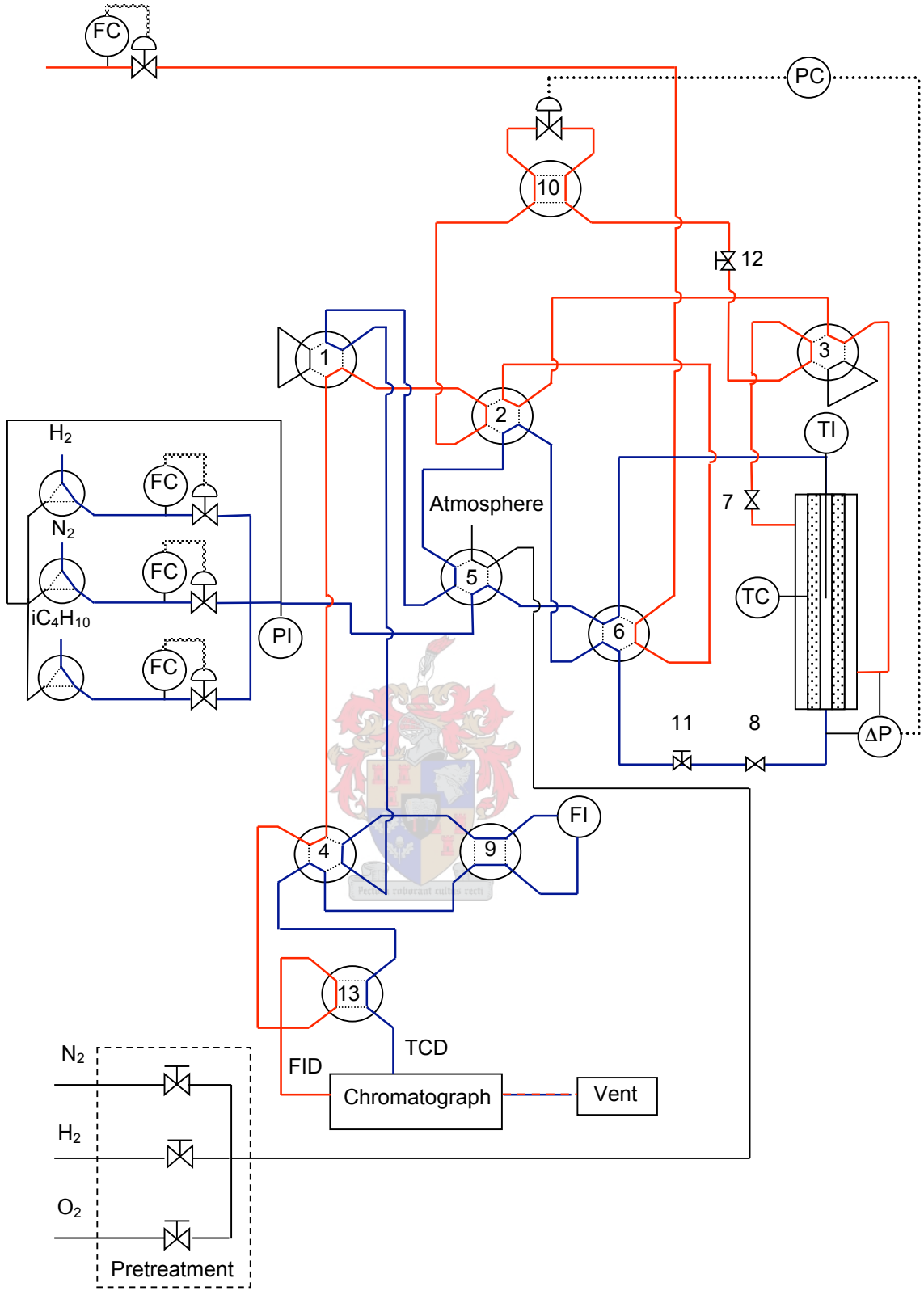

Figure 3-3 Isobutane dehydrogenation experimental bench (CNRS/IRC, France).

The flow rates of the two compartments and the feed are measured by a Drycal 500 flow meter. This can be achieved by alternating the stream to be measured by using valve 4. The flow meter may be bypassed using valve 9.

Valve 7 and 8 are shut-off valves for the one side of either the internal or external compartment.

The composition of the feed and two exit gas mixtures are analysed using a gas chromatograph (Shimatdzu – GC14A). The chromatograph is equipped with two detectors: A Flame Ionization Detector (FID) for the analyses of hydrocarbons, and a Thermal Conductivity Detector (TCD) for the analyses of hydrogen. These two detectors operate in parallel, and the stream (internal or external exit) attached to each detector is alternated by a pneumatic valve (valve 13). This valve is automatically controlled when the basic program of the integrator (Shimadzu – CR5) is run. The operating conditions of the gas chromatograph (GC) and characteristics of the packed bed columns are given in Table 3-1.

Table 3-1 Operating conditions of the gas chromatograph (GC) and characteristics of the packed bed columns.

Detector	Type	FID	TCD (Intensity 80mA)
Column	Type	"GC-Graphpac" – Packed column	Carbosphere – Packed column
	Composition	0.19 % Piric acid on GC-graphpac	
	Length	7 ft	6 ft
	Diameter	1/8"	1/8"
Carrier Gas	Type	Nitrogen (N_2)	Nitrogen (N_2)
	Flow Rate	30 ml/min	52 ml/min
Oven Temperature		313 K	313 K
Analysis Gasses		iC_4H_{10} and iC_4H_8	Hydrogen (H_2)

3.4.2 Materials

The *MFI/alumina membrane* and *Pd supported membrane* were prepared as discussed in Chapter 2. The α-alumina support membranes had top layers of 0.2 μm. The thickness of the palladium membrane was calculated to be 4.8 μm.

The *catalyst* was a trimetallic Pt-In-Ge supported on a MFI zeolite [143]. Indium and Germanium were introduced within the zeolite precursors before hydrothermal synthesis. After calcination, the final material contained 0.8 wt.% of both Indium and Germanium. Platinum (0.5 wt%) was then introduced in the zeolite via an exchange/impregnation technique using $Pt(NH_3)_4(OH)_2$ as a precursor. Before catalytic use, the solid was activated in situ under flowing H_2 at 823 K for 10 hours. The powdered catalyst was extruded into pellets using the following preparation method: The powder was thoroughly mixed with 20 wt % of kaolin. Water was slowly added to form a paste, and pressed into pellets ca. 2 mm in size using a syringe-like labscale extruder. After the pellets were formed, it was dried at 373 K and calcined at 723 K in air for 2 hours (heating rate: 1 K/min) [65].

3.4.3 Transport measurements: single gas and mixture

Before membrane testing, the membranes were pretreated. The pretreatment procedures used were described in section 2.2.4 (page 43). Single gas permeation measurements were performed for hydrogen, nitrogen and isobutane at 723 K in the dead-end mode. Separation tests on the MFI/alumina membrane were performed by a modified Wicke-Kallenbach method (transmembrane pressure was kept to zero) with a mixture of isobutane and hydrogen diluted in nitrogen. The feed rate was 1.2 l/hr (0.2 iC_4H_{10}, 0.2 H_2 and 0.6 N_2), and the temperature and counter-current sweep flow rates were varied. The MFI/alumina membrane was packed with inerts in order to simulate the catalyst pellets.

The separation factors (S_f) were determined by the following formula:

$$S_f\left(\frac{H_2}{iC_4H_{10}}\right)=\frac{\left(\left[H_2\right]/\left[iC_4H_{10}\right]\right)_{permeate}}{\left(\left[H_2\right]/\left[iC_4H_{10}\right]\right)_{retentate}} \qquad (3\text{-}1)$$

The permeance of a component in the mixture was determined with equation (2-1), using $\Delta P_{Mean(i)}$ (counter-current sweep mode), using the following equation known as the "log mean partial pressure difference":

$$\Delta P_{Mean(i)}=\frac{\Delta P_i^0-\Delta P_i}{\ln\left(\frac{\Delta P_i^0}{\Delta P_i}\right)} \qquad (3\text{-}2)$$

with $\Delta P_i^0 = P_i^{feed} - P_i^{permeate}$ and $\Delta P_i = P_i^{retentate} - P_i^{sweep}$. ΔP_i^0 is the partial pressure difference of component *i* in the feed and permeate exit streams at position L = 0, while ΔP_i is the partial pressure difference of the retentate and sweep streams at L = L.

The sweep flow rate can be expressed as a volumetric flow rate (ml/min or ml/s) or in terms of the linear velocity (m/s) of the sweep gas as it moves across the membrane outer surface. If the sweep gas moves through the shell side, as is the case here, then the sweep gas velocity can be determined with the following equation:

$$\mathbf{u}_{sweep} = \frac{\dot{v}_{sweep}}{\frac{\pi}{4}(d^2_{reactor} - d^2_{membrane_{OD}})} \tag{3-3}$$

with $\mathbf{u}_{sweep}$ the linear sweep velocity, $\dot{v}_{sweep}$ the volumetric sweep flow rate, $d_{reactor}$ the diameter of the stainless steel reactor and $d_{membrane_{OD}}$ the outer diameter of the composite membrane. It should, however, be noted that the volumetric flow rate is temperature and pressure dependent and this should be taken into account when calculating the linear velocity of the sweep gas at the membrane outer surface. The sweep gas volumetric flow rates presented in this dissertation are the values at standard temperature and pressure.

3.4.4 Isobutane dehydrogenation in a eCMR

The catalyst pellets were packed in the permeable volumes of the palladium supported and MFI/alumina composite membranes, and quartz wool was placed in the volume taken up by the enamel endings. The bulk density of the catalyst in the catalyst bed was 0.53 g/cm^3.

In order to activate the catalyst, and to prepare the Pd membrane for use, a pretreatment procedure needs to be performed. The individual pretreatment procedures for the catalyst and the membranes are not the same, and therefore a new procedure, which is a combination of the two pretreatment procedures, was developed and used.

Mériaudeau *et al*. [143] used the following catalyst activation method: Heating of the catalyst from room temperature to 593 K (heating rate 0.2 K/min) under O_2 flow. Flush the reactor with N_2 before switching to H_2 and increasing the temperature to 773 K (heating rate 1 K/min). Leaving catalyst under H_2 flow for 2 hours and cool to room temperature. Flush the reactor with N_2 before exposing the catalyst to air. The pretreatment of the Pd/alumina is explained in chapter 2.

The catalyst and membrane pretreatment methods were combined and a new procedure followed. The Pd/alumina membrane and catalyst were pretreated as follows: Heat the membrane in nitrogen to 593 K at 1 K/min. Switch from nitrogen to oxygen, and force 10 ml/min oxygen through the Pd layer and membrane wall from the feed side to the permeate side for 2 hours. Switch to nitrogen and heat from 593 K to 623 K (1 K/min).

Switch to H_2 and heat to 773 K (1 K/min) and leave for 2 hours. Cool down in nitrogen to reaction temperature (-1 K/min).

The MFI/alumina eCMR was pretreated using the standard pretreatment procedures for the MFI/alumina composite membrane and the catalyst.

Before the isobutane dehydrogenation reaction was started the feed flow rate was measured and the composition analysed. The feed flow rate was about 50 ml/min and the composition 0.2 iC_4H_{10}, 0.2 H_2 and 0.6 N_2. The reaction was performed at 723 K.

The eCMR reaction was done in the counter-current sweep flow configuration and the sweep flow rate varied between 0 and 185 ml/min. The differential pressure across the membrane was kept at zero. The compositions of the feed, retentate and permeate were analyzed on-line and the flow rates measured.

The conversion of isobutane and selectivity of the reaction to form isobutene was determined with the following equations:

$$Conversion = \frac{\left(x_{iC_4H_{10}} \cdot Q\right)_{feed} - \left[\left(x_{iC_4H_{10}} \cdot Q\right)_{retentate} + \left(x_{iC_4H_{10}} \cdot Q\right)_{permeate}\right]}{\left(x_{iC_4H_{10}} \cdot Q\right)_{feed}} \qquad (3\text{-}4)$$

$$Selectivity = \frac{\left(x_{iC_4H_8} \cdot Q\right)_{retentate} + \left(x_{iC_4H_8} \cdot Q\right)_{permeate}}{\left(x_{iC_4H_{10}} \cdot Q\right)_{feed} - \left[\left(x_{iC_4H_{10}} \cdot Q\right)_{retentate} + \left(x_{iC_4H_{10}} \cdot Q\right)_{permeate}\right]} \qquad (3\text{-}5)$$

where x is the mole fraction of isobutane (iC_4H_{10}) or isobutene (iC_4H_8), and Q is the flow rate of the feed, retentate and permeate, respectively.

The sub-/superscripts *permeate* and *retentate* refer to the exit streams of the retentate and permeate sides, while *sweep* refers to the sweep inlet/permeate inlet stream.

3.4.5 Isobutane dehydrogenation in a Conventional Reactor (CR)

The conventional packed bed reactor (CR) conversion was determined by closing the two exits of the permeate side of the eCMR, feeding to and analysing only the retentate side. These experiments were performed in conjunction with the eCMR isobutane dehydrogenation experiments and also at the same reaction conditions.

3.5 Xylene isomerization in an eCMR

Meta-xylene isomerization experiments were done in an MFI/alumina eCMR. Para-xylene was selectively extracted from the reaction zone. A description of the experimental procedures, used for the evaluation of MFI/alumina membranes for meta-xylene isomerization, will be given below.

3.5.1 Experimental set-up

The isobutane dehydrogenation experimental bench (Figure 3-3) was changed in order to allow the analysis and feeding of xylenes. Photos of the adapted isobutane dehydrogenation experimental set-up for xylene isomerization, is presented in Figure 3-4. It can clearly be seen that all the lines were heated and isolated with glass wool.

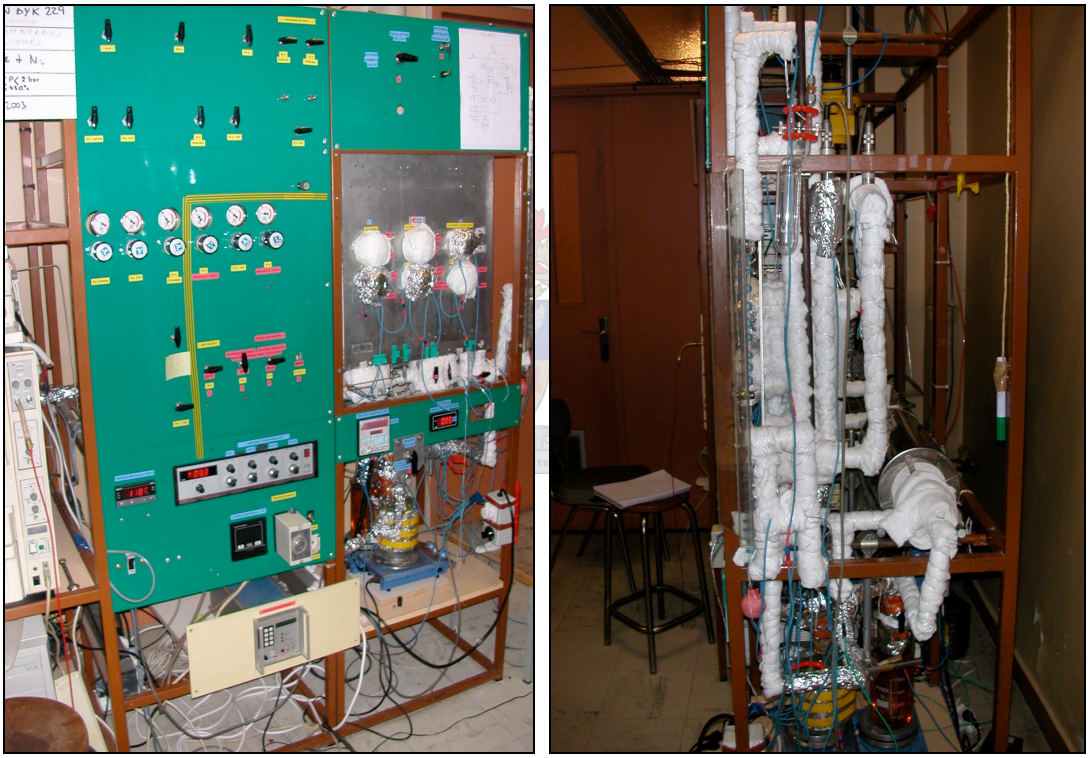

Figure 3-4 Photos of xylene isomerization experimental set-up: (left) front view and (right) side view.

Figure 3-5 is a schematic diagram of the experimental set-up used for xylene isomerization experiments (CNRS/IRC, France).

The xylenes were fed as gas phase diluted in nitrogen, using two saturators in series. The temperature in the first saturator was kept 5 K higher than the second one in order to ensure precise vapour saturation. All the pipes in the system were heated using heating tape and kept at 373 K in order to prevent any xylene condensation, and to ensure

correct xylene vapour pressure values. The flow rates of the various streams were measured using a bubble flow meter.

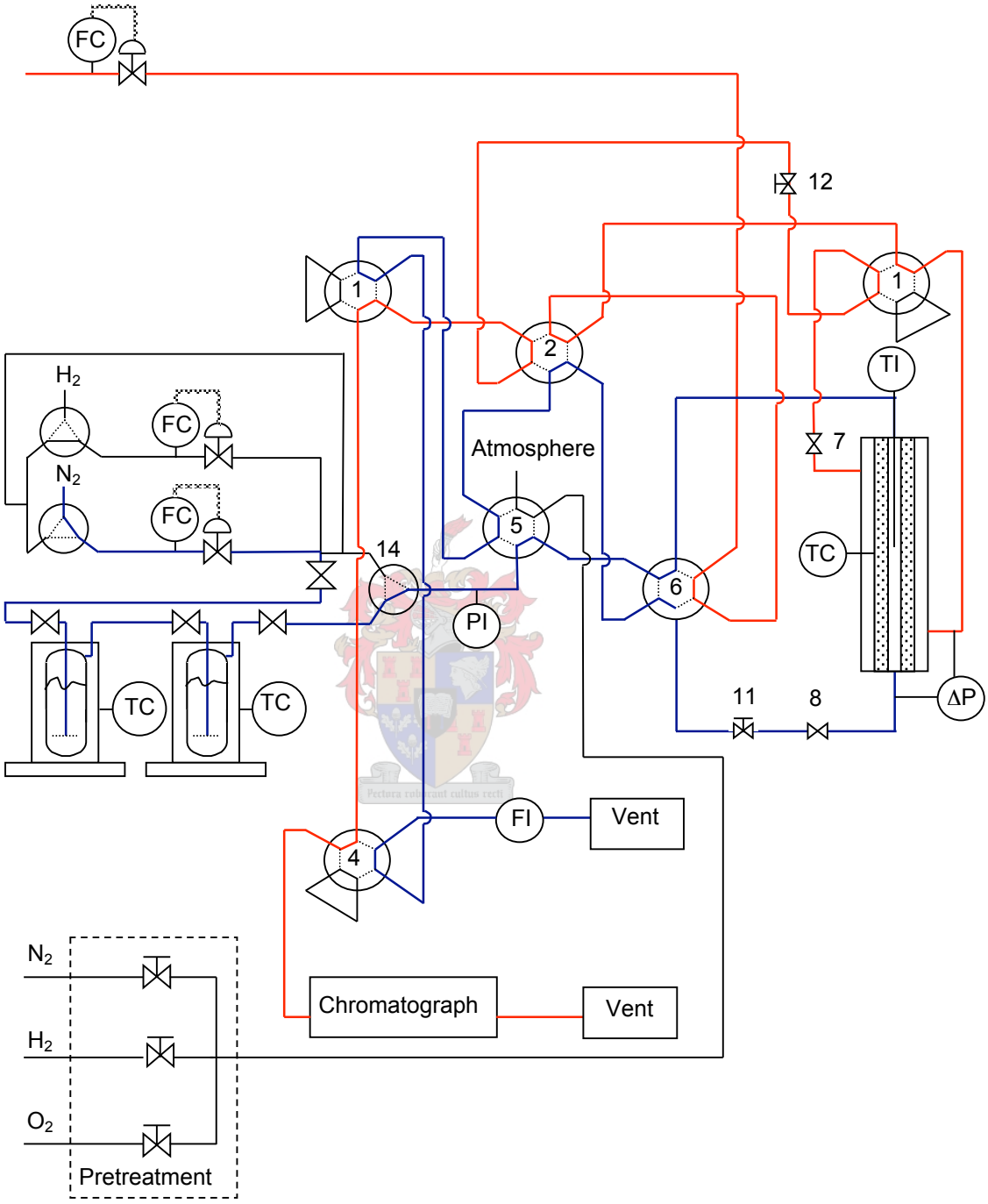

Figure 3-5 Xylene isomerization experimental bench (adapted from Figure 3-3).

The compositions of the feed, permeate and retentate streams were analyzed on-line with a gas chromatograph (Shimadzu, GC 14A), equipped with a FID detector and a

capillary column (Solgel-WAX, SGE). The GC operating conditions and capillary column properties are given in Table 3-2.

Table 3-2 Operating conditions and characteristics of the gas chromatograph for xylene isomer analysis.

Column	Type	Solgel-WAX (SGE) Capillary Column
	Composition	Polyethylene glycol in Sol-Gel matrix
	Length	30 m
	Diameter	0.51mm
Carrier Gas	Type	Hellium
	Feed Pressure	20 kPa
Split ratio		1:50
Injector Temperature		523 K
Detector	Type	Flame Ionization Detector (FID)
	Temperature	553 K
Oven Temperature		333 K

3.5.2 Materials

The *MFI/alumina composite membrane* was prepared as discussed in Chapter 2. The α-alumina support membrane had a top layer of 0.1μm.

The *catalyst* (Pt-HZSM5) was a commercial xylene isomerization catalyst (ISOXYL) from Süd-Chemie. The catalyst pellets were pulverized and diluted with kaolin powder to 5 wt% of the original and extruded into ca. 2-mm pellets, with a labscale extruder. Before catalytic use, the solid was activated in situ under H_2 flow at 673 K for 3 hrs.

Anhydrous xylene isomers were purchased from Sigma–Aldrich: meta-xylene 99+ %, para-xylene 99+ % and ortho-xylene 97 %.

3.5.3 Transport measurements: mixture

Before any membrane testing commenced, the MFI/alumina membrane was pretreated at 673 K under nitrogen flow for 4 hours.

Mixture separation tests were performed following a modified Wicke-Kallenbach method with a mixture of xylenes (1.5 kPa p-xylene, 4.5 kPa m-xylene and 1.35 kPa o-xylene) saturated in nitrogen at atmospheric pressure and 336 K. The feed flow rate was 60 ml/min and a counter-current nitrogen sweep was applied at 15 ml/min. The temperature of the membrane system was varied from 673 to 423 K and again from 423 to 673 K. The feed, retentate and permeate compositions were measured online using the GC.

The separation factors (S_f) were determined with the following formulas:

$$S_f\left(\frac{pC_8H_{10}}{mC_8H_{10}}\right)=\frac{\left([pC_8H_{10}]/[mC_8H_{10}]\right)_{permeate}}{\left([pC_8H_{10}]/[mC_8H_{10}]\right)_{retentate}} \tag{3-6}$$

$$S_f\left(\frac{pC_8H_{10}}{oC_8H_{10}}\right)=\frac{\left([pC_8H_{10}]/[oC_8H_{10}]\right)_{permeate}}{\left([pC_8H_{10}]/[oC_8H_{10}]\right)_{retentate}} \tag{3-7}$$

Equations 3-6 and 3-7 give the separation factors of para-xylene (pC_8H_{10})/meta-xylene (mC_8H_{10}) and para-xylene/ ortho-xylene (oC_8H_{10}). Equations (2-1) and (3-2) were used to determine the permeance of a component in the mixture.

3.5.4 Xylene isomerization in a eCMR

The fixed bed catalyst (weight 2.18 g) was packed (13 cm in length) in the lumen of the tubular membrane and the ends packed with quartz wool. Therefore, the catalyst bulk density in the bed was 0.43 g/cm^3. Meta-xylene vapour, saturated in nitrogen, was fed to the reactor at 330 K. The m-xylene isomerization reaction was carried out at various temperatures, feed flow rates and sweep flow rates. The differential pressure across the membrane was kept at zero by varying the external pressure of the membrane module. Nitrogen was used as a sweep gas in the counter current mode. The feed flow rates were kept high enough to keep the conversion below equilibrium in the catalytic bed, in order to avoid undesired by-product (toluene or ethylbenzene) formation. Permeate and retentate exit streams were analysed separately.

The yield of para-xylene in the retentate were determined with the following formula

$$Y_{pC_8H_{10}}^{retentate}=\frac{(x_{pC_8H_{10}}.Q)_{retentate}}{(x_{mC_8H_{10}}\cdot Q)_{feed}-\left[(x_{mC_8H_{10}}\cdot Q)_{retentate}-(x_{mC_8H_{10}}\cdot Q)_{permeate}\right]} \tag{3-8}$$

and in the permeate

$$Y_{pC_8H_{10}}^{permeate} = \frac{(x_{pC_8H_{10}}.Q)_{permeate}}{(x_{mC_8H_{10}} \cdot Q)_{feed} - \left[(x_{mC_8H_{10}} \cdot Q)_{retentate} - (x_{mC_8H_{10}} \cdot Q)_{permeate}\right]} \quad (3\text{-}9)$$

The addition of these two yields rendered the *combined mode* (CM) (permeate + retentate) para-xylene yield:

$$Y_{pC_8H_{10}}^{combined\ mode} = Y_{pC_8H_{10}}^{retentate} + Y_{pC_8H_{10}}^{permeate} \quad (3\text{-}10)$$

The reaction selectivity for para-xylene production in each stream (permeate, retentate and combined) was determined with the following formulas:

$$Selectivity_{pC_8H_{10}}^{retentate} = \frac{\left(x_{pC_8H_{10}} \cdot Q\right)_{retentate}}{\left(x_{pC_8H_{10}} \cdot Q\right)_{retentate} + \left(x_{oC_8H_{10}} \cdot Q\right)_{retentate}} \quad (3\text{-}11)$$

$$Selectivity_{pC_8H_{10}}^{permeate} = \frac{\left(x_{pC_8H_{10}} \cdot Q\right)_{permeate}}{\left(x_{pC_8H_{10}} \cdot Q\right)_{permeate} + \left(x_{oC_8H_{10}} \cdot Q\right)_{permeate}} \quad (3\text{-}12)$$

$$Selectivity_{pC_8H_{10}}^{combined\ mode} = \frac{\left(x_{pC_8H_{10}} \cdot Q\right)_{permeate} + \left(x_{pC_8H_{10}} \cdot Q\right)_{retentate}}{\left[\left(x_{pC_8H_{10}} + x_{oC_8H_{10}}\right) \cdot Q\right]_{permeate} + \left[\left(x_{pC_8H_{10}} + x_{oC_8H_{10}}\right) \cdot Q\right]_{retentate}} \quad (3\text{-}13)$$

The sub-/superscripts *permeate* and *retentate* refers to the exit streams of the retentate and permeate sides.

3.5.5 Xylene isomerization in a Conventional Reactor (CR)

Separate Conventional Reactor experiments were done. The MFI/alumina composite membrane was replaced with a stainless steel tube of identical dimensions, and the reaction conditions were kept as close as possible to the eCMR operation. The CR was fed on the retentate side, and only the feed and retentate exit streams were analyzed and measured. Each of the experiments was performed with a fresh catalyst sample. Reasons as to why a stainless steel tube was used for the new conventional reactor experiments will be presented in chapter 5.

3.6 Design and construction of an experimental bench

In this section the design and construction of a membrane reactor experimental bench at the Department of Process Engineering at the University of Stellenbosch is described. When this study started, the existing experimental bench had been dismantled and therefore it was necessary to design and construct a membrane reactor experimental bench. The experimental set-ups described in the previous sections were at the Institut Recherches sur la Catalyse (CNRS) laboratories in Lyon, France.

3.6.1 Problem statement

Designing and construction of a membrane/ membrane reactor testing bench able to do the following membrane/ membrane reactor treatment and testing on:

1. Membrane treatment/ pre-treatment.
2. Single gas membrane permeation testing (dead-end mode and Wicke-Kallenbach method).
3. Gas mixture separation testing (Wicke - Kallenbach method).
4. Gas phase reaction testing inside the membrane reactor. For this case isobutane dehydrogenation.

The idea was therefore, to design and construct a membrane reactor experimental bench similar to the ones in France, improving on the short comings, keeping the design simple, and working within the budget constraints of the Department of Process Engineering, University of Stellenbosch, South Africa.

3.6.2 Experimental set-up

All the design requirements of the experimental set-up were met, and a diagram of the experimental bench in South Africa is given in Figure 3-9.

Hastings mass flow controllers (HFC 202) (FC) (Figure 3-6) are used to feed the hydrogen (0 - 50 ml/min), nitrogen (0 - 50 ml/min) and isobutane (0 - 50 ml/min), as well as the nitrogen sweep gas (0 - 300 ml/min).

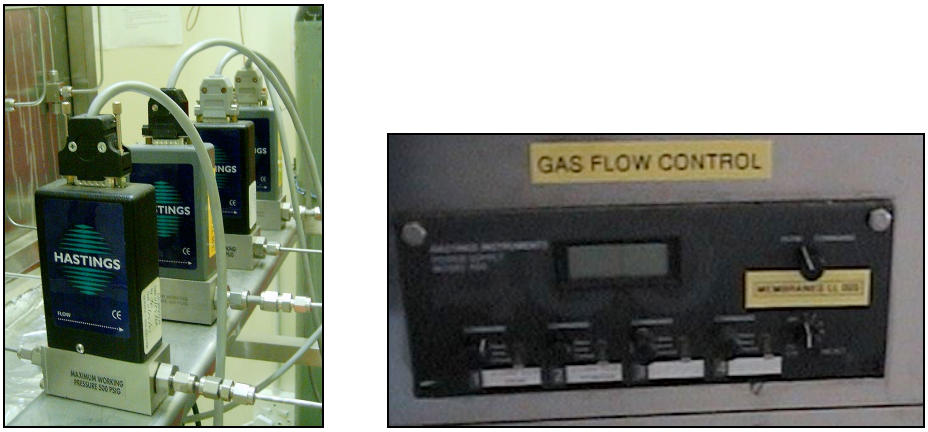

Figure 3-6 Hastings flow controllers (left) and power supply (right).

The internal pressure (Figure 3-7) is measured with a Keller PR-21S pressure probe, range 0 – 5 Bar (abs). The differential (trans-membrane) pressure between the internal and external compartments of the reactor is measured with a differential pressure indicator (Keller DP23), range +500 to –500 mBar.

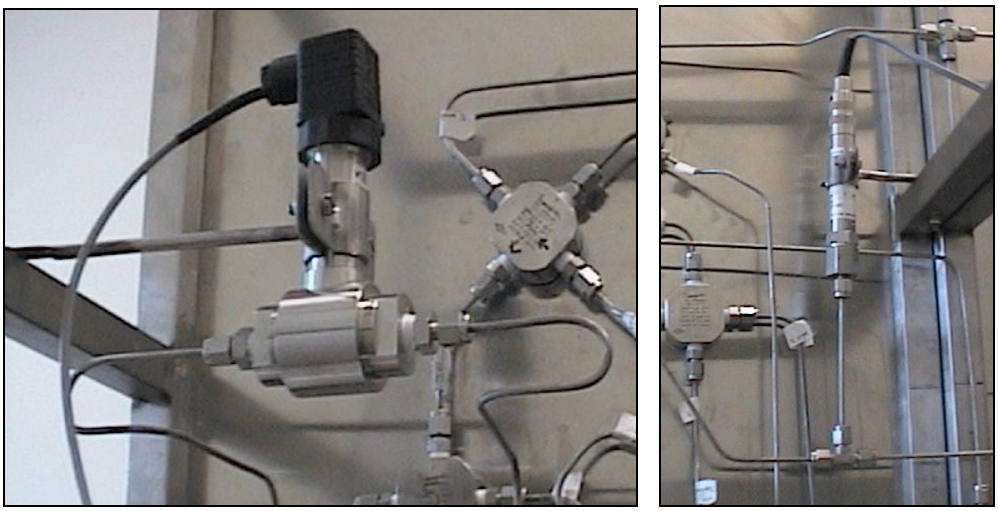

Figure 3-7 Differential pressure (left) and pressure (right) probes of the experimental bench.

Figure 3-8 Photo of the valve system of the experimental bench (view from the back).

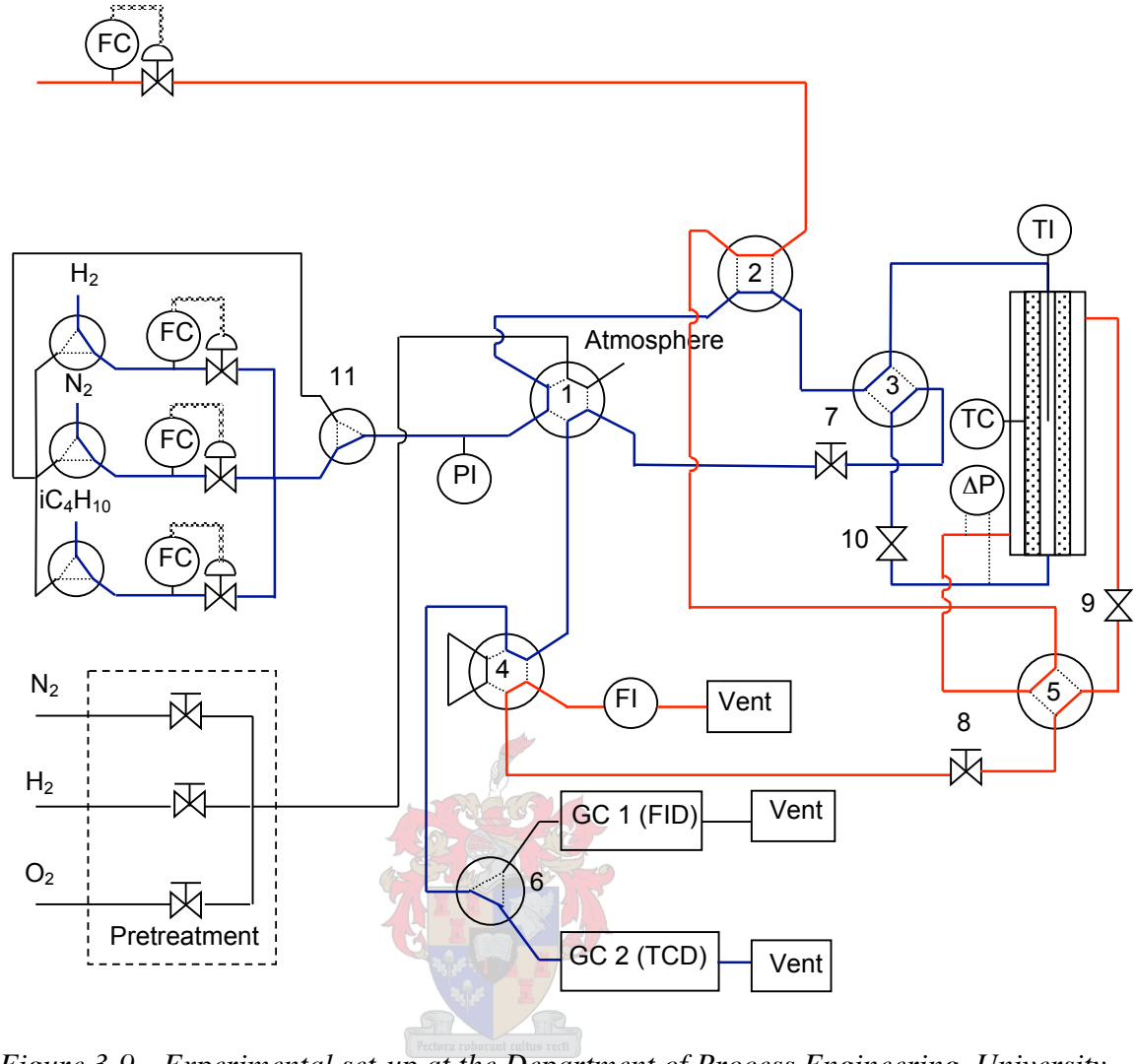

Figure 3-9 Experimental set-up at the Department of Process Engineering, University of Stellenbosch (SA).

The set-up consists of various valves (Figure 3-8 and Figure 3-9) that give the user options for changing various operating conditions.

Valve 1 Reactor bypass/Pretreatment or Membrane testing. To be used to bypass the feed from the reactor. Valve 1 is also used to choose membrane pretreatment.

Valve 2 Feed internal or external. This valve allows the use of the set-up for internal and external feeding without having to physically change the lines going to the reactor module.

Valve 3 Internal flow direction. The gas flow direction in the internal compartment can be fixed.

Valve 4 Flow meter, internal or external. Valve allowing the measurement of the flow rates of either the internal or external exit streams. When valve 1 is in the

bypass position, for feed analysis, then valve 4 should be on *internal* in order to measure the flow of the feed.

Valve 5 External flow direction. The gas flow direction in the external compartment can be fixed.

Valve 6 GC 1 (FID) or GC 2 (TCD). Due to the fact that there is no GC with FID and TCD detectors in series, the flow of the to be analyzed stream is first sent for hydrogen analysis (GC 2), and then changed manually to analyze the stream for hydrocarbons (GC 1). The characteristics of the GC columns and operating conditions are similar to Table 3-1.

Valves 7 & 8 Variable open/close valves. Allow for manual control of the differential pressure across the membrane by changing the pressure in the internal (valve 7) and external (valve 8) compartments.

Valve 9 &10 Open/ close valves. Allows for the closure of the internal exit/inlet (valve 10) and the external inlet/exit (valve 9).

The cylindrical furnace was designed by myself and manufactured by Unitemp (Cape Town). It has a length of 50 cm and inner diameter of 6 cm, where the reactor module can be placed. The heating elements in the furnace were placed in such a manner that more heat was distributed at the end parts in order to ensure an even temperature distribution. Photos of the tube furnace are given in Figure 3-10 (frontal view), Figure 3-11 (inside) and Figure 3-12 (side view). A design diagram of the cylindrical furnace is given in Appendix B.

A Gefran 800P temperature controller controls the temperature on the outside of the membrane reactor module by changing the heat input to the furnace. The temperature controller offers on-off, PI and PID control. The temperature can be preset making use of four separate different temperature programs. The thermocouple (type K), connected to the temperature controller, is situated on the external surface (in the middle) of the membrane reactor module.

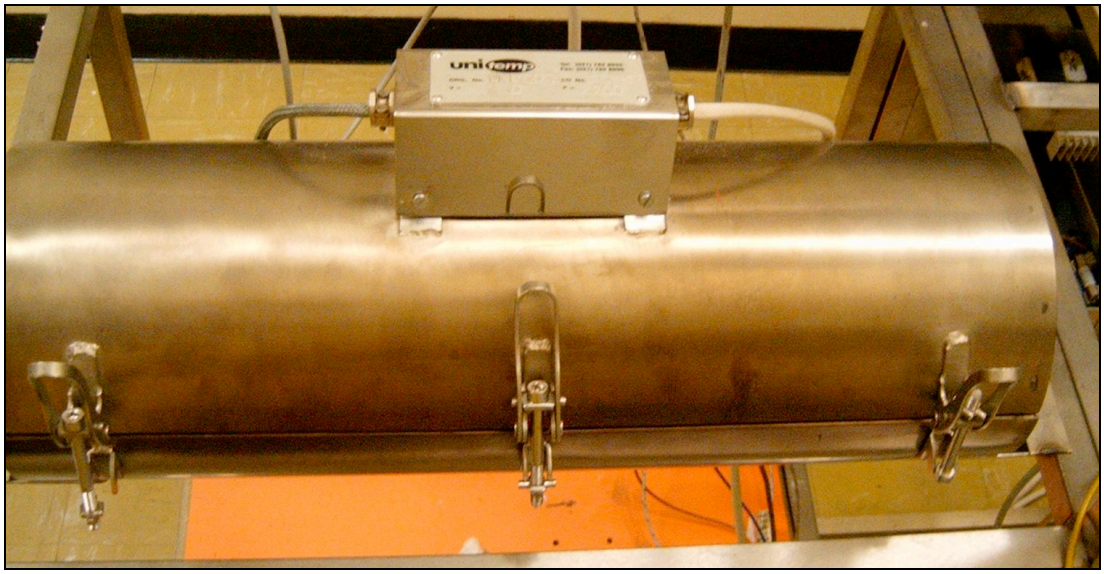

Figure 3-10 Frontal view of cylindrical furnace.

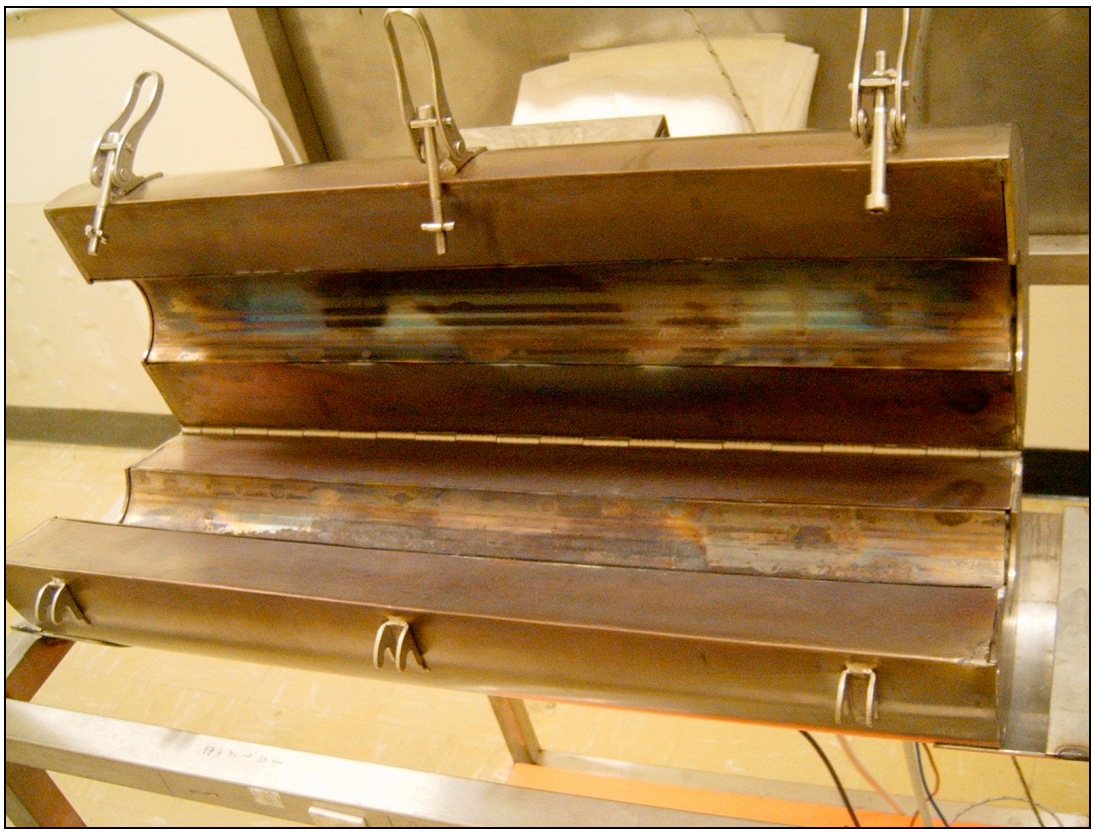

Figure 3-11 Inside view of the cylindrical furnace.

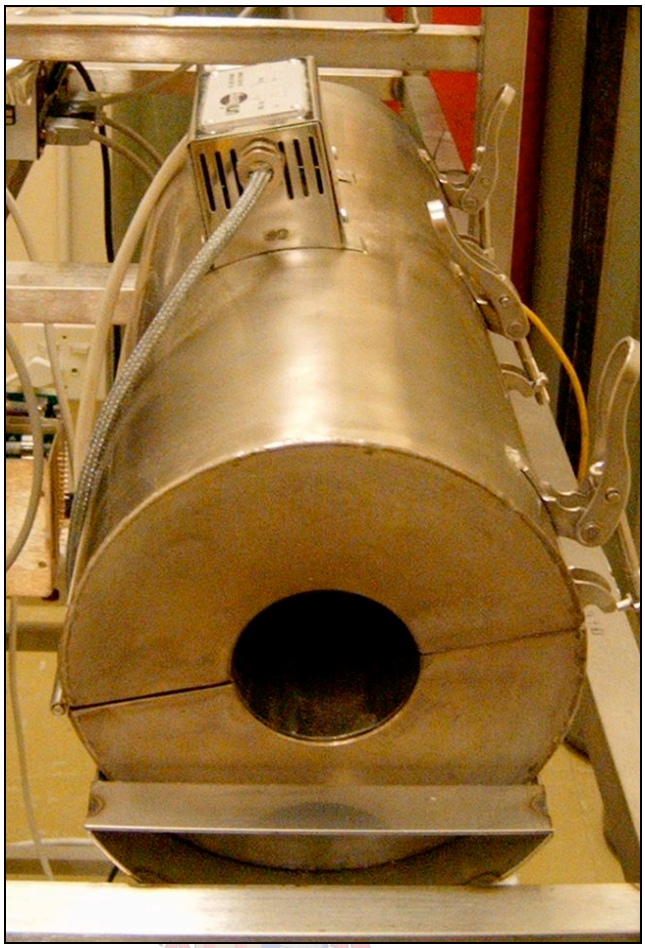

Figure 3-12 Side view of membrane reactor furnace.

The flow rates of the feed, external exit and internal exit streams are measured with an interchangeable bubble flow meter.

It can therefore, be seen that the basic functions of the SA bench are similar to the one in France. The operational procedures of the set-up are provided in appendix A.

3.6.3 Improvements on experimental design

I have made some improvements to the design compared with the set-up at the CNRS/IRC, France. A discussion will follow with the help of Figure 3-13.

a) When permeation testing is done, there is back pressure on the mass flow controllers. This may cause damage to the mass flow controllers according to the operational manual. For this reason a 3-way valve has been included in the design of the new set-up, to separate the permeate and feeding section lines, while still utilizing the same feed line to the reactor.

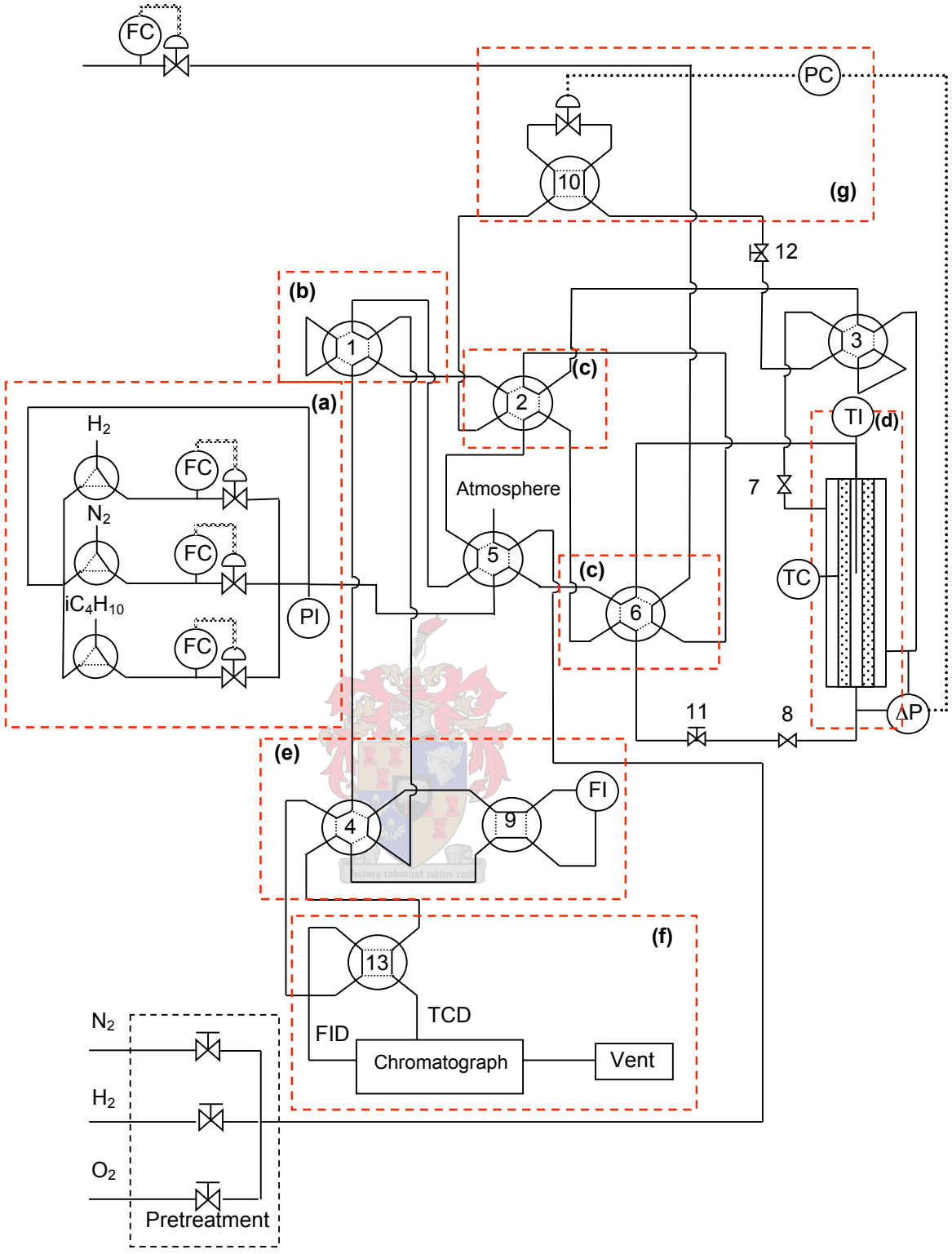

Figure 3-13 Isobutane dehydrogenation bench (CNRS/IRC) – blocks indicate points of discussion.

b) Valve 13 provides an automated change of the analysis streams to the various detectors. The GC program always starts with the retentate being analyzed first by

FID, the lines going to valve 1 can therefore, be fixed in a position to valve 4 making valve 1 unnecessary.

c) Valve 6 (Internal sweep or feed) must be operated in parallel with valve 2 (External sweep or feed), because the sweep can only be internal if the feed is external and visa versa. Valves 6 and 2 can therefore, be replaced by a single valve.

d) With valve 3 the current direction can be chosen (counter/ co-current). This valve is only connected to the external side of the reactor, and therefore only the direction of the external flow can be changed. What this means in effect, is that when the feed is in the external part, then the direction of the sweep will stay constant during a change of the flow direction, and the feed direction will be changed if the counter current mode is employed. If a catalytic membrane reactor test is done, and the feed direction is changed, this might change the reaction conditions, if the catalyst shows any signs of deactivation. The "fresher" part of the catalyst will be exposed to the higher concentration feed, and therefore more conversion will take place. In order to eliminate any problems that might arise from this, valve 3 was replaced by 2, 4-way valves. Each of the valves allows the user to choose the flow direction of the internal or the external flow. These two valves should be operated interdependently, meaning that if the flow direction of the internal part is set, and the sweep is in the external compartment then only the sweep direction should be changed.

e) The cylindrical furnace length was extended for the new set-up from 30-35 cm (CNRS\IRC) to 50 cm. Heat losses can occur at the ends of the furnace leading to an uneven temperature profile within the furnace. By extending the length of the furnace the reactor module is further away from the ends, limiting heat losses from the ends of the reactor module. The heating elements in the furnace were also placed in such a manner that more heat was distributed at the end parts in order to ensure an even temperature distribution. The temperature controller used for the new set-up furnace offers, on-off, PI and PID control with four separate temperature programs, allowing pre-programming of the various temperatures. Temperature control at the CNRS\IRC is on-off control with one temperature program.

f) Blocks f, g and h represent equipment that could not be included in the new design due to budget constraints. The functions provided by these pieces of equipment were, however incorporated in the new experimental set-up.

3.7 Summary

In this chapter the various experimental conditions for extractor Catalytic Membrane Reactor experiments were outlined. The design and construction of an experimental bench for the Department of Process Engineering, University of Stellenbosch were also described. The differences between the various experimental set-ups in France and South Africa have been highlighted.

4 The use of an eCMR to enhance reaction conversion: Isobutane dehydrogenation

The *extractor* Catalytic Membrane Reactor is used in this chapter to enhance the reaction conversion of an equilibrium restricted reaction. The first step in the production of MTBE, an octane booster for gasoline, is the dehydrogenation of isobutane to isobutene. Recent regulation about oxygenates in motor fuels, leads us to reconsider the demand for isobutene in the future. Isobutane dehydrogenation can be considered as a good model reaction for membrane reactors of the extractor type [144]. The performances of both a Pd/alumina membrane and an MFI/alumina membrane, used as hydrogen extracting membranes during isobutane dehydrogenation, are described here. This reaction has already been studied in CMRs using both dense Pd [76, 145] and porous materials [144, 146, 147], but no comparative experimental data under similar conditions have been reported.

4.1 Literature review

4.1.1 eCMRs to enhance reaction conversion

According to Le Chatelier's principle, if a dynamic equilibrium is disturbed by changing the reaction conditions (concentration or temperature or pressure (gas phase) the position of the equilibrium shifts to counteract the change and restores the equilibrium. Consequently when an *extractor* Catalytic Membrane Reactor is applied for equilibrium restricted reactions, removing one of the products from the reaction zone, leads to a shift in the equilibrium to the product side.

Hidden advantages would be that the same production rate can be maintained at lower reaction conditions, and therefore energy costs would be curtailed. Milder reaction conditions would also be advantages to the catalyst life.

Dehydrogenation Reactions

The majority of reactions to which the *extractor* Catalytic Membrane Reactor concept has been applied, are dehydrogenation reactions. During dehydrogenation in an eCMR, hydrogen is selectively removed from the reaction zone.

Alcanes

The catalytic dehydrogenation of light alkanes (C_2-C_4) is an important industrial process for the production of alkenes, which are valuable starting chemicals for a variety of applications. The dehydrogenation of light alkanes are endothermic reactions, requiring high temperatures for attainable conversion, with side-reactions being favoured above the main reaction. Gryaznov and co-workers did pioneering studies on light alkane dehydrogenation in Pd or Pd-alloy membrane reactors [36, 148]. Theses researchers, as well as Shu *et al*. [118], have published comprehensive review papers on Pd membranes reactors.

Ethane dehydrogenation

Gobina and Huges [149] performed ethane dehydrogenation in a catalytic membrane reactor, which consisted of a membrane of thin layer of Pd-23 wt% Ag on porous Vycor glass, packed with a Pd/α-alumina catalyst. The conversion of ethane could be increased typically 7 times (cocurrent mode), and 8 times (counter-current mode) higher than the equilibrium value attainable in conventional fixed bed reactors, when high sweep rates were employed. They constructed a mathematical model for the process, by investigating the various effects of the operating parameters (sweep gas flowrate, sweep/feed ratio and feed contacting times).

In another study by Champagnie *et al*. [150] ethane dehydrogenation experiments were performed in a multi-layer alumina membrane (40Å) (MEMBRALOX) impregnated with a Pt catalyst. Increased yields were obtained over calculated equilibrium values and at 823 K they obtained about 19 % conversion compared to the equilibrium value of just under 10 %.

The conversion of ethane to pure hydrogen and ethylene or BTX (Benzene, Toluene and Xylenes) at relatively mild temperatures was investigated by Wang *et al*. [151] in a membrane reactor. The membrane reactor was a Pd-based membrane, packed with a very active Re/HZSM-5 catalyst. The selectivity towards ethylene or BTX was controlled by the ethane space velocity (SV). High SV of ethane favoured the formation of ethylene, while low SV was more favourable to the production of BTX. The use of the membrane reactor enhanced the yields of ethylene and BTX, and also effectively suppressed the formation of the side product, methane.

Dehydrogenation of Propane

Ziaka *et al*. [152] did propane dehydrogenation in an γ-alumina packed with a commercial Pt/alumina catalyst. The diffusion of hydrogen through the membrane was governed by Knudsen diffusion, so the selectivities of the membrane were not very high. The membrane also suffered from the fact that γ-alumina is a meta-stable material, which at high temperatures and steam pressure evolves slowly towards the more meta-stable α-alumina. In order to achieve higher hydrogen selectivities, microporous silica membranes have been employed. Weyton *et al*. [153] used a commercial silica/alumina membrane made by CVD/CV1 with hydrogen permeance of about 1.4 mol/m^2/Pa/s and a H_2/C_3H_8 permselectivity of 70 - 90 at 773 K for propane dehydrogenation. The conversion of propane was increased by a factor of 2 at 773 K. They also found that significant increases in the conversion could only be achieved at low propane feed rates, due to the fact that the hydrogen extraction capability of the membrane was limited. A Pd/Ag membrane, which had superior hydrogen permeance and selectivity, provided better performances for this reaction.

Schafer *et al*. [154] used a sol gel SiO_2 membrane on an γ-Al_2O_3 substrate in a eCMR. The membrane showed a hydrogen permeance higher than 25 m^3/m^2/h/bar and H_2/C_3H_8 permselectivities between 30-55 at 723 - 823 K.

n-Butane dehydrogenation

Butane dehydrogenation was studied by Gobina and Hughes [155] in a Pd-Ag/Vycor® glass membrane packed with a 0.5 wt% Pd/alumina catalyst. At 673K the equilibrium conversion for this reaction was 5 %. When air was used as a sweep gas the conversion was increased to 39 %, while an 11 % carbon monoxide sweep gas gave 26 % conversion.

Rezac and co-workers [156, 157] used a thermally stable polymer-ceramic membrane for hydrogen extraction. The butane conversion in this eCMR was improved to 22 - 33 % for reaction temperatures between 753 and 813 K.

Zaspalis *et al*. [158] used an α-alumina membrane with an γ-alumina top layer (4-5 nm pore size) packed with a Pt/SiO_2 catalyst for butane dehydrogenation. A 9 % improvement in the conversion of butane was achieved at 773K (calculated equilibrium conversion by 6 %).

The dehydrogenation of isobutane in an extractor Catalytic Membrane Reactor is discussed later in this chapter.

Dehydrogenation of ethylbenzene to styrene

Styrene is one of the most important chemicals in the polymer industry. Application of membrane reactors for ethylbenzene (EB) dehydrogenation has been done through a number of studies using Pd on porous ceramics or stainless steel membrane, porous alumina membranes and microporous membranes [159-164]. These studies reported an increase in styrene yield, when compared with a conventional packed bed reactor. Tichareno-Lechuga *et al*. [160] reported that during the continuous use of the catalytic membrane reactor for EB dehydrogenation, the flux of hydrogen steadily decreases with time, due to carbon deposition on the membrane. This led to the eventual clogging of the membrane. They used a tabular ALCOA alumina membrane (50 Å) in a tube and shell arrangement, packed with a commercial Shell 105 catalyst as the membrane reactor.

Jiang and Wang [162] used a new kind of microporous membrane with H_2/EB selectivity of over 75 and hydrogen permeance of 10 – 6 mol/Pa/m^2/s in a membrane reactor. With EB liquid hour space velocity (LHSV) of 0.5 - 1.0 h^{-1}, a water/EB molar ratio of 9.86 - 16.42, in the temperature range 633-873K, the membrane reactor improved the styrene yield to a maximum of 21.5 % and a top per-pass styrene yield of 75 %. This was a 10 % improvement on yields obtained in a conventional fixed bed reactor.

In a more recent study She *et al*. [161] used a palladium/stainless steel membrane reactor for ethylbenzene dehydrogenation. The Pd reactor and a fixed-bed reactor were operated at 725 - 898K and 1.2 atm pressure with a steam/EB ratio of 6.8. As a result of the hydrogen removal, the conversion of EB was about 10 % higher in the Pd membrane reactor than in the fixed-bed reactor at temperatures higher than 873 K. Undesired side reactions were suppressed, and the selectivity towards styrene increased by 15 % in the eCMR. The use of microporous (Fe-MFI and Fe-Al-MFI) zeolite membranes for EB dehydrogenation in a membrane reactor has recently been reported by Xiongfu *et al*. [165].

This reaction has also been used to develop a few catalytic membrane reactor models [166-172].

Cyclohexane dehydrogenation to benzene

This reaction has been used in many catalytic membrane reactor modeling studies due to its well known kinetics and low operating temperatures [173-176]. The reaction has potential significance for hydrogen storage and renewable energy sources [141]. Terry *et al*. [177] studied this reaction using commercial (US filter) ceramic membranes of various

pore sizes modified by the addition of successive thin film layers of silica prepared with silica oxide particles in an iron (III) solution. A 300 % yield increase was achieved when the membrane was operated in the Knudsen regime, when compared with conventional reactor experiments at the same operating conditions. The uncoated membranes rendered higher yields than the uncoated membranes, even though both types of membranes were operated in the Knudsen regime. Studies on EB dehydrogenation in microporous, hollow-fiber carbon membranes used in an eCMR were done by Itoh and Haraya [178]. Although the membranes had high hydrogen/cyclohexane and hydrogen/benzene permselectivities they suffered from poor mechanical stability. Due to this fact the fibres were protected from the fixed-bed catalyst using a porous tube of sintered metal. A 300 % enhancement in the conversion with respect to the equilibrium was achieved. Thermally resistant, polymeric membranes provide promise for use in catalytic membrane reactor applications for this reaction [179, 180].

Alcohols

The dehydrogenation of alcohols has been studied by a number of groups. Deng *et al*. [181] studied *ethanol* dehydrogenation in alumina membranes (500 nm pore size) with an γ-alumina layer containing Pd, Pt, Cu or Ni top layer, packed with a Cu-P/SiO_2 catalyst. Cu and Ni-modified alumina membrane reactors yielded similar results as the alumina membrane reactor. The best results were obtained with the Pd and the Pt-modified alumina membranes with acetaldehyde yields being further improved on by increasing the space time and/or the sweep gas flow rates.

Raich and Foley [182] studied ethanol dehydrogenation in a Pd tube with a wall thickness of 7 μm at operating temperatures between 448 and 498 K. The Pd membrane was packed with Pt/silica or Cu/silica catalysts. The best results were obtained with a Cu/silica catalyst, which gave higher selectivities, but lower activity and lower overall yield. When the Palladium membrane packed with the Cu/silica catalyst was compared with a conventional reactor the ethanol conversion was increased from 60 % to almost 90 %, the selectivity to acetaldehyde from 35 % to 70 %, and the yield from 21 % to 63 %.

In another study by Liu and co-workers [183] two kinds of Ni-P alloy/ ceramic membranes were used. The one type of membrane was prepared by the conventional electroless plating technique, and the other by a subsequent recrystallization method. Ethanol conversion in the reactor with the conventionally prepared Ni-P amorphous alloy membranes was higher, than in the membrane reactor using the re-crystallized membranes.

This group also studied the same reaction using Rh-modified γ-alumina membranes [184]. Ethanol conversions and acetaldehyde selectivities in the Rh-modified γ-alumina reactor were higher than those in the γ-alumina membrane reactor. The Rh-modified γ-alumina membrane displayed higher hydrogen permeabilities and separation factors than the γ-alumina membrane. The same group also used an amorphous Ni-B alloy membrane, prepared by electroless plating, for ethanol dehydrogenation [185]. This membrane had catalytic activity as well as high hydrogen permselectivity for hydrogen, which led to a significant promotion effect for the reaction.

Keuler [14] did ethanol dehydrogenation with a Pd-Ag/α-alumina membrane reactor packed with an optimized 14.4 wt% Cu/silica catalyst. The best results were obtained at 548 K, which gave improved conversion (compared with conventional) of ethanol from 45 % to 60 % at low feed flow rates and from 36 % to 46 % at high feed flow rates. The Pd-Ag/α-alumina membrane that was used, displayed a hydrogen permeance of 4 μmol/Pa/s/m^2 and a hydrogen/ nitrogen permselectivity of 221 at 563 K.

The same membrane reactor was used for the dehydrogenation of *2-butanol*. The maximum conversion in a plug flow reactor at 513 K was 80 %, and that increased to above 90 % for the membrane reactor.

The dehydrogenation of *isopropanol* was studied by Mouton *et al*. [186] and Trianto *et al*. [187]. Mouton used a Pd-Cu/α-alumina membrane packed with a Cu/silica catalyst while Trianto *et al*. used a modified Vycor® glass membrane. During both studies, the conversion of isopropanol to isopropanoon was improved.

The catalytic dehydrogenation of *metanol* to methyl formate has been studied by a number of groups. Lefu *et al*. [188] studied this reaction in a Pd-Ag/γ-alumina membrane reactor packed with a very active CuO-ZnO-ZrO_2/Al_2O_3 catalyst, which showed superior performances to that of a fixed-bed reactor. Gorshkov *et al*. investigated hydrogen permeance through a Pd-Ru membrane during the dehydrogenation reaction and without any reaction taking place. CO presence in the membrane during the reaction did not deactivate the membrane during the reaction, but rapid deactivation of the membrane occurred when exposed to CO in the absence of the catalyst and reaction. Amandusson *et al*. [189] studied methanol dehydrogenation in a Pd membrane reactor. The Pd of the membrane also acted as a catalyst for the reaction. At 623 K under continuous methanol feeding the methanol absorbs onto the Pd surface and decomposes, leading to adsorbed hydrogen and a carbonaceous surface top layer. This eventually leads to a decline, and

eventual termination of hydrogen diffusion through the membrane. In order to prevent this from happening, oxygen was co-fed, which reacted with the C on the surface to form CO, therefore enabling the maintenance of the hydrogen permeation rate.

Other catalytic reactions

A number of decomposition (H_2S, NH_3 and H_2O) reactions have been studied with the extractor Catalytic Membrane Reactor. Ma *et al*. [190] studied the *decomposition of* H_2S in a Vycor® porous glass membrane packed with a molybdenum sulfide catalyst, with no sweep gas employed. They concluded, that in order to shift the reaction equilibrium significantly, a highly selective membrane would have to be employed. Although Edlund and Pledger [191] used a very selective Pt-V membrane for H_2S decomposition, which was more stable than a Pd membrane, this membrane was less permeable and not free of other problems associated with dense metallic membranes. Kajiwara *et al*. [192] compared CVD Pt and electroless plated Pd on alumina membranes for H_2S decomposition. The CVD Pt membranes gave comparable hydrogen fluxes to the Pd membrane, but showed less defect formation after contact with a gas stream containing hydrogen sulphide.

The *decomposition* of dilute mixtures of NH_3, for potential treatment of coal gasification streams, was studied by Collins and Way [193] as well as Gobina *et al*. [194], using Pd-alloy catalytic membrane reactors. Laboratory results showed promise, but no evidence was presented as to whether the membranes would be robust enough for use in the gas-coal environment.

Early investigations on H_2O *decomposition* for hydrogen production were done by Lede and co-workers [195], using a calcia-stabilized zirconia membrane at high temperatures (1673 – 2073 K). Other studies focused on using mixed conducting electrolyte membranes to extract oxygen from the reaction zone.

Methane steam reforming is one of the most widely applied commercial processes for the production of hydrogen from synthesis gas. The reactions are very endothermic and require high operating temperatures (T < 1123 K) [196]

$$CH_4 + H_2O \rightleftharpoons CO + H_2 \qquad (4\text{-}1)$$

$$CH_4 + 2H_2O \rightleftharpoons CO_2 + 3H_2 \qquad (4\text{-}2)$$

Shu *et al*. [196] indicated, through mathematical modelling, that hydrogen removal through the membrane could best be exploited at temperatures between 773 and 873 K. Using porous stainless steel supported Pd and Pd-Ag membranes, packed with Ni/Al_2O_3

catalyst, significant improvements with the membrane reactor were obtained by Shu and co-workers. Methane conversion was 1.4 times higher in the membrane reactor at 773 K, 136 kPa and a steam to methane ratio of 3.

The focus of research in this area has shifted to hydrogen production for mobile fuel cell applications. Lin and Rei [197, 198] proposed a double-jacketed membrane reactor for methanol steam reforming. The reactor is a concentric module, consisting of a supported Pd membrane in the centre and two stainless steel tubes assembled separately as the outer jackets. A Cu-based catalyst was placed in the annulus between the membrane, and the inner stainless steel tube for the methanol reforming reaction. A Pd/Al_2O_3 catalytic oxidation catalyst was placed between the two stainless steel tubes to oxidize the retentate, in order to generate heat to drive the endothermic reaction. An automated operation could be achieved with hydrogen recoveries in the range of 70-80 %, with additional heating being provided through electric heating if required. At 623 K and reactor pressures above 12 atm, a recovery yield of 97 %, and a hydrogen flux of 3.7 $m^3/m^2/h$ were obtained for a load to surface ratio of 50 $mol/m^3/h$, which is much higher than the conventional yield of 75 %.

Frustreri *et al*. [199] used a Ru impregnated zeolite membrane/ Cu-based catalyst catalytic membrane reactor for methanol steam reforming. The catalyst was placed on the outside of the membrane, in the annular space between the membrane and the reactor external shell. The membrane did not show any beneficial effect due to equilibrium conversion displacement, because stability restrictions dictated the use of the reactor at temperatures higher than 573 K.

4.1.2 Isobutane dehydrogenation reaction

It is more than likely that the demand for MTBE, as oxygen boosters for fuels, will decrease in the future, and consequently, the demand for isobutene will also decrease.

A possible solution for this problem is the use of iso-ether technology, proposed by Snamprogetti S.p.A. Research & Development Division. Isobutylene can be selectively dimerized from any source to a non-oxygen-containing alkylate-like stream (mainly iso-octane), which possesses excellent blending and engine performance properties. The iso-ether technology coupled with isobutane dehydrogenation allows one to economically convert butanes into large amounts of an Iso-Octane-based superior alkylate to be sold as a commodity, making these complexes economically viable [200].

Features of the reaction

The dehydrogenation of isobutane to form isobutene is an endothermic reaction ($\Delta H_{R,\,298K}$ = 118 kJ/mol), and can be represented by the following equation:

$$i\text{-}C_4H_{10} \rightleftharpoons i\text{-}C_4H_8 + H_2 \qquad (4\text{-}3)$$

Attainable conversions are limited by thermodynamics of the reaction and therefore high temperatures (Figure 4-1), and low pressures favour reaction conversion. Despite high reaction temperatures, the reaction is slow. Furthermore side reactions like isomerization, thermal cracking and coking are thermodynamically and kinetically favoured over the main reaction, and can occur at the required reaction conditions. The use of a catalyst is therefore necessary in order to get high conversion rates, while obtaining a high selectivity toward the desired olefin [201].

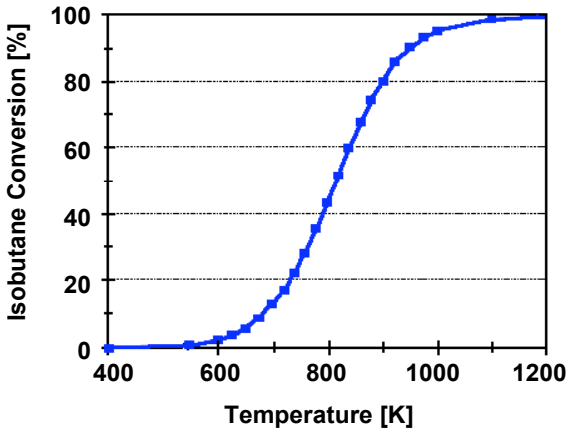

Figure 4-1 Isobutane dehydrogenation equilibrium conversion at different temperatures (Pressure 1 atm) [65]

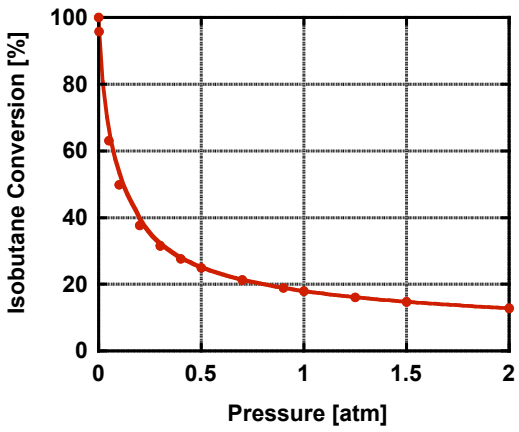

Figure 4-2 Isobutane equilibrium conversion at 723 K and various pressures [65]

Isobutane dehydrogenation catalysts

An alcane dehydrogenation catalyst normally consists of a support doped with one or more active site and some have alkali metals present. Catalysts that are most often used for isobutane dehydrogenation, are chromium oxide and supported platinum catalysts.

Chromium oxide

For many years now chromium oxide catalysts have been used for the dehydrogenation of isobutane. The active site are the mononuclear Cr(III) species with two coordinative unsaturations and adjacent O^{2-} of the support [202]. The activity of the catalyst increases linearly with the Cr_2O_3 content up to a maximum of 12 % by weight.

De Rossi *et al.* [203] investigated the effects of the support type (Al_2O_3, SiO_2 and ZiO_2) on the dehydrogenation of propane and found that Cr_2O_3 supported on ZiO_2 afforded higher turnover frequencies than the loaded Al_2O_3 or SiO_2. Extended studies into the dehydrogenation of isobutane with a Cr_2O_3/ ZiO_2 catalyst gave a conversion of 45 % with a selectivity of 95 % at 823 K. It was, however, noticed that marked deactivation of the catalyst occurred within the first 60 min of the reaction [202].

The addition of CaO or MoO_3 as promoters, increase the reaction stability but lesser activity of the catalyst is observed. Coke formation can be decreased by neutralizing the acid sites on the support through the addition of alkali metals, or alkali earth metals like K_2O, LiO and MgO in small quantities (0.5 – 3 %). Catalyst stability is also improved by adding TiO_2, Sb_2O_3 or MnO_3 [65].

However, it must be noted that chromium is a heavy metal and is known to be toxic. Frequent regeneration of these chromia catalysts are also required [204].

Supported noble metal (usually platinum) catalysts

Platinum has a strong capacity to selectively break C-H connections, with the rupture of C-C bonds being much more difficult. Due to this fact, platinum constitutes the principle element of most dehydrogenation catalysts. The platinum catalyst is very active and therefore, deactivation occurs quickly. Secondary reactions that can occur are cracking, isomerization and coke forming. Sn inhibits major dehydrogenation and the reagents are thus, less strongly adsorbed, and can migrate on the support. A reason for this behaviour was given by Cortright *et al.* [204]. Accordly, hydrogenolysis and isomerization reactions require surface ensembles, containing at least several Pt atoms. When surface ensembles are absent, like the case would be with small platinum particles, then hydrogenolysis and isomerizations reactions are inhibited. A fairly large ensemble of surface Pt atoms is also required for reactions which lead to coke formation. Adding Sn to Pt/SiO_2 suppresses isomerization and hydrogenolysis of isobutane, and enhances the dehydrogenation selectivity. Sn interacts with the supported Pt to produce a Pt/Sn alloy, therefore reducing the size of the surface Pt ensembles on Pt/Sn alloy particles.

Alkaline metal addition such as Li, K or Mg makes it possible to decrease the quantity of coke formed during the reaction, by neutralizing acid sites of the support and metal ions in charge of coke formation [65]. The addition of K to Pt/SiO_2 has the same effect as Sn addition (reducing the area of Pt ensembles on the catalyst) and it was found that the dehydrogenation reaction rate increases by stabilizing the reactive intermediates.

Gueguen *et al.* [205] did isobutane dehydrogenation over various platinum supported metalophosphate oxynitrate catalysts (MM`PON where M=Al, M`=Ga, Cr). They found that these catalysts have a high ability to transform isobutane into isobutene. The influence on reactivity was investigated by cationic and anionic substitution in the AlM`PON (M` = Ga, Cr) support. The best results in terms of isobutane conversion and selectivity was obtained with the AlGaPON support. Gallium induces a large increase in conversion, due to the fact that it has the potential to recombine hydrogen in molecular form.

Cortright *et al.* [204] reported that Pt-Sn supported on K-L-zeolite exhibited a high activity and selectivity towards isobutane dehydrogenation. The catalyst was selective and stable at low hydrogen partial pressures, and moderate temperatures (i.e. $T < 800$ K).

Isobutane dehydrogenation catalysts have alo been studied within our group. Casanava *et al.* [65] compared the performances of various catalysts containing chromium

and platinum for isobutane dehydrogenation. The catalyst containing platinum was the most active, however the support type played a dominating role on the stability of the catalyst. The commercial catalyst Pt-Sn/Al_2O_3 was found to be unstable and the catalyst was modified by neutralizing the acid sites with an adequate amount of potassium, which led to a reduction in the amount of coke formed during the reaction. It was also found that the partial pressure of hydrogen within the system, influenced the stability of the catalyst and reduced the amount of coke formed. Another catalyst that was studied was a Pt-In supported on silicalite catalyst and it was found that the catalyst displayed good stability, and its selectivity for isobutane dehydrogenation was close to 100 %. A reason given for the good stability is that the narrow channels of the silicalite (5.6 Å) could, in the form of selectivity, block the formation of precursory polymeric intermediate products of coke. This catalyst was also used in the continuation of the study, which involved isobutane dehydrogenation in membrane reactors.

Isobutane dehydrogenation in an eCMR

Isobutane dehydrogenation has been studied in a Pd-Ag membrane packed with a Cr_2O_3/Al_2O_3 catalyst by Guo *et al.* [206]. The membrane was hydrogen selective with separation factors for H_2/N_2 and H_2/Ar close to infinite and a hydrogen flux of 0.76 mol/s/m^2 at 773 K (ΔP = 1.9 atm). The conversion of isobutane with a gas hour space velocity of 150 h^{-1} and sweep flow rate of 200 ml/min was 50.5 %. The equilibrium conversion of isobutane at these conditions is 18.8 % and conversion in a fixed-bed 15.5 %. It was also found that complete extraction of hydrogen led to the deactivation of the catalyst and therefore, it was suggested to maintain a certain hydrogen pressure on the reaction side.

Sheintuch and Dessau [207] use a Pd/Ru membrane packed with a Pt/alumina catalyst for isobutane dehydrogenation. Butene yields (isobutene and n-butene) of up to 76 % could be achieved at 773 K compared with the equilibrium value of 32 %. The attained yields were limited at low feed rates by suppressed catalyst activity in the absence of H_2. Fast deactivation of the catalyst was found at high sweep/feed molar ratios. Yields under high internal pressure conditions (18 psi isobutane) were similar to those attained under atmospheric conditions in the membrane reactor, but with the added advantage of higher purity hydrogen.

In another study by Matsuda *et al.* [208] palladium/alumina membrane (Pd outer surface of tube) was used in the membrane reactor. Two different catalysts were used, a

very active Pt/Al_2O_3 catalyst and a Cr_2O_3-Al_2O_3 catalyst. Although the Pt catalyst showed greater activity, lower isobutane yields were obtained in the membrane reactor compared to the Cr_2O_3 catalyst. The Pt catalyst deteriorated more rapidly in the CMR, due to the deposition of carboneous material. Side reaction was suppressed by adding Sn to the Pt/Al_2O_3 catalyst, leading to increased yields in isobutene and less coke formation.

This reaction has also been studied extensively in our group at the CNRS/IRC [144, 209]. Hydrogen and isobutane permeation and separation using the MFI-zeolite membrane, were studied by Ciavarella *et al*. [112]. In the mixture, the strongly adsorbed isobutane molecules in the micropores hindered permeation of hydrogen through the membrane at low temperatures. H_2/iC_4H_{10} separation experiments showed a maximum separation factor of 25 at 723 K, with H_2:iC_4H_{10}:N_2 ratio in the feed of 12:15:73. The isobutane flux showed a maximum at 450 K, while hydrogen flux decreased with increasing temperature.

MFI-zeolite membranes prepared by the same pore plugging technique were used in the dehydrogenation of isobutane using a Pt-In zeolite catalyst [144]. The influences of various operating conditions were investigated (temperature, feed flow rate, sweep flow rates and direction). The isobutane was converted to hydrogen and isobutene, with ca 90 % selectivity towards isobutene. When counter and co-current sweep flow rates were employed, similar conversions of isobutane were obtained, although the hydrogen extraction in the counter-current flow mode was higher. The conversion increased with an increase in sweep flow rate. In the conventional packed-bed reactor an increase in the isobutane feed flow rate had almost no effect on the conversion, but an increase had a significant impact on the isobutane conversion in the membrane reactor. The conversion decreased with an increase in feed flow rate. This group came to the conclusion that the isobutane dehydrogenation reaction was limited by the transport properties when a co-current mode was employed. In counter-current mode, the reaction was limited by reaction kinetics [210]. This chapter presents work that is a continuation of these studies.

The results of the various studies are summarized in Table 4-1.

Table 4-1 Dehydrogenation of isobutane in eCMRs (Y = Isobutene Yield, C = Isobutane Conversion, C_{eq} = Equilibrium conversion at CMR conditions and Y_{FBR} = Yield fixed bed reactor at the same feed conditions as CMR).

Membrane	**Catalyst**	**T [K]**	**Results**	**Ref.**
Pd/ alumina (Pd outside)	Pt/ Al_2O_3	673	C = 25 % Y = 22 % (C_{eq} = 11 %; Y_{FBR} = 6 %)	[208]
SiO_2/Vycor	Cr_2O_3-Al_2O_3	773	C – *not given* Y = 36.4% (C_{eq} = 33 %; Y_{FBR} = 29 %)	[146]
MFI-zeolite	Pt-Sn/γ-Al_2O_3	723	C - *not given* Y = 22.4 % (C_{eq} - *not given*, Y_{FBR} = 13 %)	[209]
2% Ru/Pd	Pt/Al_2O_3	773	C = 81 % Y = 68 % (C_{eq} = 33 %; Y_{FBR} – *not given*)	[207]
Pd/alumina	Pt-In/SiO_2	723	C = 33 %; Y = 32 % (C_{eq} = 8 %; Y_{FBR} - *not given*)	[76]
MFI-zeolite	Pt-In/SiO_2	723	C = 43 % Y = 40 % (C_{eq} = 8 %; Y_{FBR} = 14 %)	[144]
Pd-Ag/ceramic	Cr_2O_3-Al_2O_3	723	C = 50.5 % Y = 48 % (C_{eq} = 18.8 %; Y_{FBR} = 15.5 %	[206]

4.2 Transport measurements: Mixture separation and single gas permeation testing

A description of the experimental procedures are presented in chapter 3 (section 3.4).

4.2.1 Results

Pd membrane

The thickness of the Pd membrane was 4.8 μm, determined from the mass gain of the substrate assuming a continuous Pd layer. Table 4-2 reports single gas (H_2, iC_4H_{10} and N_2) permeation results for both the MFI and Pd membrane.

Gas mixture separation testing was also performed at 723 K, feed rate 50ml/min and feed composition of 0.26 H_2:0.2 iC_4H_{10}:0.54 N_2. as a function of sweep flow rate employing counter- and cocurrent sweep flow modes. The H_2/iC_4H_{10} separation factors can be seen in Figure 4-3. The separation factor increases with an increase in sweep flow rate up to a value of 40 for counter-current at 125 ml/min, and 35 for a cocurrent sweep flow rate of 175 ml/min.

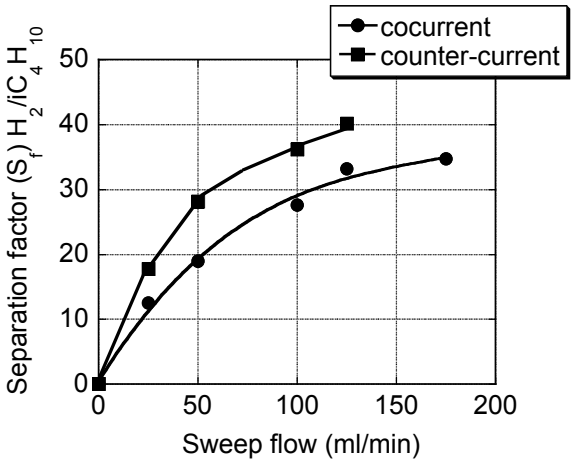

Figure 4-3 Hydrogen/Isobutane separation factors at 723 K, feed flow rate 50 ml/min, feed composition 0.26 H_2:0.2 iC_4H_{10}:0.54 N_2 as a function of sweep mode and rate.

Table 4-2 Single gas permeation data for MFI and Pd membranes

Membrane	Nitrogen [μmol/Pa.s.m^2]	Isobutane [μmol/Pa.s.m^2]	Hydrogen [μmol/Pa.s.m^2]
MFI	0.2	0.01	0.5
Pd	0.05	0.05	3

Zeolite membrane

Single gas permeation results for the MFI membrane are reported in Table 4-2. The hydrogen/isobutane separation experiments were performed under conditions (temperature, feed flow rates, sweep) similar to those used during catalytic tests. From Figure 4-4 it can be seen that the separation factor $S_f(H_2/iC_4H_{10})$ is highly dependent on the temperature and the sweep flow rate. At room temperature the separation factor is close to 1 and increases up to ca. 10 at high temperature (reaction conditions).

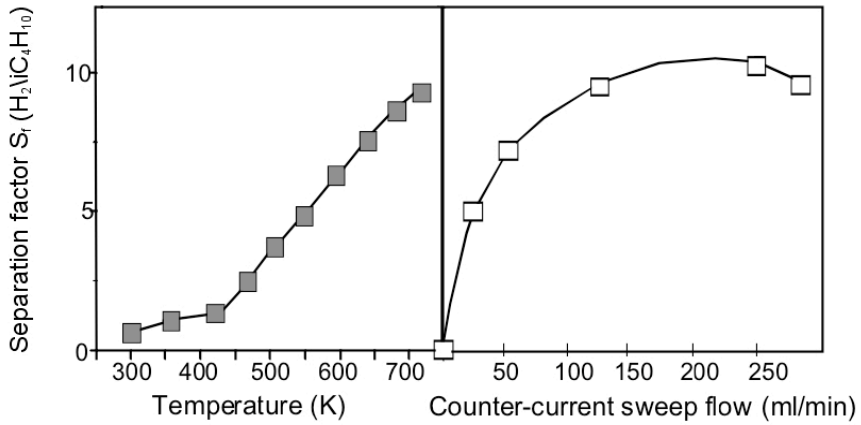

Figure 4-4 Separation factor S_f as a function of temperature (left) and counter-current sweep flow rate (right)

4.2.2 Discussion

Pd membrane

Dense Pd membranes are only permeable to hydrogen, and therefore the permeance of isobutane and nitrogen are an indication of some defects in the membrane, or leaks at the graphite seal interface. However, the overall performance (permeance and selectivity) of the Pd membrane is sufficient for eCMR operation, and different enough from the zeolite membrane's characteristics in order to provide interesting comparison. In Figure 2-46 the ideal permselectivity (H_2/N_2) for this membrane is given (120) after manufacture and subsequent single gas testing. This is a higher value than was obtained when the membrane was used for eCMR experiments and therefore, it is possible that some structural changes took place in the Pd film.

However, the H_2/N_2 permselectivity is 60, which is higher than that based on Knudsen transport (3.7). This shows that the H_2 permeance mainly occurs through metallic palladium. Due to the fact that hydrogen and isobutane transport proceeds

essentially through independent pathways, the performance of the Pd membrane in H_2/iC_4H_{10} separation during CMR operation can be estimated on the basis of the calculated permselectivity (60 in this case).

Mixture separation testing (Figure 4-3) indicates that the separation in the counter current flow mode leads to an improved selectivity of hydrogen over isobutane, when compared to the co-current mode. The separation factor increases with an increase in sweep slow rate for both sweep flow modes. It is expected from extrapolating the data for the counter-current mode that the separation factor at 185 ml/min would be around 43. From these values it appears that the separation factor is 2/3 of the permselectivity at this sweep flow rate.

MFI membrane

The mixture gasses (H_2, N_2, iC_4H_{10}) permeate through the same porous network, essentially that of the MFI material (defects contribution is limited [102]). The selectivity of the transport is governed by adsorption in the MFI-zeolite structure. At low temperatures iC_4H_{10} is strongly adsorbed in the MFI pores and blocks permeation of other species. However, due to the very small diffusivity of iC_4H_{10}, its transfer through the membrane is low and close to the limited amount of H_2 that may permeate, essentially through defects.

Hence, at room temperature, the H_2/iC_4H_{10} separation factor, S_f , is low (Figure 4-4). At higher temperature the adsorption and occupancy of iC_4H_{10} decrease. As a result, the H_2 permeation increases, leading to an increase in the separation factor.

Figure 4-4 also shows how the separation factor S_f varies with the sweep flow rate. There is a large increase of S_f in the 0-100 ml/min sweep range, then S_f goes through a maximum, close to 10. At high sweep flow rates the extraction of iC_4H_{10} increases in non negligible amounts leading to a decrease in the separation factor at high sweep flow rates.

Comparison of the two membranes

When compared to the MFI membrane under CMR operation conditions (T, feed, sweep), the Pd membrane shows a better performance for the H_2 permeance (ca. 4 - 6 times higher).

As far as the H_2/iC_4H_{10} separation factor is concerned, it is clear from the separation tests that the Pd membrane performs better in terms of selectivity than the MFI membrane for separation.

Therefore, it is concluded that the Pd membrane has a higher hydrogen extraction capacity than the MFI membrane and that it is more selective towards hydrogen than the MFI membrane.

4.3 CMR performance

4.3.1 Results

Pd membrane reactor

Figure 4-5 shows the results (iC_4H_{10} conversion and iC_4H_8 yield) as a function of the sweep flow-rate. In the absence of sweep, the reactor works as a conventional packed–bed reactor (no permeation through the membrane) and the isobutane conversion (14 %) corresponds to that predicted by the thermodynamic equilibrium. Isobutane conversion in the conventional reactor was checked before each eCMR test and the value stayed constant through all the runs. This means that the catalyst was active enough to reach isobutane equilibrium and that it did not suffer from deactivation during the test.

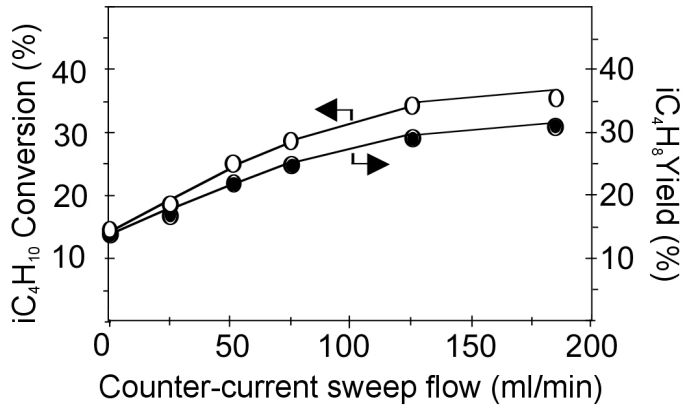

Figure 4-5 Isobutane conversion and isobutene yield in the Pd membrane reactor. Feed flow rate: 50 ml/min, feed composition: $H_2/iC_4/N_2$ =20/20/60

The isobutane conversion increased (Figure 4-5) up to ca. 37 % for a sweep flow rate of 185 ml/min (3.7 times the feed flow) in the eCMR. In all the sweep flow rates employed, the extraction of hydrogen led to an increase in the conversion when compared with the conventional packed-bed reactor. The increase in conversion does however come at the cost of a slightly lower selectivity (isobutene yield/ isobutane conversion) towards isobutene, 100 % to ca. 90 %.

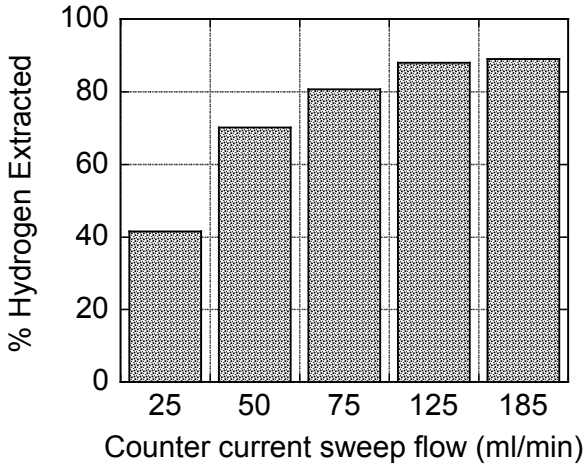

Figure 4-6 % Hydrogen extracted from the reaction zone

Figure 4-6 represents the various percentages of hydrogen extracted from the reaction zone at different counter-current sweep flow rates. As the conversion increases, more hydrogen is produced and consequently more hydrogen is available for extraction. At low counter current sweep flow rates the driving force for permeation (partial pressure difference of H_2) is low, but increases with an increase in the sweep flow rate. At 125 ml/min and 185 ml/min the presence of hydrogen in the reaction zone is low, around 10 %. The selectivity towards isobutene decreases with an increase in hydrogen extraction and therefore it can be concluded that the presence of hydrogen in the reaction zone has a positive effect on the selectivity of the catalyst towards isobutene.

Zeolite membrane reactor

Figure 4-7 shows the effect of the sweep on the isobutane conversion. van Dyk *et al*. [211] demonstrated that the selectivity towards isobutene was also negatively affected by the sweep, and varied in a similar way and range as for the Palladium eCMR. At the highest sweep flow rate the selectivities were: isobutene 90 %, n-butane 5 %, n-butene 3 %, C_3-C_1 products 2 %.

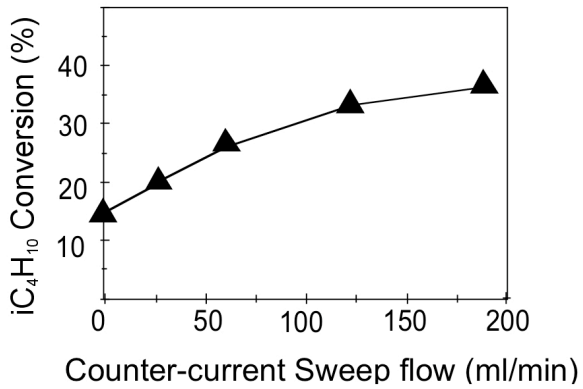

Figure 4-7 Isobutane conversion yield in the MFI membrane reactor. Feed flow rate: 50 ml/min, feed composition: $H_2/iC_4/N_2$ =20/20/60 [211]

4.3.2 Discussion

Comparison of CMRs performances

Figure 4-5 and Figure 4-7 show very similar behaviours for the MFI and Pd eCMRs. It is logical that the two systems will give the same conversion at zero sweep (conventional fixed-bed reactor). What is surprising is that, under high sweep flow rates the Pd eCMR does not draw any benefit from the better transport performances (H_2 permeance and selectivity) of the Pd membrane.

Previous work in our group by Ciavarella *et al.* [144] reported on the effect of sweeping mode on the performance of the MFI eCMR for the same reaction. It was found that in the co-current sweep mode, the membrane controlled the eCMR's performance, but that this was not the case in the counter-current sweep mode. Owing to the very high driving force that existed for hydrogen permeation, in the counter-current mode, at the outlet of the reactor, the catalyst was not able to establish equilibrium at the exit of the catalyst bed [144]

That interpretation is confirmed by the results shown here. It can therefore be said that the isobutane conversion in the eCMR (MFI and Pd) is not controlled by the membrane's hydrogen extraction capabilities, but rather by the catalysts ability to produce hydrogen. Therefore, the MFI and Pd eCMRs (packed with the same catalyst) showed similar performance when operated at the same reaction conditions.

One can speculate how to increase the catalyst performance to overcome this situation.

If the fixed-bed Pt-based catalyst is considered here as a "black-box" producing hydrogen, in competition with the membrane extracting hydrogen, it has been previously reported that this catalyst did not suffer, under similar conditions, of diffusive limitations [65]. The catalyst works therefore, under chemical regime.

This catalyst has been selected after a screening of different state-of-the-art active phases in dehydrogenation reactions [65] and showed excellent activity and stability under the present conditions. It has been patented [10].

Conventional ways to improve the catalyst performance, like temperature or contact time increases, would have only limited effects. As a matter of fact, a simple calculation shows that the hydrogen production rate, at the catalyst, is much lower than the permeation rate through the membrane, at the outlet of the CMR. This extends to a factor of up to 30 for the MFI membrane, and 80 for the Pd membrane, depending on the experimental conditions. Moreover, a temperature increase may deactivate the catalyst and change the selectivity. An increase in contact time could result in diffusion limitations in the active phase. Furthermore, increases in temperature and contact time, could even improve the membrane performance, increasing again this rate gap, which is not the targeted effect.

As far as catalytic selectivity is concerned, both systems give, when increasing sweep flow, the same and limited decrease of isobutene selectivity (from 100 to 90 %). This is what can be expected in the case of isobutane dehydrogenation on a Pt-zeolite-based catalyst. As a matter of fact, in this reaction, the main side reaction, isomerization (leading to the linear butane and butenes formation), goes through a dehydrogenation step of iC_4H_{10} [204]. Therefore, the higher the sweep, the higher the isobutane dehydrogenation and, the lower the isobutene selectivity. The fact that the two Pd and MFI eCMRs give the same selectivity results also suggests that the membrane has little effect on the catalysis itself.

In order to verify the conclusion drawn here, the eCMR has been modelled though a simple model assuming that the catalyst does not suffer from the negative effects of hydrogen extraction (kinetic model for microreactor experiments are valid for the eCMR).

4.4 Modeling

4.4.1 Model formulation

The model presented [211] here is a modified and more simple version of a detailed model previously presented by Casanave *et al*. [210]. The simplified version is however, well adapted for the purpose of this study.

A one-dimensional model was developed using the reaction rate expression and transport parameters of the membranes. The following assumptions were made in the derivation of the model:

- operation in steady-state,
- isothermal conditions,
- negligible transmembrane pressure,
- plug flow prevails in each compartment, axial dispersion negligible,
- pressure drops through packed-bed and shell side are negligible, and
- gaseous components behave as ideal gases.

Transport parameters were obtained from the permeation measurements, as described previously in this chapter. The reaction rate expression (Equation (4-4)) employed is that obtained by Casanave and co-workers [212] on a similar catalyst, using a differential microreactor. When operating in the vicinity of thermodynamic equilibrium its expression is:

$$r = \frac{k_1 K_{iC_4}\left(P_{iC_4} - P_{iC_4=}P_{H_2}/K_{eq}\right)}{\left(1 + K_{iC_4}P_{iC_4} + K_{iC_4=}P_{iC_4=} + \sqrt{K_{H_2}P_{H_2}}\right)^2} \qquad (4\text{-}4)$$

In order to take into account back permeation of the sweep gas, variations of the overall molar flow in the tube and shell sides are considered, owing to the chemical reaction and mass transfers through the porous media. Under the experimental conditions, Fick's law is sufficient to describe mass transfers through the membrane. The simulation was done for the membrane reactor operated in the counter current sweep configuration.

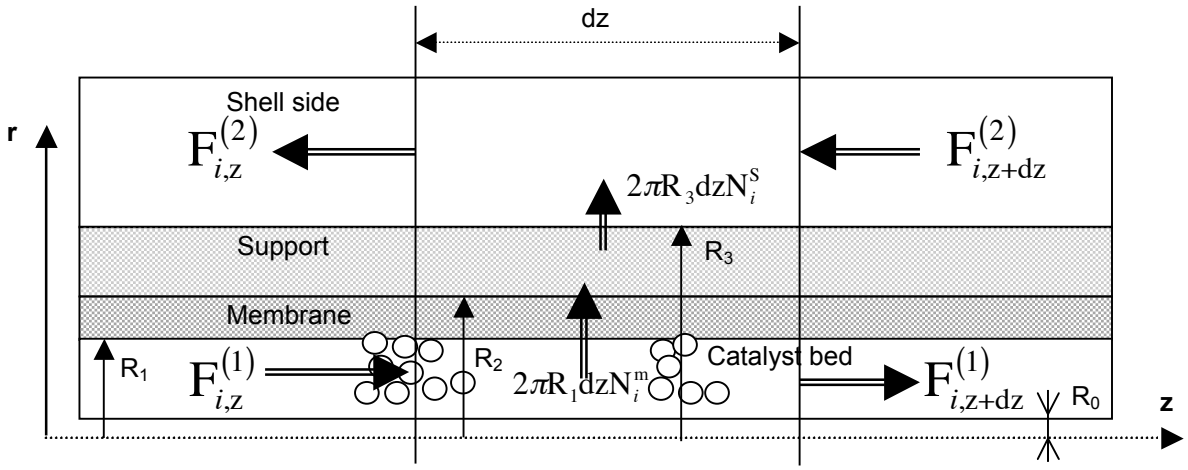

Figure 4-8 Schematic view of the eCMR in the counter current mode. The reactor is divided into four zones: Catalyst bed, membrane layer, and support and shell side.

A detailed description of the model and derivation thereof can be found in appendix B. For an elemental reactor length, dz, (see Figure 4-8, schematic of the eCMR) the differential equations describing mass balances in the axial direction for components i = iC_4H_{10} (isobutane, also noted iC_4), iC_4H_8 (isobutene, also noted iC_4=), H_2 and N_2 are:

Tube side:

The evolution of the molar flow rate of component i along the reactor length can be written as:

$$\frac{dF_i^{(1)}}{dz} = \nu_i \eta \rho \pi \left(R_1^2 - R_0^2\right) r + 2\pi \frac{P}{RT} \frac{D_i^m \varepsilon_m}{\tau_m} \frac{1}{\ln\frac{R_2}{R_1} + \frac{D_i^m \varepsilon_m}{D_i^s \varepsilon_s}\frac{\tau_s}{\tau_m}\ln\frac{R_3}{R_2}} \left(\frac{F_i^{(2)}}{F_T^{(2)}} - \frac{F_i^{(1)}}{F_T^{(1)}}\right) \tag{4-5}$$

The second term on the right-hand side of equation (4-5) represents the molar flow rate of component i through the porous membrane. The apparent density ρ is defined as the mass of catalyst with respect to the tube unit volume, ν_i is the algebraic stoichiometric coefficient of component i. The effectiveness factor, η, is introduced to account for some limiting effects on the activity of the catalyst in the eCMR, when compared to that measured in the differential micro-reactor. It should be noted that η has nothing to do with the diffusion limitations in the catalyst. It is just an adjustment term that will be used to quantify differences between model data (kinetics and transmembrane transfers analyzed separately) and experimental results obtained in the eCMR.

Terms D_i^s are molecular diffusivities that were calculated from the kinetic theory of gases.

The overall mass balance on the tube side is obtained by writing out equation (4-4) for each component in the gas stream and adding them together, and considering the fact that the operation pressure is constant:

$$\frac{dF_T^{(1)}}{dz} = -2\pi \frac{P}{RT} \sum_{j \neq I} \frac{\left(D_I^m - D_j^m\right) \varepsilon_m}{\tau_m} \frac{1}{\ln\frac{R_2}{R_1} + \frac{D_j^m \varepsilon_m}{D_j^s \varepsilon_s} \frac{\tau_s}{\tau_m} \ln\frac{R_3}{R_2}} \left(\frac{F_j^{(2)}}{F_T^{(2)}} - \frac{F_j^{(1)}}{F_T^{(1)}}\right) + \eta\rho\pi\left(R_1^2 - R_0^2\right) r\Delta\nu \tag{4-6}$$

where: $\Delta\nu = \sum_i \nu_i$

Shell side material balance:

For component *i*, $i \neq$ I (I being an inert or sweep gas)

$$\frac{dF_i^{(2)}}{dz} = (-1)^{n+1} 2\pi \frac{P}{RT} \frac{D_i^m \varepsilon_m}{\tau_m} \frac{1}{\ln\frac{R_2}{R_1} + \frac{D_i^m \varepsilon_m}{D_i^s \varepsilon_s} \frac{\tau_s}{\tau_m} \ln\frac{R_3}{R_2}} \left(\frac{F_i^{(2)}}{F_T^{(2)}} - \frac{F_i^{(1)}}{F_T^{(1)}}\right) \tag{4-7}$$

(n =1 for counter current)

The overall mass balance in the shell side is:

$$\frac{dF_T^{(2)}}{dz} = (-1)^n 2\pi \frac{P}{RT} \sum_{j \neq I} \frac{\left(D_I^m - D_j^m\right) \varepsilon_m}{\tau_m} \frac{1}{\ln\frac{R_2}{R_1} + \frac{D_j^m \varepsilon_m}{D_j^s \varepsilon_s} \frac{\tau_s}{\tau_m} \ln\frac{R_3}{R_2}} \left(\frac{F_j^{(2)}}{F_T^{(2)}} - \frac{F_j^{(1)}}{F_T^{(1)}}\right) \tag{4-8}$$

The boundary conditions for equations (4-5) to (4-8) are:

Tube side:

At z = 0

$$F_i^{(1)} = F_{i,0}^{(1)} \tag{4-9}$$

$$F_T^{(1)} = \sum_i F_{i,0}^{(1)} \tag{4-10}$$

Shell side:

At z = L (counter current)

$$F_i^{(2)} = F_{i,0}^{(2)} \tag{4-11}$$

$$F_T^{(2)} = \sum_i F_{i,0}^{(2)} \tag{4-12}$$

The system of differential equations (4-5) to (4-8) was rearranged by introducing dimensionless length.

Orthogonal collocation was applied for numerical discretization of the above-mentioned equations and IMSL routine DN2QNF was used for resolution.

Numerical parameters that have been used for the simulation are given in Table 4-3. Diffusivities D have been deduced from experimental values of single gas permeation.

The diffusivity coefficients D_i^m were estimated from permeation measurements with the membrane. Terms D_i^s are molecular diffusivities that were calculated from the kinetic theory of gases.

Table 4-3 Parameters used for simulation

$k_1 = 67\mu mols^{-1}g^{-1}$	$R_1 = 3.5mm$	$\varepsilon_s = 0.26$
$K_{ic_4} = 0.9atm^{-1}$	$R_2 = 3.505mm$	$\varepsilon_m = 0.5$
$K_{iC_4=} = 2.1atm^{-1}$	$R_3 = 5mm$	$\tau_s = 1.5$
$K_{H_2} = 0.8atm^{-1}$	$R_4 = 8mm$	$\tau_m = 1$
$K_{eq} = 0.033$	$R_0 = 0.08mm$	
$\rho = 0.53gcm^{-3}$	$L = 100mm$	

Zeolite	Palladium
$D^m_{iC_4} = 6.10^{-4}mm^2s^{-1}$	$D^m_{iC_4} = 3.10^{-3}mm^2s^{-1}$
$D^m_{iC_4=} = 6.10^{-4}mm^2s^{-1}$	$D^m_{iC_4=} = 3.10^{-3}mm^2s^{-1}$
$D^m_{H2} = 0.036mm^2s^{-1}$	$D^m_{H2} = 0.09mm^2s^{-1}$
$D^m_{N_2} = 0.012mm^2s^{-1}$	$D^m_{N_2} = 3.10^{-3}mm^2s^{-1}$

4.4.2 Results

The modeling approach shed some light on the comparison of the two eCMRs. Figure 4-9 (Pd eCMR) and Figure 4-10 (MFI eCMR) compare to the experimental conversions with those deduced from the modeling.

The thermodynamic equilibrium conversion in a conventional reactor is also given under similar conditions. This conversion slightly changes with the sweep flow rate in the eCMRs, owing to the pressure increase on the catalyst side. This is due to the fact that the increase of the sweep flow rate produces a pressure rise in the sweep side and a drop in the set-up pressure. To keep the transmembrane differential pressure to zero, the pressure on the catalyst side has to be increased. Figure 4-9 and Figure 4-10 show that both eCMRs perform better than the conventional system.

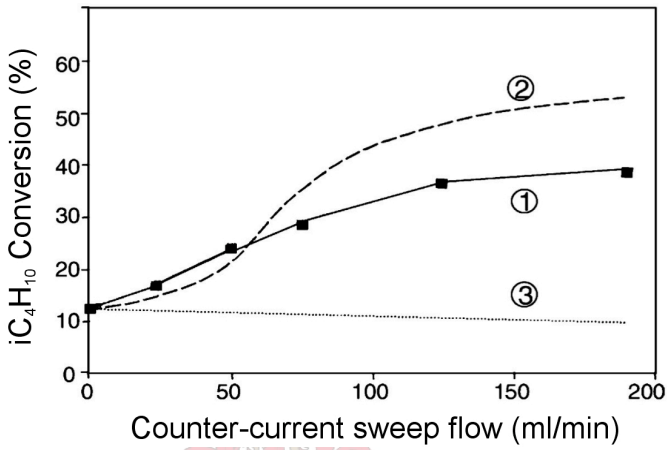

Figure 4-9 Pd CMR. Comparison of experimental data (curve 1) and modelling results (curve 2). Curve 3 represents the performance of a conventional reactor at equilibrium.

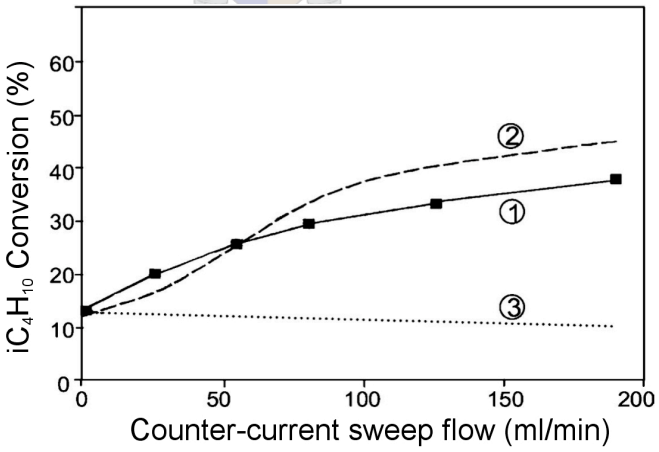

Figure 4-10 MFI CMR. Comparison of experimental data (curve 1) and modelling results (curve 2). Curve 3 represents the performance of a conventional reactor at equilibrium.

4.4.3 Discussion

As the model makes use of a kinetic law that has been obtained in a conventional microreactor, it predicts a performance that would have been observed if the catalyst was not limiting. The conversion given by the model corresponds to a situation where the catalyst would be efficient enough to take into account the high hydrogen extraction and re-establish the equilibrium under conditions prevailing at the exit of the catalyst bed.

The better the membrane separative performance, the larger the gap observed between experiments and modeling. This gap can be estimated using the factor η, as introduced in the modeling (equation (4-5)), to account for the catalyst efficiency in the CMR. These η values are obtained by adjusting the model response to the experimental data. For the MFI CMR, η is 0.6 and only 0.4 for the Pd CMR.

Therefore, as eCMRs are composed of a membrane and catalyst, each of these two materials may control the whole performance of the reactor. Until new catalysts are developed for eCMRs use, the only effective way to draw full benefit of the extraction ability would be to optimize the ratio of the membrane permeable area to catalyst weight. A way of calculating the optimum catalyst weight to membrane area ratio would be to fit a value for η onto the experimental values and then using this η, calculate the catalyst weight necessary to obtain the same conversion as for $\eta = 1$ (using the original catalyst weight). This optimization of the ratio would only be useful at sweep flow rates where the reaction is too slow to keep up with the extraction ability of the membrane. Another option would be to employ these membranes to dehydrogenation reactions in which more that one mole of hydrogen is produced per mole of hydrocarbon converted (e. g. cyclohexane to benzene).

4.5 Summary

The Pd and MFI eCMR, differed only on the basis of the membrane used. Isobutane dehydrogenation was performed at the same reaction conditions in order to assess the benefit of using a membrane with a higher hydrogen extraction capacity and selectivity for yield enhancement of the isobutane dehydrogenation reaction. The eCMR results of the two different membranes were similar. It has been shown that in order for the extractor-type CMR to completely draw benefit from their combination for yield enhancement, a very active catalyst should be developed, able to sustain the high extraction ability of the membrane.

This observation is consistent with those already reported [11] and may be extended to other types of eCMRs [144]. As a matter of fact, in an eCMR, the catalyst is often placed in a reactive medium different from that existing in conventional reactors, for which catalysts have been generally designed [10].

The need of an adapted catalyst may be a general feature of eCMRs, which receive less attention than that dedicated to membranes.

Another direction would be to look at reactions producing slower permeating products, to synchronise extraction with reaction. This concept is illustrated in the next chapter.

5 The use of an eCMR to enhance reaction selectivity: Meta-xylene isomerization

The *extractor* Catalytic Membrane Reactor can be used to enhance the selectivity of a reaction, if in a consecutive reaction network, the desired product is a reaction intermediate and it is extracted before further conversion of this product occurs.

Xylenes (Figure 5-1) are industrially important chemicals. Para-xylene is used to manufacture dimethyl terephthalate (DMT) and terephthalic acid (TPA), polyester resins. Polyester resin, in turn is used to manufacture polyester fibres, film and fabricated items (e.g. beverage bottles). Ortho-xylene is a raw material for phthalic anhydride, which is converted into phthalate plasticizers used in flexible polyvinyl chloride (PVC). Meta-xylene is converted into iso-phthalic acid, mainly used for the synthesis of polyster resins [213].

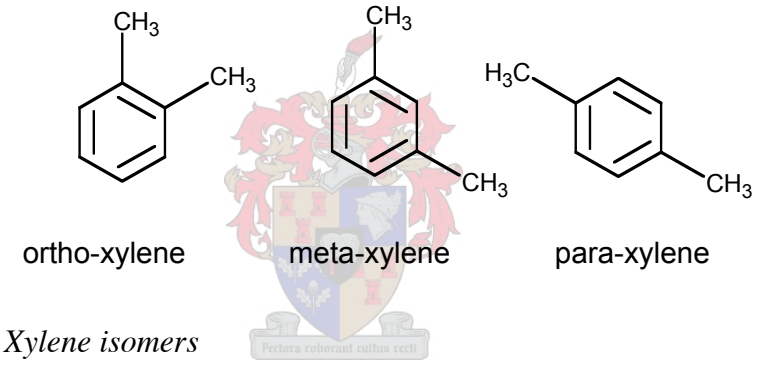

Figure 5-1 Xylene isomers

In 2003 the wordwide demand for xylenes was about 22 million metric tons, with para-xylene holding 80% of the market share. Ortho-xylene comprises 11% and about 8% of the output goes for meta-xylene and solvents. The remaining 1% is used as blending stocks in gasoline [214].

Principle sources of xylene isomer mixtures are catalytically reformed naphthas and pyrolysis distillates [213]. The C_8 aromatic cut from these sources contains a mixture of xylenes (50 – 60 % of meta-xylene and 20 – 25 % ortho- and para-xylene) and ethylbenzene (20% and 50% EB in the C_8 fractions originating from naphtha reforming and steam cracking respectively) [215]. Commercial isomerization is the conversion of surplus ortho- and meta-xylene into the more valuable para-xylene [216].

In this part of the dissertation, the eCMR (MFI-zeolite membrane packed with a Pt-HZSM5 catalyst) is used to simultaneously, convert meta-xylene to a mixture of xylenes and to separate para-xylene, with the objective to enhance the reaction selectivity towards

para-xylene. The work presented in this chapter has been accepted for publication in Catalysis Today [217].

5.1 Literature review

5.1.1 Xylene isomerization

A number of commercial xylene isomerization processes exists: MHAI, MVPI, XYMAX, Octafinning and Isomar. The first three processes are available from Mobil. Octafinning-I/II are available from Acreon Catalysts of Houston, Tex., formally known as Engelhard Corporation and the Isomar processes are available from UOP, Inc. of Des Plaines [216, 218].

Thermodynamic Equilibrium of Xylene Isomerization

Xylene isomerization is a thermodynamic equilibrium restricted reaction network (Figure 5-2). K_1 (m-xylene ⇋ o-xylene), K_2 (p-xylene ⇋ m-xylene) and K_3 (p-xylene ⇋ o-xylene) are the thermodynamic equilibrium constants of the various isomerization reactions.

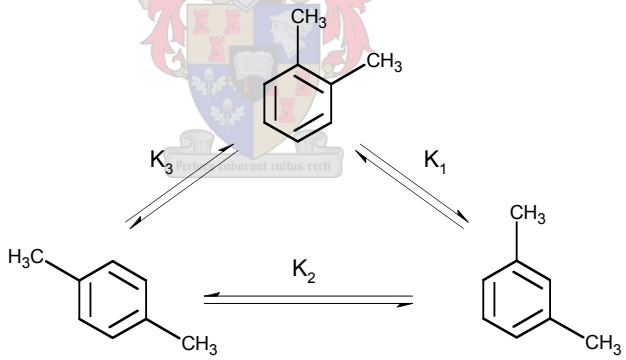

Figure 5-2 Xylene isomerization reaction network. K_1 (m-xylene ⇋ o-xylene), K_2 (p-xylene ⇋ m-xylene) and K_3 (p-xylene ⇋ o-xylene) are the thermodynamic equilibrium constants of the various isomerization reactions.

Recent thermodynamic equilibrium calculations based upon new calorimetric and physical property measurements of para-, meta- and ortho-xylene have been done by Chirico and Steele [219]. Figure 5-3 shows the change of the equilibrium constants in the standard state (ideal gas at p = p° = 101.325 kPa) for temperatures between 250 and

1500 K. It should be noted that values at 600 – 1500 K were calculated by extrapolation of the calorimetric results.

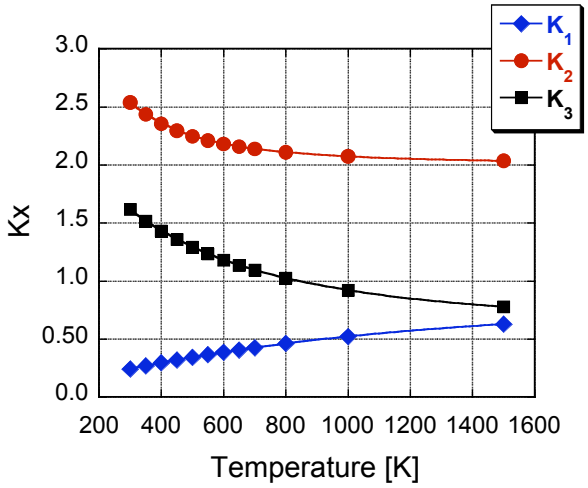

Figure 5-3 Equilibrium reaction constants K_x over the temperature range 250 – 1500 K [$x = 1$ (m-xylene ⇋ o-xylene), $x = 2$ (p-xylene ⇋ m-xylene) and $x = 3$ (p-xylene ⇋ o-xylene] [219].

The equilibrium constant of a reversible reaction characterizes the *position* of the equilibrium. The larger the equilibrium constant, the more equilibrium favours the products; the smaller the equilibrium constant, the more the equilibrium favours reactants [220]. When we have a reaction network as in Figure 5-2, where all the reaction products are linked, it is difficult to apply the above-mentioned definition of the equilibrium constant in order to see the extent of the equilibrium. It is therefore, more convenient to look at the combined product distribution (or net-effect) of the three dependent reactions with temperature (Figure 5-4).

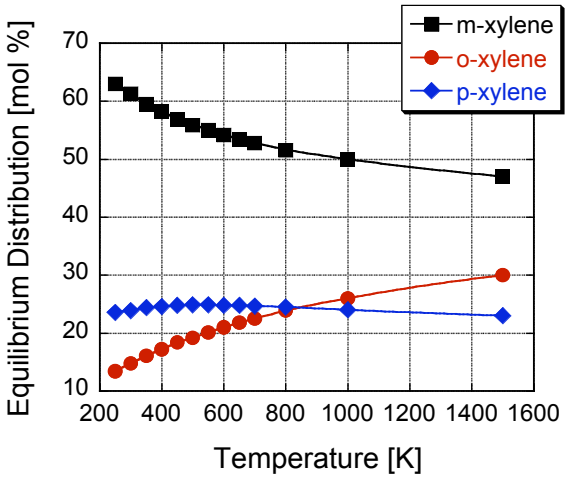

Figure 5-4 Equilibrium product distribution (mol %) for xylene isomerization in the standard state (ideal gas at p = p° = 101.325 kPa) as a function of temperature [219].

Some observations can be made from Figure 5-4. Temperature does not influence the equilibrium conversion of para-xylene significantly. Temperature has a bigger influence on the thermodynamic equilibrium conversion of meta- and otho- xylene. Ortho-xylene conversion displays an increase with temperature, while meta-xylene conversion decreases with temperature. It seems as though the gain in ortho-xylene conversion is a direct consequence of the loss in meta-xylene conversion, because the para-xylene conversion stays relatively constant over the temperature range. This is particularly true for temperatures ranging from 450 – 700 K, where the change in para-xylene conversion is ±1 %.

Xylene isomerization catalysts

The commercial C_8 aromatic cut from principle sources (naphthas and pyrolysis distillates) contains ethylbenzene (EB) and therefore two broad categories of xylene isomerization catalysts exits: EB isomerization catalysts, which convert ethyl benzene into additional mixed xylenes and EB dealkylation catalysts, which converts ethyl benzene to a valuable benzene co-product [221].

Practically all of the currently working isomerization plants are using catalysts with base mordenite or ZSM-5 [222]. Other catalysts that have been studied with this reaction includes: zirconia modified by tungsten oxide [223], H-Y zeolite [222, 224], HFAU [225], zeolite beta [222], UZM-5 and UZM-6 zeolites [226], active amorphous silica [227] and modified catalysts derived from above mentioned catalysts, to name but a few. Adair *et al.*

[228] also studied the reaction of m-xylene over all known intersecting medium zeolites and compared the results to values obtained with zeolites of large and large pores.

Xylene isomerization is an acid-catalyzed reaction. Gas phase isomerization of xylene over solid acidic catalysts can occur through an intramolecular mechanism (Figure 5-5) involving bensonium–ion intermediates and/ or through an intermolecular mechanism (Figure 5-6) involving successive xylene disproportionation reactions and fast transalkylation between trimethylbenzene and reactant xylene molecules.

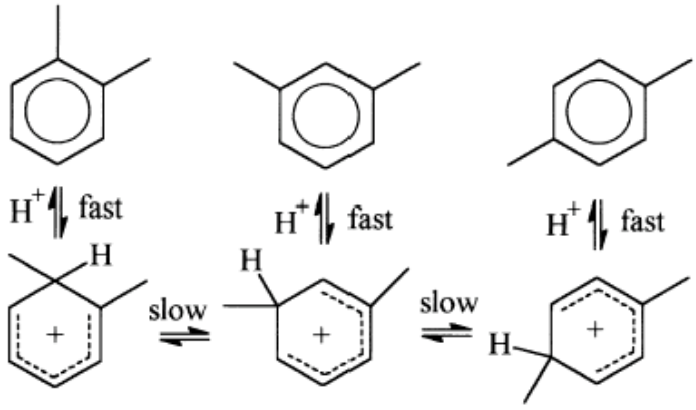

Figure 5-5 Xylene isomerization: Intramolecular mechanism.

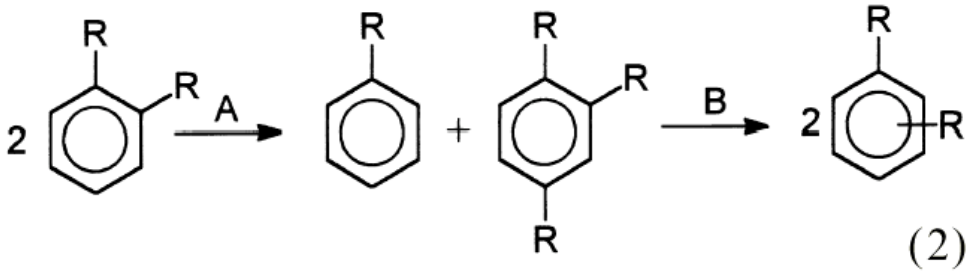

Figure 5-6 Xylene Isomerization: Intermolecular mechanism.

Xylene isomerization occurs predominantly through the intramolecular mechanism on *fresh* catalysts and also:

- when steric constraints in the vicinity of the acid sites limits (large pore zeolites such as EMT, BEA, etc.) or inhibit (for zeolites with average pore size, like MFI) the formation of bulky diphenylmethane intermediates of transalkylation;
- when catalysts possesses very strong acid sites e.g. protonic sites of HFAU in interaction with extra-framework aluminum species. These sites are

unable to catalyse transalkylation because diphenylmethane intermediates of this reaction are transformed into coke precursors; and

- when the pores are too large (e.g, amorphous silica-alumina) for allowing a concentration effect, which favours bimolecular reactions such as transalkylation.

The intermolecular mechanism becomes predominant with HFAU samples in which localized groups of weak protonic acid sites exists and is the only mechanism observed for isomerization with mesoporous MCM-41 aluminosilicates. Last mentioned catalysts displays a shape selectivity called "tunnel shape selectivity", due to the fact that xylene molecules undergo, successive reactions of disproportionation and transalkylation, before desorption, in the long , non-interconnected channels of these molecular sieves [216].

The ZSM-5 catalyst was developed by Mobil and its development for commercial use as a xylene isomerization catalyst took about 17 years [218]. The medium pore size ZSM-5 zeolite is of great interest due to its unique shape-selectivity characteristics which gives it a good selectivity with respect to para-xylene and also in its selectivity with respect to undesired secondary dismutation reactions, which is lower than those recorder for zeolites with large pores [229]. A kinetic study of the isomerization of xylene on the pellet form of HZSM-5 zeolites were done by Li and Jun [230]. It is generally considered that xylene isomerization over ZSM-5 is monomolecular and does not require the formation of a bimolecular intermediate. From the results obtained during the study they proposed a triangular network of reactions and suggested that the toluene present were due to the dealkylation of xylene isomers and not disproportionation, because no trimethylbenzene were found in the effluents of the isomerization reactions. It was assumed that the reaction follows simple order kinetics with respect to the sorbed phase concentration and the kinetic parameters for the reactions are given at four temperatures.

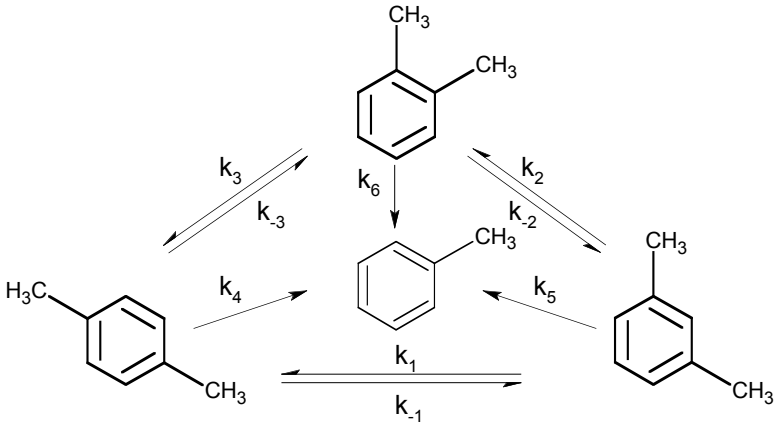

Figure 5-7 Triangular reaction network: Xylene isomerization HZSM-5 [230].

Bauer *et al.* [231] compared m-xylene isomerization on a Pt/HZMS-5 catalyst and a pre-coked Pt/ HZSM-5 catalyst to demonstrate that the para-xylene selectivity could be enhanced by surface modification by a pre-coking treatment. They assumed an intramolecular 1,2-methyl group shift model for the m-xylene isomerization. Their proposed meta-xylene isomerization reaction network is presented in Figure 5-8.

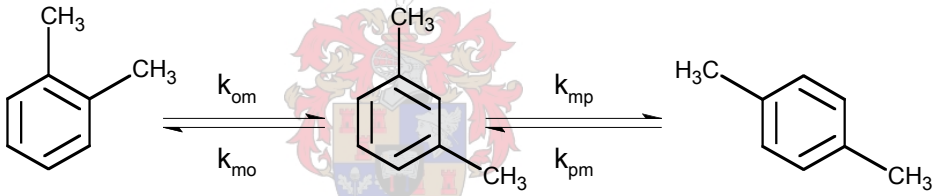

Figure 5-8 Reaction pathway of meta-xylene isomerization on Pt/HZSM-5 as proposed by Bauer et al. [231].

Therefore, in literature two reaction pathways for m-xylene isomerization over HZSM-5 catalysts have been proposed. Both were used to fit kinetic data with equal success making it difficult to say which one is more suited for the reaction. The triangular mechanism is readily adopted because it is said that due to the fact that the ortho- and meta-xylene undergo a number of "isomerizations" in the zeolite pores before it escapes as para-xylene, the global mechanism appears to indicate a reaction between para- and ortho-xylene.

Large pore size opening zeolites like mordenite (12 MR, opening with 12 oxygen atoms) do not have properties of geometric selectivity. Their selectivities towards p-xylene are lower that those obtained by ZSM-5 zeolites, irrespective of their Si/Al ratio. The production of trimethylbenzenes by disproportionation is promoted, because the microporous system is more open than ZSM-5 [229]. Henriques *et al.* [232] studied the

coke formation during o-xylene isomerization over two H-mordenites (framework SiO_2/ Al_2O_3 ratios of 15 and 75) at various temperatures. They found that o-xylene isomerization was very temperature dependent. At 523 K, low conversions were obtained with m-xylene being the only product. At 623 and 723 K disproportionation of xylene were observed as a secondary reaction and the product stream contained all the xylene isomers, toluene and trimethylbenzenes. At 723 K isomerization equilibrium conversion for o-xylene were obtained with the H-mordenite catalyst with a framework SiO_2/ Al_2O_3 ratio of 75. These results were better than those obtained with the other H-mordenite (framework SiO_2/ Al_2O_3 ratio 15) and was explained by the fact that the reagents had better access to the active sites because of its bigger pore system, making it more active even though its acidity were lower. This H-mordenite catalyst sample (SiO_2/ Al_2O_3 ratio of 75) was more resistant towards deactivation, because its larger pores decreased its susceptibility to blockage by coke.

Another large pore zeolite Y-zeolite has also been studied for the isomerization of xylene. Unimolecular and bimolecular pathways of xylene isomerization are possible over HY zeolites [225]. Through the bimolecular pathway direct p-xylene to o-xylene (and vice versa) can occur. This bimolecular isomerization would occur through two successive steps, disproportionation of the xylene reactant followed by a transalkylation reaction between trimethylbenzene and the reactant.

(5-1)

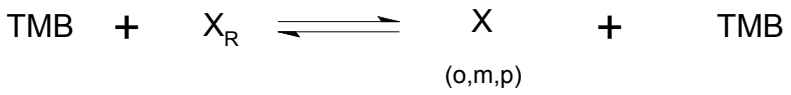

(5-2)

Where X_R, T and X (o,m,p) are the xylene used as reactant, toluene, and xylene mixture respectively.

For direct isomerization of xylenes the kinetic rate constant of the second reaction must be faster than the first. Gendy and Pratt [224] developed kinetic models for o-xylene isomerization over a HY zeolite, taking into account the catalyst activity decay functions. The model does not mention the possibility of a bimolecular isomerization, although two models were investigated: one with o-xylene—p-xylene interconversion and one without. Both models made provision for disproportionation of xylenes.

5.1.2 Xylene isomer separation

As mentioned previously the C_8 aromatic cut contains a mixture of xylenes and ethylbenzene, and hence in order to obtain the more valuable para-xylene, separation from its isomers and ethylbenzene is essential. The recovery of ortho-xylene is possible by fractional distillation, but due to the close boiling points (Table 5-1) of the other compounds in this mixture separation through distillation is difficult. A way to overcome this problem is to recover para-xylene by fractional crystallization, taking advantage of the differences in the melting points of the compounds [233].

Table 5-1 Boiling and melting points of xylene isomers and ethylbenzene [234].

Xylene Isomer	Boiling Point [K]	Melting Point [K]
ortho-xylene	417	248
meta-xylene	412	225
para-xylene	411	286
ethylbenzene	409	178

Para-xylene can also be recovered through selective adsorption (separation of chemical compounds by structural class). Para-xylene is adsorbed from the isomer mixture by an adsorbent (solid) and stripped from the adsorbent with a desorbent (liquid). Para-xylene is then separated from the desorbent by fractional distillation. Adsorbents employed in this process includes molecular sieves like type A, X or Y zeolites or silicalite [235]. This concept has been used in the simulated moving bed (SMB), which is a large-scale version of high-performance liquid chromatography used in laboratories to purify or separate mixtures of compounds. SMB is a continuous process in which a solvent and the compounds to be separated are injected into and withdrawn from a ring of chromatographic columns at rotating points between the columns. This technique simulates movement of the chromatographic packing material, or bed, against the solvent stream and allows for continuous recovery of the desired compound [236]. SMB has been used for decades in large-scale separations, notably the Parex process pioneered by Des Plaines, III-based UOP for extraction of p-xylene from mixed xylenes.

Recent research efforts focus on using MFI-zeolite membranes for xylene separation, a potentially more energy-efficient separation method [81, 237-239].

Xylene separation in MFI-zeolite membranes

The MFI zeolite pore structure consists of straight, circular pores (0.54 × 0.56 nm), interconnected with sinusoidal, elliptic pores (0.51 × 0.54 nm) [89]. These pore sizes are close to the kinetic diameter of para-xylene (d_k = 0.58 nm), and it is expected that its bulkier isomers (d_k = 0.68 nm) would diffuse at a slower rate, and adsorb to a lesser extent in the MFI framework due to their size and shape [238]. Therefore, xylene isomer separation in MFI-zeolite membranes relies on intracrystalline molecular sieving.

Moreover, the molecule of m-xylene will enter the pores of the zeolite with more difficulty than that of o-xylene. The o-xylene molecule has two methyl groups at 4 and 5 positions in the benzene ring. The neighbouring methyl groups of the molecule may distort and the whole molecule can slowly squeeze into the micropores of the zeolite. As for the m-xylene, two methyl groups are located at the position of 1- and 3-in benzene ring, which makes it more difficult for the molecule to enter.

It is well-known that the framework symmetry of MFI-type zeolites are strongly related to the nature and amount of guest molecules sorbed in the channel system of the zeolite. It has been shown experimentally and through molecular dynamics studies that in the p-xylene/MFI system the *orthorombic* MFI undergoes a phase transition with increasing loading of p-xylene from the ORTHO phase (2 < p-xylene/unit cell ≤ 4) to the PARA phase at higher para-xylene loadings (4 < p-xylene/unit cell ≤ 8). Besides the fact that the cross channel in PARA MFI is rather skewed, there is little difference between the PARA and ORTHO structures, but this difference is significant enough to cause a change in adsorption behavior. At coverage lower than 4 the sorbed p-xylene are located at the channel-intersections. At a coverage greater than 4 molecules per unit cell, sorbates occupy sites along the cross channels. The sites along the straight channels between intersections are left largely unoccupied owing to steric hindrance by the sorbates at the intersections [240, 241].

A number of research groups have carried out studies in this area with different results. Baertsch *et al*. [237] studied para- and ortho-xylene separation with a silicalite-1 membrane containing a large amount of non-zeolitic pores (N_2/SF_6 permeance ratio of 86 and N_2 permeance of 2 μmol/Pa.s.m^2). No separation could be achieved with a feed mixture of ~ 3 mol% p-xylene, 3 mol% o-xylene and 94 mol% He, over the temperature range 380 to 480 K, even though p-/o-xylene ideal selectivities were as high as 12. This behaviour was attributed to single-file diffusion, which according to this group is the

controlling mass transfer mechanism at high p- and o-xylene concentrations, as was the case here. When single file diffusion occurs the channels in the membrane are not large enough for molecules to pass one another and therefore the molecule with the slowest permeation rate limits diffusion. At the high concentrations used, it was equally probable for o-xylene and p-xylene to enter the pores of the membrane. The lack of separation may, however, only be due to diffusion through defects, which will render no separation.

Gump *et al*. [89] studied the fluxes of aromatic molecules (p-xylene, o-xylene and benzene), through several molecular sieve membranes (SAPO-5, SAPO-11 and mordenite) as well as three types of MFI membranes (silicate-1, ZSM-5 and boron substituted ZSM-5), as a function of pressure and temperature. They found that surface diffusion and what they called "activated gas transport" were the controlling mechanisms for MFI membranes. The boron-substituted ZSM-5 membrane displayed the highest p-xylene/ o-xylene selectivities. The best selectivities, 130 (ideal) and 60 (separation), were obtained at 425 K and feed partial pressures of 2.1 kPa. p-Xylene preferentially permeated through the zeolite pores, while o–xylene preferentially permeated through non-zeolite pores. The permeation of p-xylene however, takes 8 hours to reach a steady state. They claimed higher pressures of p-xylene distorted the film-like membrane framework leading to higher o-xylene permeation and reduced selectivity. The flux of p-xylene through the zeolite pores was stable for at least 10 hours after steady state was reached. The flux of o-xylene through non-zeolite pores was stable at 373 K, but continuously decreased for at least 12 hours at 405 K.

Masuda *et al*. [46] used a ZSM-5 zeolite membrane reactor in order to convert methanol to olefins. The zeolite layer, which was deposited on the outer layer of a cylindrical alumina ceramic filter, acted as the catalyst. In order to ensure that the zeolite contained no cracks single gas p-xylene, m-xylene and diethylbenzene permeation tests were carried out with the membrane. The membrane was sealed at one end and the inside of the membrane was evacuated from the other end, while pure vapour filled the apparatus in which the membrane was mounted. The ZSM-5 zeolite membrane (8 μm) displayed an ideal p/m-xylene selectivity of 2.7 with a p-xylene permeability of 0.07 nmol.m/m^2.s.Pa at 303 K. When using different ZSM-5 membrane, which had some cracks, the membrane showed no molecular sieving ability and the ideal selectivity of p/m-xylene was 1.

Matsufuji *et al*. [242] performed single and mixture gas permeation measurements of butane isomers at 300 - 375K along with xylene isomer pervaporation tests with MFI-

zeolite membranes at 303 K, supported on α-alumina flat disks. n-Butane was preferentially adsorbed in the binary system, displaying separation factors (nC_4H_{10}/iC_4H_{10}) of 28 at 300 K, 40 at 335 K and 69 at 375 K, which was always better than the ideal selectivity. During pervaporation tests for single liquid components the flux of p-xylene was the largest among the three kinds of isomers and were explained by the size effect (kinetic diameters p-xylene 0.59 nm, m-xylene and o-xylene 0.68 nm). When a mixture of p-xylene/m-xylene (50:50) was used, the flux of p-xylene was initially higher than that of m-xylene for the first 660 minutes, but decreased thereafter. The flux of p-xylene was also the highest in a unary mixture of p-xylene, m-xylene and o-xylene (24:51:25) for the first 500 minutes, but thereafter m-xylene permeated preferably followed by o-xylene and then p-xylene. It was concluded that the permeation of p-xylene might have been blocked by strongly adsorbed m-xylene and o-xylene, which were slower components.

Keizer *et al*. [243] reported p-xylene/o-xylene selectivities as a function of time between 293 and 475 K for a silicalite-1 membrane (supported on a flat α-alumina disks). For a feed mixture of 0.31 kPa p-xylene, 0.26 kPa o-xylene and 99.4 kPa helium, they obtained values of ~ 1 (298 K) to > 200 (375 - 415K) with a maximum at ~400K. The selectivity was 25 at 473K. The same experiments were conducted with a feed of 0.62 kPa p-xylene and 0.52 kPa o-xylene and the same temperature dependence was observed as at the lower xylene concentration. The o-xylene flux did not influence the p-xylene flux at low temperature and therefore, no blocking effect was observed. The maximum p-xylene flux at 400 K was said to be due to opposing effects of sorption and diffusion.

Researchers from Exxon [244] reported xylene separation testing at temperatures between 443 K and 573 K, with xylene mixture feeds of 1 ml/min and a argon sweep gas flowrates between 100 and 400 cc/min in their ZSM-5 zeolite membranes made by seeded growth. The pressure of both argon and the xylene feed were fixed at 1 atm (abs). The best separation factors for p-xylene over its isomers (either meta- or ortho-xylene) were < 1.75 (ranging between 1.0 - 1.4) for the as-prepared membranes (c-orientated ZSM-5 zeolite layer). These results for maximum selectivities were less than expected (for experimental range selectivities expected > 2.5 determined from diffusion coefficient of xylene isomers in type MFI crystals used) and it was determined experimentally that the membranes suffered from defects after the separation tests. Polyimide protective layers were consequently deposited on the ZSM-5 layers and selectivities of 4 - 10 were obtained, showing selectivity enhancement due to the polyimide protective layer.

Xomeritakis *et al.* [238, 245, 246] conducted an extensive study of xylene vapour permeation through orientated MFI-zeolite membranes. Single gas permeation tests at feed partial pressures of 0.86 and 0.64 kPa for p-xylene and o-xylene were performed in the temperature range 295 - 548 K for c-orientated MFI membranes. It was found that p-xylene permeance displayed weak temperature dependence, while o-xylene permeance displayed a minimum at 373 K. When p-xylene was added in the o-xylene feed, the flux of o-xylene was greatly enhanced. Also, as the partial pressure of p-xylene in the feed mixture enhanced from 43 to 430 Pa, the selectivity dropped from 48 to a value of 3. Only when feeds of p-xylene partial pressures < 0.05 kPa were introduced over the MFI membranes, were separation factors up to ~ 20 observed. It was found that the addition of n-hexane in a binary feed mixture of para-and ortho-xylene resulted in an improvement of mixture separation factors up to 60. The same research [247] group successfully synthesized b-orientated siliceous ZSM-5 membranes, using the same seeded growth method, but adding organic polycations as zeolite crystal modifiers to enhance the growth rates along the desired direction. These b-orientated ZMS-5 membranes showed superior performance for the separation of para- and ortho-xylene, with para-xylene permeance values as high ~ 0.2 μmol/Pa.s.m^2 and p-/ o-xylene separation factors between 200 - 450 for a feed mixture of 0.45 kPa p-xylene and 0.35 kPa o-xylene at 473 K. However, in this last case, the conclusion of higher selectivity for b-orientated samples has to be taken with care, as the differently orientated samples may have included different membrane defect density.

Sakai *et al.* [239] used self-supporting MFI zeolite membranes to carry out vapour permeation by the Wicke-Kallenbach method in nitrogen flow to examine p-xylene separation from the ternary mixture of xylene isomers as a function of time (0 – 72 hours), temperature (303 – 673 K), para-xylene feed partial pressure (0.3 - 5.1 kPa) and membrane thickness (60 - 130 μm). The p-xylene permeation flux showed a maximum at 473 K and a partial pressure of 0.3 kPa, with a permeance of 82 nmol/Pa.m^2.s. The maximum was described by the competitive effects between the amount of equilibrium adsorption and diffusivity. m-Xylene and o-xylene showed similar permeances, which were small and almost constant between 473 and 673 K. The separation factors of p- /m-xylene and p- /o-xylene showed a maximum value of 250 at 473K. The permeation flux was proportional to the para-xylene partial pressure for both single component feed and the ternary mixture

of xylene isomers from 473 to 673 K. In the experimental range studied here, the thickness of the membrane (130 – 60 μm) had little effect on the p-xylene permeation flux.

Hedlund *et al.* [248] did xylene separation studies at high pressures and temperatures. They used ultra thin MFI membranes (film thickness of 0.5 μm) supported on α-alumina membrane supports. The membranes were produced by a two-step support masking technique and a monolayer of colloidal nucleation seeds, followed by in situ hydrothermal growth. A separation factor of 3.2 was obtained for a binary feed mixture of 0.27 kPa p-xylene/ 0.59 kPa o-xylene, with a p-xylene permeance of 0.6 μmol/(Pa.s.m^2) at 373 K. For the same feed composition at 663 K the separation factor increased to 16, while the p-xylene permeance dropped to 0.3 μmol/(Pa.s.m^2). The high permeances for p-xylene achieved in this study were attributed to the thin nature of the zeolite film. High pressure xylene separation tests were carried out at 100 kPa hydrocarbon partial pressure (200 kPa) and 773 K. The permeance of p-xylene was 0.11 μmol/(Pa.s.m^2) while a p-/m-xylene separation factor of 13 was obtained. The selectivity and p-xylene permeance dropped to 5 and 27.5 nmol/(Pa.s.m^2) when the hydrocarbon partial pressure increased to 0.5 MPa (1.8 MPa total pressure). The drop in p-xylene permeance was attributed to an increased loading of the zeolite channels.

In a patent by NGK [249] they claim to have developed a method for separation of p-xylene from a mixture of xylenes and ethylbenzene at high temperature and high pressure using a MFI-zeolite membrane. The inventors found that at a low p-xylene partial pressure region, the p-xylene adsorption increased sharply with a p-xylene partial pressure increase, but the increase became small when the partial pressure reached a certain level and higher. It was recommended that the temperature at which separation is done should be equal or higher than 473 K, while the p-xylene partial in the retentate should be kept at 100 kPa or higher and the p-xylene partial pressure on the permeate side should be kept at 20 kPa or lower.

Conclusions

From the above studies a few general conclusions can be drawn for xylene isomer separation through MFI-zeolite membranes:

- At high xylene isomer concentrations single file diffusion may occur, due to the high occupancy of the isomers on the external surface blocking para-xylene from entering the pores. It could, however, also just be that the membrane contains defects.

- MFI-membranes with defects renders little to no separation of the xylene isomers, even though some show satisfactory separation of other molecules e.g. butane isomers, nitrogen and sulphur hexafluoride. Meta- and ortho-xylene permeate preferentially through defects, while para-xylene permeates through zeolitic pores. Xylene isomer separation by MFI-zeolite membranes is therefore, a widely accepted test for benchmarking their molecular sieving ability. Separation relies on intracrystalline molecular sieving and is therefore, an ideal testing method to determine the presence of nano-scale defects and describe intercrystalline transport pathways.
- Para-xylene permeance through MFI-zeolite membranes displays a maximum due to the opposing effects of adsorption and diffusion through the zeolite pores. Some groups have also observed so-called *activated diffusion* at higher temperatures.
- Single gas permeation of meta- and ortho-xylene is possible through MFI-zeolite membranes.

5.1.3 Xylene isomerization in an eCMR

Research in this area is limited, with one reference in literature made to experimental laboratory scale studies on the subject. Research on xylene isomerization in a MFI membrane reactor was conducted by Mabanda *et al.* [250], but their results indicated that the separation of xylenes through the membrane was not sufficient enough to improve on the performance of the conventional reactor.

ExxonMobil [233] owns a patent in which they postulate the use of eCMR technology for the process of para-xylene production. Figure 5-9 is a process flow diagram, one of six, in which they proposed the use of a MFI type zeolite membrane in para-xylene production. This specific one refers to the membrane separation and reaction being in one unit (CMR). Fresh feed containing xylenes are fed to a xylene splitter in which xylenes are separated from higher boiling components (may include ortho-xylene). The overhead stream, withdrawn from the splitter, contains xylenes and ethylbenzene and is fed to the xylene recovery unit. The xylene recovery unit can use fractional crystallization and/or molecular sieve separation to separate para-xylene form other components. The para-xylene depleted stream is then sent to the eCMR for isomerization of ortho-and meta-xylene to para-xylene and the conversion of ethylbenzene to benzene and/or xylenes. Para-xylene is selectively extracted from the reaction zone to the permeate

stream. The retentate stream should ideally be at equilibrium or near equilibrium. These two streams may be treated separately (not shown in Figure 5-9) or the streams can be combined and sent for C_5^- (and lighter compound) removal and then for toluene (and lighter compound) removal (DETOL). The xylenes and heavier compounds are then sent back to the Xylene splitter unit. Fresh feed can also be fed to the eCMR along with the para-xylene depleted stream from the para-xylene recovery unit.

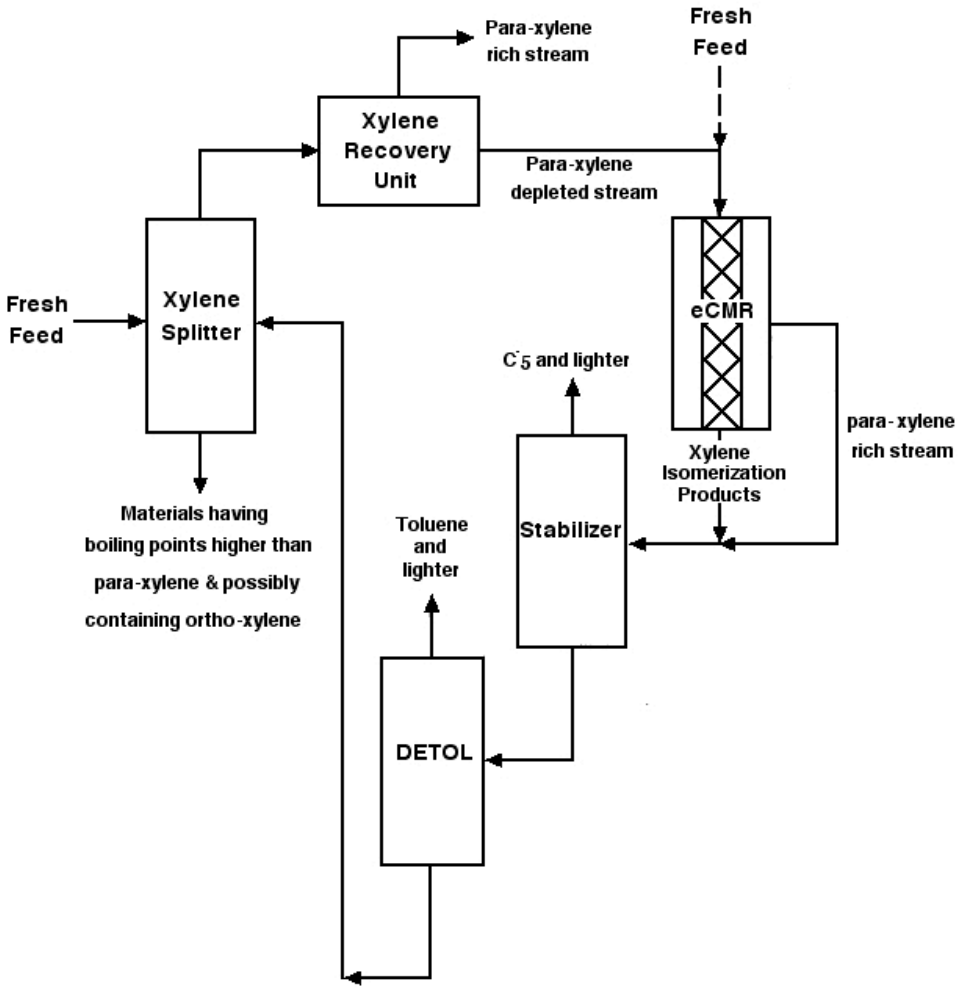

Figure 5-9 ExxonMobil Patented process for production of para-xylene.

It can therefore, be seen that this technology is novel and has industrial application and interest, even though no real evidence exists in the literature to confirm whether or not para-xylene selectivity enhancement through xylene isomerization in a eCMR is achievable with existing membranes.

5.2 Mixture separation

Experimantal procedures for the mixture separation are provided in chapter 3.

5.2.1 Results

Figure 5-10 shows a diagram of the para-xylene permeance values obtained from the separation testing (1.5 kPa p-xylene, 4.5 kPa m-xylene and 1.35 kPa o-xylene). Samples were withdrawn after 90-minute temperature steps starting at 673 K. The temperature was then decreased and samples analysed down to 423 K and again up to 673 K. Over this temperature range, para-xylene was the only detectable component in the permeate stream. The accuracy/detection limit of the GC corresponded to a permeance of about 0.12 nmol/s/m^2/Pa for meta-xylene and 0.45 nmol/s/m^2/Pa for ortho-xylene, as represented in Figure 5-10.

These results correspond to separation factor values that must be more than 73 and 27 for p-/m-xylene as well as more than 21 and 7 for p-/o-xylene at 423 and 673 K, respectively. It can be seen in the 673-423 K range that, in the ternary mixture, para-xylene permeance is a function of temperature with a maximum value of 10.2 nmol/s/m^2/Pa at 450 K. The permeance decreases with an increase in temperature, down to a value of about 3.6 nmol/s/m^2/Pa at 673 K. The permeance values for 423 to 673 K were similar.

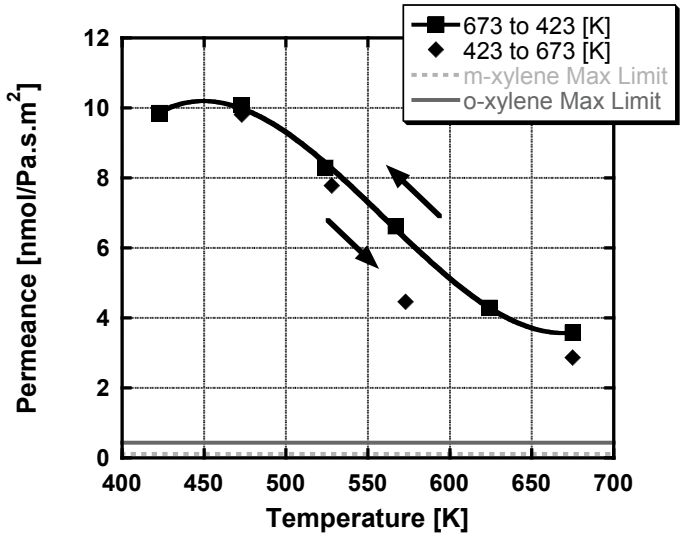

Figure 5-10 Permeance of para-xylene in a ternary isomer mixture (■ & ◆: para-xylene permeance when decreasing and increasing the temperature respectively, dotted gray line: detection limit for meta-xylene, dark gray line, detection limit for ortho-xylene).

5.2.2 Discussion

From the separation experiment results, it can be concluded that para-xylene can be selectively separated from a ternary mixture of xylene isomers with the MFI-zeolite membranes prepared in this study. A maximum value in the permeance of para-xylene can be seen close to 450 K. It can be explained as follows: as we consider the transport to be controlled by the zeolite pores, it is adsorption driven. At low temperatures the coverage of para-xylene on the pore surface is higher. With an increase in temperature the coverage decreases, and is counterbalanced by the increase of the diffusion coefficient up to a certain point, leading to a further global decrease in permeance, as observed for all gases previously studied on this type of membrane [101, 102, 112, 144, 209].

This study did not provide any hint of further permeance increase at higher temperatures, as commonly quoted (*gas activated transport*) on different gases [81, 89, 251-253] and also on xylenes [89, 238, 239, 243]. This may be related to the support pore-plugging structure of the membrane [100].

The membranes used in this work have micron-size MFI-zeolite crystals (0.2-1 μm) in the pores of the 0.2 or 0.1 μm α-alumina substrate top layer. The pores are completely plugged with crystals running along several pores (see the TEM characterisation in chapter 2). On the other hand, film-shape membranes commonly described in the literature have rather large zeolite crystals (1 μm). Taking into account the negative thermal expansion coefficient of the MFI at high temp [254], then a contraction of the grain size would lead to an opening to a large extent between zeolite crystals, which can lead to an increase in the permeance of molecules. On the other hand, the membranes used in this work had micron-size MFI-zeolite crystals (0.2-1 μm) plugging the pores of the 0.2 or 0.1 μm α-alumina substrate top layer. The pores were completely plugged with crystals running along several pores (see the TEM characterisation in chapter 2). This composite structure may lead to different thermal behaviour of the whole material, as the two phases (MFI and alumina) can be seen to be linked together at the atomic level on the TEM characterisations. This may explain why no intercrystalline pores open at higher temperature with the membranes used in this work.

It was shown in chapter 2 that the MFI/alumina composite membrane used in this study is highly selective towards n-butane from a n-butane/hydrogen mixture at low temperatures, while the single gas hydrogen permeance at room temperature was high 0.25 μmol/Pa/s/m^2. Transport of n-butane in a mixture of n-butane/hydrogen at low

temperature occurs through the adsorption of n-butane in the zeolite pores, blocking hydrogen from entering the pore structure. This, along with the fact that only para-xylene is present in the permeate stream, suggests that this membrane is free from nano-size intercrystalline or larger defects.

In Table 5-2 results of xylene isomer separation testing in MFI-zeolite membranes by various research groups are presented, along with findings of this study. Most of the studies done on xylene vapour separation in MFI-zeolite membranes focus on two component separation of either para– and ortho-xylene or para- and meta-xylene. It can be seen that the data varies considerably between the different research groups. Sakai *et al.* [239] performed the only other vapour ternary mixture separation, but at low xylene isomer partial feed pressures. The para-xylene permeance obtained by them is higher than in this study (82 compared to 10.2 nmol/Pa/s/m^2 at 473 K), but some meta- and ortho-xylene were present in the permeate stream (S_f = 250 for both para/meta and para/ortho). In the case of b-orientated (MFI straight channels perpendicular to the support surface) membranes the para-xylene permeance and para-/ortho-xylene separation factors are high. However, as stated before, the higher separation factors and permeance values for b-orientated samples have to be considered with caution, as the differently orientated samples may have included different membrane defect densities. The membranes used in this study show high separation performance compared to other studies, but with lower para-xylene permeance.

Table 5-2 Xylene separation in literature

Group	Membrane	Support	Thickness [μm]	Area [cm^2]	Feed Composition	T [K]	p-xylene Permeance [$nmol/Pa/s/m^2$]	Separation factor (p/o)
Beartsch *et al.* [237]	Silicalite-1	γ-alumina tube	2-10	-	~3 mol % p-xylene, 3mol % o-xylene carrier gas He	380	0.5	1
						480	4	1
Sakia *et al.[239]*	MFI	α-alumina disk	90	0.33	0.3 kPa p-xylene 0.27 kPa o-xylene 0.27 kPa m-xylene	473	82	250
						303	-	1
Noble et. al. [89]	B-ZSM5	stainless steel tube	-	~5.1	2.1 kPa p-xylene 2.1 kPa o-xylene carrier gas He	425	2.6 [247]	60
Keizer *et. al.* [243]	Silicalite-1	α-alumina disk	3	~1.9	0.31 kPa p-xylene 0.26 kPa o-xylene carrier gas He	400	12.5 [247]	555
						473	9 [247]	25
Xiomeritikakis et al. [238]	MFI (c-orientated)		12-18	~	0.45 kPa p-xylene 0.35 kPa o-xylene carrier gasHe	373	29.8	3 (flux ratio)

Table 5-2 Xylene separation in literature (continued)

Group	Membrane	Support	Thickness [μm]	Area [cm^2]	Feed Composition	T [K]	p-xylene Permeance [$nmol/Pa/m^2/s$]	Separation factor [p/o]
Xiomeritikakis *et al.* [238]	ZSM-5 [101] orientated	α-alumina disk	2	-	0.45 kPa p-xylene, 0.35 kPa o-xylene carrier gas He	403	40	60
Hudlund *et al.* [255]	MFI	α-alumina disk	0.5	~4.9	0.27 kPa p-xylene 0.59 kPa o-xylene carrier gas He	373	600	3.2
						663	300	16
					1 kPa p-xylene 1 kPa o-xylene	773	110	13 (p/m)
Lai *et al.* [247]	ZSM-5 (b-orientated)	α-alumina disk	1	-	0.45 kPa p-xylene, 0.35 kPa o-xylene carrier gas He	423	260	400
						473	200	200-450
This study	MFI/alumina pore plugged	α-alumina tube	-	28.6	1.5 kPa p-xylene 4.5 kPa m-xylene 1.35 kPa o-xylene carrier gas N_2	673	3.6	∞ (p/o & p/m)
						473	10.2	∞ (p/o & p/m)

5.3 Xylene isomerization in an eCMR and conventional packed-bed reactor

Experimental procedures for the eCMR operation and the conventional packed-bed reactor experiments have been described in chapter 3.

5.3.1 Results

Extractor CMR

Figure 5-11 is a graphic representation of the results one would expect from a catalytic membrane reactor experiment (577 K, 450 μl/min, 10 ml/min counter-current sweep flow rate), showing the feed and exit streams (permeate and retentate) as well as the combination of the two exit streams. The para-xylene yield (η) is the amount of formed para-xylene in the stream(s) divided by the total meta-xylene feed. It therefore, represents the contribution made by each stream towards the total para-xylene yield in the system. The selectivity (sel) value is the amount of para-xylene present divided by the amount of reaction products (para-xylene + ortho-xylene) in each stream.

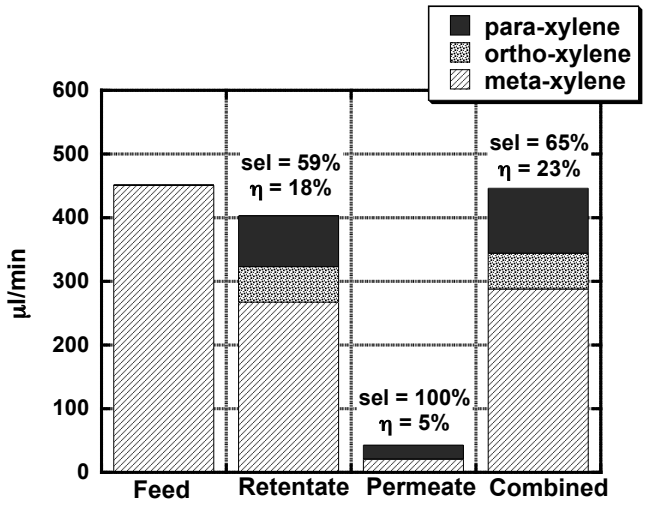

Figure 5-11 CMR operation at 577 K, 450 μl/min meta-xylene feed, 10 ml/min sweep flow (sel: selectivity of para-xylene; η: para-xylene yield). The combined result would be obtained by mixing of both retentate and permeate streams after the reactor.

The feed to the reactor only includes meta-xylene diluted in nitrogen. Only para- and meta-xylene are detectable in the permeate stream. The para-xylene selectivity in the retentate is 59 %, compared to the 100 % in the permeate, which means that all the ortho-

xylene formed during the reaction leaves the reaction zone via the retentate stream. The amount of para-xylene in the permeate constitutes 5 % of the total para-xylene yield, while the rest leaves the reactor through the retentate. Mixing both streams after the reactor would provide the *combined CMR* mode result.

The results presented for the CMR, depicted in Figure 5-11 (referred to as standard conditions), operated at the above reaction conditions are compared with results obtained at a different feed flow rate, temperature and sweep flow rate, and shown in Table 5-3. The membrane stays para-xylene selective, compared to ortho-xylene at all reaction conditions. If the meta-xylene feed flow rate is increased to 1150 ml/min, the para-xylene yield decrease to 13 % in the retentate and 2 % in the permeate. The selectivity in the permeate remains constant with an increase in feed flow rate, while the selectivity in the retentate increases (up to 66 %) while the yield decreases.

Lowering the sweep flow rate to 7 ml/min brings about a slight decrease in the para-xylene selectivity of the retentate (58 %) and permeate yield (4 %). The para-xylene yield in the retentate stays constant. With an increase in temperature to 633 K, the selectivity in the retentate drops to 55 %, indicating a higher ortho-xylene yield for the reaction. The retentate para-xylene yield is 19 %, while the permeate para-xylene yield decreases to 4 %, rendering an unchanged total para-xylene yield.

Table 5-3 Comparison of CMR results at various meta-xylene feed flow rates, nitrogen sweep flow rates and temperature, including, as a reference, the standard condition results shown in Figure 5-11 (in italics and between brackets).

(Standard Conditions)		Retentate		Permeate	
		selectivity	yield	selectivity	yield
		(59%)	*(18%)*		*(5%)*
Feed [µl/min]	1150 *(450)*	66%	13%	100%	2%
Sweep [ml/min]	7 *(10)*	58%	18%		4%
Temperature [K]	633 *(577)*	55%	19%		4%

Comparison of the CMR results with Conventional Reactor results

In Figure 5-12, the combined CMR result is compared with the conventional reactor (CR) mode and xylene isomerization equilibrium at 577 K, for the same feed conditions. The conventional para-xylene selectivity is 58 % and the para-xylene yield 21 %, to be compared to equilibrium values of 46 % and 24.9 %, respectively. When the reactor is operated as a combined mode CMR, the yield of para-xylene increases slightly (23 %) while para-xylene selectivity (65 %) increases with 7 % compared to the CR mode.

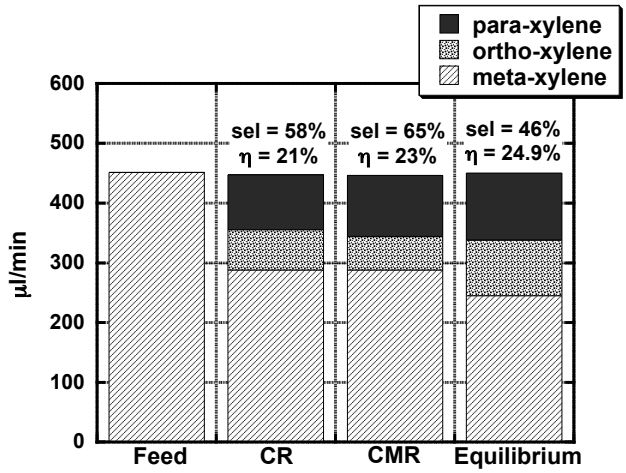

Figure 5-12 Comparison between conventional reactor (CR), combined mode catalytic membrane reactor (CMR) and xylene isomerization equilibrium [219] at 577 K (sel: selectivity of para-xylene; η: para-xylene yield).

In Table 5-4 the conventional reactor and combined CMR xylene isomer distribution in the product streams at 577 K are compared. At the low feed flow rate (450 µl/min) the ortho-xylene in the product streams decrease slightly (15 % to 14 % and 15% to 14%) while para-xylene production increase in the combined CMR (21 % to 22 % and 21 % to 23 %). At a sweep of 7 ml/min the conversion of meta-xylene stays constant, but an increase in the sweep flow rate to 10 ml/min leads to a slight decrease in meta-xylene conversion. At the higher feed rate (1150 µl/min) the ortho-xylene yield stays constant, while the para-xylene yield increase from 12 to 14 %. At this reaction condition more meta-xylene is converted (21% compared to 19%).

Table 5-4 Xylene Isomer distribution in the product streams of the conventional reactor and combined CMR at 577 K.

		combined CMR			Conventional Reactor		
Feed	Sweep	para	meta	ortho	para	meta	ortho
450 µl/min	7 ml/min	22	64	14	21	64	15
	10 ml/min	23	65	12	21	64	15
1150 µl/min	7 ml/min	14	79	7	12	81	7

In Table 5-5 the conventional reactor and combined CMR xylene isomer distribution in the product streams at 633 K are compared. The values for the conventional reactor were taken from the retentate values. At the low feed flow rate (450 μl/min) the ortho-xylene in the product streams decrease slightly (17 % to 16 %) while para-xylene production increases in the combined CMR (23 % to 21 %) for both sweep rates (7 ml/min and 10 ml/min). The meta-xylene conversion increases slightly. At the higher feed rate (1150 μl/min) the ortho-xylene yield stays constant, while the para-xylene yield increases from 15 to 17 %. At this reaction condition more meta-xylene is converted (26 % compared to 24 %).

Table 5-5 Xylene Isomer distribution in the product streams of the conventional reactor and combined CMR at 633 K.

		combined CMR			Conventional Reactor*		
Feed	Sweep	para	meta	ortho	para	meta	ortho
450 μl/min	7 ml/min	23	61	16	21	62	17
	10 ml/min	23	61	16	21	62	17
975 μl/min	7 ml/min	17	74	9	15	76	9

* *conventional reactor results were calculated from the retentate conversion*

5.3.2 Discussion

Extractor CMR

Meta-xylene isomerization in an extractor catalytic membrane reactor leads to an increase in the para-xylene selectivity of the reaction. This is due to the selective extraction of para-xylene compared to ortho-xylene. Throughout the runs no ortho-xylene was detected in the permeate stream. The meta-xylene present in the permeate stream may be due to permeation of meta-xylene in the first part of the reactor, when the para-xylene concentration is still too low to block the zeolite pores by adsorption [46]. Simple calculations suggest that the observed meta-xylene transmembrane flow cannot be due to poor membrane separation, considering the high separation ability of the membrane for p-/m-xylene, e.g. S_f higher than 53 at 577 K.

An increase in meta-xylene feed flow rate decreases the overall conversion of meta-xylene. The fact that the para-xylene selectivity improves in the retentate stream

indicates that the reaction becomes more para-xylene selective at higher feed rates, as could be expected. The amount of para-xylene that diffuses also decreases, due to the concentration decrease of para-xylene in the membrane reaction zone.

It is expected that with a decrease in sweep flow rate the para-xylene permeance would also decrease. This has been seen in chapter 4 for hydrogen extraction in CMR experiments with similar membranes as used in this study [211][Chapter 4]. With a decrease in sweep flow rate from 10 to 7 ml/min a small decrease in para-xylene permeance is observed. This, together with the fact that the yield of para-xylene in the retentate stays constant while the para-xylene selectivity in the retentate decreases also slightly, indicates that when less para-xylene is extracted more ortho-xylene is formed in the reaction.

When the temperature is changed from 577 to 633 K, the selectivity in the retentate decreases, indicating more ortho-xylene production at this temperature. The yield in the retentate is only slightly higher, but the yield in the permeate is lower indicating the effect of temperature on the para-xylene permeance from the mixture, as seen during the separation testing.

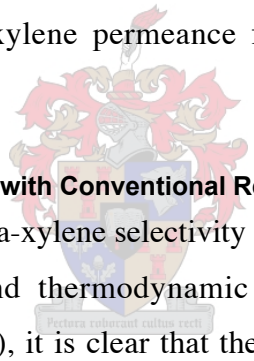

Comparison of the CMR results with Conventional Reactor results

When the yield and para-xylene selectivity values (Figure 5-12) of the conventional packed bed reactor (CR) and thermodynamic equilibrium are compared at 577 K (450 μl/min meta-xylene feed), it is clear that the reactor is not operated at equilibrium. Conventional reactor tests performed with the undiluted catalyst indicated that if the catalyst is too active and the reaction operates near equilibrium some toluene and ethylbenzene forms. Toluene and ethylbenzene will compete with para-xylene to permeate through the MFI/ alumina membrane, leading to an increase in the production of the undesired products. In order to prevent the formation of toluene and ethylbenzene the catalyst was diluted to 5 wt % of the original and the feed conditions chosen such that one did not operate close to equilibrium. A weight hour space velocity (WHSV) of 215 hr^{-1} was used at the reactor operation presented in Figure 5-12.

CMR operation increases the reaction selectivity compared to conventional conditions, due to the fact that no ortho-xylene is present in the permeate stream. The results obtained for the conventional reactor is similar to that of the retentate (sel = 59 % and η = 20 %). A relative improvement in para-xylene yield of about one tenth (23%

compared to 21 %) is achieved. It is expected that this improvement can be enhanced upon if no meta-xylene was present in the permeate stream.

At 633 K (Table 5-5), an increase in the sweep flow rate does not change the amount of para-xylene formed (23 % at 7 ml/min and 10 ml/min). This could be due to the fact that little advantage can be drawn from the slight increase in sweep flow rate, considering that only a slight improvement was obtained at 577 K (Table 5-4), where the permeance was higher than at 633 K.

What is interesting from both Table 5-4 and Table 5-5 is that at the higher meta-xylene feed flow rates (1150 μl/min and 975 μl/min), there is no change in the ortho-xylene yield when the combined CMR is used. If we consider the reaction network of Figure 5-7 then this would indicate that at higher flow rates the influence of the reaction between para-and ortho-xylene becomes insignificant. The improvement in the para-xylene yield would therefore, be the direct consequence of an increased meta-xylene conversion.

Conventional Reactor experiments

Conventional reactor experiments were performed separately from the eCMR experiments. The membrane was replaced with a stainless steel tube of similar dimensions as the membrane and feed and retentate outlet compositions and flow rates were measure. The reason for this deviation from the standard procedure of just closing off the permeate side of the membrane, whereby creating a *simulated* conventional packed bed reactor, is that some mass balance problems were observed for the *simulated* conventional reactor. The conversion of meta-xylene was more than the amount of para- and ortho-xylene formed, and there was no indication of any byproduct formation. This indicated that some meta-xylene or products had *disappeared* from the reaction zone.

The same mass balance problems were not experienced when the data of the eCMR were analyzed, indicating that the loss occurred somewhere near the reactor and was not a leak in the experimental system.

First we considered the fact that the lost xylenes might be trapped in the space between the membrane and the stainless steel reactor module (permeate chamber volume). Calculations however indicated that the space could be filled easily by the *lost* xylenes and back-permeation into the reaction zone will occur.

This led to another theory, adsorption of xylenes within the MFI-zeolite framework. m-xylene and o-xylene can fill up to 4 molecules/MFI unit cell, while para-

xylene fills up to 8 molecules/MFI unit cell. Taking into account that about 3.5 μmol/min xylene was lost at 577 K and we continue the experiment for let say 10 hours which would give around 1.2×10^{21} molecules. Therefore if we assume that the amount of MFI zeolite in the membrane (ca. 0.5g) can absorb 4 molecules/ unit cell then the unit cell density will have to be 6×10^{20} unit cells/g MFI-zeolite.

Conventional reactor experiments done at 577 K gave similar results to the conventional reactor results. Results obtained at 633 K done with a fresh different catalyst sample gave a different product distribution than the retentate of the eCMR (at 633 K, 450μl/min, para/meta/ortho is 25:53:22). This product distribution corresponds to thermodynamic equilibrium. Therefore the product distribution presented for the conventional reactor presented in Table 5-5 was determined from the eCMR retentate product distribution. The difference may be attributed to the fact that a different catalyst sample was used and that the reaction conditions differed slightly from the eCMR experiments. Catalyst deactivation during eCMR experiments can also not be excluded as a possible reason.

Influence on productivity by using the eCMR for xylene isomerization

In Table 5-6, the results of the conventional reactor, permeate-only CMR and combined mode CMR are compared in terms of para-xylene selectivity and productivity. It is calculated for the reaction condition (CMR: feed,450 μl/min, sweep, 10 ml/min and 577 K) where the highest increase in selectivity was observed compared to the conventional reactor. The productivity is related to para-xylene per unit bed volume of the reactor.

Table 5-6 Comparison of Conventional Reactor (CR), Permeate-only (CMR) mode and Combined mode Catalytic Membrane Reactor (CMR)

	Conventional Reactor (CR)	Permeate-only (CMR)	Combined mode CMR
Para-xylene selectivity	58%	100%	65%
Productivity (mmol/s/m^3)	10.2	2.4	11.2

If one considers the CMR in the permeate-only mode, when compared to CR, the para-xylene selectivity is improved to 100% - almost double. This would, however, lead to a significant reduction in the para-xylene production throughput (2.4 compared to 10.2 [mmol/m^3/s]). However, when the catalytic membrane reactor is used in combined mode (mixing both the retentate and permeate feed after the reactor), the para-xylene productivity noticeably increases over the conventional reactor (11.2 compared to 10.2 mmol/m^3/s) with a lower amount of ortho-xylene in the product. This demonstrates that including both the separative membrane, and the catalytic bed in the same device (as per definition of a CMR) leads to an improvement when compared to separated catalytic and membrane separation units.

5.4 Summary

It has been shown that the pore-plugged MFI-zeolite membranes used in this study can selectively extract para-xylene from a mixture of xylenes. It has been shown in this preliminary study that using an extractor type catalytic membrane reactor instead of a conventional fixed-bed reactor for meta-xylene isomerization, can lead to higher para-xylene selectivities. The para-xylene selectivity can even be improved to 100% if the CMR is operated in the permeate-only mode, but this comes at a price of lower para-xylene yields. When operated in combined mode (i.e. mixing both permeate and retentate streams after the reactor), the CMR shows an improvement on both para-xylene productivity (ca. 10 % maximum at conditions studied) and selectivity when compared to the conventional reactor. When the CMR was used to carry out meta-xylene isomerization, some meta-xylene was extracted as well. This was attributed to the fact that in the front-end part of the reactor no para-xylene was present, in contact with the membrane, to block the pores, and therefore some single-gas meta-xylene permeantion could occur.

6 Conclusions

The first part of the dissertation described the various uses of catalytic membrane reactors and introduced the reader to this field of research. The rest of the dissertation focus on achieving the following objectives set out in the beginning of the study:

- To design and construct a new generation membrane reactor testing bench for the Department of Process Engineering, University of Stellenbosch.
- To study the internal eCMR mechanism in the case where it has been applied in order to increase reaction conversion (isobutane dehydrogenation), by studying the influence and nature of the membrane material (palladium and MFI-zeolite).
- To explore the use of an eCMR to increase the selectivity of a reaction, using xylene isomerization as an example and using an MFI-zeolite membrane.

6.1 Design and construction of a new generation Membrane Reactor testing bench

A new experimental membrane reactor testing bench was successfully designed and constructed by myself for the Department of Process Engineering, University of Stellenbosch. The membrane bench can be used for the following membrane tests:

- Membrane treatment/ pre-treatment.
- Single gas membrane permeation testing (dead-end mode and Wicke-Kallenbach method).
- Gas mixture separation testing (Wicke - Kallenbach method).
- Gas phase reaction testing inside the membrane reactor. For this case isobutane dehydrogenation.

It is versatile and easy adaptable for other types of reactions. The membrane reactor testing bench design and constructed, is an improvement on membrane reactor testing benches used by me during my studies at the CNRS/IRC. For example, the new tube furnace design offers better temperature profile control within the membrane.

6.2 Isobutane dehydrogenation in an eCMR

A Pd and MFI eCMR were used to carry out isobutane dehydrogenation. They differed only on the bases of the membrane used. Hydrogen/ isobutane separation testing

revealed that the Pd membrane was able to extract more hydrogen and with a higher separation factor, than the MFI-zeolite/alumina composite membrane. Isobutane dehydrogenation was performed at the same reaction conditions in order to assess the benefit of using a membrane with a higher hydrogen extraction capacity and selectivity for conversion enhancement of the isobutane dehydrogenation reaction. The eCMR results of the two different eCMRs were similar. It has been shown that in order for the an extractor-type CMR to completely draw benefit from their combination for yield enhancement, a very active catalysts should be developed, able to sustain the high extraction ability of the membrane. This observation is consistent with those already reported [11] and may be extended to other types of eCMRs [144]. As a matter of fact, in an eCMR, the catalyst is often placed in a reactive medium different from that existing in conventional reactors, for which catalysts have been generally designed [10].

A simple one-dimensional model was satisfactory to describe the function of the eCMR mathematically.

6.3 Xylene isomerization in an eCMR

Para-xylene was selectively separated from a mixture of xylene isomers with the MFI-zeolite membrane, prepared by a pore plugging technique. The extractor type catalytic membrane reactor (MFI-membrane packed with a PtO-HZSM-5) operated in combined mode (i.e. mixing both permeate and retentate streams after the reactor) improved on both para-xylene productivity (up to ten percent) and selectivity when compared to the conventional reactor. The para-xylene selectivity can be improved to 100% when the CMR is operated in the permeate-only mode, but this comes at the expense of para-xylene production. To the best of our knowledge this is the first time in the literature that a successful improvement on selectivity enhancement was reported for this reaction.

7 Future Work

The palladium membrane fabrication has led to some questions about the fabrication procedure and therefore, it is necessary to develop a standard procedure for the production of palladium membranes. Standard testing procedures for the membrane supports and characterization procedures for the membranes must be developed to better describe membranes. Life-time endurance studies to determine the durability of the membranes need attention.

The need to design speciality catalysts for the eCMRs exists. These catalysts should be able to perform in the *foreign* environment of the catalytic membrane reactor.

The isomerization of meta-xylene was a preliminary study to assess whether it was possible to improve the reaction selectivity towards para-xylene. Further improvements on the system are necessary, with higher cross-membrane para-xylene fluxes being the most important. Optimizing the zeolite membrane and working under higher feed xylene partial pressures may achieve higher para-xylene fluxes. In order to avoid meta-xylene permeance in the eCMR operation optimization of the catalyst location along the membrane is necessary in order to avoid that part of the membrane may be in contact with only meta-xylene. In other words, some para-xylene should already have formed by the time the mixture reaches the permeable area of the membrane. The catalyst needs to be optimised in order to ensure no undesirable by-products at equilibrium, for example toluene and ethylbenzene, which may compete with para-xylene to diffuse through the membrane. Operation of the CMR at lower temperatures is necessary to investigate the advantages of the higher para-xylene permeance at lower temperatures. Modeling and scale-up studies are also needed to investigate the practical and economical feasibility of this process.

In terms of process development it is suggested that a membrane be placed before the eCMR, extracting ethylbenzene from the C_8 mixture. The presence of ethylbenzene in the eCMR feed mixture may hinder the permeance of para-xylene.

8 References

1. *Oxford Dictionary*. 2002.
2. Hsieh, H.P., *Inorganic membranes for separation and reaction.* Membrane Science and Technology. Vol. 3. 1996, New York: Elsevier Science Publishing Company, New York, USA. 1-610.
3. Sanchez, J.G. and T.T. Tsotsis, *Catalytic Membranes and Membrane Reactors*. 2002: Wiley-VCH. 261.
4. Julbe, A., D. Farrusseng, and C. Guizard, Journal of Membrane Science, 2001. **181**(1): p. 3-20.
5. Soria, R., Catalysis Today, 1995. **25**(3-4): p. 285-290.
6. Keizer, K., J.R. Uhlhorn, and T.J. Burggraaf, *Gas separation using inorganic membranes*, in *Membrane Separations Technology. Principles and Applications*, R.D. Noble and S.A. Stern, Editors. 1995, Elsevier Science B.V: Amsterdam. p. 553-588.
7. Sanchez, J. and T.T. Tsotsis, *Current developments and future research in catalytic membrane reactors*, in *Fundamentals of Inorganic Membrane Science and Technology*, A.J. Burggraaf and L. Cot, Editors. 1996, Elsevier: Amsterdam. p. 708.
8. Koros, W.J., Y.H. Ma, and T. Shimidzu, Journal of Membrane Science, 1996. **120**(2): p. 149-159.
9. Tsotsis, T.T., A.M. Champagnie, S.P. Vasileiadis, Z.D. Ziaka, and R.G. Minet, Chemical Engineering Science, 1992. **47**(9-11): p. 2903-2908.
10. Dalmon, J.-A., *Catalytic Membrane Reactors*, in *Handbook of Heterogeneous Catalysis*, G. Ertl, H. Knözinger, and J. Weitkamp, Editors. 1997, VCH Publishers: Weinheim. p. 2541.
11. Mota, S., S. Miachon, J.-C. Volta, and J.-A. Dalmon, Catalysis Today, 2001. **67**(1-3): p. 169-176.
12. Agarwalla, S. and C.R.F. Lund, Journal of Membrane Science, 1992. **70**(2-3): p. 129-141.
13. Keuler, J.N. and L. Lorenzen, Journal of Membrane Science, 2002. **202**: p. 17-26.
14. Keuler, J.N., *Optimising catalyst and membrane performance and performing a fundamental analysis on the dehydrogenation of ethanol and 2-butanol in a*

catalytic membrane reactor, in *Process Engineering*. 2000, University of Stellenbosch: Stellenbosch. p. 433.

15. Keuler, J.N. and L. Lorenzen, Journal of Membrane Science, 2002. **195**: p. 203-213.
16. Keuler, J.N., L. Lorenzen, and S. Miachon, Separation Science and Technology, 2002. **37**: p. 379-401.
17. Cruz-López, A., N. Guilhaume, S. Miachon, and J.-A. Dalmon, Catalysis Today, 2004. **Submitted**.
18. Farrusseng, D., A. Julbe, and C. Guizard, Separation and Purification Technology, 2001. **25**(1-3): p. 137-149.
19. Kölsch, P., Q. Smejkal, M. Noack, R. Schafer, and J. Caro, Catalysis Communications, 2002. **3**(10): p. 465-470.
20. Kölsch, P., M. Noack, R. Schafer, G. Georgi, R. Omorjan, and J. Caro, Journal of Membrane Science, 2002. **198**(1): p. 119-128.
21. Mallada, R., M. Menéndez, and J. Santamaría, Catalysis Today, 2000. **56**(1-3): p. 191-197.
22. Diakov, V., D. Lafarga, and A. Varma, Catalysis Today, 2001. **67**(1-3): p. 159-167.
23. Diakov, V., B. Blackwell, and A. Varma, Chemical Engineering Science, 2002. **57**(9): p. 1563-1569.
24. Brinkmann, T., S.P. Perera, and W.J. Thomas, Chemical Engineering Science, 2001. **56**(6): p. 2047-2061.
25. Tonkovich, A.L.Y., J.L. Zilka, D.M. Jimenez, G.L. Roberts, and J.L. Cox, Chemical Engineering Science, 1996. **51**(5): p. 789-806.
26. Coronas, J., M. Menendez, and J. Santamaria, Industrial & Engineering Chemistry Research, 1995. **34**: p. 4229-4234.
27. Klose, F., T. Wolff, S. Thomas, and A. Seidel-Morgenstern, Applied Catalysis A: General, 2004. **257**(2): p. 193-199.
28. Julbe, A., D. Farrusseng, J.C. Jalibert, C. Mirodatos, and C. Guizard, Catalysis Today, 2000. **56**(1-3): p. 199-209.
29. Pantazidis, A., J.A. Dalmon, and C. Mirodatos, Catalysis Today, 1995. **25**(3-4): p. 403-408.
30. Alfonso, M.J., M. Menendez, and J. Santamaria, Catalysis Today, 2000. **56**(1-3): p. 247-252.

31. Ge, S.H., C.H. Liu, and L.J. Wang, Chemical Engineering Journal, 2001. **84**(3): p. 497-502.
32. Téllez, T., M. Menéndez, and J. Santamaría, AIChE Journal, 1997. **43**(3): p. 777-784.
33. Zeng, Y. and Y.S. Lin, AIChE Journal, 2001. **47**(2): p. 436-444.
34. Omata, K., S. Hashimoto, H. Tominaga, and K. Fujimoto, Applied Catalysis, 1989. **52**(1): p. L1-L4.
35. Anshits, A.G., A.N. Shigapov, S.N. Vereshchagin, and V.N. Shevnin, Catalysis Today, 1990. **6**(4): p. 593-600.
36. Gryaznov, V.M., V.I. Vedernikov, and S.G. Gul'yanova, Kinet. Catal., 1986. **27**: p. 142.
37. Balachandran, U., J.T. Dusek, P.S. Maiya, B. Ma, R.L. Mieville, M.S. Kleefisch, and C.A. Udovich, Catalysis Today, 1997. **36**(3): p. 265-272.
38. Rebeilleau-Dassonneville, M., S. Rosini, A.C. van Veen, D. Farrusseng, and C. Mirodatos, Catalysis Today, 2004. **Submitted for publication**.
39. van Veen, A.C., M. Rebeilleau, D. Farrusseng, and C. Mirodatos, Chemical Communications, 2003. **1**: p. 32-33.
40. Daub, K., V.K. Wunder, and R. Dittmeyer, Catalysis Today, 2001. **67**: p. 257-272.
41. Coronas, J. and J. Santamaria, Catalysis Today, 1999. **51**(3-4): p. 377-389.
42. Miachon, S., V. Perez, G. Crehan, E. Torp, H. Raeder, R. Bredesen, and J.-A. Dalmon, Catalysis Today, 2003. **82**(1-4): p. 75-81.
43. Ilinitch, O.M., F.P. Cuperus, L.V. Nosova, and E.N. Gribov, Catalysis Today, 2000. **56**(1-3): p. 137-145.
44. Pina, M.P., M. Menendez, and J. Santamaria, Applied Catalysis B: Environmental, 1996. **11**(1): p. L19-L27.
45. Torres, M., L. Lopez, J.M. Dominguez, A. Mantilla, G. Ferrat, M. Gutierrez, and M. Maubert, Chemical Engineering Journal, 2003. **92**(1-3): p. 1-6.
46. Masuda, T., T. Asanuma, M. Shouji, S.R. Mukai, M. Kawase, and K. Hashimoto, Chemical Engineering Science, 2003. **58**(3-6): p. 649-656.
47. Lange, C., S. Storck, B. Tesche, and W.F. Maier, Journal of Catalysis, 1998. **175**(2): p. 280-293.
48. Sloot, H.J., G.F. Versteeg, and W.P.M. Van Swaaij, Chemical Engineering Science, 1990. **45**(8): p. 2415-2421.

49. Veldsink, J.W., R.M.J. van Damme, G.F. Versteeg, and W.P.M. van Swaaij, Chemical Engineering Science, 1992. **47**(9-11): p. 2939-2944.
50. Peureux, J., M. Torres, H. Mozzanega, A. Giroir-Fendler, and J.-A. Dalmon, Catalysis Today, 1995. **25**(3-4): p. 409-415.
51. Wu, S., J.-E. Gallot, M. Bousmina, C. Bouchard, and S. Kaliaguine, Catalysis Today, 2000. **56**(1-3): p. 113-129.
52. Iojoiu, E.E., S. Miachon, and J.-A. Dalmon, Topics in Catalysis, 2004. **Accepted for publication**.
53. Raeder, H., R. Bredesen, G. Crehan, S. Miachon, J.-A. Dalmon, A. Pintar, J. Levec, and E.G. Torp, Separation and Purification Technology, 2003. **32**: p. 349-355.
54. Vospernik, M., A. Pintar, G. Betcic, J. Levec, J. Walmsley, H. Raeder, E.E. Iojoiu, S. Miachon, and J.-A. Dalmon, Chemical Engineering Science, 2004. **59**(22-23): p. 5363-5372.
55. Iojoiu, E.E., J.C. Walmsley, H. Raeder, S. Miachon, and J.-A. Dalmon, Catalysis Today, 2004. **Submitted for publication**.
56. Vankelecom, I.F.J., R.F. Parton, M.J.A. Casselman, J.B. Uytterhoeven, and P.A. Jacobs, Journal of Catalysis, 1996. **163**(2): p. 457-464.
57. Giorno, L. and E. Drioli, Trends in Biotechnology, 2000. **18**: p. 339-349.
58. Giorno, L., L. Donato, S. Todisco, and E. Drioli, Journal of Separation Science and Technology, 1998. **33**(5): p. 739-756.
59. Wenten, I.G. and I.N. Widiasa, Desalination 149, 2002. **149**: p. 279-285.
60. Hua, L., Z.-H. Sun, Y. Leng, and Z.-Q. Hu, Process Biochemistry, 2005. **40**(3-4): p. 1137-1142.
61. Howell, J.A., Desalination, 2004. **162**: p. 1-11.
62. Wandrey, C., A. Liese, and D. Kihumbu, Organic Process Research & Development, 2000. **4**: p. 286-290.
63. ltinger, J.W., A.S. Bommarius, K. Drauz, and C. Christian Wandrey, Organic Process Research & Development, 2001. **5**: p. 241-248.
64. Dittmeyer, R., V. Hollein, and K. Daub, Journal of Molecular Catalysis A: Chemical, 2001. **173**(1-2): p. 135-184.
65. Casanave, D., *Etude de la dehydrogenation de l'isobutane dans un reacteur catalytique a membrane poreuse conception mise en ouvre et modelisation.* 1996, L'Univesite Claude Bernard - Lyon 1: Lyon. p. 242.

66. van de Graaf, J.M., *Permeation and separation properties of supported Sillicate-1 membranes*. 1999, University of Delft: Delft.
67. Höllein, V., M. Thornton, P. Quicker, and R. Dittmeyer, Catalysis Today, 2001. **67**: p. 33-42.
68. Gryaznov, V.M., V.I. Vedernikov, and S.G. Gul'yanova, Trans. Kinet. Katal., 1986. **27**: p. 142.
69. ten Elshof, J.E., *Dense inorganic membranes Studies on transport properties, defect chemistry and catalytic behaviour*, in *Department of Chemical Engineering*. 1997, University of Twente: Twente. p. 149.
70. Shelekhin, A.B., S. Pien, and Y.H. Ma, Journal of Membrane Science, 1995. **103**(1-2): p. 39-43.
71. Uemiya, S., N. Sato, H. Ando, Y. Kude, T. Matsuda, and E. Kikuchi, Journal of Membrane Science, 1991. **56**(3): p. 303-313.
72. Bryden, K.J. and J.Y. Ying, Materials Science and Engineering A, 1995. **204**(1-2): p. 140-145.
73. Souleimanova, R.S., A.S. Mukasyan, and A. Varma, Chemical Engineering Science, 1999. **54**(15-16): p. 3369-3377.
74. Souleimanova, R.S., A.S. Mukasyan, and A. Varma, AIChE Journal, 2002. **48**(2): p. 262-268.
75. Li, W., G. Xiong, J. Gu, and Zheng, Journal of Membrane Science, 1996. **110**: p. 257-260.
76. Shu, J., B.P.A. Grandjean, S. Kaliaguine, P. Ciavarella, A. Giroir-Fendler, and J.-A. Dalmon, The Canadian Journal of Chemical Engineering, 1997. **75**: p. 712-720.
77. Mardilovich, P.P., Y. She, Y.H. Ma, and M.-H. Rei, AIChE Journal, 1998. **44**(2): p. 310 - 322.
78. Bakker, W.J.W., F. Kapteijn, J. Poppe, and J.A. Moulijn, Journal of Membrane Science, 1996. **117**(1-2): p. 57-78.
79. Lee, D.-W., Y.-G. Lee, S.-E. Nam, S.-K. Ihm, and K.-H. Lee, Journal of Membrane Science, 2003. **220**(1-2): p. 137-153.
80. Armor, J.N., Journal of Membrane Science, 1998. **147**(2): p. 217-233.
81. Flanders, C.L., V.A. Tuan, R.D. Noble, and J.L. Falconer, Journal of Membrane Science, 2000. **176**(1): p. 43-53.

82. Biesheuvel, M.P. and H. Verweij, Journal of Membrane Science, 1999. **156**(1): p. 141-152.
83. Caro, J., M. Noack, P. Kolsch, and R. Schafer, Microporous and Mesoporous Materials, 2000. **38**(1): p. 3-24.
84. Xu, X., W. Yang, J. Liu, and L. Lin, Microporous and Mesoporous Materials, 2001. **43**(3): p. 299-311.
85. Pina, M.P., M. Arruebo, M. Felipe, F. Fleta, M.P. Bernal, J. Coronas, M. Menendez, and J. Santamaria, Journal of Membrane Science, 2004. **244**(1-2): p. 141-150.
86. Xu, X., W. Yang, J. Liu, L. Lin, N. Stroh, and H. Brunner, Journal of Membrane Science, 2004. **229**(1-2): p. 81-85.
87. Ido, H., J. Horii, and K. Yura, Zeolites, 1995. **15**(4): p. 382.
88. Bernal, M.P., E. Piera, J. Coronas, M. Menendez, and J. Santamaria, Catalysis Today, 2000. **56**(1-3): p. 221-227.
89. Gump, C.J., V.A. Tuan, R.D. Noble, and J.L. Falconer, Industrial Engineering and Chemistry Research, 2000. **40**: p. 565-577.
90. Poshusta, J.C., V.A. Tuan, J.L. Falconer, and R.D. Noble, Industrial Engineering and Chemistry Research, 1998. **37**: p. 3924 -3929.
91. Dong, J. and Y.S. Lin, Industrial Engineering and Chemistry Research, 1998. **37**: p. 2404 -2409.
92. Braunbarth, C.M., L.C. Boudreau, and M. Tsapatsis, Journal of Membrane Science, 2000. **174**(1): p. 31-42.
93. Tuan, V.A., S. Li, J.L. Falconer, and R.D. Noble, Chemistry of Materials, 2002. **14**: p. 489-492.
94. Breck, D.W., *Zeolite molecular sieves: Structure, chemistry and use*. 1974, New York: John Wiley & Sons.
95. Lin, Y.S., I. Kumakiri, B.N. Nair, and H. Alsyouri, Separation and Purification Reviews, 2002. **31**(2): p. 229-379.
96. Baerlocher, C., W.M. Meier, and D.H. Olson, *Atlas of Zeolite Framework Types*. 5th ed. 2001, Amsterdam: Elsevier. 308.
97. Krishna, R. and R. Baur, Chemical Engineering Journal, 2004. **97**: p. 37-45.
98. Artioli, G., A. Pavese, G.L. Marra, and C. Lamberti, *Structure study of hydroxyl groups in silicalite*. 1997, ISIS Experimental Report: Milano. p. 1.

99. Yamahara, K., K. Okazaki, and K. Kawamura, Catalysis Today, 1995. **23**: p. 397-402.
100. Kumakiri, I., O. Pachtova, S. Miachon, H. Mozzanega, E. Landrivon, Y. Sun, N. Guilhaume, and J.-A. Dalmon, Journal of Membrane Science. **To be submitted**.
101. Chau, C., I. Prévost, S. Miachon, and J.-A. Dalmon, *Procédé de préparation de membrane zéolithique supportée par cristallisation contrôlée en température*. 2001: Europe.
102. Giroir-Fendler, A., J. Peureux, H. Mozzanega, and J.-A. Dalmon, Studies in Surface Sciences and Catalysis, 1996. **101A**: p. 127-136.
103. Pachtová, O., I. Kumakiri, M. Kocirik, S. Miachon, and J.-A. Dalmon, Journal of Membrane Science, 2003. **226**(1-2): p. 101-110.
104. Bernal, M.P., G. Xomeritakis, and M. Tsapatsis, Catalysis Today, 2001. **67**(1-3): p. 101-107.
105. Xu, W., J. Dong, J. Li, J. Li, and J. Wu, Journal of Chemical Society: Chemical Communications, 1990. **10**: p. 755.
106. Nishiyama, N., K. Ueyama, and M. Matsukata, Microporous Materials, 1996. **7**(6): p. 299-308.
107. Barrer, R.M., Journal of the Chemistry Society: Faraday Transactions, 1990. **86**(7): p. 1123-1130.
108. Van de Graaf, J., F. Kapteijn, and J.A. Moulijn, AIChE Journal, 1999. **45**: p. 497-511.
109. Krishna, R. and J.A. Wesselingh, Chemical Engineering Science, 1997. **52**: p. 861-911.
110. Krishna, R. and D. Paschek, Chemical Engineering Journal, 2002. **87**: p. 1-9.
111. Krishna, R. and R. Baur, Separation and Purification Technology, 2003. **33**: p. 213-254.
112. Ciavarella, P., H. Moueddeb, S. Miachon, K. Fiaty, and J.-A. Dalmon, Catalysis Today, 2000. **56**(1-3): p. 253-264.
113. Krishna, R. and L.J.P. van den Broeke, The Chemical Engineering Journal and the Biochemical Engineering Journal, 1995. **57**(2): p. 155-162.
114. Kapteijn, F., W.J.W. Bakker, J.v.d. Graaf, G. Zheng, J. Poppe, and J.A. Moulijn, Catalysis Today, 1995. **25**(3-4): p. 213-218.

115. *Hydrogen in Metals II: Application-Orientated Properties*, ed. G. Alefeld and J. Völkl. 1978, New York: Springer-Verlag.
116. Tripodi, P., D. Di Gioacchino, and J. Darja Vinko, Brazilian Journal of Physics, 2004. **34**(3B): p. 1177-1184.
117. Avdjukhina, V.M., A.A. Katsnelson, and G.P. Revkevich, Platinum Metals Review, 2002. **46**(4): p. 169-176.
118. Shu, J., B.P.A. Grandjean, A. Van Neste, and S. Kaliaguine, The Canadian Journal of Chemical Engineering, 1991. **69**: p. 1036-1060.
119. De Ninno, A., V. Violante, and A. La Barbera, Physical Review B, 1997. **56**(5): p. 2417-2420.
120. Aoki, K., S. Yokoyama, K. Kusakabe, and S. Morooka, The Korean Journal of Chemical Engineering, 1996. **13**(5): p. 530-537.
121. Knapton, A.G., Platinum Metals Review, 1977. **21**: p. 44-50.
122. Miachon, S., A. Mazuy, and J.-A. Dalmon. *Catalysis of palladium salt reduction in a gas-liquid membrane reactor*. in *12th International Congress on Catalysis*. 2000. Granada (Spain): Elsevier.
123. Henry, J.R., Metal Finishing, 2000. **1998**: p. 424-435.
124. Cheng, Y.S. and K.L. Yeung, Journal of Membrane Science, 2001. **182**: p. 195-203.
125. Shipley, C.R., Plating and Surface Finishing, 1984. **71**: p. 92-99.
126. Wu, L.-Q., N. Xu, and J. Shi, Industrial Engineering and Chemistry Research, 2000. **39**: p. 342-348.
127. Ward, T.L. and T. Dao, Journal of Membrane Science, 1999. **153**: p. 211-231.
128. Yeung, K.L., S.C. Christiansen, and A. Varma, Journal of Membrane Science, 1999. **159**: p. 107-122.
129. Shu, J., B.P.A. Grandjean, E. Ghali, and S. Kaliaguine, Journal of Membrane Science, 1993. **77**: p. 181-195.
130. Wong, W.C., L.T.Y. Au, C.T. Ariso, and K.L. Yeung, Journal of Membrane Science, 2001. **191**(1-2): p. 143 - 163.
131. Geus, E.R., M.J. den Exter, and H. van Bekkum, Journal of the Chemistry Society Faraday Transactions, 1992. **88**(20): p. 3101-3109.
132. Ciavarella, P., *Etude experimentale et modelisation du transport gazeux dans les membranes zeolithiques de type MFI. Application a la dehydrogenation de*

l'isobutane en reacteur catalytique a membrane. 1999, L'Universite Claude Bernard - Loyn 1: Lyon. p. 277.

133. Huang, T.-C., M.-C. Wei, and H.-I. Chen, Chemical Engineering Communications, 2002. **189**: p. 1340 - 1359.
134. Xomeritakis, G. and Y.S. Lin, Journal of Membrane Science, 1996. **120**: p. 261-272.
135. Hollek, G.L., Journal of Physical Chemistry, 1970. **74**: p. 503-511.
136. Rothenberger, K.S., A.V. Cugini, B.H. Howard, R.P. Killmeyer, M.V. Ciocco, B.D. Morreale, R.M. Enick, F. Bustamante, I.P. Mardilovich, and Y.H. Ma, Journal of Membrane Science, 2004. **244**(1-2): p. 55-68.
137. Weyten, H., J. Luyten, K. Keizer, L. Willems, and R.U. Leysen, Catalysis Today, 2000. **56**(1-3): p. 3-11.
138. Li, A., W. Liang, and R. Hughes, Journal of Membrane Science, 2000. **165**: p. 135-141.
139. Shu, J., B.E.W. Bongondo, B.P.A. Grandjean, and S. Kaliaguine, Journal of Materials Science Letters, 1997. **16**: p. 294-297.
140. Dixon, A.G., International Journal of Chemical Reactor Engineering, 2003. **Review R6**: p. 1-35.
141. Saracco, G., H.W.J.P. Neomagus, G.F. Versteeg, and W.P.M. Van Swaaij, Chemical Engineering Science, 1999. **54**: p. 1997-2017.
142. Drioli, E. and M. Romano, Industrial Engineering and Chemistry Research, 2001. **40**: p. 1277-1300.
143. Mériaudeau, P., C. Naccache, A. Thangaraj, C.L. Bianchi, R. Carli, and S. Narayanan, Journal of Catalysis, 1995. **152**: p. 313-321.
144. Ciavarella, P., D. Casanave, H. Moueddeb, S. Miachon, K. Fiaty, and J.-A. Dalmon, Catalysis Today, 2001. **67**(1-3): p. 177-184.
145. Raich, B.A. and H.C. Foley, Applied Catalysis A: General, 1995. **129**(2): p. 167-188.
146. Ionnides, T. and G.R. Gavalas, Journal of Membrane Science, 1993. **77**: p. 207-220.
147. Zhu, Y., R.G. Minet, and T.T. Tsotsis, Catalysis Letters, 1993. **18**: p. 48.
148. Gryaznov, V.M., Platinum Metals Review, 1992. **36**: p. 70-79.
149. Gobina, E. and R. Hughes, Journal of Membrane Science, 1994: p. 11-19.

150. Champagnie, A.M., T.T. Tsotsis, R.G. Minet, and I.A. Webster, Chemical Engineering Science, 1990. **45**: p. 2423-2429.
151. Wang, L., K. Murata, and M. Inaba, Catalysis Today, 2003. **82**: p. 99-104.
152. Ziaka, Z.D., R.G. Minet, and T.T. Tsotsis, AIChE Journal, 1993. **39**(3): p. 526-529.
153. Weyten, H., K. Keizer, A. Kinoo, J. Luyten, and R. Leysen, AIChE Journal, 1997. **43**: p. 1819-1827.
154. Schafer, R., M. Noack, P. Kolsch, S. Thomas, A. Seidel-Morgenstern, and J. Caro, Separation and Purification Technology, 2001. **25**: p. 3-9.
155. Gobina, E. and R. Hughes, Applied Catalysis A: General, 1996. **137**: p. 119-127.
156. Rezac, M.E., W.J. Koros, and S.J. Miller, Industrial Engineering and Chemistry Research, 1995. **34**: p. 862-868.
157. Rezac, M.E., W.J. Koros, and S.J. Miller, Jounal of Membrane Science, 1994. **93**: p. 193-201.
158. Zaspalis, V.T., W. van Praag, K. Keizer, J.G. van Ommen, J.R.H. Ross, and A.J. Burggraaf, Applied Catalysis, 1991. **74**: p. 223-234.
159. Zhang, X.F., J.Q. Wang, H.O. Liu, and C.H. Liu, Gao Xiao Hua Xue Gong Cheng Xue Bao/Journal of Chemical Engineering of Chinese Universities, 2001. **15**: p. 121-126.
160. Tiscareno-Lechuga, F., C.G.J. Hill, and M.A. Anderson, Applied Catalysis A: General, 1993. **96**: p. 33-51.
161. She, Y., J. Han, and Y.H. Ma, Catalysis Today, 2001. **67**: p. 43-53.
162. Jiang, Z. and J. Wang, Separation Science and Technology, 1998. **33**: p. 1379-1385.
163. Wu, J.C.S., T.E. Gerdes, J.L. Pszczolkowski, R.R. Bhave, P.K.T. Liu, and E.S. Martin, Separation Science and Technology, 1990. **25**: p. 1489-1510.
164. Quicker, P., V. Hollein, and R. Dittmeyer, Catalysis Today, 2000. **56**: p. 21-34.
165. Xiongfu, Z., L. Yong, W. Jinqu, and T. Huairong. in *Proc. 6th International Congress on Inorganic Membranes*. 2000. Montpellier, France.
166. Dittmeyer, R., V. Hoellein, P. Quicker, G. Emig, G. Hausinger, and F. Schmidt, Chemical Engineering Science, 1999. **54**: p. 1431-1439.
167. Abdalla, B.K. and S.S.E.H. Elnashaie, AIChE Journal, 1994. **40**: p. 2055-2059.
168. Hermann, C., P. Quicker, and R. Dittmeyer, Jounal of Membrane Science, 1997. **136**: p. 161-172.

169. Becker, Y.L., A.G. Dixon, W.R. Moser, and Y.H. Ma, Jounal of Membrane Science, 1993. **77**: p. 233-244.
170. Assabumrungrat, S., K. Suksomboon, P. Praserthdam, T. Tagawa, and S. Goto, Journal of Chemical Engineering of Japan, 2002. **35**: p. 263-273.
171. Fukuhara, C. and A. Igarashi, Journal of Chemical Engineering of Japan, 2003. **36**: p. 530-539.
172. Wu, J.C.S. and P.K.T. Liu, Industrial Engineering and Chemistry Research, 1992. **31**: p. 322-327.
173. Jeong, B.-H., K.-I. Sotowa, and K. Kusakabe, Chemical Engineering Journal, 2003. **103**: p. 69-75.
174. Mondal, A.M. and S. Ilias, Separation and Purification Technology, 2001. **36**: p. 1101-1116.
175. Kokugan, T., A. Trianto, and H. Takeda, Journal of Chemical Engineering of Japan, 1998. **31**: p. 596-603.
176. Koukou, M.K., G. Chaloulou, N. Papayannakos, and N.C. Markatos, International Journal of Heat and Mass Transfer, 1997. **40**: p. 2407-2417.
177. Terry, P.A., M. Anderson, and I. Tejedor, Journal of Porous Material, 1999. **6**: p. 267.
178. Itoh, N. and K. Haraya, Catalysis Today, 2000. **56**: p. 103-111.
179. Koros, W.J. and D.G. Woods, Journal of Membrane Science, 2001. **181**: p. 157-166.
180. Rezac, M.E. and B. Schoberl, Jounal of Membrane Science, 1999. **156**(2): p. 211-222.
181. Deng, J., Z. Cao, and B. Zhou, Applied Catalysis A: General, 1995. **132**: p. 9-20.
182. Raich, B.A. and H.C. Foley, Industrial Engineering and Chemistry Research, 1998. **37**(10): p. 3888-3895.
183. Liu, B.S., W.L. Dai, G.H. Wu, and J.-F. Deng, Catalysis Letters, 1998. **49**(3-4): p. 181.
184. Liu, B.S., G.H. Wu, G. Niu, and J.F. Deng, Applied Catalysis A: General, 1999. **185**(1): p. 1-10.
185. Xue, D., H. Chen, G.H. Wu, and J.F. Deng, Applied Catalysis A: General, 2001. **214**(1): p. 87-94.

186. Mouton, D.W., *The development of a membrane reactor for the dehydrogenation of isopropanol*, in *Department of Process Engineering*. 2003, University of Stellenbosch: Stellenbosch.

187. Trianto, A., W.L. Qiao, and T. Kokugan, Journal of Chemical Engineering of Japan, 2001. **34**(8): p. 1065-1068.

188. Lefu, W., J. Hongbing, and Z. Jie. in *4th International Conference on Catalysis in Membrane Reactors*. 2003.

189. Amandusson, H., L.G. Ekedahl, and H. Dannetun, Surface Science, 1999. **442**: p. 199-205.

190. Ma, Y.H., W.R. Moser, S. Pien, and A.B. Shelekhin. in *Proc. 3rd International Conference on Inorganic Membranes*. 1994. Worcester, MA, USA.

191. Edlund, D.J. and W.A. Pledger, Journal of Membrane Science, 1994. **94**: p. 111-119.

192. Kaijwara, M., S. Uemiya, and T. Kojima, International Journal of Hydrogen Energy, 1999. **24**: p. 839-844.

193. Collins, J.P. and J.D. Way, Journal of Membrane Science, 1994. **96**: p. 259-274.

194. Gobina, E.N., J.S. Oklany, and R. Huges, Industrial Engineering and Chemistry Research, 1995. **34**(11): p. 3777-3783.

195. Lede, J., F. Lapicque, J. Villeurmaux, B. Cales, A. Ounali, J.F. Baumard, and A.M. Antony, International Journal of Hydrogen Energy, 1982. **7**: p. 939-950.

196. Shu, J., B.P.A. Grandjean, and S. Kaliaguine, Catalysis Today, 1995. **25**: p. 327-332.

197. Lin, Y.M. and M.-H. Rei, Catalysis Today, 2001. **67**(1-3): p. 77-84.

198. Lin, Y.M. and M.-H. Rei, International Journal of Hydrogen Energy, 2000. **25**(3): p. 211-219.

199. Frustreri, F., A. Mezzapic, F. Arena, A. Parmaliana, A. Tavolaro, A. Basile, A. Regina, and E. Drioli. in *Proc. International Conference on Catalysis with Membrane Reactors - 2000*. 2000. Zaragoza, Spain.

200. Sanfilippo, D., Cattech, 2002. **4**: p. 56-72.

201. Miracca, I. and L. Piovesan, Catalysis Today, 1999. **52**: p. 259-269.

202. De Rossi, S., G. Ferraris, S. Fremiotti, V. Indovina, and A. Cimino, Catalysis A: General, 1995. **106**: p. 125-141.

203. De Rossi, S., G. Ferraris, S. Fremiotti, A. Cimino, and V. Indovina, Applied Catalysis A: General, 1992. **81**: p. 113-132.

204. Cortright, R.D., J.M. Hill, and J.A. Dumesic, Catalysis Today, 2000. **55**: p. 213-223.

205. Gueguen, E., S. Delsarte, V. Peltier, R. Conanec, R. Marchand, Y. Laurent, and P. Grange, Journal of the European Ceramic Society, 1997. **17**: p. 2007-2010.

206. Guo, Y., G. Lu, Y. Wang, and R. Wang, Separation and Purification Technology, 2003. **32**: p. 271-279.

207. Sheintuch, M. and R.M. Dessau, Chemical Engineering Science, 1996. **51**(4): p. 535-547.

208. Matsuda, T., I. Koike, N. Kubo, and E. Kikuchi, Applied Catalysis A: General, 1993. **96**: p. 3-13.

209. Casanave, D., A. Giroir-Fendler, J. Sanchez, R. Loutaty, and J.-A. Dalmon, Catalysis Today, 1995. **25**: p. 309-314.

210. Casanave, D., P. Ciavarella, K. Fiaty, and J.-A. Dalmon, Chemical Engineering Science, 1999. **54**(13-14): p. 2807-2815.

211. van Dyk, L., S. Miachon, L. Lorenzen, M. Torres, K. Fiaty, and J.-A. Dalmon, Catalysis Today, 2003, 82: p. 167-177.

212. Casanave, D., K. Fiaty, J.-A. Dalmon, and M. Forissier, *Kinetics and mechanism studies of the catalytic dehydrogenation of isobutane on platinum-indium catalyst (p. 367)*. Studies in Surface Sciences and Catalysis, ed. G.F. Froment and K.C. Waugh. Vol. 122. 1999: Elsevier. 490.

213. McKetta, J.J., *Encyclopedia of Chemical Processing and design*. Encyclopedia of Chemical Processing and design. Vol. 67. 1999, New York: Marcel Dekker Inc. 147.

214. Graph, G., *Price shifts roil market as demand improves*, in *Purchasing Magazine*. 2003.

215. Franck, H.-G. and J.W. Stadelhofer, *Industrial Aromatic Chemistry, Raw Materials, Process, Products*. 1988, Berlin, Germany: Springer-Verlag. 283.

216. Guisnet, M., N.S. Gnep, and S. Morin, Microporous and Mesoporous Materials, 2000. **35-36**: p. 47-59.

217. van Dyk, L., L. Lorenzen, S. Miachon, and J.-A. Dalmon, Catalysis Today, 2005. **In press.**

218. Chen, N.Y., Industrial & Engineering Chemistry Research, 2001. **40**: p. 4157-4161.
219. Chirico, R.D. and V. Steele, Journal of Chemical Engineering Data, 1997. **42**: p. 784-790.
220. Fogler, H.S., *Elements of Chemical Reaction Engineering*. 1992, New York: Prentice Hall International. 838.
221. Koehler, E., G. Burgfels, P. Roeger, J. Osbourne, and H. Takeda. *Improved Economics from new Generation of Xylene Isomerization Catalysts*. in *AIChE 2001 Spring National Meeting*. 2001. New Orleans.
222. Corma, A. and E. Sastre, Journal of Catalysis, 1991. **129**: p. 177-185.
223. Wilson, R.D., D.G. Barton, C.D. Beartsch, and E. Iglesia, Journal of Catalysis, 2000. **194**: p. 175-187.
224. Gendy, T.S. and K.C. Pratt, Chemical Engineering Science, 1982. **37**: p. 37-43.
225. Morin, S., N.S. Gnep, and M. Guisnet, Journal of Catalysis, 1996. **159**: p. 296-304.
226. Jan, D.-Y., G.J. Lewis, J.G. Moscoso, M.A. Miller, and Q. Chen, *Xylene isomerization process using UZM-5 and UZM-6 zeolites*, in *US Patent 6,388,159*. 2002, UOP LLC (Des Plaines, IL): United States.
227. Young, D.A. and J.W. Koepke, *Chemical reaction promoted by catalytically active amorphous silica*, in *US Patent 4,501,925*. 1985, Union Oil Company of California (Los Angeles, CA): United States.
228. Adair, B., C.-Y. Chen, K.-T. Wan, and M.E. Davis, Microporous Materials, 1996. **7**: p. 261-270.
229. Benazzi, E., J.-F. Joly, J.M. Da Silva, G. Ribeiro, M.F. Gomes Ribeiro, and US Patent 6, 704, *Catalyst with a base of modified MFI zeolite, and its use in the isomerization of a C_8 aromatic cut*, in *US Patent 6,245,704*. 2001, Institut Francais du Petrole (FR): United States.
230. Li, Y.-G. and H. Jun, Applied Catalysis A: General, 1996. **142**: p. 123-137.
231. Bauer, F., W.-H. Chen, H. Ernst, S.-J. Huang, A. Freyer, and S.-B. Liu, Microporous and Mesoporous Materials, 2004. **72**: p. 81-89.
232. Henriques, C.A., J.L.F. Monteiro, P. Magnoux, and M. Guisnet, Journal of Catalysis, 1997. **172**: p. 436-445.
233. Ferraro, J.M., R.M. Osman, J.D.-Y. Ou, G.I. Cox, J.R. Lattner, and K.R. Clem, *Process for production of para-xylene*, in *US 6,376,733 B1*. 2002, ExxonMobil Chemical Patents Inc.: United States.

234. Burger, B.V., C.W. Holzapfel, D.F. Schneider, and H.F. Strauss, *Inleiding tot die organiese chemie*. 1985, Johannesburg: Butterworth – CO Ltd. 336.

235. Hamm, D.A., *Adsorptive separation product recovery by fractional distillation*, in *US Patent 6,395,951*. 2002, UOP LLC (Des Plaines, IL): United States.

236. Blehaut, J. and R.-M. Nicoud, Analusis Magazine, 1998. **26**: p. M60-M70.

237. Baertsch, C.D., H.H. Funke, J.L. Falconer, and R.D. Noble, Journal of Physical Chemistry, 1996. **100**: p. 7676-7679.

238. Xomeritakis, G., L. Zhiping, and M. Tsapatsis, Industrial & Engineering Chemistry Research, 2001. **40**(2): p. 544-552.

239. Sakai, H., T. Tomita, and T. Takahashi, Separation and Purification Technology, 2001. **25**(1-3): p. 297-306.

240. Mentzen, B.F. and P. Gelin, Materials Reasearch Bulletin, 1995. **30**: p. 373-380.

241. Mohanty, S., H.T. Davis, and A.V. McCormick, Chemical Engineering Science, 2000. **55**: p. 2779-2792.

242. Matsufuji, T., N. Nishiyama, M. Matsukata, and K. Ueyama, Jounal of Membrane Science, 2000. **178**: p. 25-34.

243. Keizer, K., A.J. Burggaaf, Z.A.E.P. Vroon, and H. Verweij, Journal of Membrane Science, 1998. **147**: p. 159-172.

244. Deckman, H.W., E.W. Corcoran (Jr.), J.A. Mc Henry, F. Lai, L.R. Czarnetzki, and W.E. Wales, *Zeolite containing composition with a selectivity enhancing coating*, in *US Patent 5,968,366*. 1999, Exxon Research and Engineering Company (Florham Park, NJ): United Sates.

245. Xomeritakis, G., S. Nair, and M. Tsapatsis, Chemical Materials, 1999. **11**: p. 875.

246. Xomeritakis, G., S. Nair, and M. Tsapatsis, Microporous and Mesoporous Materials, 2000. **38**: p. 61-73.

247. Lai, Z., G. Bonilla, I. Diaz, J.G. Nery, K. Sujaoti, M.A. Amat, E. Kokkoli, O. Terasaki, R.W. Thompson, M. Tsapatsis, and D.G. Vlachos, Science, 2003. **300**: p. 456-460.

248. Hedlund, J., J. Sterte, M. Anthonis, A.-J. Bons, B. Cartensen, N. Corcoran, D. Cox, H. Deckman, W. De Gijnst, P.-P. de Moor, F. Lai, J. McHenry, W. Mortier, J. Reinoso, and J. Peters, Microporous and Mesoporous Materials, 2002. **52**: p. 179-189.

249. Takahashi, T., H. Sakai, and N. Ogawa, *Method for separation of p-xylene*, in *US 6,646,177*. 2003, NGK Insulators, Ltd. (Nagoya, JP): United States.

250. Mabande, G.T.P., A. Avhale, W. Schwieger, M. Hanebuth, and R. Dittmeyer. *MFI membrane reactor for xylene isomerization: Concept and testing*. in *6th International Conference on Catalysis in Membrane Reactors (ICCMR-6)*. 2004. Lahnstein/GERMANY.

251. Sommer, S., T. Melin, J.L. Falconer, and R.D. Noble, Journal of Membrane Science, 2003. **224**(1-2): p. 51-67.

252. Noble, R.D. and J.L. Falconer, Catalysis Today, 1995. **25**(3-4): p. 209-212.

253. Bai, C., M.-D. Jia, J.L. Falconer, and R.D. Noble, Journal of Membrane Science, 1995. **105**(1-2): p. 79-87.

254. Jayaraman, V.K., B.D. Kulkarni, and A. Rao, Chemical Engineering Journal, 2001. **84**(3): p. 475-483.

255. Hedlund, J., J. Sterte, M. Anthonis, A.-J. Bons, B. Carstensen, N. Corcoran, D. Cox, H. Deckman, W.D. Gijnst, P.-P.d. Moor, F. Lai, J. McHenry, W. Mortier, J. Reinoso, and J. Peters, Microporous and Mesoporous Materials, 2002. **52**: p. 179-189.

Appendix A: Operating procedures of the Membrane Reactor Testing Bench

A new generic experimental membrane reactor testing bench for the Department of Process Engineering, University of Stellenbosch was designed and constructed. In the following section the general operating procedures of the bench will be given.

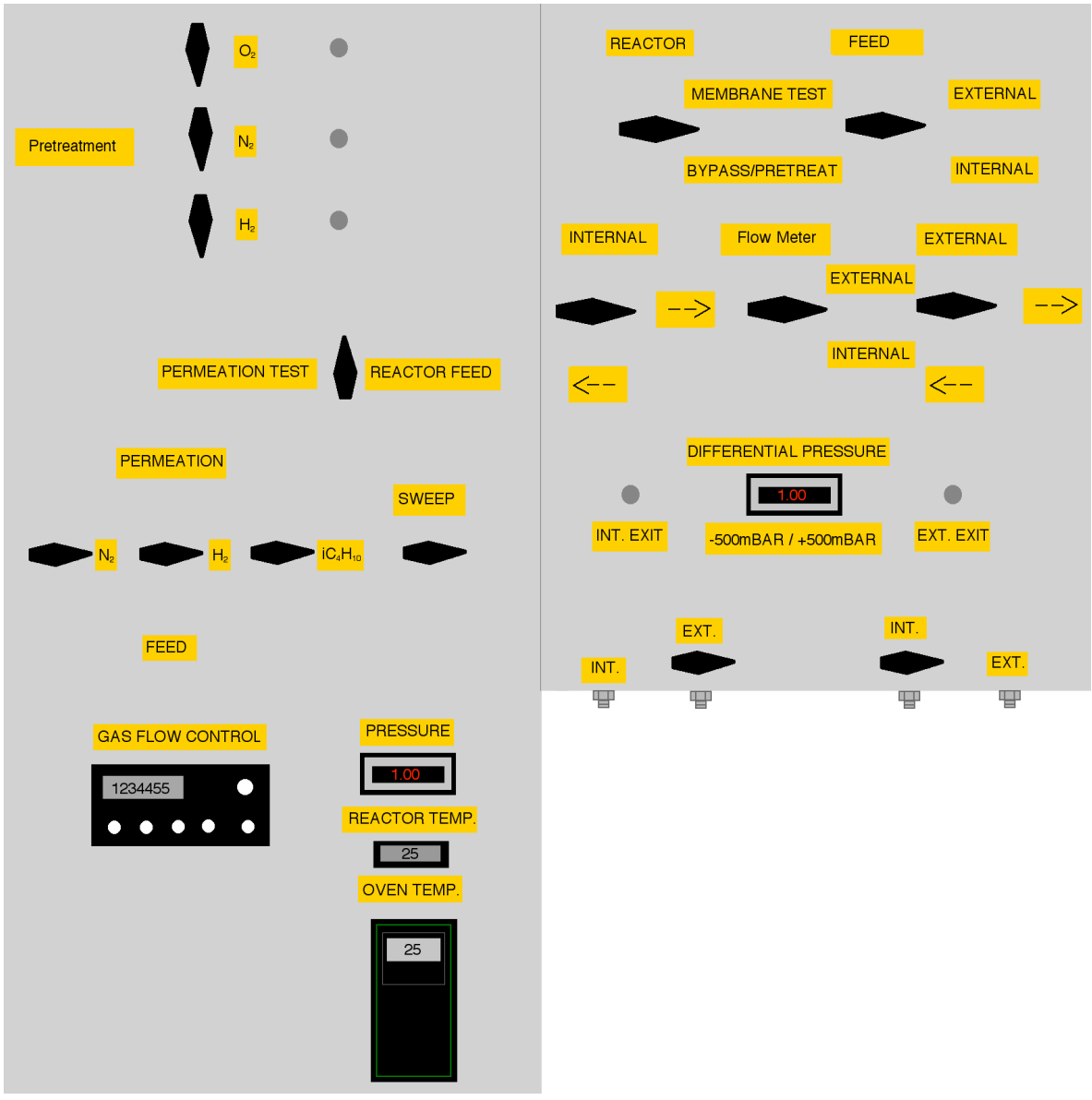

Figure A-1 Frontal view of Membrane Testing Bench at the Department of Process Engineering (University of Stellenbosch)

A.1 Membrane Treatment/ Pre-treatment

Membrane set-up Settings (membrane layer on inside of support)

- Valve 1 (Reactor): Bypass/ Pretreat.
- Valve 2 (Feed): Internal.
- Valve 3 (Internal): – –›
- Valve 5 (External): – –›
- Valve 4 (Flow meter): Internal or External
- Sweep (open/close) valve: Open
- Flow controller channel --- open and set at required flow rate

Procedure

- Place membrane inside the membrane reactor module and connect the membrane module to the lines of the membrane reactor testing bench.
- Program the temperature controller
- Select pretreatment gas and open the feeding valve
- Tune the variable pretreatment gas valve until the correct flow rate is obtained by measuring the internal flow rate with the bubble flow meter.
- Start temperature programme

Comments

Before doing the pretreatment open N_2 gas cylinders, settings: N_2 sweep pressure 400 kPa, and *suggested* N_2 pretreatment pressure 100 kPa. The N_2 pretreatment cylinder's feeding pressure can be changed in order to ensure a regulated gas flow on the internal part.

A.2 Single gas permeation testing (Dead-end mode)

Membrane set-up Settings (membrane layer on inside of support)

- Valve (11) - Permeation test position
- Valve (1) - Reactor: Membrane Test
- Valve 2 (Feed): Internal.
- Valve 3 (Internal): – –›
- Valve 5 (External): – –›
- Valve 9 (Ext. open/close): Close.
- Valve 10 (Int. open/close): Close.
- Valve 4 (Flow meter): External

- Sweep (open/close) valve: Close.
- Permeation gas: Valves in permeation position.

Procedure

- Do membrane pretreatment
- Adjust temperature to the required permeation temperature
- Use gas cylinder regulator to regulate the internal pressure inside the membrane (displayed on the pressure indicator).
- Record pressure
- Measure the flow rate of the external compartment and record.

Comments

The flow meter can also be connected directly onto the membrane reactor external outlet. The feed exit and internal inlet can be closed off directly on the reactor module as well. If the above method is used it should be insured that the external pressure do not rise above 500 mBar, due to the fact the gas pass through the differential pressure guage.

A.3 Feed composition and feed rate analysis

Procedure

- Set feed rates on the flow controllers.
- Valve 11: Reactor feed
- Valve 1 (Reactor): Bypass
- Valve 4 (Flow meter): Internal – measure the flowrate and record
- Valve 4 (Flow meter): External
- If analysing for hydrocarbons, then put valve 6 in FID position and inject.
- If analysing for hydrogen, then put valve 6 in TCD position and inject.

A.4 Mixture gas permeation

Measuring feed flow composition and rate

Membrane set-up Settings (membrane layer on inside of support)

- Valve (11): Reactor feed
- Valve 1 (Reactor): Membrane Test

- Valve 2 (Feed): Internal.
- Valve 3 (Internal): – –›
- Valve 5 (External): – –› (co-current) OR ‹– – (counter-current)
- Valve 4 (Flow meter): Internal or External. When flow meter on external then the internal stream will go to the gas chromatograph and visa versa.
- Sweep (open/close) valve: Open
- Feed gas valves: Feed
- Flow controller channels open and set at required flow rates
- Valves 9, 10, 7 and 8: Open

Procedure

- Place membrane inside the membrane reactor module and connect the membrane module to the lines of the membrane reactor testing bench. The membrane can be packed with inerts to simulate the catalyst or not.
- Program the temperature controller.
- Do pretreatment.
- Set temperature to required set point.
- Do feed composition and feed flow rate analysis procedure
- Switch Valve 1 to Membrane Test
- Set differential pressure to 0 by adjusting the internal or external pressure by tuning valves 7 or 8.
- Measure internal flowrate (Flow meter: Internal).
- Switch Valve 4 to External position.
- Switch Vale 6 to FID position and inject.
- Switch Valve 6 to TCD position and inject.
- Wait for analysis and measure internal flowrate.
- Switch Valve 4 to Internal position.
- Switch Vale 6 to FID position and inject.
- Switch Valve 6 to TCD position and inject.
- Adjust parameters and repeat procedure for mixture gas separation measurements.

Comments

All the gas cylinder feed pressures should be on 400 kPa.

A.5 Membrane reactor testing

The operating procedures for the membrane reactor testing is identical to the mixture separation testing, except that the membrane is now packed with a catalyst. The pretreatment procedure will now depend on the pretreatment procedure of the catalyst and membrane combined.

Before doing the membrane test, the conventional reactor test needs to be done. This can either be done by replacing the membrane with a stainless steel tube of similar dimensions, only analyzing the feed and retentate compositions and flow rates OR it can be done in series with the CMR tests by just closing the external compartment of the membrane reactor module and analyzing the feed and retentate flow rates and compositions.

Appendix B: One-dimensional simple eCMR model

A one-dimensional model was developed to describe the operation on the CMR for isobutane dehydrogenation [211]. Figure B-1 is a schematic view of the reactor in counter current sweep mode. The reactor is divided into four zones: Catalyst bed, membrane layer, and support and shell side.

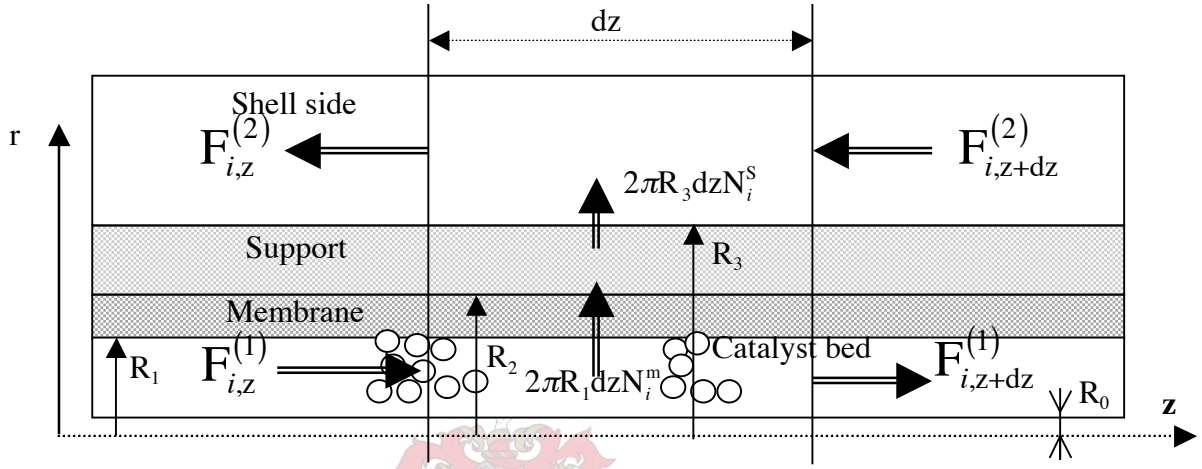

Figure B-1 Schematic view of the reactor in counter current sweep mode. The reactor is divided into four zones: Catalyst bed, membrane layer, and support and shell side.

Model assumptions

- Operation in steady-state
- Isothermal conditions
- Negligible transmembrane pressure
- Plug flow prevails in each compartment, axial dispersion negligible
- Pressure drops through packed-bed and shell side are negligible
- Gaseous components behave as ideal gases.
- Model development

Tube side

In the catalyst bed, 0 < z < L, the mass balance on each component is:

$$\frac{dF_i^{(1)}}{dz} = \nu_i \eta \rho \pi \left(R_1^2 - R_0^2\right) r - 2\pi R_1 N_i^m \Big|_{r=R_1^+} \qquad \text{B-1}$$

ρ is the catalyst apparent density defined as the mass of catalyst per internal compartment unit volume and ν_i is the algebraic stoichiometric coefficient of component i,

η the effectiveness factor introduced to take into account the limiting effects on catalyst activity in comparison with the one measured in the differential microreactor and r the kinetic rate. N_i^m is the molar flux of mixture component *i* through the membrane.

Shell side

The differential equation describing mass balance in the axial direction is:

$$\frac{dF_i^{(2)}}{dz} = (-1)^n 2\pi R_3 N_i^s \Big|_{r=R_3^-} \qquad \text{B-2}$$

with n = 0 for co current and n =1 for counter current. N_i^s is the molar flux of mixture components through the support.

Membrane

In the membrane the conservation of the mass is given by:

$$\frac{1}{r}\frac{\partial}{\partial r}\left(rN_i^m\right) = 0 \qquad \text{B-3}$$

with $N_i^m = -\frac{D_i^m}{RT}\frac{\varepsilon_m}{\tau_m}\frac{\partial P_i^m}{\partial r}$ given by Fick's Law B-4

Membrane Support

A similar expression can be derived for mass transport in the support:

$$\frac{1}{r}\frac{\partial}{\partial r}\left(rN_i^s\right) = 0 \qquad \text{B-5}$$

and $N_i^s = -\frac{D_i^s}{RT}\frac{\varepsilon_s}{\tau_s}\frac{\partial P_i^s}{\partial r}$ B-6

Expressions B-3 and B-5 are solved analytically using the following boundary conditions:

At r = R1 $\qquad P_i^m\Big|_{r=R_1^+} = P_i^{(1)} = \frac{F_i^{(1)}}{F_T^{(1)}}P$ B-7

At r = R2 $\qquad P_i^m\Big|_{r=R_2^-} = P_i^s\Big|_{r=R_2^+}$ B-8

At r = R3 $\qquad P_i^s\Big|_{r=R_3^-} = P_i^{(2)} = \frac{F_i^{(2)}}{F_T^{(2)}}P$ B-9

At the membrane/support (R2) interface $N_i^m \Big|_{r=R_2} = N_i^s \Big|_{r=R_2}$.

The following equation of the molar flux through the membrane is:

$$N_i^m \Big|_{r=R_1^+} = -\frac{1}{R_1}\frac{D_i^m\varepsilon_m}{\tau_m}\frac{1}{\ln\frac{R_2}{R_1} + \frac{D_i^m\varepsilon_m}{D_i^s\varepsilon_s}\frac{\tau_s}{\tau_m}\ln\frac{R_3}{R_2}}\frac{P}{RT}\left(\frac{F_i^{(2)}}{F_T^{(2)}} - \frac{F_i^{(1)}}{F_T^{(1)}}\right) \qquad \text{B-10}$$

The mass balance in the tube side is obtained by substituting equation B-10 into equation B-1 giving the following expression:

$$\frac{dF_i^{(1)}}{dz} = \nu_i \eta \rho \pi \left(R_1^2 - R_0^2\right) r + 2\pi \frac{P}{RT} \frac{D_i^m \varepsilon_m}{\tau_m} \frac{1}{\ln\frac{R_2}{R_1} + \frac{D_i^m \varepsilon_m}{D_i^s \varepsilon_s}\frac{\tau_s}{\tau_m}\ln\frac{R_3}{R_2}} \left(\frac{F_i^{(2)}}{F_T^{(2)}} - \frac{F_i^{(1)}}{F_T^{(1)}}\right) \qquad \text{B-1'}$$

At steady state there will be a conservation of the flux at the interface membrane/support in the radial direction:

$$N_i^s \Big|_{r=R_3^-} = \frac{R_1}{R_3} N_i^m \Big|_{r=R_1^+} \qquad \text{B-11}$$

Substitution of equation B-10 into B-11 and subsequent substitution into B-2 gives an new expression for the mass flow in the shell side:

$$\frac{dF_i^{(2)}}{dz} = (-1)^{n+1} 2\pi \frac{P}{RT} \frac{D_i^m \varepsilon_m}{\tau_m} \frac{1}{\ln\frac{R_2}{R_1} + \frac{D_i^m \varepsilon_m}{D_i^s \varepsilon_s}\frac{\tau_s}{\tau_m}\ln\frac{R_3}{R_2}} \left(\frac{F_i^{(2)}}{F_T^{(2)}} - \frac{F_i^{(1)}}{F_T^{(1)}}\right) \qquad \text{B-2'}$$

Due to chemical reaction and back permeation, the total molar rate vary along the membrane length and it is therefore necessary to take this change into account. A way of doing this is to also solve the equation of the total molar flux in tube $F_T^{(1)}$ and shell side $F_T^{(2)}$. $F_T^{(1)}$ is obtained from a overall mass balance over the tube side by adding together equation B-1 written for each component of the gaseous mixture:

$$\frac{dF_T^{(1)}}{dz} = -2\pi R_1 \sum_i N_i^m \Big|_{r=R_1^+} + \eta \rho \pi \left(R_1^2 - R_0^2\right) r \Delta\nu \qquad \text{B-12}$$

where $\Delta\nu = \sum_i \nu_i$

The total molar flux at the membrane tube interface is defined as:

$$\sum_i N_i^m \Big|_{r=R_1^+} = -\frac{1}{RT} \sum_i \frac{D_i^m \varepsilon_m}{\tau_m} \frac{\partial P_i^m}{\partial r}\Bigg|_{r=R_1^+} \qquad \text{B-13}$$

It was assumed that the total pressure is constant and therefore the variation of the inert partial pressure through the membrane is:

$$\frac{\partial P_I^m}{\partial r} = -\sum_{j \neq I} \frac{\partial P_j^m}{\partial r} \qquad \text{B-14}$$

with *I* referring to the inert component or sweep gas. By substituting equation B-14 into equation B-13, and this with equation B-4 and equation B-10 , the radial total molar flux can be determined by the following expression:

$$\sum_i N_i^m\Big|_{r=R_1^+} = \frac{1}{R_1}\frac{P}{RT}\sum_{j\neq I}\frac{\left(D_I^m - D_i^m\right)\varepsilon_m}{\tau_m}\frac{1}{\ln\frac{R_2}{R_1} + \frac{D_i^m\varepsilon_m}{D_i^s\varepsilon_s}\frac{\tau_s}{\tau_m}\ln\frac{R_3}{R_2}}\left(\frac{F_i^{(2)}}{F_T^{(2)}} - \frac{F_i^{(1)}}{F_T^{(1)}}\right) \quad \text{B-15}$$

The overall mass balance on the tube side can then be obtained by substituting equation B-15 into equation B-12:

$$\frac{dF_T^{(1)}}{dz} = -2\pi\frac{P}{RT}\sum_{j\neq I}\frac{\left(D_I^m - D_i^m\right)\varepsilon_m}{\tau_m}\frac{1}{\ln\frac{R_2}{R_1} + \frac{D_i^m\varepsilon_m}{D_i^s\varepsilon_s}\frac{\tau_s}{\tau_m}\ln\frac{R_3}{R_2}}\left(\frac{F_i^{(2)}}{F_T^{(2)}} - \frac{F_i^{(1)}}{F_T^{(1)}}\right) + \eta\rho\pi\left(R_1^2 - R_0^2\right)r\Delta v \quad \text{B-16}$$

Similarly the overall mass balance in the shell side will be given by the sum of the component mass balances in the shell side:

$$\frac{dF_T^{(2)}}{dz} = (-1)^n 2\pi R_3\sum_i N_i^s\Big|_{r=R_3^-} \quad \text{B-17}$$

By substituting equation B-11 and equation B-15 into equation B-17, the overall mass balance in the shell side becomes:

$$\frac{dF_T^{(2)}}{dz} = (-1)^n 2\pi\frac{P}{RT}\sum_{j\neq I}\frac{\left(D_I^m - D_i^m\right)\varepsilon_m}{\tau_m}\frac{1}{\ln\frac{R_2}{R_1} + \frac{D_i^m\varepsilon_m}{D_i^s\varepsilon_s}\frac{\tau_s}{\tau_m}\ln\frac{R_3}{R_2}}\left(\frac{F_i^{(2)}}{F_T^{(2)}} - \frac{F_i^{(1)}}{F_T^{(1)}}\right) \quad \text{B-18}$$

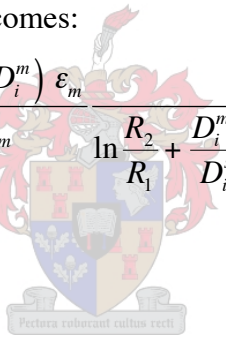

Appendix C: Published papers

Catalysis Today 82 (2003) 167-177

L. van Dyk, S. Miachon, L. Lorenzen, M. Torres, K. Fiaty and J-A. Dalmon

Comparison of Microporous MFI and Dense Pd Membrane Performances in an Extractor-type CMR.

Catalysis Today (2005): In Press

Lizelle van Dyk, Leon Lorenzen, Sylvain Miachon & Jean-Alain Dalmon

Xylene isomerization in an extractor type Catalytic Membrane Reactor

Comparison of Microporous MFI and Dense Pd Membrane Performances in an Extractor-type CMR.

L. van Dyk[1], S. Miachon[2], L. Lorenzen[1], M. Torres[3], K. Fiaty[4] and J-A. Dalmon[2]*

[1]*Unversity of Stellenbosch, Matieland, 7602 Stellenbosch, South Africa*
[2]*IRC-CNRS-Lyon, 2 av. Albert Einstein, 69626 Villeurbanne cedex (France)*
[3] *Universidad Autonoma Metropolitana (Azcapotzalco)*
[4]*LAGEP, UCB-CPE Lyon, 43 bd. du 11 Nov. 1918, 69622 Villeurbanne cedex (France)*
**dalmon@catalyse.univ-lyon1.fr*

Abstract

An extractor-type CMR, including a Pt-based fixed-bed catalyst, was combined with two different membranes, either a Pd membrane, obtained by electroless plating, or an MFI zeolite membrane, obtained by hydrothermal synthesis. These two configurations were compared in isobutane dehydrogenation. Both CMRs give better results than conventional reactors. However, though the two membranes presented different separative properties, the two CMRs showed very similar yields. This has been attributed to the limitation of both CMRs by the catalyst lack of efficiency, when compared to the membrane performance. A modeling approach that combines catalyst kinetic law and membrane gas transfer equations also contributes to the description of the CMRs performance.

Introduction

According to a recently proposed classification of CMRs [1], in an extractor, the role of the membrane is to selectively remove (extract) from the reactor a product of the reaction. When compared to conventional reactors, this may lead either to an improved yield in the case of equilibrium-restricted reactions, like hydrocarbon dehydrogenation [2], or to an improved selectivity in consecutive reactions when the permeation favours the extraction of a primary product [3].
Here we report on the performances of a Pd membrane or an MFI membrane, used as hydrogen extracting membranes during the isobutane dehydrogenation. If this reaction has been already studied in CMRs using either dense Pd [4-6] or porous materials [7-9], no comparative experimental data under similar conditions have been reported. The dehydrogenation of isobutane to isobutene is the first step in the production of MTBE, an octane booster for gasoline. Though recent regulation about oxygenates in motor fuels leads to reconsider the isobutene demand in the future, the isobutane dehydrogenation can be considered as a good model reaction for membrane reactors of the extractor type [9].
Identical reaction conditions were used in order to compare the performances of these two membranes that possess very different characteristics and properties. In principle, Pd membranes are perfectly selective for hydrogen, as permeation is due to the formation of palladium hydrides. However, they are expensive and may present stability problems [10]. On the other hand, transport through zeolite membranes is very often controlled by diffusivity parameters and adsorption properties. Their selectivity may be strongly temperature-dependent.
Finally, the catalyst itself, here located as fixed-bed in the lumen of the tubular membrane, may operate under conditions that are quite different from that of a conventional reactor. A modeling approach has been developed in order to illustrate how the CMR works.

Experimental

Materials

Catalyst

The *catalyst* was a trimetallic Pt-In-Ge supported on a MFI zeolite [11]. Indium and Germanium were introduced within the zeolite precursors before hydrothermal synthesis. After calcination the final material contained 0.8 wt. % of both Indium and Germanium. Platinum (0.5 wt. %) was then introduced in the zeolite via an exchange/impregnation technique using $Pt(NH_3)_4(OH)_2$ as a precursor. Before catalytic use, the solid was activated in situ under flowing H_2 at 823 K during 10 h. For experiments in the membrane reactor, and in order to avoid an excessive pressure drop in the catalyst bed, the catalyst powder was transformed into pellets of ca. 2 mm size, using a lab extruder.

Membranes

The separative phases (Pd or MFI) were applied on ceramic tubular supports (Pall-Exekia T1-70), consisting of three macroporous α- alumina layers (from outer to inner side, respective average pore sizes: 12, 0.8, 0.2 μm and thicknesses 1500, 40, 20 μm).

Pd membrane

The Palladium membrane was prepared by a batch electroless plating technique. A detailed discussion description of the plating procedure and equipment is given in [12]. The pretreated support membrane was sealed in a teflon reactor and placed in a warm bath (345 K), after which 8 ml of plating solution (Table 1) was introduced in the inner volume of the tubular support. Hydrazine was only added at the start of a plating session and increased with time (Table 2). An initial layer of 1 μm was plated without a vacuum being drawn and the membrane cleaned with 15 wt% ammonia solution. For subsequent layers a vacuum was drawn on the membrane.

Table 1 Composition of palladium (1625ppm Pd) plating bath per litter of plating solution

$(NH_3)_4PdCl_2.H_2O$ [g]	4.00
28 wt % Ammonia [ml]	325
EDTA [g]	65
35 wt % Hydrazine	Hydrazine: Pd = 0.35:1 (start reaction) Increased with time
Temperature [°C]	72

Table 2 Plating procedure for producing Pd films

Reaction Time (Total) (8 ml plating solution) [min]	1.75 wt % Hydrazine Added (8 ml plating solution) [µl]
0	84.8
20	56.5
40	283
Stop reaction after 60 minutes	

Zeolite membrane

The MFI membrane was obtained by synthesis of zeolite crystals inside the pores of the macroporous tubular support (pore-plugging method) [13]. The precursor solution of the MFI zeolite was obtained by mixing silica (Aerosil 380) and a template (tetrapropylammonium hydroxide, TPAOH). After a 3-day ageing period, that solution was poured in a Teflon-lined autoclave containing the porous ceramic tube. Hydrothermal synthesis was then performed at 443 K for 3 days, and the membrane was calcined at 773 K under a flow of 5% O_2 diluted in N_2. Characterization of the membrane showed it could be considered defect-free (i.e. the transport through the membrane is controlled by the micropores of the MFI structure).

Transport measurements: single gas and mixtures

The membranes were sealed with cylindrical graphite seals in a stainless steel module, equipped with temperature control. The lumen of the tubes was packed with inerts in order to simulate the catalysts pellets. Before membrane testing the palladium and MFI membranes were pretreated. The Pd membrane was pretreated at 593 K first in nitrogen then in oxygen; the same procedure was repeated at 723 K [12]. The MFI membrane was heated to 773 K in nitrogen and left for 4 hours.

Single gas permeation measurements were performed for hydrogen, nitrogen and isobutane at 723 K in the dead-end mode. Separation tests on the MFI membrane were performed by a modified Wicke-Kallenbach method with a mixture of isobutane and hydrogen diluted in nitrogen, feed rate of 1.2 l/h (0.2 H_2, 0.2 iC_4H_{10}, 0.6N_2) with 1.2 l/h counter current nitrogen sweep. The separation factor (S_f) was determined with the following formula:

$$S_f\left(H_2/iC_4\right) = \frac{\left(\frac{[H_2]}{[iC_4]}\right)_{permeate}}{\left(\frac{[H_2]}{[iC_4]}\right)_{feed}} \qquad (1)$$

CMR operation and set-up

The fix-bed catalyst was packed in the lumen of the tubular membrane and the isobutane dehydrogenation reaction was carried out at 723 K and 50 ml/min feed flow (0.2 H_2: 0.2 iC_4H_{10} and 0.6N_2). The differential pressure across the membrane was kept at zero by varying the external pressure of the membrane module. Nitrogen was used as a sweep gas in the counter current mode at different flow rates. The feed and sweep flow rates were

controlled with mass flow controllers (Brooks MFC). The compositions of the feed, permeate and retentate were analyzed on-line with a gas chromatograph (Shimadzu, GC 14A) equipped with two detectors: TCD for hydrogen and FID for hydrocarbons. The flow rates of the permeate and retentate were measured with an automatic flowmeter (Bios, Dry Cal DC-Lite).

Modeling

In order to interpret the results, the membrane reactor has been described through a theoretical model, combining transport equations and catalysis kinetics. A detailed model was previously presented by Casanave et al [14]. Here, we will give a modified and more simple version, which is well adapted for the purpose of this study.
Transport parameters were obtained from permeation measurements, as described in a previous section. The reaction rate expression employed is that obtained by Casanave and co-workers [15] on a similar catalyst, using a differential microreactor. When operating in the vicinity of thermodynamic equilibrium its expression is:

$$r = \frac{k_1 K_{iC_4}\left(P_{iC_4} - P_{iC_4=}P_{H_2}/K_{eq}\right)}{\left(1 + K_{iC_4}P_{iC_4} + K_{iC_4=}P_{iC_4=} + \sqrt{K_{H_2}P_{H_2}}\right)^2} \qquad (2)$$

From this equation and the transport parameters, a one-dimensional model was developed using the following simplifying assumptions: operation in steady-state, isothermal conditions, negligible transmembrane pressure, plug flow prevails in each compartment, axial dispersion negligible. Pressure drops through packed-bed and shell side are negligible. Gaseous components behave as ideal gases.
In order to take into account back permeation of the sweep gas, variations of the overall molar flow in the tube and shell sides are considered, owing to the chemical reaction and mass transfers through the porous media. Under the experimental conditions, Fick's law is sufficient to describe mass transfers through the membrane. Only the simulation results of the countercurrent configuration will be presented here.
Let us consider an element of length dz (see Figure 1, schematic of the CMR). The differential equations describing mass balances in the axial direction for i = iC_4H_{10} (isobutane, also noted iC_4), iC_4H_8 (isobutene, also noted iC_4=), H_2 and N_2 are (see appendix for details) can be obtained as follows:

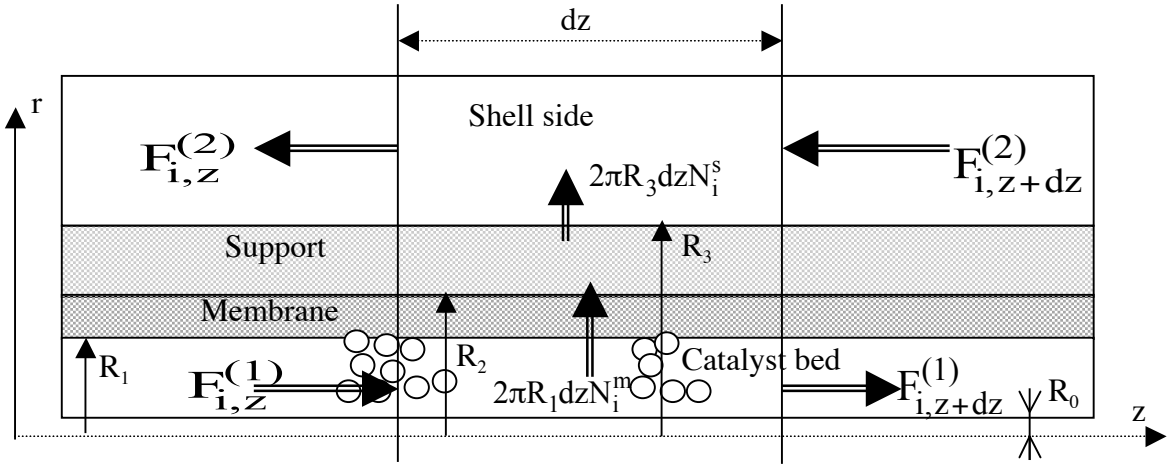

Figure 1. Schematic view of the reactor in counter current mode. The reactor is divided into four zones: Catalyst bed, membrane layer, and support and shell side.

***Tube side*:**
For each component i, the evolution of the molar flow rate along the reactor length is:

$$\frac{dF_i^{(1)}}{dz} = \nu_i \eta \rho \pi \left(R_1^2 - R_0^2\right) r + 2\pi \frac{P}{RT} \frac{D_i^m \varepsilon_m}{\tau_m} \frac{1}{\ln\frac{R_2}{R_1} + \frac{D_i^m \varepsilon_m}{D_i^s \varepsilon_s}\frac{\tau_s}{\tau_m}\ln\frac{R_3}{R_2}} \left(\frac{F_i^{(2)}}{F_T^{(2)}} - \frac{F_i^{(1)}}{F_T^{(1)}}\right) \quad (3)$$

The second term on the right-hand side of Eq. 3 renders the molar flow rate through the porous membrane. The apparent density ρ is defined as the mass of catalyst with respect to the tube unit volume, ν_i is the algebraic stoichiometric coefficient of component i. The effectiveness factor, η, is introduced to account for some limiting effects on the activity of the catalyst in the CMR, when compared to that measured in the differential micro-reactor. Let us underline that η here has nothing to do with diffusion limitations in the catalyst. It is just an adjustment term that will be used to quantify differences between model data (kinetics and transmembrane transfers analyzed separately) and experimental results obtained in the CMR. The diffusivity coefficients D_i^m were estimated from permeation measurements with the membrane. Terms D_i^s are molecular diffusivities that were calculated from the kinetic theory of gases.
Adding Eqs. 3 for each component of the gas stream and considering that the operation pressure is constant, the overall mass balance is:

$$\frac{dF_T^{(1)}}{dz} = -2\pi \frac{P}{RT} \sum_{j \neq I} \frac{\left(D_I^m - D_j^m\right) \varepsilon_m}{\tau_m} \frac{1}{\ln\frac{R_2}{R_1} + \frac{D_j^m \varepsilon_m}{D_j^s \varepsilon_s}\frac{\tau_s}{\tau_m}\ln\frac{R_3}{R_2}} \left(\frac{F_j^{(2)}}{F_T^{(2)}} - \frac{F_j^{(1)}}{F_T^{(1)}}\right) + \eta \rho \pi \left(R_1^2 - R_0^2\right) r \Delta\nu \quad (4)$$

where: $\Delta\nu = \sum_i \nu_i$

Shell side material balance:
For each component i ≠ I (I being an inert or sweep gas)

$$\frac{dF_i^{(2)}}{dz} = (-1)^{n+1} 2\pi \frac{P}{RT} \frac{D_i^m \varepsilon_m}{\tau_m} \frac{1}{\ln\frac{R_2}{R_1} + \frac{D_i^m \varepsilon_m}{D_i^s \varepsilon_s}\frac{\tau_s}{\tau_m}\ln\frac{R_3}{R_2}} \left(\frac{F_i^{(2)}}{F_T^{(2)}} - \frac{F_i^{(1)}}{F_T^{(1)}}\right) \quad (5)$$

(n =1 for counter current)
The overall mass balance in the shell side is:

$$\frac{dF_T^{(2)}}{dz} = (-1)^n 2\pi \frac{P}{RT} \sum_{j \neq I} \frac{\left(D_I^m - D_j^m\right) \varepsilon_m}{\tau_m} \frac{1}{\ln\frac{R_2}{R_1} + \frac{D_j^m \varepsilon_m}{D_j^s \varepsilon_s}\frac{\tau_s}{\tau_m}\ln\frac{R_3}{R_2}} \left(\frac{F_j^{(2)}}{F_T^{(2)}} - \frac{F_j^{(1)}}{F_T^{(1)}}\right) \quad (6)$$

The boundary conditions for equations (3)-(6) are:
tube side:
at z = 0

$$F_i^{(1)} = F_{i,0}^{(1)} \quad (7)$$

$$F_T^{(1)} = \sum_i F_{i,0}^{(1)} \quad (8)$$

shell side:
at z = L (counter current)

$$F_i^{(2)} = F_{i,0}^{(2)} \quad (9)$$

$$F_T^{(2)} = \sum_i F_{i,0}^{(2)} \quad (10)$$

The system of differential equations (3)-(6) was rearranged by introducing dimensionless length.

Orthogonal collocation was applied for numerical discretization of the above mentioned equations and IMSL routine DN2QNF was used for resolution.

Numerical parameters that have been used for the simulation are given in Table 3. Diffusivities D have been deduced from experimental values of single gas permeation.

Table 3 Parameters used for simulation

$k_1 = 67\mu mols^{-1}g^{-1}$	$R_1 = 3.5mm$	$\varepsilon_s = 0.26$
$K_{ic_4} = 0.9atm^{-1}$	$R_2 = 3.505mm$	$\varepsilon_m = 0.5$
$K_{iC_4=} = 2.1atm^{-1}$	$R_3 = 5mm$	$\tau_s = 1.5$
$K_{H_2} = 0.8atm^{-1}$	$R_4 = 8mm$	$\tau_m = 1$
$K_{eq} = 0.033$	$R_0 = 8mm$	
$\rho = 0.53gcm^{-3}$	$L = 100mm$	

Zeolite	Palladium
$D^m_{iC_4} = 6.110^{-4}mm^2s^{-1}$	$D^m_{iC_4} = 3.10^{-3}mm^2s^{-1}$
$D^m_{iC_4=} = 6.110^{-4}mm^2s^{-1}$	$D^m_{iC_4=} = 3.10^{-3}mm^2s^{-1}$
$D^m_{H2} = 0.036mm^2s^{-1}$	$D^m_{H2} = 0.09mm^2s^{-1}$
$D^m_{N_2} = 0.012mm^2s^{-1}$	$D^m_{N_2} = 3.10^{-3}mm^2s^{-1}$

Results

Transport

Pd membrane

First, the thickness of the Pd membrane was estimated to be 4.8µm from the mass gain of the substrate assuming a continuous layer deposition. Accordingly, there was undoubtedly enough Pd to form a separative layer.

Table 4 reports permeation results. As dense Pd membranes are only permeable to hydrogen, the permeance of isobutane and nitrogen through the membrane is an indication that the separative layer contains defects or that gas leaking occurs at or in the graphite seals. However, tests with an impermeable metallic tube showed the seals were gas-tight under the present conditions.

Table 4. Single gas permeation data for MFI and Pd membranes

Membrane	Nitrogen [μmol/Pa.s.m^2]	Isobutane [μmol/Pa.s.m^2]	Hydrogen [μmol/Pa.s.m^2]
MFI	2.10^{-1}	10^{-2}	5.10^{-1}
Pd	5.10^{-2}	5.10^{-2}	3

Zeolite membrane

Single-gas permeation results are reported in Table 4 that shows MFI permeances are different from those obtained with the Pd membrane. The hydrogen/isobutane separation experiments were performed under conditions (temperature, feed flow rates, sweep) similar to those used during catalytic tests. Fig. 2 shows the separation factor $S_{f(H2/iC4)}$ is highly dependent on both temperature and sweep flow rate. At room temperature the separation factor is close to 1 and increases up to ca. 10 at high temperature (reaction conditions).

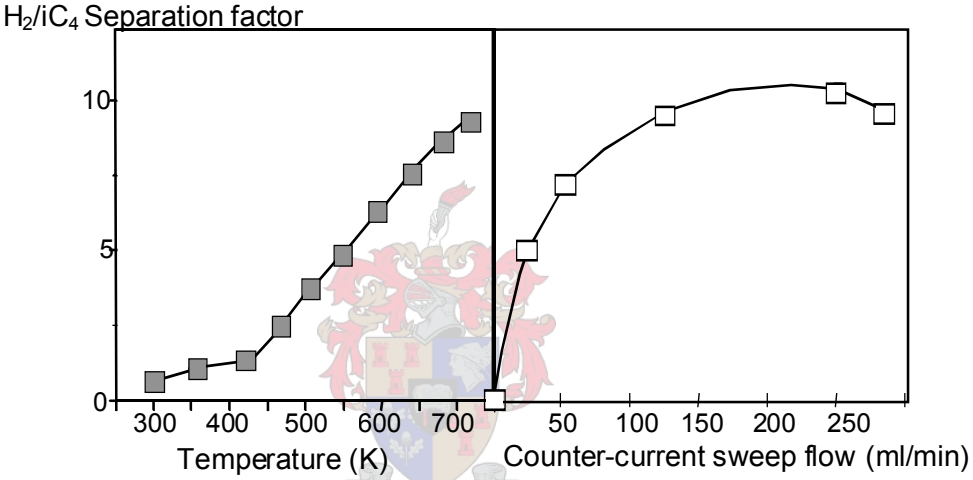

Fig 2. H_2/iC_4 Separation factor S_f as a function of temperature (left) and countercurrent sweep flow rate (right)

CMR performance

Pd membrane reactor

Figure 3 shows the results (iC_4H_{10} conversion and iC_4H_8 yield) as a function of the sweep flow-rate. In the absence of sweep, the reactor works as a conventional one (no permeation through the membrane) and the butane conversion (14%) corresponds to that predicted by the thermodynamic equilibrium. This means that the catalyst is active enough to reach this value and that it does not suffer from deactivation during the test. These data will serve as a reference to be compared with the CMR performance.

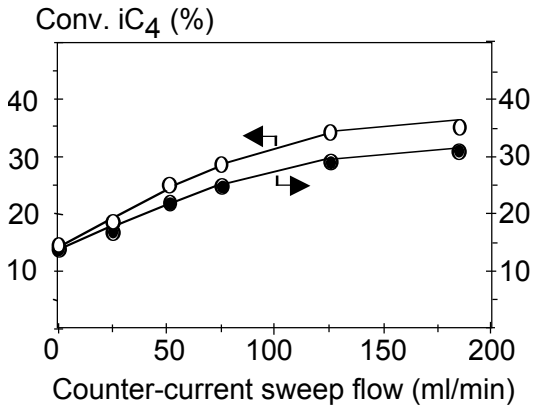

Fig 3. Isobutane conversion and isobutene yield in the Pd membrane reactor
Feed flow rate: 50 ml/min, feed composition: $H_2/iC_4/N_2$ =20/20/60

When using a sweep, the isobutane conversion increases (figure 3) up to ca. 40% for a sweep flow rate of 175 ml/min (3.5 times the feed flow). This increase in conversion does however come at the cost of a slightly lower selectivity that decreases from 100 to 90 %.

Zeolite membrane reactor

Most of the data have been already reported [9] and Figure 4 shows the effect of the sweep on the isobutane conversion. The selectivity towards isobutene is also negatively affected by the sweep and varies in a similar way and range. For the highest sweep flow rate, selectivities are: isobutene 90%, n-butane 5%, n-butene 3%, C3-C1 products 2%.

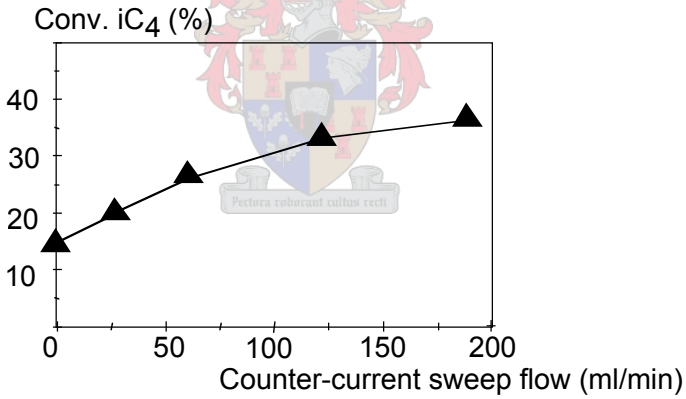

Fig 4. Isobutane conversion yield in the MFI membrane reactor
Feed flow rate: 50 ml/min, feed composition: $H_2/iC_4/N_2$ =20/20/60

Discussion

Transport properties

Pd membrane

When compared to data from the literature, the present Pd membrane does not show a very high performance, due to the presence of some defects. The fact that nitrogen and isobutene exhibit the very same permeances (Table 3) suggests these defects are macroporous and likely correspond to pores of the support that are not covered by Pd.

However, the H_2/N_2 permselectivity (60) is clearly higher than that based on Knudsen transport (3.7). This shows the H_2 permeance mainly occurs through metallic palladium.

Erratum: Paragraph 1 – "When using a sweep, the isobutane conversion increases (figure 3) up to ca. 37% for a sweep flow rate of 185 ml/min (3.7 times the feed flow).

As hydrogen and isobutane transports proceed essentially through independent pathways, the performance of the Pd membrane in H_2/iC_4H_{10} separation during CMR operation can be estimated on the basis of the calculated permselectivity (here, 60).

MFI membrane

In this case, species (H_2, N_2, iC_4) permeate through the same porous network, essentially that of the MFI material (defects contribution is limited [13]). Adsorption phenomena in the zeolite structure will rule the selectivity of the transport. At low temperature iC_4H_{10} is strongly adsorbed in the MFI pores and blocks permeation of other species. However, owing to the very small diffusivity of iC_4, its transfer through the membrane is low and close to the limited amount of H_2 that may permeate, essentially through defects. Therefore, at room temperature, the H_2/iC_4H_{10} separation factor, S, is low (Figure 1). At higher temperature, iC4 adsorption and occupancy decrease, leading to an increase of both H_2 permeation and separation factor.

Figure 2 also shows how this separation factor S_f varies with the sweep flow rate. There is a large increase of S_f in the 0-100 ml/min sweep range, then S goes through a maximum, close to 10, as high sweeps extract also iC_4 in non negligible amounts.

Comparison of the two membranes

When compared to the MFI membrane under CMR operation conditions (T, feed, sweep), the Pd membrane shows a better performance for the H_2 permeance (ca. 6 times higher).

As far as the H_2/iC_4H_{10} separation factor is concerned, the quantitative comparison is not so easy, as no direct measurement has been performed with the Pd membrane. However, it has been observed that most (up to 90%) of the hydrogen (coming from the feed or produced by the reaction) is extracted by the Pd membrane during CMR operation. This observation, combined with the H_2/iC_4H_{10} permselectivity of 60 deduced from single gas measurements, suggests the separation efficiency of the Pd membrane is certainly better than that of the MFI membrane under CMR operation.

Comparison of CMRs performances

Figures 3 and 4 show a very similar behavior of the two MFI and Pd CMRs when increasing the countercurrent sweep flow rate.

If it logical that the two systems give the same conversion at zero sweep (conventional reactor), it is surprising that under high sweep the Pd CMR does not draw any benefit from the better transport performances (H_2 permeance and selectivity) of the Pd membrane.

In a previous publication [9], we reported on the effect of sweeping mode on the performance of the MFI CMR for the same reaction. Let us recall that, if, in the co-current sweep mode, the CMR performance was clearly controlled by the membrane, this was no more the case in the counter-current sweep mode. In fact, owing to the very high driving force for hydrogen permeation that exists, in the counter-current mode, at the outlet of the reactor, the catalyst was not able to establish equilibrium at the exit of the catalyst bed [9].

This interpretation is confirmed by the results shown here. As a matter of fact, the Pd membrane, with higher permeation and separation abilities, will not change the situation, as the CMR is limited by the efficiency of the (same) catalyst. Therefore, the two MFI and Pd CMRs showed similar performances.

One can speculate how to increase the catalyst performance to overcome this situation.

If the fixed-bed Pt-based catalyst is considered here as a "black-box" producing hydrogen, in competition with the membrane extracting hydrogen, it has been previously reported that this catalyst did not suffer, under similar conditions, of diffusive limitations [16]. The catalyst works therefore under chemical regime.

This catalyst has been selected after a screening of different state-of-the-art active phases in dehydrogenation reactions [16] and showed excellent activity and stability under the present conditions. It has been patented [17].
Conventional ways to improve the catalyst performance, like temperature or contact time increases, would have only limited effects. As a matter of fact, a simple calculation shows that the hydrogen production rate, at the catalyst, is much lower than the permeation rate through the membrane, at the outlet of the CMR. This extends to a factor of 30 for the MFI membrane and to a factor of 80 for the Pd membrane. Moreover, a temperature increase may deactivate the catalyst and change the selectivity. A contact time increase could result in diffusion limitations in the active phase. Furthermore, temperature and contact time increases could even improve the membrane performance, increasing again this rate gap, which is not the targeted effect.

As far as catalytic selectivity is concerned, both systems give, when increasing sweep flow, the same and limited decrease of isobutene selectivity (from 100 to 90 %). This is what can be expected in the case of isobutane dehydrogenation on a Pt-zeolite-based catalyst. As a matter of fact, in this reaction, the main side reaction, isomerization (leading to the linear butane and butenes formation), goes through a dehydrogenation step of iC_4H_{10}. Therefore, the higher the sweep, the higher the isobutane dehydrogenation and, the lower the isobutene selectivity.
The fact that the two Pd and MFI CMRs give the same selectivity results also suggests that the membrane has little effect on the catalysis itself.

The modeling approach also shed some light on the comparison of the two CMRs. Figures 5 (Pd CMR) and 6 (MFI CMR) compare the experimental conversions with those deduced from the modeling.
The thermodynamic equilibrium conversion in a conventional reactor is also given under similar conditions, that slightly changes with the sweep flow rate in the CMRs. As a matter of fact, owing to the pressure drop in the set-up, an increase of the sweep flow produces a pressure rise in the sweep side. To keep the transmembrane differential pressure to zero, there is a parallel pressure increase on the catalyst side. Figures 5 and 6 show that both CMRs perform better than the conventional system.

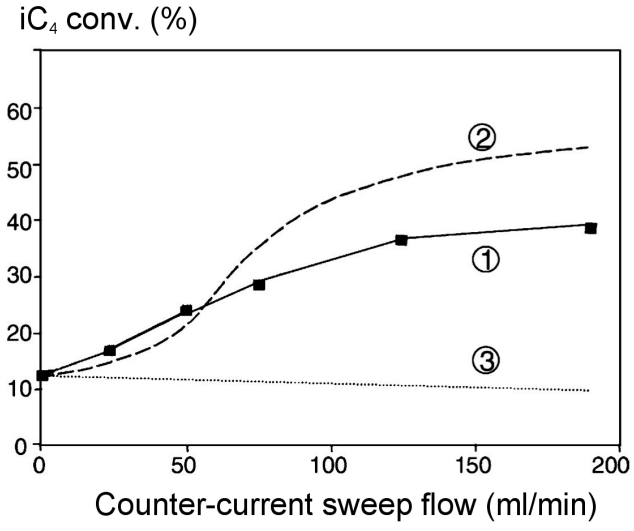

Figure 5. Pd CMR. Comparison of experimental data (curve 1) and modelling results (curve 2). Curve 3 performance of a conventional reactor at equilibrium.

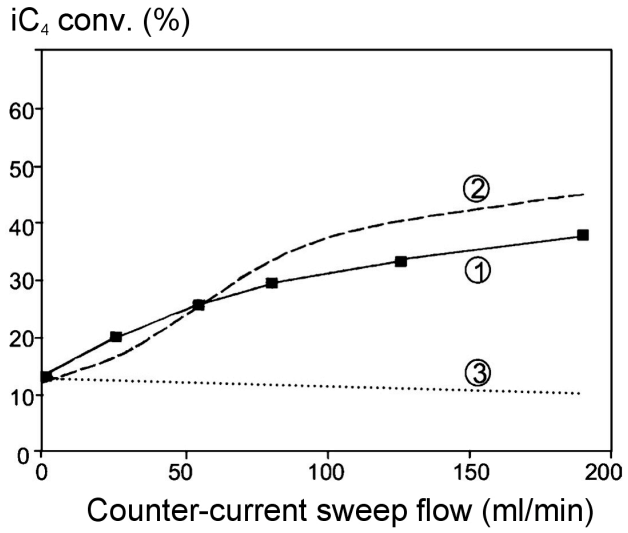

Figure 6. MFI CMR. Comparison of experimental data (curve 1) and modelling results (curve 2). Curve 3 performance of a conventional reactor at equilibrium.

As the model makes use of a kinetic law that has been obtained in a conventional microreactor, it predicts a performance that would have been observed only if the catalyst was not limiting. The conversion given by the model corresponds to a situation where the catalyst would be efficient enough to take into account the high hydrogen extraction and re-establish the equilibrium under conditions prevailing at the exit of the catalyst bed.
The better the membrane separative performance, the larger the gap observed between experiments and modeling. This gap can be estimated using the factor η, as introduced in the modeling (Eq. 3), to account for the catalyst efficiency in the CMR. These η values are obtained by adjusting the model response to the experimental data. For the MFI CMR, η is 0.6 and only 0.4 for the Pd CMR.

Conclusion

As CMRs are made of a membrane and a catalyst, each of these two materials may control the whole performance of the reactor. In the present study of an extractor-type CMR, it has been shown that, to completely draw benefit from their combination, there was a need of developing very active catalysts, able to follow the high extraction ability of the membrane.
This observation is consistent with those already reported [1] and may be extended to other types of CMRs [9]. As a matter of fact, in a CMR, the catalyst is often placed in a reactive medium different from that existing in conventional reactors, for which catalysts have been generally designed [18].
The need of an adapted catalyst may be a general feature of CMRs, which perhaps received less attention than that dedicated to membranes.

NOTATION

D_i^m	diffusion coefficient of species i through the membrane ($mm^2.min^{-1}$)
D_i^s	molecular diffusivity of species i ($mm^2.min^{-1}$)
$F_i^{(k)}$	molar flow rate of species i in zone k ($mol.min^{-1}$)
$F_{i,0}^{(k)}$	inlet molar flow rate of species i in zone k ($mol.min^{-1}$)
$F_T^{(k)}$	total molar flow rate in zone k ($mol.min^{-1}$)
k_1	kinetic constant for reaction ($mol.min^{-1}.g^{-1}$)
K_{eq}	equilibrium constant (atm^{-1})
K_{iC4}	adsorption equilibrium constant of isobutane (atm^{-1})
$K_{iC4=}$	adsorption equilibrium constant of isobutene (atm^{-1})
K_{H2}	adsorption equilibrium constant of hydrogen (atm^{-1})
L	reactor length (mm)
P	Total pressure in the catalyst bed and in the shell side (atm)
P_{H2}	partial pressure of hydrogen (atm)
P_{iC4}	partial pressure of isobutane (atm)
$P_{iC4=}$	partial pressure of isobutene (atm)
Q	reaction quotient (atm^{-1})
R	gas law constant
r:	rate of reaction ($mol.min^{-1}.g^{-1}$)
r:	radial coordinate (in appendix)
R_0	radius of the thermometric tube (mm)
R_1	inner radius of the membrane tube (mm)
R_2	outer radius of the membrane tube (mm)
R_3	inner radius of the shell tube (mm)
R_4	outer radius of the shell tube (mm)
S_f	separation factor
T	reaction temperature (K)
z	axial coordinate

Greek letters

ε_m, ε_s	porosity of membrane, support
η	effectiveness factor
ν_i	algebraic stoechiometry coefficient of specie i
ρ	catalyst apparent density ($g.mm^{-3}$)
τ_m, τ_s	tortuosity of membrane, support

REFERENCES

[1] S. Mota, S. Miachon, J.-C. Volta, and J.-A. Dalmon, Cat. Today, 67 (2001) 169.
[2] H.P. Hsieh, Inorganic Membranes for Separation and Reaction, Elsevier, (1996) p. 299.
[3] E. Piera, C. Tellez, J. Coronas, M. Menendez and J. Santamara, Cat. Today, 67 (2001) 127.
[4] T. Matsuda, I. Koike, N. Kubo and E. Kikuchi, Appl. Catal. A, 96 (1993) 3.
[5] B.A. Raich and H.C. Foley, Appl. Catal. A, 129 (1995) 167.
[6] J. Shu, B.P.A. Grandjean, S. Kaliaguine, P. Ciavarella, A. Giroir-Fendler and J-A. Dalmon, Canadian Journal of Chemical Engineering, 75 (1997) 712.
[7] T. Ionnides and G.R. Gavalas, J. Membrane Sc., 77 (1993) 207.
[8] Y. Zhu, R.G. Minet and T.T. Tsotsis, Catal. Lett., 18 (1993) 48.
[9] P. Ciavarella, D. Casanave, H. Moueddeb, S. Miachon, K. Fiaty and J-A. Dalmon, Cat. Today, 67 (2001) 177.
[10] U. Illgen, R. Schäfer, M. Noack, P. Kölsch, A. Kühnle and J.Caro, Catalysis Communications, 2 (2001) 339.
[11] P. Mériaudeau, A. Thangaraj, C. Naccache, Stud. Surf. Sci. Catal. 101B (1996) 1313.
[12] J. Keuler, L. Lorenzen and S. Miachon, accepted in Sep. Sci. & Tech.
[13] A. Giroir-Fendler, J. Peureux, H. Mozzanega, J-A. Dalmon, Stud. Surf. Sci. Catal. 101A (1996) 127.
[14] D. Casanave, P. Ciavarella, K. Fiaty and J-A. Dalmon, Chem. Eng. Sc., 54 (1999) 2807.
[15] D. Casanave, K. Fiaty, J-A. Dalmon, M. Forissier, Stud. Surf. Sci. Catal., 122 (1999) 367.
[16] D. Casanave, PhD thesis, Lyon University, 1996.
[17] P. Mériaudeau, P. Nascimento, G. Sapaly and C. Naccache, Eur. Patent EP98400371.5-2104.
[18] J-A. Dalmon, Handbook of Heterogeneous Catalysis. Eds Ertl, Knözinger, Weitkamp, VCH, 1997, Chapter 9.3, 1387.

Appendix: Model development

In catalyst bed, 0 < z < L the mass balance on each component is:

$$\frac{dF_i^{(1)}}{dz} = \nu_i \eta \rho \pi \left(R_1^2 - R_0^2\right) r - 2\pi R_1 N_i^m \Big|_{r=R_1^+} \quad (1)$$

ρ is the catalyst apparent density defined as the mass of catalyst per internal compartment unit volume and νi is the algebraic stoichiometric coefficient of component i, η the effectiveness factor introduced to take into account the limiting effects on catalyst activity in comparison with the one measured in the differential microreactor and r the kinetic rate. N_i^m is the molar flux of mixture component i through the membrane.

In the shell side, the differential equation describing mass balance in the axial direction is:

$$\frac{dF_i^{(2)}}{dz} = (-1)^n 2\pi R_3 N_i^s \Big|_{r=R_3^-} \quad (2)$$

with n = 0 for co current and n =1 for counter current. N_i^s is the molar flux of mixture components through the support.

In the membrane the conservation of the mass balance is

$$\frac{1}{r}\frac{\partial}{\partial r}\left(rN_i^m\right) = 0 \quad (3)$$

$$\text{with } N_i^m = -\frac{D_i^m}{RT}\frac{\varepsilon_m}{\tau_m}\frac{\partial P_i^m}{\partial r} \quad (4)$$

In the support a similar expression is derived:

$$\frac{1}{r}\frac{\partial}{\partial r}\left(rN_i^s\right) = 0 \quad (5)$$

$$\text{and } N_i^s = -\frac{D_i^s}{RT}\frac{\varepsilon_s}{\tau_s}\frac{\partial P_i^s}{\partial r} \quad (6)$$

Expressions (3) and (5) are solved analytically taking into account the following boundary conditions:

at r = R1 $\quad P_i^m\Big|_{r=R_1^+} = P_i^{(1)} = \frac{F_i^{(1)}}{F_T^{(1)}}P \quad (7)$

at r = R2 $\quad P_i^m\Big|_{r=R_2^-} = P_i^s\Big|_{r=R_2^+} \quad (8)$

at r = R3 $\quad P_i^s\Big|_{r=R_3^-} = P_i^{(2)} = \frac{F_i^{(2)}}{F_T^{(2)}}P \quad (9)$

and the continuity of flux at the interface membrane/support ($N_i^m = N_i^s$) to obtain the following equation of the molar flux through the membrane:

$$N_i^m \Big|_{r=R_1^+} = -\frac{1}{R_1}\frac{D_i^m \varepsilon_m}{\tau_m}\frac{1}{\ln\frac{R_2}{R_1} + \frac{D_i^m \varepsilon_m}{D_i^s \varepsilon_s}\frac{\tau_s}{\tau_m}\ln\frac{R_3}{R_2}}\frac{P}{RT}\left(\frac{F_i^{(2)}}{F_T^{(2)}} - \frac{F_i^{(1)}}{F_T^{(1)}}\right) \quad (10)$$

Substituting eq10 in eq1 the mass balance in the tube can be written as:

$$\frac{dF_i^{(1)}}{dz} = \nu_i \eta \rho \pi \left(R_1^2 - R_0^2\right) r + 2\pi \frac{P}{RT}\frac{D_i^m}{\tau_m}\frac{\varepsilon_m}{\ln\frac{R_2}{R_1} + \frac{D_i^m \varepsilon_m}{D_i^s \varepsilon_s}\frac{\tau_s}{\tau_m}\ln\frac{R_3}{R_2}}\left(\frac{F_i^{(2)}}{F_T^{(2)}} - \frac{F_i^{(1)}}{F_T^{(1)}}\right) \quad (1')$$

Using at steady state the conservation of the flux at the interface membrane/support in the radial direction:

$$N_i^s\big|_{r=R_3^-} = \frac{R_1}{R_3} N_i^m\big|_{r=R_1^+} \tag{11}$$

Eq2 becomes:

$$\frac{dF_i^{(2)}}{dz} = (-1)^{n+1} 2\pi \frac{P}{RT} \frac{D_i^m \varepsilon_m}{\tau_m} \frac{1}{\ln\frac{R_2}{R_1} + \frac{D_i^m \varepsilon_m}{D_i^s \varepsilon_s}\frac{\tau_s}{\tau_m}\ln\frac{R_3}{R_2}} \left(\frac{F_i^{(2)}}{F_T^{(2)}} - \frac{F_i^{(1)}}{F_T^{(1)}}\right) \tag{12}$$

Due to chemical reaction and back permeation, the total molar rate vary along the membrane length. The total molar flux in tube $F_T^{(1)}$ is obtained from overall mass balance by adding together eq1 written for each component of the gaseous mixture:

$$\frac{dF_T^{(1)}}{dz} = -2\pi R_1 \sum_i N_i^m\big|_{r=R_1^+} + \eta\rho\pi\left(R_1^2 - R_0^2\right) r\Delta\nu \tag{13}$$

where $\Delta\nu = \sum_i \nu_i$

The total molar flux at the interface membrane tube is defined by:

$$\sum_i N_i^m\Big|_{r=R_1^+} = -\frac{1}{RT}\sum_i \frac{D_i^m \varepsilon_m}{\tau_m}\frac{\partial P_i^m}{\partial r}\Bigg|_{r=R_1^+} \tag{14}$$

We assume the total pressure to be constant, therefore the variation of the inert partial pressure through the membrane is:

$$\frac{\partial P_I^m}{\partial r} = -\sum_{j\neq I}\frac{\partial P_j^m}{\partial r} \tag{15}$$

where 'I' symbolizes the inert component or sweep gas. Substituting eq15 in eq14 combined with eq4 and eq10 , the radial total molar flux can be determined by the expression:

$$\sum_i N_i^m\Big|_{r=R_1^+} = \frac{1}{R_1}\frac{P}{RT}\sum_{j\neq I}\frac{\left(D_I^m - D_i^m\right)\varepsilon_m}{\tau_m} \frac{1}{\ln\frac{R_2}{R_1} + \frac{D_i^m \varepsilon_m}{D_i^s \varepsilon_s}\frac{\tau_s}{\tau_m}\ln\frac{R_3}{R_2}} \left(\frac{F_i^{(2)}}{F_T^{(2)}} - \frac{F_i^{(1)}}{F_T^{(1)}}\right) \tag{16}$$

Substituting eq16 in eq13, the overall mass balance is:

$$\frac{dF_T^{(1)}}{dz} = -2\pi\frac{P}{RT}\sum_{j\neq I}\frac{\left(D_I^m - D_i^m\right)\varepsilon_m}{\tau_m} \frac{1}{\ln\frac{R_2}{R_1} + \frac{D_i^m \varepsilon_m}{D_i^s \varepsilon_s}\frac{\tau_s}{\tau_m}\ln\frac{R_3}{R_2}} \left(\frac{F_i^{(2)}}{F_T^{(2)}} - \frac{F_i^{(1)}}{F_T^{(1)}}\right) + \eta\rho\pi\left(R_1^2 - R_0^2\right) r\Delta\nu) \tag{17}$$

In the shell side the material balances for all the components is:

$$\frac{dF_T^{(2)}}{dz} = (-1)^n 2\pi R_3 \sum_i N_i^s\big|_{r=R_3^-} \tag{18}$$

By substituting eq11 and eq16 in eq18, the overall mass balance becomes:

$$\frac{dF_T^{(2)}}{dz} = (-1)^n 2\pi\frac{P}{RT}\sum_{j\neq I}\frac{\left(D_I^m - D_i^m\right)\varepsilon_m}{\tau_m} \frac{1}{\ln\frac{R_2}{R_1} + \frac{D_i^m \varepsilon_m}{D_i^s \varepsilon_s}\frac{\tau_s}{\tau_m}\ln\frac{R_3}{R_2}} \left(\frac{F_i^{(2)}}{F_T^{(2)}} - \frac{F_i^{(1)}}{F_T^{(1)}}\right) \tag{19}$$

Xylene isomerization in an extractor type Catalytic Membrane Reactor

Lizelle van Dyk[1,2], Leon Lorenzen[1], Sylvain Miachon[2,*] & Jean-Alain Dalmon[2]
1. University of Stellenbosch, Stellenbosch, South Africa
2. Institut de Recherches sur la Catalyse, CNRS, Villeurbanne, France

to whom correspondence should be addressed: smiachon@catalyse.cnrs.fr

Abstract

A zeolite / alumina pore plugging membrane was used to successfully separate xylene isomers. It was then applied as a selective membrane in an extractor type Catalytic Membrane Reactor (CMR), used to enhance the xylene isomerization reaction selectivity towards para-xylene. The results of the CMR in different configurations (permeate-only and combined permeate-&-retentate mode) were compared to conventional fixed-bed reactor results. In both cases, the selectivity was significantly enhanced (up to 100% in permeate-only mode). In the combined mode, the CMR also provided a net increase in productivity over the conventional reactor.

Keywords:

para-xylene, meta-xylene, ortho-xylene, isomerization, zeolite membrane, Catalytic Membrane Reactor, extractor, selectivity, productivity.

Introduction

In 2003 the worldwide demand for xylenes was about 22 million tons, with para-xylene (a precursor for polyesters) holding 80% of the market share [1]. Principal sources of xylene isomer mixtures are catalytically reformed naphthas and pyrolysis distillates [2], with the distribution of xylene isomers being approximately 50-60% of meta-xylene and 20-25% ortho- and para-xylene. In order to meet the para-xylene demand the much less used ortho- and meta-xylenes are converted via the xylene isomerization reaction, a major industrial process for this aromatic [3]. Xylene isomerization is a thermodynamic equilibrium restricted reaction, and therefore total conversion is impossible in conventional conditions. Equilibrium product distributions in the standard state (atmospheric pressure) for temperatures 250-1500 K, range from 63-47% for meta-xylene, 13.4-30% for ortho-xylene and 23.6-23% for para-xylene [4].

Separation of para-xylene from its isomers is essential, but this is difficult due to their close boiling points. Para-xylene (T_b = 411.3 K) and meta-xylene (T_b = 412.1 K) are normally separated by crystallization, selective adsorption or chromatographic techniques. Recent research efforts focus on using MFI-zeolite membranes for xylene separation, a potentially more energy-efficient separation method [5-8]. The MFI zeolite pore structure consists of straight, circular pores (0.54 × 0.56 nm), interconnected with sinusoidal, elliptic pores (0.51 × 0.54 nm) [9]. These pore sizes are close to the kinetic diameter of para-xylene (d_k = 0.58 nm), and it is expected that its bulkier isomers (d_k = 0.68 nm) would diffuse at a slower rate, and adsorb to a lesser extent in the MFI framework due to their size and shape [6].

A number of research groups have carried out studies in this area with different results. Baertsch *et al*. [5] studied permeation of p- and o-xylene through silicalite-1 membranes containing large amounts of non-zeolite pores. They found that for a mixture of ~3 mol% p-xylene, 3 mol% o-xylene and 94 mol% He over the temperature range 380-480 K, no separation occurred. Keizer *et al*. [10] reported separation factors of p-/o-xylene as a function of time between 298 and 473 K and gave values of ~ 1 at 298 K to > 200 at 375-415 K with a maximum at ~400 K. The separation factor was 25 at 473 K. The partial pressures of components in the feed were low (p-xylene 0.31 kPa, o-xylene 0.26 kPa). A maximum p-xylene flux at 400 K was said to be due to opposing effects of adsorption and diffusion. Gump *et al*. [9] studied the fluxes of aromatic molecules (p-xylene, o-xylene and benzene), through several molecular sieve membranes (SAPO-5, SAPO-11 and mordenite) as well as three types of MFI membranes (silicate-1, ZSM-5 and boron substituted ZSM-5), as a function of pressure and temperature. They found that surface diffusion and what they identified as *activated gas transport* were the controlling mass transfer mechanisms for MFI membranes. Boron-substituted ZSM-5 membrane displayed the highest p-xylene/o-xylene separation, up to 60, obtained at 425 K for partial feed pressures of 2.1 kPa per isomer. Higher pressures of p-xylene were reported to distort the membrane framework, leading to higher o-xylene permeation and reduced separation.

An extensive study of xylene vapour permeation was performed by Xomeritakis *et al*. [6,11,12]. Single gas permeation tests at feed partial pressures of 0.86 and 0.64 kPa for p-xylene and o-xylene were done in the temperature range 295 to 548 K for c-oriented MFI membranes. It was found that p-xylene permeance displayed weak temperature dependence, while o-xylene permeance displayed a minimum at 373 K. Also, as the partial pressure of p-xylene in the feed mixture was increased from 43 to 430 Pa, the p-/o- xylene separation factor dropped from 48 to 3. In order to get rid of defect influence, Sakai *et al*. [7] used self-supporting MFI zeolite membranes of a thickness between 60 and 130 μm. The p-xylene permeation flux showed a maximum at 473 K and a partial pressure at 0.3 kPa, and was described by the competitive effects between equilibrium adsorption and diffusivity. The permeation of m- and o-xylene was small, and almost constant between 473 and 673 K. The separation factors of p- to m-xylene and p- to o-xylene reached a maximum value of 250 at 473 K. On the other hand, high-pressure, high-temperature gas separation of xylenes were carried out by Hedlund *et al*. [13] using ultra thin MFI films (0.5 μm) on porous α-alumina supports produced by a two-step support masking technique, and a monolayer of colloidal nucleation seeds, followed by in situ hydrothermal growth. High permeance values were obtained (up to 0.6 μmol/s/m^2/Pa at 373 K), together with p-/o-xylene separation factors somewhat lower than expected (3 to 17) [14]. Similar interesting results were obtained recently by Lai and co-workers [15,16].

Separation of para-xylene from its isomers is therefore possible through MFI-zeolite membranes. However, the presence of defects shows a strong influence on separation factors found in the literature, particularly at higher temperatures. In particular, supported zeolite films may suffer from defects opening during calcinations or temperature increase, as a consequence of the difference in thermal expansion coefficient between the zeolite and the support [7]. We show here the use of a zeolite /alumina nanocomposite membrane of the *pore-plugging* type.

Catalytic membrane reactors (CMRs) have been classified, in previous publications from our team, into three groups, depending on the function of the membrane: extractor,

distributor and contactor [17]. By using a membrane capable of separating p-xylene from the mixture of the three isomers, we propose to study the behaviour of the catalytic reaction taking place in the CMR. Therefore, this paper reports on the use of an extractor type CMR for the selectivity enhancement of the meta-xylene isomerization reaction towards para-xylene. Nevertheless, whereas extractor CMRs are commonly reported to enhance conversion, this work concentrates on improving selectivity.

Experimental

Materials

The MFI-zeolite membrane was synthesized in the wall of a porous ceramic tubular support (Pall-Exekia T1-70), consisting of three macroporous α-alumina layers (from outer to inner side, respective average pore sizes: 12, 0.8, 0.1 μm and thicknesses 1500, 40, 20 μm). It had an outer diameter of 10 mm, inner diameter of 7 mm and an effective membrane length of 13 cm. The MFI membrane was obtained by synthesis of zeolite crystals inside the pores of the macroporous tubular support (*pore-plugging* method) [18,19]. The MFI zeolite precursor solution was obtained by mixing silica (Aerosil 380) and a template (tetrapropylammonium hydroxide, TPAOH). After a 3-day ageing period, the solution was poured in a Teflon-lined autoclave containing the porous ceramic tube. Hydrothermal synthesis was then performed at 443 K for 3 days, and the membrane was calcined at 773 K under airflow. Low temperature butane / hydrogen separation through the membrane showed it could be considered close to defect-free (i.e. the transport through the membrane is controlled by the micropores of the MFI structure).

The *catalyst* (Pt on zeolite) was a commercial xylene isomerization catalyst (ISOXYL) from Süd-Chemie. The catalyst was diluted with kaolin to 5 wt% of the original and extruded into ca 2-mm pellets, with a labscale extruder. The same mass of 2.18 g of the obtained solid was used in every experiment. Before catalytic use, the solid was activated in situ under H_2 flow at 673 K for 3 hrs.

Anhydrous xylene isomers were purchased from Sigma–Aldrich: meta-xylene 99+%, para-xylene 99+% and ortho-xylene 97%.

Set-up

Figure 1 shows a schematic diagram of the experimental set-up used for the separation tests, as well as the catalytic membrane reactions. The xylenes were fed as gas phase diluted in nitrogen, using two saturators in series. The temperature in the first saturator was kept 5 K higher than the second one, in order to ensure precise vapour saturation. The flow through the compartments could be either co- or counter current (valve 3). The carrier gas, and sweep gas flow rates were controlled with Brooks mass flow controllers (FC). The internal pressure was measured by help of a pressure gauge (Keller PAA23). The trans-membrane or differential pressure between the internal and external compartments of the reactor was measured (Keller DP22), and could be manually regulated by using valves 11a and b. The flow rates were measured with a soap bubble flow meter. All the pipes in the system were heated using heating tape and kept at 373 K in order to prevent any xylene condensation, and ensure correct xylene vapor pressure values. The compositions of the feed, permeate and retentate streams were analyzed on-line with a gas chromatograph

(Shimadzu, GC 14A) equipped with a FID detector and a capillary column (Solgel-WAX, SGE). Reactor by-pass was possible if needed.

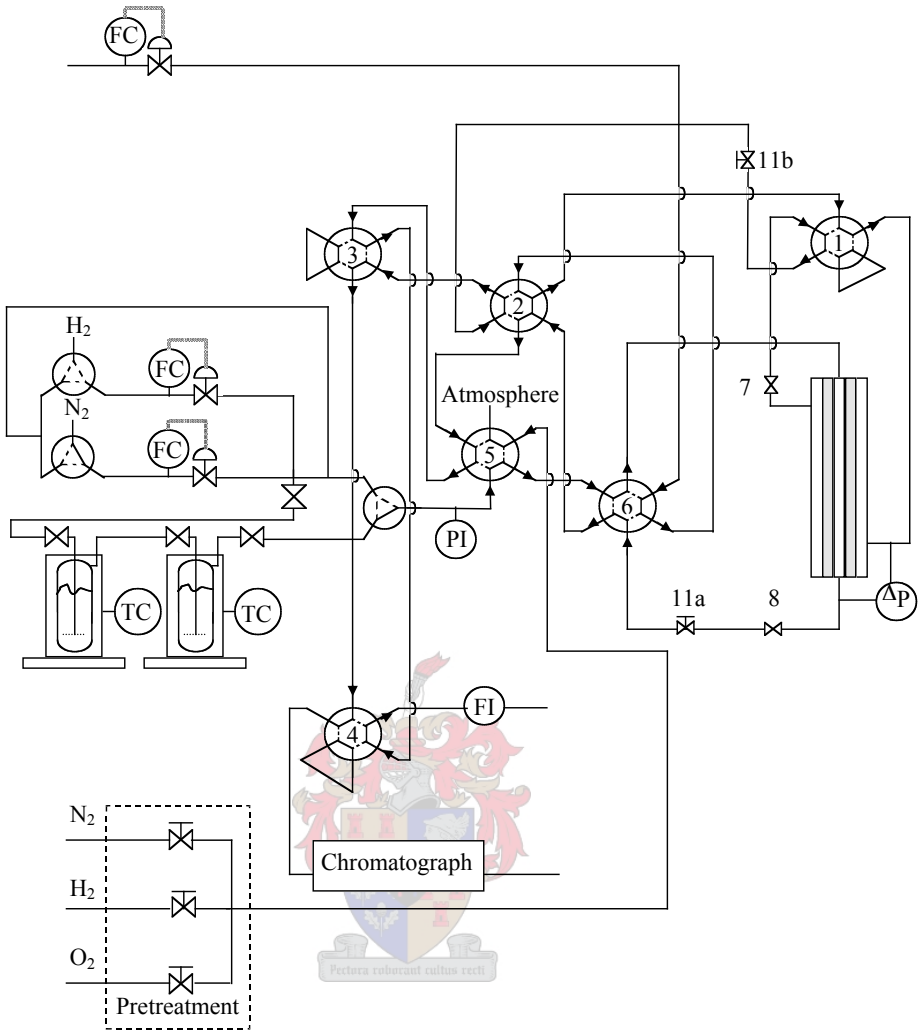

Figure 1. Schematic diagram of the experimental set-up (FC: mass flow controller, ΔP: transmembrane pressure gauge, FI: flow meter, PI: feed pressure gauge, TC: temperature controllers).

Transport measurements: mixture

The membrane was sealed with cylindrical graphite seals in a stainless steel module, equipped with temperature control. Before any membrane testing, the MFI membrane was pre-treated at 673 K under nitrogen flow for 4 hours.

Separation tests were performed on the MFI membrane following a modified Wicke-Kallenbach method with a mixture of xylenes (1.5 kPa p-xylene, 4.5 kPa m-xylene and 1.35 kPa o-xylene) saturated in nitrogen at atmospheric pressure and 336 K. The feeding rate was 60 ml/min with a counter-current nitrogen sweep of 15 ml/min. The temperature of the membrane system was varied from 673 to 423 K and again from 423 to 673 K. The feed, retentate and permeate compositions were measured online using the GC.

The separation factor (S_f) is defined here as an enrichment factor of one component to another in the permeate, as compared to the feed composition ratio:

$$S_{f,x/y} = \frac{x_P / x_F}{y_P / y_F}$$

with $x_{F,P}$ and $y_{F,P}$ the molar fractions of components x and y in the feed (F) or permeate (P) streams.

CMR operation and set-up

The fixed bed catalyst was packed in the lumen of the tubular membrane and the m-xylene isomerization reaction was carried out at various temperatures, feed flow rates and sweep flow rates. The differential pressure across the membrane was kept zero by varying the external pressure of the membrane module. Nitrogen was used as a sweep gas in the counter current mode. The feed flow rates were kept high enough to keep the conversion below equilibrium in the catalytic bed, in order to avoid undesired by-product (toluene or ethylbenzene) formation. The permeate and retentate exit streams were analysed separately. Adding up both streams provided the total amount of products obtained in the reactor (combined CMR mode).

We take as our *standard conditions*: temperature 577 K, 450 µl/min meta-xylene volumetric feed flow rate (diluted in nitrogen up to a total feed flow rate of 7 ml/min) and 10 ml/min sweep flow rate. In both separation and CMR experiments, very little nitrogen back permeation was observed, owing to the limited difference of nitrogen partial pressure between the feed and sweep sides of the membrane.

Conventional fixed-bed Reactor (CR)

The zeolite-based membrane was replaced with a stainless steel tube of identical dimensions, and the reaction conditions were kept as close as possible to the CMR operation, feeding and analyzing only the retentate side.

Results

Separation

Figure 2 shows a diagram of the para-xylene permeance values obtained from the separation testing. Samples were withheld after 90 minute temperature steps starting at 673 K. The temperature was then decreased and samples analysed down to 423 K and again up to 673 K. Over this temperature range, para-xylene was the only detectable component in the permeate stream. The accuracy/detection limit of the GC corresponded to a permance of about 0.12 nmol/s/m^2/Pa for meta-xylene and 0.45 nmol/s/m^2/Pa for ortho-xylene, as represented in figure 2.

Therefore, these results correspond to separation factor values that must be above 73 and 27 for p-/m-xylene as well as above 21 and 7 for p-/o-xylene at 473 and 673 K respectively. It can be seen in the 673-423 K range that, in the ternary mixture, para-xylene permeance is a function of temperature with a maximum value of 10.2 nmol/s/m^2/Pa at 450 K. The permeance decreases with an increase in temperature, down to a value of about 3.6 nmol/s/m^2/Pa at 673 K. The permeance values on the 423 to 673 K way are similar.

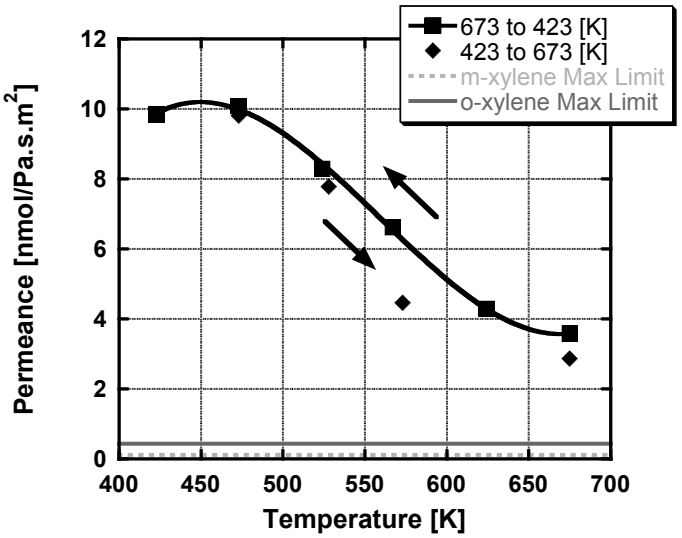

Figure 2. Permeance of para-xylene in a ternary isomer mixture (■ & ◆: para-xylene permeance when decreasing and increasing the temperature respectively, dotted gray line: detection limit for meta-xylene, dark gray line, detection limit for ortho-xylene).

Extractor CMR

Figure 3 is a graphic representation of a typical catalytic membrane reactor result (577 K, 450 μl/min xylene volumetric feed flow rate, 10 ml/min counter-current sweep flow rate), showing the feed and exit streams (permeate and retentate) as well as the combination of the two exit streams. The para-xylene yield (η) is the amount of formed para-xylene in the stream(s) divided by the total feed. It therefore represents the contribution made by each stream to the total yield in the system. The selectivity (sel) value is the percentage of para-xylene present divided by the amount of reaction products (para + ortho) in each stream.

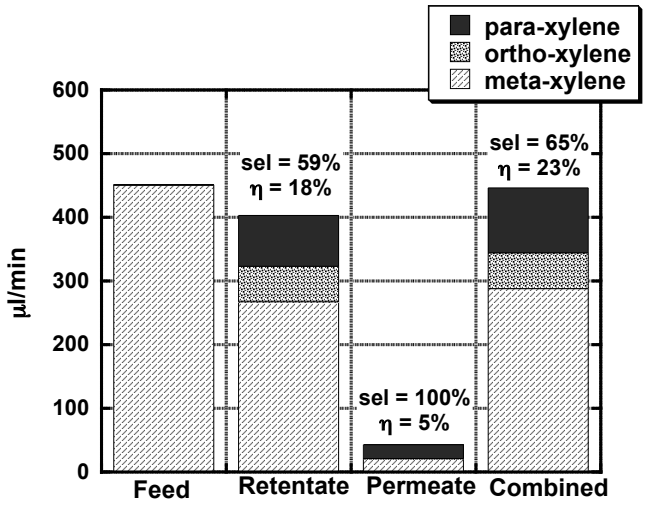

Figure 3. CMR operation at 577 K, 450 µl/min meta-xylene feed, 10 ml/min sweep flow (sel: selectivity of para-xylene; η: para-xylene yield). The combined result is obtained by mixing of both retentate and permeate streams after the reactor.

The feed to the reactor only includes meta-xylene diluted in nitrogen. Only para-and meta-xylene are detectable in the permeate stream. The para-xylene selectivity in the retentate is 59%, compared to the permeate 100%, meaning all the ortho-xylene formed during the reaction leaves the reaction zone via the retentate stream. The amount of para-xylene in the permeate making up 5% total para-xylene yield, while the rest leaves the reactor through the retentate. Mixing both streams after the reactor provides the *combined CMR* mode.

The results obtained for the CMR, operated at the above reaction conditions (referred to as the *standard conditions*: temperature 577 K, 450 µl/min meta-xylene volumetric feed flow rate (diluted in nitrogen) and 10 ml/min sweep flow rate) are compared with results obtained at a different feed flow rate, temperature and sweep flow rate, and shown in table 1. The membrane stays para-xylene selective, compared to ortho-xylene at all reaction conditions. If the meta-xylene feed flow rate is increased to 1150 ml/min, the para-xylene yield decrease to 13% in the retentate and 2% in the permeate. The selectivity in the permeate remains constant with an increase in feed flow rate, while the selectivity in the retentate increases (up to 66%) while the yield decreases.

Lowering the sweep flow rate to 7 ml/min brings about a slight decrease in the para-xylene selectivity of the retentate (58%) and permeate yield (4%). The para-xylene yield in the retentate stays constant. With an increase in temperature to 633 K, the selectivity in the retentate drops to 55% indicating a higher ortho-xylene yield for the reaction. The retentate para-xylene yield is 19%, while the permeate para-xylene yield decreases to 4% rendering an unchanged total para-xylene yield.

Table 1. Comparison of CMR results at various meta-xylene feed flow rates, nitrogen sweep flow rates and temperature, including, as a reference, the standard condition results shown in figure 3 (in italics and between brackets).

(Standard Conditions)		Retentate		Permeate	
		selectivity	yield	selectivity	yield
		(59%)	*(18%)*		*(5%)*
Feed [µl/min]	1150 *(450)*	66%	13%	100%	2%
Sweep [ml/min]	7 *(10)*	58%	18%		4%
Temperature [K]	633 *(577)*	55%	19%		4%

In Figure 4, the combined CMR result is compared with the conventional fixed-bed reactor (CR) mode and xylene isomerization equilibrium at 577 K, for the same feed conditions. The CR para-xylene selectivity is 58% and the para-xylene yield 21%, to be compared to equilibrium values of 46% and 24.9%, respectively. When the reactor is operated in combined CMR mode, the yield of para-xylene increases slightly (23%) while para-xylene selectivity (65%) increases with 7% compared to the CR mode.

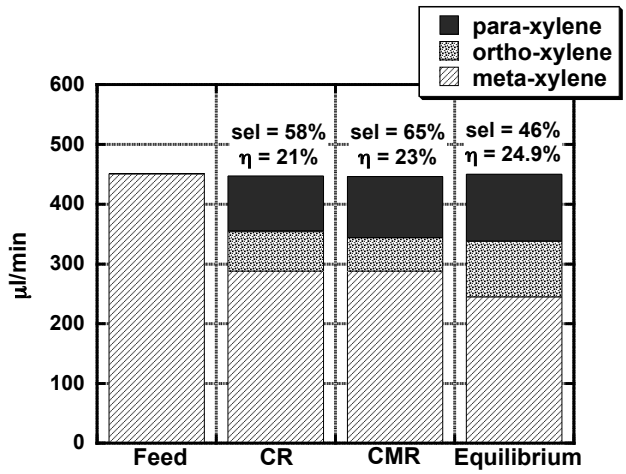

Figure 4. Comparison between conventional fixed-bed reactor (CR), combined mode catalytic membrane reactor (CMR) and xylene isomerization equilibrium [4] at 577 K (sel: selectivity of para-xylene; η: para-xylene yield)

In table 2, the results of the conventional reactor, permeate-only CMR and combined mode CMR are compared in terms of para-xylene selectivity and productivity. The productivity is related to para-xylene per unit bed volume of the reactor.

Table 2. Comparison of Conventional fixed-bed Reactor (CR), Permeate-only (CMR) mode and Combined mode Catalytic Membrane Reactor (CMR)

	Conventional Reactor (CR)	Permeate-only (CMR)	Combined mode CMR
Para-xylene selectivity	58%	100%	65%
Productivity (mmol/s/m^3)	10.2	2.4	11.2

Discussion

From the separation experiment results it can be concluded that para-xylene can be selectively separated from a ternary mixture of xylene isomers with the MFI zeolite membranes prepared in this study. A maximum value in the permeance of para-xylene can be seen close to 450 K. It can be explained as follows: as we consider the transport to be controlled by the zeolite pores, it is driven by a competition between adsorption and diffusivity temperature dependence. At low temperatures the coverage of para-xylene on the pore surface is higher. With an increase in temperature the coverage decreases, and is counterbalanced by the increase of the diffusion coefficient up to a certain point, leading to a further global decrease in permeance, as observed for all gases previously studied on this type of membrane [18-22].

It is interesting to note this study did not provide any hint of further permeance increase at higher temperatures, as commonly quoted (*gas activated transport*) on different gases [8,9,23-25] and also on xylenes [6,7,9,10]. This may be related to the support pore-plugging structure of the membrane, and will be detailed in another paper [26].

Meta-xylene isomerization in an extractor catalytic membrane reactor leads to an increase in the para-xylene selectivity of the reaction. This is due to the selective extraction of para-xylene compared to ortho-xylene. Throughout the runs no ortho-xylene was detected in the permeate stream. The meta-xylene present in the permeate stream may be due to permeation of meta-xylene in the first part of the reactor, when the para-xylene concentration is still too low to block the zeolite pores by adsorption [27]. As a matter of fact, calculations based on a para/meta-xylene separation factor above 53 at the reaction temperature, assuming an averaged lumen gas composition after reaction close to that used in the separation experiments, were carried out. They suggest that the observed meta-xylene trans-membrane flow is far too high when compared to separation conditions.

An increase in meta-xylene feed flow rate decreases the overall conversion of meta-xylene. The fact that the para-xylene selectivity improves in the retentate stream indicates that the reaction becomes more para-xylene selective at higher feed rates, as could be expected. The amount of para-xylene that diffuses also decreases, due to the concentration decrease of para-xylene in the membrane reaction zone.

It is expected that with a decrease in sweep flow rate the para-xylene permeance would also decrease. This has been seen for hydrogen extraction in CMR experiments with similar membranes as used in this study [28]. With a decrease in sweep flow rate from 10 to 7 ml/min a small decrease in para-xylene permeance is observed. This, together with the fact that the yield of para-xylene in the retentate stays constant while the para-xylene selectivity in the retentate also decreases slightly, indicates that when less para-xylene is extracted, more ortho-xylene is formed in the reaction.

When the temperature is changed from 577 to 633 K, the selectivity in the retentate decreases indicating more ortho-xylene production at this temperature. The yield in the retentate is only slightly higher, but the yield in the permeate is lower indicating the effect of temperature on the para-xylene permeance from the mixture, as seen during the separation testing.

When the yield and para-xylene selectivity values (fig. 4) of the conventional fixed-bed reactor and those calculated using thermodynamic equilibrium are compared, it is clear that the reactor is not operated at equilibrium. A WHSV of 215 hr^{-1} was used in these conditions. CMR operation increases the reaction selectivity when compared to conventional conditions, due to the fact that no ortho-xylene is present in the permeate stream. The results obtained for the conventional fixed-bed reactor is similar to that of the retentate (sel = 59% and η = 20%). A relative improvement in para-xylene yield of about one tenth (23% compared to 21%) is achieved. It is expected that this improvement can be enhanced upon if no meta-xylene was present in the permeate stream.

If one considers the CMR in the permeate-only mode, when compared to CR, the para-xylene selectivity is improved up to 100% - almost double. This would however lead to a significant reduction in the para-xylene production throughput (2.4 compared to 10.2 $mmol/m^3/s$). However, when the catalytic membrane reactor is used in combined mode (mixing both the retentate and permeate feed after the reactor), the para-xylene productivity is noticeably increased over the conventional fixed-bed reactor (11.2 compared to 10.2 $mmol/m^3/s$) with a lower amount of ortho-xylene in the product. This demonstrates that including both the separative membrane, and the catalytic bed in the same device (as per definition of a CMR) leads to an improvement when compared to separated catalytic and membrane separation units.

Conclusions

Using an extractor type catalytic membrane reactor instead of a conventional fixed-bed reactor for meta-xylene isomerization, can lead to higher para-xylene selectivities. The para-xylene selectivity can even be improved to 100% if the CMR is operated in the permeate-only mode, but this comes at a price of lower para-xylene yields. When operated in combined mode (i.e. mixing both permeate and retentate streams after the reactor), the CMR shows an improvement on both para-xylene productivity and selectivity when compared to the conventional fixed-bed reactor.

To the best of our knowledge there are no comparable results in literature. Research on xylene isomerization in a MFI membrane reactor was conducted by Mabanda *et al.*[29], but their results indicated that the separation of xylenes through the membrane was not sufficient enough to improve on the performance of the conventional fixed-bed reactor.

Prospects

Further improvements on the system are necessary, with higher cross-membrane para-xylene fluxes being the most important. Optimizing the zeolite membrane (in performance and/or geometry), the catalyst location along the membrane and/or working under higher feed xylene partial pressures may achieve this. In particular, the observed permeation of meta-xylene through the membrane during CMR operation could benefit from pre-conversion of meta-xylene or recycling of the permeate.

The catalyst needs to be optimised in order to ensure no undesirable by-products at equilibrium, for example ethylbenzene, would compete with para-xylene to diffuse through the membrane. Operation of the CMR at lower temperatures is necessary to investigate the advantages of the higher para-xylene permeance at lower temperatures. These two arguments show once again, that catalysts for CMRs need specific designs [28,30].

Modeling and scale-up studies are also needed to investigate the practical and economical feasibility of this process.

Acknowledgements

The authors would like to thank Süd-Chemie for kindly providing the catalyst and the Centre National de la Recherche Scientifique (Direction des Relations Internationales) and National Research Foundation (South Africa) for financial assistance.
Special thanks to Emmanuel Landrivon for technical help.

References

[1] G. Graph, Purchasing Magazine (2003) [http://www.manufacturing.net/pur/].

[2] J.J. McKetta, Encyclopedia of Chemical Processing and design, Marcel Dekker Inc., New York, 1999.

[3] M. Guisnet, N.S. Gnep, S. Morin, Microporous and Mesoporous Materials, 35-36 (2000) 47.

[4] R.D. Chirico, V. Steele, Journal of Chemical Engineering Data, 42 (1997) 784.

[5] C.D. Baertsch, H.H. Funke, J.L. Falconer, R.D. Noble, Journal of Physical Chemistry, 100 (1996) 7676.

[6] G. Xomeritakis, L. Zhiping, M. Tsapatsis, Industrial & Engineering Chemistry Research, 40 (2001) 544.

[7] H. Sakai, T. Tomita, T. Takahashi, Separation and Purification Technology, 25 (2001) 297.

[8] C.L. Flanders, V.A. Tuan, R.D. Noble, J.L. Falconer, Journal of Membrane Science, 176 (2000) 43.

[9] C.J. Gump, V.A. Tuan, R.D. Noble, J.L. Falconer, Industrial Engineering and Chemistry Research, 40 (2000) 565.

[10] K. Keizer, A.J. Burggaaf, Z.A.E.P. Vroon, H. Verweij, Journal of Membrane Science, 147 (1998) 159.

[11] G. Xomeritakis, S. Nair, M. Tsapatsis, Microporous Mesoporous Materials, 38 (2000) 61.

[12] G. Xomeritakis, S. Nair, M. Tsapatsis, Chemical Materials, 11 (1999) 875.

[13] J. Hedlund, J. Sterte, M. Anthonis, A.-J. Bons, B. Cartensen, N. Corcoran, D. Cox, H. Deckman, W. De Gijnst, P.-P. de Moor, F. Lai, J. McHenry, W. Mortier, J. Reinoso, J. Peters, Microporous and Mesoporous Materials, 52 (2002) 179.

[14] J. Hedlund, F. Jareman, A.-J. Bons, M. Anthonis, Journal of Membrane Science, 222 (2003) 163.

[15] Z. Lai, G. Bonilla, I. Diaz, J.G. Nery, K. Sujaoti, M.A. Amat, E. Kokkoli, O. Terasak, R.W. Thompson, M. Tsapatsis, D.G. Vlachos, Science, 300 (2003) 456.

[16] Z. Lai, M. Tsapatsis, Industrial & Engineering Chemistry Research, 43 (2004).

[17] J.-A. Dalmon, in G. Ertl, H. Knözinger, J. Weitkamp (Editors), in Handbook of Heterogeneous Catalysis, VCM Publishers, Weinheim, 1997, p. 2541.

[18] C. Chau, I. Prévost, S. Miachon, J.-A. Dalmon, Patent 02290252.2-2113 (US6.582.495) (Europe), 4.02.2001 (ext. to US 24.06.2003).

[19] A. Giroir-Fendler, J. Peureux, H. Mozzanega, J.-A. Dalmon, Studies in Surface Sciences and Catalysis, 101A (1996) 127.

[20] P. Ciavarella, D. Casanave, H. Moueddeb, S. Miachon, K. Fiaty, J.-A. Dalmon, Catalysis Today, 67 (2001) 177.

[21] P. Ciavarella, H. Moueddeb, S. Miachon, K. Fiatty, J.-A. Dalmon, Catalysis Today, 56 (2000) 253.

[22] D. Casanave, A. Giroir-Fendler, J. Sanchez, R. Loutaty, J.-A. Dalmon, Catalysis Today, 25 (1995) 309.

[23] S. Sommer, T. Melin, J.L. Falconer, R.D. Noble, Journal of Membrane Science, 224 (2003) 51.

[24] R.D. Noble, J.L. Falconer, Catalysis Today, 25 (1995) 209.

[25] C. Bai, M.-D. Jia, J.L. Falconer, R.D. Noble, Journal of Membrane Science, 105 (1995) 79.

[26] I. Kumakiri, O. Pachtova, S. Miachon, H. Mozzanega, E. Landrivon, Y. Sun, N. Guilhaume, J.-A. Dalmon, Journal of Membrane Science (to be submitted).

[27] T. Masuda, T. Asanuma, M. Shouji, S.R. Mukai, M. Kawase, K. Hashimoto, Chemical Engineering Science, 58 (2003) 649.

[28] L. van Dyk, S. Miachon, L. Lorenzen, M. Torres, K. Fiaty, J.-A. Dalmon, Catalysis Today, 82 (2003) 167.

[29] G.T.P. Mabande, A. Avhale, W. Schwieger, M. Hanebuth, R. Dittmeyer, (Proc. of 6th International Conference on Catalysis in Membrane Reactors (ICCMR-6)) (2004).

[30] S. Miachon, J.-A. Dalmon, Topics in Catalysis, 29 (2004) 59.

Nomenclature

A	Area	m^2
B_C	Mobility of component	$mol.Pa^{-1}.m^{-1}.s^{-1}$
d	Diameter	m or nm
D^s	Corrected transport diffusivity on the surface	$m^2.s^{-1}$
D^{Kn}	Knudsen diffusivity	$m^2.s^{-1}$
D^F	Fickian diffusivity	$m^2.s^{-1}$
D	Transport diffusivity	$m^2.s^{-1}$
D_{ij}^{MS}	Cross term Maxwell-Stefan diffusivity	$m^2.s^{-1}$
D^{MS}	Maxwell-Stefan diffusivity	$m^2.s^{-1}$
D_i^m	Diffusion coefficient of component i through the membrane	$mm^2.min^{-1}$
D_i^S	Molecular diffusivity of component i	$mm^2.min^{-1}$
D_0^∞	Intrinsic diffusivity at infinite temperature	$m.s^{-1}$
D_0	Intrinsic diffusion coefficient	$m.s^{-1}$
E_a	Activation energy	$J.mol^{-1}$
F_P	Permeance	$mol.Pa^{-1}.s^{-1}.m^{-2}$
$F_i^{(k)}$	Molar flow rate of component i in zone k	$mol.min^{-1}$
$F_{i,0}^{(k)}$	Inlet molar flow rate of component i in zone k	$mol.min^{-1}$
$F_T^{(k)}$	Total molar flow rate in zone k	$mol.min^{-1}$
f	Fugasity	
g	Geometric factor	
ΔH_{ads}	Adsorption Enthalpy	$J.mol^{-1}.K^{-1}$
k_1	Kinetic constant for reaction	$mol.min^{-1}.g^{-1}$
K	Adsorption equilibrium constant	Pa^{-1}
K_{eq}	Equilibrium constant	atm^{-1}
K_{iC_4}	Adsorption equilibrium constant of isobutane	atm^{-1}
K_{iC_4}	=Adsorption equilibrium constant of isobutene	atm^{-1}
K_{H_2}	Adsorption equilibrium constant of hydrogen	atm^{-1}
L	Reactor length (eCMR modeling)	mm
l	Effective thickness of the membrane	mm or m

M	Molecular weight	kg.mol^{-1}
N	Molar Flux	mol.m^{-2}.s^{-1}
$\dot{n}$	Molar flow rate at 298K and 1 atm	mol.s^{-1}
$\bar{p}$	Average pressure	Pa
ΔP	Differential pressure	Pa
p, P	Total pressure or partial pressure	atm, Pa or mBar
P_{H_2}	Partial pressure of hydrogen	atm
P_{iC_4}	Partial pressure of isobutane	atm
P_{iC_4} =	Partial pressure of isobutene	atm
Q	Reaction quotient (eCMR modeling)	atm^{-1}
Q	Molar flow rate	mol.s^{-1}
P^m	Permeance	mol/Pa.s.m^2
P^{er}	Permeability	mol.m/Pa.s.m^2
q	Molecular loading	mol.m^{-3} or mol.g^{-1} or mol.kg^{-1}
r	Rate of reaction	mol.min^{-1}.g^{-1}
r	Radial coordinate (in Appendix B)	
r_p	(Mean) pore radius	m
R	Universal Gas Law constant	8.314 J.mol^{-1}.K^{-1}
R_0	Radius of thermometric tube	mm
R_1	Inner radius of the membrane tube	mm
R_2	Outer radius of the membrane tube	mm
R_3	Inner radius of the shell tube	mm
R_4	Outer radius of the shell tube	mm
ΔS_{ads}	Adsorption Entropy	J.mol^{-1}.K^{-1}
S_f	Separation factor	
T	Temperature	K
ΔU_{ads}	Adsorption Energy	J.m^{-1}.K^{-1}
$\boldsymbol{u}$	Linear velocity	m.s^{-1}
$\dot{v}$	Volumetric flow rate	ml.min^{-1} or ml.s^{-1}
x	Mole fraction	
z	Axial coordinate	

Greek Symbols

δ	Membrane Thickness	m
η	Dynamic Viscosity	Pa.s
θ	Occupancy	
μ^0	Standard state chemical potential	J.mol^{-1}
μ	Chemical potential	J.mol^{-1}
ρ	Density	g.m^{-3} or kg.m^{-3}
Θ	Molecule loading within pores	moles/unit cell
Γ	Thermodynamic correction factor or matrix of thermodynamic factors	
$\varepsilon_m, \varepsilon_s$	Porosity of membrane, support	
η	Effectiveness factor (eCMR modeling)	
v_i	Algebraic stroichiometric coefficient of component i	
ρ	Catalyst apparent density	g.mm^{-3}
τ_m, τ_s	Tortuosity of membrane, support	

Subscripts and exponents

h	High
g	Configuration diffusion
i, j	Component i or j
k	Kinetic
l	Low
p	Pore
P	Permeate
R	Retentate
s	Surface
sat	Referring to saturation conditions
z	Zeolite